ABSTRACT

KILIC, ALI. Improving Electret Filter Efficiency by Modifying Fibrous Webs with Melt Additives. (Under the direction of Dr. Behnam Pourdeyhimi and Dr. Eunkyoung Shim).

Having a long history in aerosol filtration technologies, electret filters still have challenging problems such as low initial efficiency and stability of filtration. One way to modify charging properties of such polymeric filter media is incorporation of additives. Even though particularly in industry several polymer additives were used so far, there is not an extensive study that explains effect of those additives on efficiency and stability of electret filters. This study addresses the effect of various polymer additives on electret and electrostatic filtration properties of high efficiency nonwoven electret filters. Undoubtedly incorporation of such additives will result in changes in chemical structure and morphology of fibers which were investigated with various techniques such as DSC, XRD, FTIR, EDS and dielectric spectroscopy. Modified nonwoven webs were also analyzed by means of surface chemistry and morphology. Relation between those structural data and both their electret and electrostatic filtration properties were compared. Surface potential and electrostatic filtration properties were analyzed as resultant characteristics of those webs. The project was not limited to selection of additives, since the electrostatic filtration efficiency strongly depends on charging method. Due to chemistry and electronic structure, additives may require investigation of specific charging conditions, which was also one of the targets of the project.

Improving Electret Filter Efficiency by Modifying Fibrous Webs with Melt Additives

by
Ali Kilic

A dissertation submitted to the Graduate Faculty of
North Carolina State University
in partial fulfillment of the
requirements for the Degree of
Doctor of Philosophy

Fiber and Polymer Science

Raleigh, North Carolina

2012

APPROVED BY:

_____	_____	_____
Dr. Richard Spontak Committee member	Dr. Saad A. Khan Committee member	Dr. Bong Yeol Yeom Committee member

_____	_____
Dr. Behnam Pourdeyhimi Committee Chair	Dr. Eunkyoung Shim Committee Co-Chair

BIOGRAPHY

Ali Kilic was born on March 14, 1983 in Ankara, Turkey. He received his Bachelor's degree in Textile Engineering from Istanbul Technical University, Istanbul, Turkey. After graduation, he started pursuing his master degree in textile engineering program at ITU in the fall semester of 2006. In January 2009, he was admitted into the PhD program in Fiber and Polymer Science and held a research assistantship with the Nonwovens Institute in the College of Textiles at NCSU. Upon finishing his graduate studies in NC State, he will be returning to his home country to pursue his career as an academician.

ACKNOWLEDGMENTS

This dissertation work would have never been accomplished without the valuable guidance and support of Dr. Behnam Pourdeyhimi, Dr. Eunkyoung Shim, and Dr. Bong Yeol Yeom. This is almost 4 year with them which was extremely enlightening to draw my future. I have learned tremendously from them to improve my writing, presentation, and technical skills as well as methodologies for solving problems. I am extremely thankful to Dr. Richard Spontak and Dr Saad Khan for valuable discussions and agreeing to be on my graduate committee.

I wish to acknowledge the financial support of this research by the Nonwoven Research Cooperative Center (NCRC). Special thanks to Dr. Benoît Mazé, Dr. Nagendra Anantharamaiah, Dr. Yogeshwar Velu (DuPont), Y. van der Zijpp (Colbond), Steve Cox and Dave Healey (H&V) for their help and fruitful discussions during the research. I would also like to thank Amy Minton, Birgit Andersen, Roberto Garcia, Chuck Mooney for their patience during analyzing my samples. I would also like to thank my friends especially "NCRC student members" who have made my graduate school years bearable even sometimes enjoyable. I would like to extend my appreciation to our Turkish community in the Triangle area.

Finally, I would like to thank my dearest family, Professors Demir, Ulcay and Oznergiz for their support they provided me during my lonely years abroad.

TABLE OF CONTENTS

LIST OF TABLES

LIST OF FIGURES

CHAPTER 1

1 Introduction

Aerosol filter media is a highly engineered nonwoven product designed to remove various suspended particles such as microorganisms, fine dusts, and pollens from the air stream. Production of air with the lowest concentration of suspended particles such as microorganisms, fine dusts, and pollens in indoor is still a challenging issue in both academic and industrial world. Increase in the number of pandemic cases, environmental pollution and strict clean room and operation room requirements forces high growth rates in filtration industry.

There are two main approaches to improve filter efficiency. One approach is the use of finer fibers, thus increasing the efficiencies of capture mechanisms such as diffusion and interception. However, this will also result in high pressure drop, which is unfavorable for filtration. A second approach -which is in the scope of this dissertation-, is imparting electrostatic charge on filtration medium without changing web structure. Those are called as "electret filters" or "electrostatic filters" [1]. A conventional filter such as a glass fiber filter media may have high collection efficiency (>99%). However, the resistance would be high up to 30-40 mmH_2O [2]. Significant portion of filtration efficiency of electret filter media can be attributed to electrostatic capture mechanism, whereas contribution of mechanical capture mechanism can be as low as 30-50% of total filtration efficiency. These media can have very

low resistance (3-6 mmH_2O) compared to glass filter media. Electrostatic capture contribution on the efficiency of some commercial filter media is shown in Figure 1.1[4]. In all three filters, discharging causes large drops in filtration efficiency since it removes contribution of electrostatic capture mechanism. It indicates electrostatic charge is essential part of such high efficiency filter products.

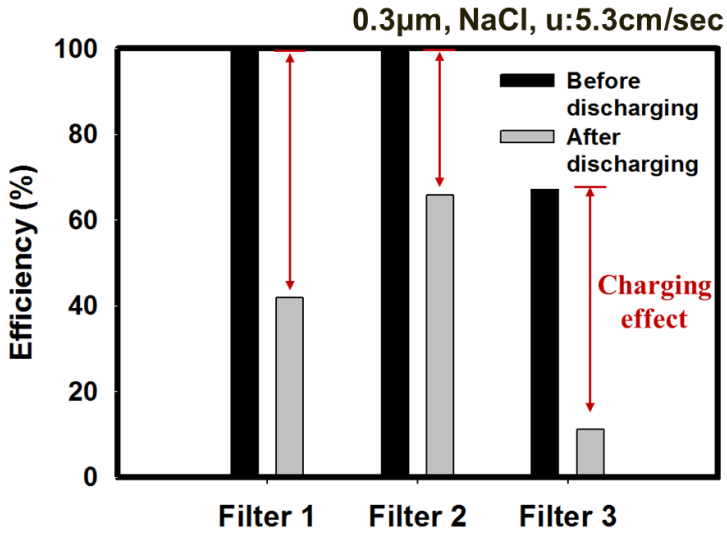

Figure 1.1 Effect of electrostatic charging on total filtration efficiency [4]

Reliability of those filters will highly depend on stability of charges since only mechanical capture mechanisms act upon loss of charge property. This will be catastrophic since generally the web structure of electret filter is designed more open. Such a failure in

filtration facilities of a medium size hospital may cause the death of tens in a couple of hours, which is irrecoverable. In semiconductor labs a minimal change in aerosol concentration will stop production for days, which means loss of millions of dollars. Although it may not be as important as previous scenarios, this will give irrecoverable damage to the fame of the hospitals and companies. Another important use of the electrets filters is facemasks. Again without electrostatics lower efficiency of facemasks against microorganisms at particular diameter range will allow penetration through respiratory system[3]. This will be fatal, since those portable devices are still a largely accepted solution for protecting individuals during pandemics. Moreover without electrostatic charging, facemask will be composed of densely packed fine fibers, which will give rise to the pressure drop. That will come up with enormous difficulty in breathing comfort. Employers will be in need of replacing such facemask too often, which will increase the operational expenses. Due to all those scenarios significant investments have been done on electret filters by many companies. It is still a question under debate that under harsh filtration conditions, ie with high humidity, high temperature, or high ionic concentration, decay of imparted charges accelerates abruptly. An unstable electret filter is nothing more than a conventional filter that has efficiency below 50-60% as shown in Figure 1.1. Therefore, use of additives and improving electrostatic charge density and its stability are critical for high efficiency electret filter media.

One way to modify charging properties of polymeric filter media is incorporation of additives. Even though particularly in industry several polymer additives were used so far,

there is not an extensive study that explains effect of those additives on efficiency and stability of electret filters. This study addresses the effect of various polymer additives on electret and electrostatic filtration properties of high efficiency nonwoven electret filters. Undoubtedly incorporation of such additives will result in changes in chemical structure and morphology of fibers which are also planned to be investigated with various techniques. At the end of the study modified nonwoven webs will be analyzed by means of not only bulk chemistry and morphology, but also surface chemistry and morphology. Relation between those structural data and both their electret and electrostatic filtration properties will be compared. Specific objectives also include interaction of additives with host polymer and effect of this interaction on electrostatic properties. The project is not limited to selection of additives, since the electrostatic filtration efficiency strongly depends on charging method. Due to chemistry and electronic structure, additives may require specific charging conditions. It will be one of the targets of the study, to investigate influences of charging procedure via negative corona charger and a probable triboelectrification method separately for selected additives.

The dissertation is presented here as a collection of papers and review articles. As a result the redundancy of introductory information would be noticed because the papers are intended to be sufficiently independent. A short summary of each is provided below to help readers navigate through this dissertation.

Chapter 2 includes review of literature. It gives detailed account of the theory electrostatic charging, polymer additives and electret filters. Other than conventional use of such additives, their possible interaction with host polymer is also briefly explained.

Chapter 3 explains the electrostatic properties of barium titanate and maleic anhydride containing polypropylene (PP) filaments.

In Chapter 4 it was shown that there is no compatibility issue with PP and $BaTiO_3$. So fibers produced free from compatibilizer. Also regarding with ferroelectric properties of $BaTiO_3$ charging procedure was modified.

Chapter 5 deals with incorporation of $BaTiO_3$ as an electret additive into PP meltblown webs, which was resulted with high efficiency stable filters.

Chapter 6 includes effect of nucleating agents to enhance charging properties of PP filaments.

Chapter 7 is about the effect of stabilizers on electrostatic properties.

In Chapter 8 effects of surface crystallinity on charging properties of PP fibers were discussed.

Chapter 9 explains electrostatic filtration properties of nucleating agent containing webs. Dielectric properties of nucleating agent containing webs were found to be acting on their charging and filtration characteristics.

Chapter 10 is about the effects of stabilizers on electrostatic filtration properties. It was shown that exclusion of stabilizers resulted with unstable filtration characteristics.

In Chapter 11 effects of surface crystallinity on electrostatic filtration properties of PP webs were discussed.

Conclusions and suggested future works were covered in Chapters 12 and 13.

Appendix 1 is related with measurement of electrostatic properties of fibrous samples. Current methods were reviewed and the proposed isothermal surface potential decay technique was discussed.

1.1 References

1. Klaase, P. T. . & Van Turnhout, J. *Method for manufacturing an electret filter medium*. (Google Patents: 1986).
2. Barrett, L. W. & Rousseau, A. D. Aerosol loading performance of electret filter media. *American Industrial Hygiene Association* 59, 532–539 (1998).
3. Kowalski, W. J., Bahnfleth, W. P. & Whittam, T. S. Filtration of airborne microorganisms: modeling and prediction. *ASHRAE TRANS* 105, 4–17 (1999).
4. Yeom, B. Y. 08-114 NCRC Project Proposal. (2008).

CHAPTER 2

2 Literature Review

2.1 Electrets

Dielectrics may be classified in two groups; either active or passive. Passive dielectrics are used for insulation purposes. Active dielectrics have an electrical property that may be manipulated and used for various applications. Piezoelectricity, pyroelectricity are examples for such applications. Electrets are also classified under the group of active dielectrics, since the electric field resulting from its quasipermanent charge property is used somehow[1]. Although it sounds all concepts are very similar to dielectrics used in capacitors; dielectrics in capacitors possess an induced polarization that is only transient, dependent on the potential applied on the dielectric, while electrets may exhibit quasi-permanent charge storage or dipole polarization in addition [2].

The history of electrets goes back to 18th century. The first information about charged/polarized state of matter can be seen in the works of Gray and later Faraday. The term "electret" was introduced by Heaviside, combining "electric" and "magnet". In early 1900s more significant results were discovered by Eguchi, who found thermoelectret from solidified mixture of carnuaba wax, resin and beeswax in the presence of a high DC electric field[3]. By exposing a dielectric under light radiation and electric field simultaneously, Nadzakov reported photoelectret effect in 1937[4]. In 1930s very first applications of electret filters, so called Hansen filters were introduced for military use[5]. In 1966 Sessler came up

with another commercial application on film electrets [4]. This was the electret condenser microphone which is used in many areas of life such as tape recorders, stereos, telephones, cordless and cellular phones and hearing aids.

Microphones are transducers that convert sound as mechanical energy into electric signals. Unlike other capacitor microphones electret microphones do not require polarizing voltage in use. A thin Mylar film which was exposed to high DC field under elevated temperatures was used for very first applications by Sessler and West. A strong polarization of the foil results in a surface potential of 200 V[6]. Detected sound signals will vibrate the film and which will produce an electrical image of the sound as a potential value which is proportional to the sound signal.

Another commercial application is radiation sensors, which is based on measuring change in potential of electret periodically in suspected areas that has a high radioactive matter concentration. The potential decay rate will be high in emergency conditions [7].

In general to exhibit electret characteristics polymer should have sufficiently deep trapping levels for electrons and deep potential wells for ions and dipole molecules. Besides conductivity should not exceed 10^{-8}-10^{-10} Ωcm^{-17} Basic electret characteristics will be discussed in detail in section 2.3.

Either nonpolar or polar polymers would exhibit electret characteristics. Nonpolar electrets can be formed via charge injection from accelerated energetic carriers or a

contact/friction based (triboelectrification) methods, whereas dipolar species within polar dielectrics should be polarized at high temperatures and frozen instantly[7]. Methods for charging electrets are summarized in section 2.4.

2.2 Electret Filters

The efficiency of conventional filter media is based on four mechanisms, which are Brownian diffusion, interception, inertial impact and gravitational settling. If combined action of airflow and Brownian motion brings a particle into contact with a fiber, this is diffusional deposition. Smaller particles will particle will rapidly came into thermal energy equilibrum with the gas and this sharing will result in Brownian motion. The coefficient of diffusion of particles is related to their mobility, μ by Einstein equation:

$$D = \mu . k_B . T \qquad \text{Equation 1.1}$$

where

$$\mu(B) = Cn / 3\pi\eta d_p \qquad \text{Equation 1.2}$$

The particles are so small that they slip between gas molecules. That is why Cunningham correction factor is incorporated into equation. Correction factor can be calculated from;

$$Cn = 1 + 2.52\lambda / d$$ Equation 1.3

where λ is the mean free path .

Diffusional capture depends on relative magnitude of convective versus diffusional motion of air. This is explained with well know Peclet number [Equation 2.4]. Diffusional capture efficiency will increase as Pe increases.

$$Pe = \frac{2uR}{D}$$ Equation 1.4

where u is velocity and R is the particle radius.

Direct interception is for particles that are following a streamline and being captured by coming into contact with fiber. Particles behave in a passive way with respect to the airflow. Since larger particles may change direction, particles should be smaller than fiber diameter. Capture is velocity independent during direct interception. If capture is affected by deviation of a particle from a streamline because of its own inertia, this is inertial impaction. Inertia causes perturbation in particle's trajectory Particle ignores the flow field and experiences Stokes drag with the formula:

$$m\frac{du}{dt} = -3\pi\eta d_p u$$ Equation 1.5

Gravitational settling is related with large particles that doesnot follow streamline, due to weight. However efficiency coming from gravitational settling drops if velocity

increases, since particle will tend to follow streamlines. It is easy to measure due to dependency to the direction of airflow.[58]. Those mechanisms were illustrated in Figure 1.2.

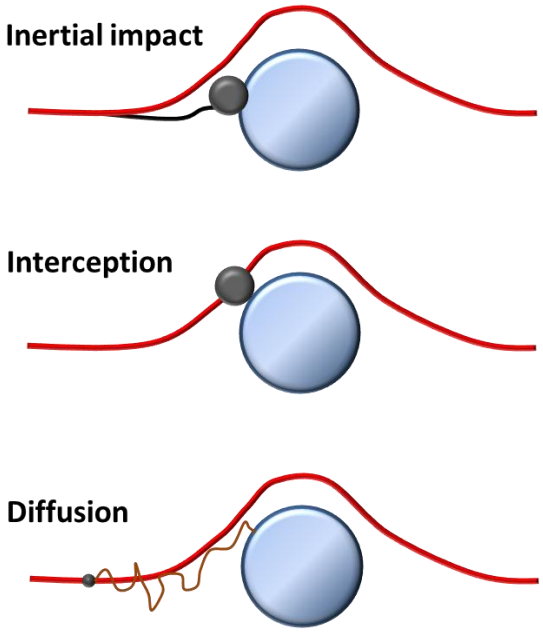

Figure 1.2 Mechanical capture mechanisms [adapted from[5]]

Besides mechanical capture mechanisms, electrostatic capture will be effective in electret filters. Charged aerosol particles will be pulled towards the fibers by Coulombic force. If the particles are neutral, filtration mechanism will involve induced capture. Neutral particles will polarized under the electric field produced by charged/polarized webs and will be captured under this electric field[9]. Induced capture and Coulombic attraction mechanisms

were illustrated in Figure 1.3 and summarized in Table 2.1.

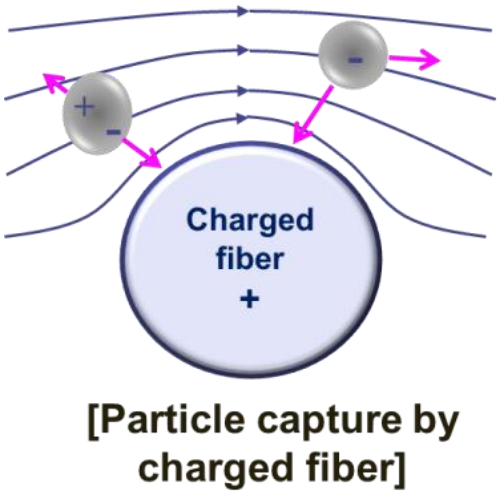

Figure 1.3 Aerosol capture mechanisms [adapted from [10]]

Table 1.1 Capture mechanisms in submicron range

Web	**Particle (submicron range)**	**Mechanisms**
Discharged	Neutral	Diffusion, interception (mostly)
Charged	Neutral	Diffusion, interception, induced capture
Charged	Charged	Diffusion, interception, induced and Coulombic capture

The contribution of mechanical interactions will lessen according to strength of electric field that is created within web. Presence of electrostatic forces will allow us to design a web with a more open structure which will result in drop in resistance against flow. Resistance of a filter media, which is generally called as pressure drop, will determine process expenses. It is also a direct indication for breath comfort in portable filter media, ie facemasks. The performance of air filter is mostly described according to quality factor which is the ratio of negative natural log of penetration to pressure drop. ($QF=-\ln P/\Delta p$). Thus both factors will be involved. In Figure 1.4 the quality factor values obtained from tests on mechanical and electrostatic filters are compared.

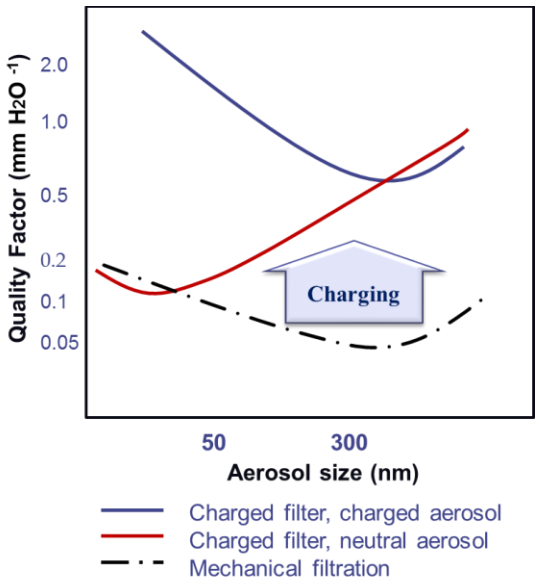

Figure 1.4 Comparison between mechanical and electrostatic filtration [9]

The charged electret fibers not only attract charged particles, but also uncharged ones. If particles are charged inherently, they are pulled towards the fibers by a strong Coulombic force, giving the highest quality factor. When they are not charged, they are polarized by the strong field around the electret fiber. So they are converted into macroscopic dipoles and attracted by the fibers. The efficiency on neutral particles is not as high as charged particles due to lower Coulombic forces[11].

On the other hand as shown in Figure 1.5 in a particle diameter range, mechanical filters are insufficient for particle capturing by means of either Brownian diffusion or interception. The lower most level in this well is defined as "most penetrating particle size". Unfortunately diameter of many microorganisms and significant amount of aerosol particles take place in this region[8,12]. To improve the efficiency at this region electrostatic capture mechanism seems to be must.

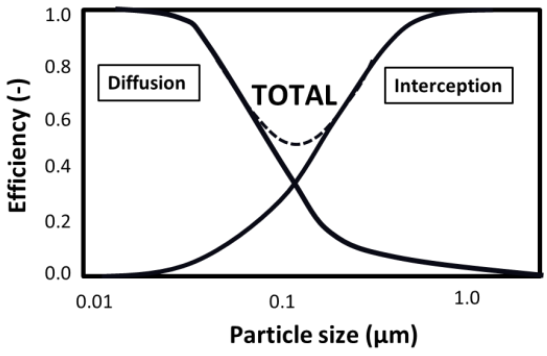

Figure 1.5 Efficiency for mechanical capture mechanisms[12]

Due to scope of this study we will focus on the changes on electrostatic filtration efficiency upon additive incorporation. Electrostatic filtration efficiency can be measured by subtracting the mechanical filtration efficiency from total filtration efficiency.

$$\zeta_{Total} = \zeta_{Electrostatic} + \zeta_{Mechanical} \qquad \text{Equation 1.6}$$

Mechanical filtration efficiency of the webs can be tested by subjecting neutral aerosols on discharged webs using TSI instrument. Similarly after charging the webs total filtration efficiency can be measured. Here what we thought is if we can have fixed mechanical filtration efficiency for all webs, the effect of electrostatic filtration can be obtained and compared easily. As a result electrostatic charging characteristic upon any modification can be obtained thereof.

As mentioned mechanical filtration at this particle range will occur due to Brownian diffusion and interception. There are various models that explain those mechanisms. Referring to model developed by Liu and Rubow, the capture efficiencies due to diffusion and interception will be as follows [13]:

$$\zeta_d = 1.6\left(\frac{1-a}{F_K}\right)^{1/3}.Pe^{-2/3} \qquad \text{Equation 1.7}$$

$$\zeta_r = \frac{1}{\varepsilon}\left(\frac{1-a}{F_K}\right)\left(\frac{N_r^2}{1+N_r}\right) \qquad \text{Equation 1.8}$$

where ζ stands for filtration efficiency, a for packing density, F_K for Kuwabara hydrodynamic factor, Pe for Peclet number, ε for web correction factor, N_r for diameter ratio [13].

If the samples are completely free from charges only mechanical capture mechanism will be effective. This situation can be provided soaking samples, either charged/uncharged, into isopropyl alcohol which is described in EN 779 test procedure. However one needs to be careful on this treatment since instead of discharging, sample can be charged significantly upon contact with this kind of polar liquids[14].

As a result it can be understood both of these capture mechanisms are highly dependent on fiber diameter, web packing density, and web uniformity. Those parameters will also have influence on electrostatic filtration., since both induced and Coulombic capture depends on them. Brown introduced induced and Coulombic force factors [15] depending on the value of Kuwabara correction factor. Single fiber efficiencies for both mechanisms could be calculated using these two values.

$$h_k = a - 0.5\ln a - 0.25a^2 - 0.75 \qquad \text{Equation 1.9}$$

and

$$\zeta_{in} = 1.48K_{in}^{0.93}; \qquad 10^{-4} < K_{in} < 10^{-2} \qquad \text{Equation 1.10}$$

$$\zeta_{in} = 0.51 h_k^{-0.35} K_{in}^{0.73} \; ; \; 10^{-2} < K_{in} < 10^{0}$$ Equation 1.11

$$\zeta_{in} = 0.54 h_k^{-0.60} K_{in}^{0.40} \; ; \; 10^{0} < K_{in} < 10^{2}$$ Equation 1.12

where

$$K_{in} = \frac{(\varepsilon_p - 1) C_c \pi^2 Q_f^2 d_p^2}{6(\varepsilon_p + 2)\varepsilon_0 (1+\varepsilon_f)^2 \mu d_f u}$$ Equation 1.13

and

$$\zeta_C = 0.78 K_C \; ; \; 10^{-3} < K_C < 10^{1}$$ Equation 1.14

$$\zeta_C = 0.59 h_k^{-0.17} K_C^{0.83} \; ; \; 10^{-1} < K_C < 10$$ Equation 1.15

where

$$K_C = \frac{C_c n_p e Q_f}{6\varepsilon_0 (1+\varepsilon_f) \mu d_p u}$$ Equation 1.16

K_{in}: Induced force parameter, K_C: Coulombic force parameter, h_K: Kuwabara hydrodynamic factor, a:solidity, C_c: Cunningham correction factor, Q_f: Fiber charge density, ε_p: dielectric constant of the particle, ε_0: space permittivity, ε_f: dielectric constant of the fiber, d_p: particle diameter, μ: fluid viscosity, u: filtration velocity, N_p: charge of the particle, e: unit elementary charge.

According to our approach if samples have similar fiber diameters and solidities, it may be said that similar mechanical capture efficiencies are effective. The difference between measured mechanical capture (using discharged webs and particles) and total efficiency (using charged web) will be resultant electrostatic capture efficiency. Obtained electrostatic capture efficiency will indicate if the selected additive is useful as an electret additive.

Another option to understand the change in electrostatic filtration would be to check the change in efficiency by changing surface velocity, since only diffusion and electrostatic capture mechanisms are dependent on efficiency; however this will also cover diffusion and would not be indicative. Interception mechanism depends on particle and fiber diameter and solidity of web, but not surface velocity.

2.3 Basic Electret Characteristics

Electrical properties of the polymers are traditionally described with two factors: Conductivity and Permittivity [16]. Being a long term dielectric, for electrets more than these properties, the material is characterized with overall charge density and stability. Again such an explanation will be too broad, since the physical processes that occur during charging and discharging have dependency at molecular[17,18], conformational[17,1920] and morphological level[21,22]. In this chapter physics behind resultant charge density and stability will be

explained in details. The observations in the experimental parts will be tried to be explained under the light of this knowledge.

2.3.1 Charging and Polarization Phenomena

Charge density may be a combination of inherent and injected charges, and also polarization, whereas stability will depend on charge transport and combination processes. For a nonpolar polymer, such as PP, electrostatic property is generally based on inherent and injected charges. However impurities and inevitably used additives such as antioxidants and stabilizers can cause polarization.

To elucidate the electrical behaviors of insulating materials, concept derived from semiconductor physics is used. However structure of insulating materials is too complicated when compared to semiconductors. On the other hand it is very weak intermolecular interactions in polymers that cause contentions on the application of band theory. However intramolecular forces are large that band scheme might hold for chain [17,23]. Despite those of the challenges, band gap theory still enlightens many specific findings within insulators.

As mentioned earlier polypropylene is the most widely used polymer in electret filters. Pure PP is nonpolar and has a very large band gap above 8eV, which leads superior insulating properties [24] [Figure 1.6]. However various impurities such as catalyst residues will be already incorporated. Being one of the most sensitive polymer against oxidation due

to tertiary hydrogen, contains antioxidants and oxidation products at a level [25,26]. Such molecular level defects act as deep traps within PP. However should be engineered carefully to reach long term charge stability. For instance carbonyl containing groups are found to be acting as deepest traps in a recent study[27]. Deep traps are important since the formation of space charges is related with their concentration. However those of the groups coming from oxidation are known to be catalyzing the decay process due to resulting increase in hydrophilicity [28]. On the other hand various studies concerned on space charge formation since they are thought to be reasons behind the electrical breakdown of the dielectric[29].

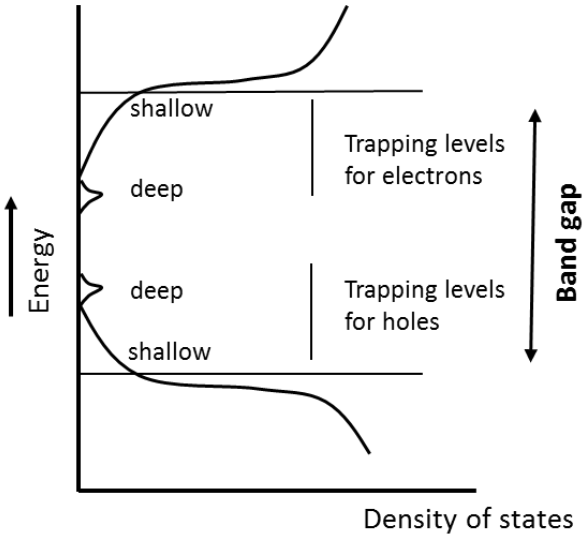

Figure 1.6 Schematic representation of state density within a dielectric [adapted from[17]]

Besides chemical defects imparting deep traps, there are physical defects originating from conformational and morphological structure. Looking at most common crystal structure in PP, α-crystal, it is composed of monoclinic unit cells consisting of four 3_1 helical chains which are composed of three propylene $[CH_2CH(CH_3)]$– units forming the ‘‘pitch’’ of the helix[27]. This helical structure is originated from conformational interactions between neighboring methyl groups[30]. Conformational properties are important on electret stability since some of the arrangements other than all-*trans* can act as shallow traps. Charging properties of PP having different conformational properties and stereo structures were investigated. It was shown that mmrm and rrrm sequences can provide more stable traps, whereas mmrr and short heterotactic sequencies fail. It was asserted that structural breaks in tacticity may result in increase in molecular mobility of polymer[20]. Those of the localized states resulting from conformational disorders may have a density of $10^{22}cm^{-3}$[17].

Lastly the presence of impurities and conformational (physical) defects will lead to drop in crystallization. Crystallization is important for electrostatic properties of polymers. For instance crystalline PE has a positive, amorphous PE has a negative electron affinity. So amorphous phase is expected to behave like trapping sites at a depth of 1eV [17]. Effects on dielectric properties attributable to those material discontinuities are called Maxwell-Wagner effects. These could be contact points with electrodes or boundary layer formed by discharged ions. Other heterogeneities could be cracks, voids, different conductivity regimes. Maxwell (1892) showed that charges will accumulate in time at the interfaces between the

layers whenever $\varepsilon_1\sigma_1 \neq \varepsilon_2\sigma_2$. Wagner brought mathematical explanation for sparsely distributed impurities of small spheres inside dielectric matrix. Sillars demonstrated the importance of the shape of conductive inclusions. Amorphous sections will have higher free volume which result in different dielectric constant. Also it was shown that conductivity of amorphous structures is lower than that of crystal parts[31]. Effect of crystallinity will be explained in chapter 2.5.2. Defective structures were summarized in Table 1.2.

Table 1.2 Defective structures, their origins and effects [adapted from[17,32]]

Size	**Origin**	**Effect**
Molecular	Oxidation products, antioxidant and catalyst residues, by-products, electret additives	Deep traps, dipoles
Conformational	Chain orientation and interaction, molecular weight distribution, free volume	Shallow traps
Morphological	Amorphous-crystalline boundaries	Interfacial polarization

Charge generation is also a complicated phenomenon, since various processes can take place. A significant ratio of real charges was contributed to inherent charges coming from early history of electret[33]. During a subsequent charging process such as corona, not only injection takes role, but also injection through electrode will occur. Charge injection at electrode is through field assisted thermoionic emission (also called Schottky emission). A

current depending on exponential function of square root of field is generated. Interestingly barrier height tested experimentally is found to be lower than theoretical values, which makes this kind of injection more effective[17]. Ionic conduction will occur at a level, however carrier ions can move through the amorphous region of the polymer only. Therefore an increase in crystallinity may give rise to reduction of the mean free path of the ionic carriers[22]. Those of the ions are thought to be originating from antioxidants, oxidation products and water[34].Ionic conduction dominates in polymers such as PVC and nylon.[23]

In summary typical physical trap energy ranges below 1.0eV, whereas chemical defects are deeper but lower in concentration[17,18] Particularly chemical defects containing carbonyl or conjugated double bonds produce the deepest traps, whereas non-conjugated double bonds and hydroxyl groups are found to be shallower[19] Shallow traps are located within specific conformational regions and amorphous-crystalline boundaries, while charges with higher release energy are trapped in molecular defects within crystal structures[35–37]

Various experimental analyze techniques were developed, which are based on stimulating those of the charges/polarized species somehow and measuring discharge current. Kravtsov *et al.* obtained three peaks form the thermally stimulated discharge (TSD) analysis of PP filaments (Figure 1.7). TSD is a quantitative method, works on the principle of discharging the sample by increasing the temperature at a fixed rate and measuring discharge current simultaneously. The first peak obtained at low-temperature (T_{max} 30–50 ° C) shows the Maxwell–Wagner polarization in which electric charge is localized at interfacial trapping

sites due to the difference in electrical conductivity of the microstructures. The medium-temperature peak between 100 and 130 °C is attributed by the release of both inherent and injected charge carriers. And, at high temperature fiber treatment, the release of both inherent and injected charges is obtained in the appearance of highest-temperature TSC peaks, which is very close to the melting temperature. This peak is thought to be a combination of two components. The first component (at T_{max} 165 °C) is due to decay of inherent charges and is lower in magnitude than the second one (at T_{max} 170 °C), which is thought to be related with injected charge relaxation[33].

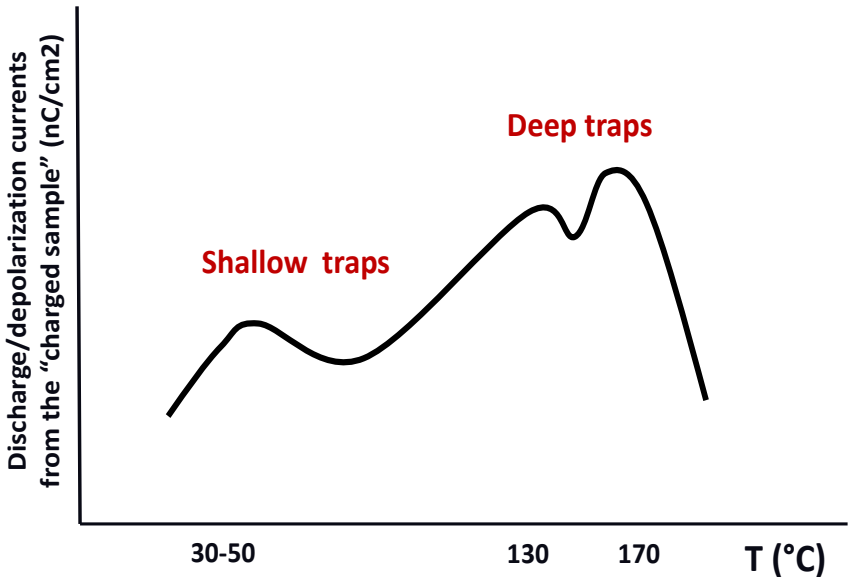

Figure 1.7 TSD curve for pure PP obtained by Kravtsov et al[33]

Same group claims[38,39] six possible charge trapping mechanism in polypropylene electrets:

- Trapping by structural defects of polymer

- Trapping at interfaces of crystalline/amorphous structures

- Self-trapped electrons in the polymer bulk[40]

- Polar groups and charged molecular fragments by thermal degradation of polymer

- Macromolecules oxidation and polar group formation by ozone, atomic oxygen, nitrogen oxides

- Dipole polarization from the heterolytic breakage of chemical bonds in polymer.

Besides charging polarization is an effective method to produce electrets. There are four polarization mechanisms which are electronic (P_e), ionic (P_a), dipole (P_d) and interfacial polarization (P_d)[41,42].

i. Electronic polarization is due to motion of valance electron cloud of the ions in the materials with respect to positive nucleus. This mechanism has a very high frequency (10^{15} Hz, UV range). The index of refraction of the material depends on the electronic polarization.

ii. At IR range (10^{12} - 10^{13} Hz) atomic or ionic polarization occurs. The positive and negative ions in the material displace with respect to each other. For instance when an electric field is applied to Si-O bond, ions will repel each other.

iii. In the subinfrared range of frequencies dipole (orientational) polarization occurs largely as a result of motion of charged ionic or molecular dipoles, producing a net dipolar orientation in the direction of applied electric field. This type of polarization is observed in two cases:

- An asymmetrical dipole moment will produce oscillations at very high frequencies, such as 10^{11} Hz. Si-O-Si bond in an equilibrium position under a sinusoidal ac field, or OH group bonded to Si will provide that kind of dipole polarization. In linear dielectrics dipole polarization is largely due to motion of charged ions between the interstitial positions.

- Second case is generally observed in nonlinear dielectrics, which involves the rotation of dipoles between two equivalent equilibrium positions. For instance Ti atom in a $BaTiO_3$ crystal will cause that kind of polarization. This will also provide ferroelectric manner of dielectric and very high dielectric constants, 10^4 or more.

iv. Space charge (interfacial) polarization occurs when mobile charge carriers are injected, but they are impeded by a physical barrier that inhibits charge migration. The charges will be collected at the barrier and produce localized polarization of the material. In some cases that type of polarization can have the same frequency with dipole polarization[41,42].

As explained in Figure 2.7, polarization of a dielectric depends on frequency of the applied field. [41,43]. All types of polarization mechanisms will be effective when DC electric field is used, which is generally preferred in electret studies.

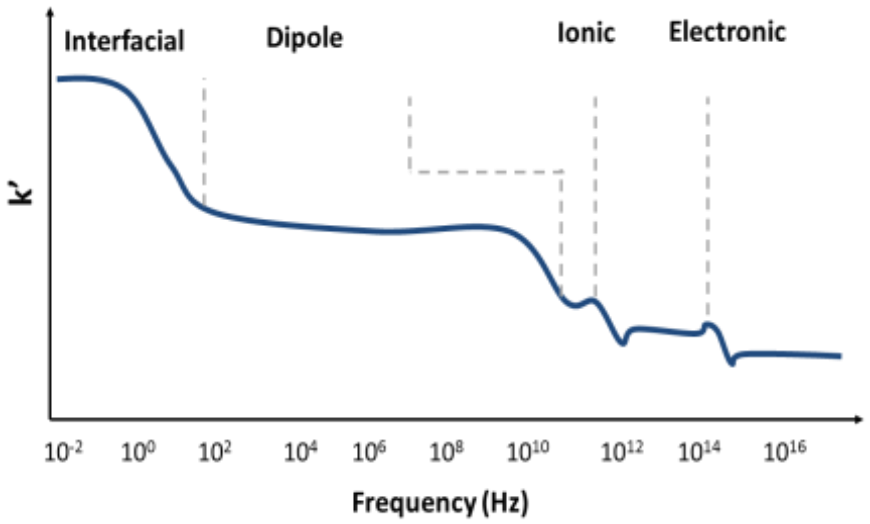

Figure 1.8 Frequency dependence of polarization mechanisms in dielectrics [41,43]

2.3.2 Charge Motions within Electrets

Based on electrical resistivity, materials can be divided into three groups: Conductor (conductivities 10^{-3} - 10^{6} S/cm), semiconductor (10^{-7} - 10^{-3} S/cm), or insulator (10^{-18} - 10^{-5} S/cm)[47]. For a perfect insulator it might not be an expected property to allow transport or to hold charges at a degree. It is again the inevitable impurities, conformational and

configurational disorders and intentionally incorporated additives that causes not only charge trapping, but also charge motions[35,48–50]. For instance PE has a band gap width of 8.8eV, which correspond to an intrinsic conductivity of 10^{-45}S/m[17], however impurities and defective structures will increase this value upto 10^{-16}S/m[51].

For the case of shallow traps the residence time of the carriers ranges from 10^{-13}s for a level at 0.1eV to about 500s for a level at 1eV. Charges can move trap to trap either each time transition to extended state which is called hoping or without undergoing to extended state, which is called tunneling (phonon-assisted tunneling) mechanism. The energy separating extended states from localized states is called mobility edge. The carrier mobility will be zero below mobility edge, whereas above this limit mobility will be infinite. Deep traps are produced by chemical disorders. Those are a lower concentration when compared to shallow traps. Space charge formation is thought to be controlled by deep traps[17]. So electret properties would be enhanced via processing deep traps, since compared to shallow traps they contribute less to conduction.

It is possible to move charge between densely spaced localized states by thermal excitation. Such conduction requires the electron to move discrete jumps across energy barrier and through space from one site to the next. As shown in Figure 1.9 electrons may hop, tunnel through barrier. Hopping and tunneling progress depends on three factors which are shape of barrier, separation of sites, and availability of thermal energy. Electrons must have sufficient energy to pass through the barrier to hop. On the other hand site separation

must be small for tunneling. Hopping conduction is trapped electron movement can be between states of same energy level. Tunneling mostly occurs under high electric field.[31]

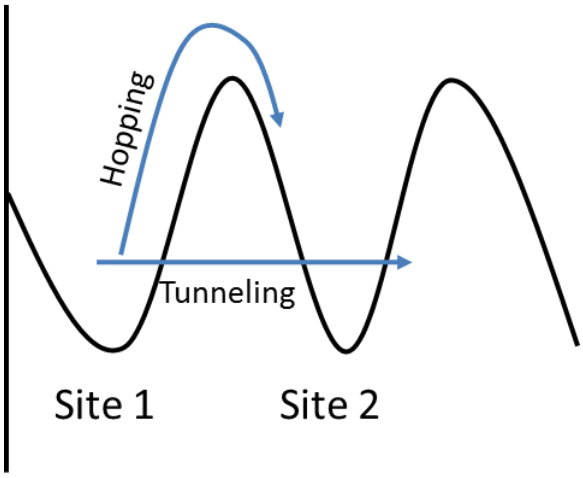

Figure 1.9 Hopping and tunneling mechanisms [adapted from [31]]

Some exceptions were asserted so far. For instance in the presence of an electric field, the thermal barrier for electron transport will not remain same. This is called Poole-Frenkel effect. This seems an important finding for electrets since it deals with deep traps. Secondly according to space-charge limited current model at a sufficient carrier concentration the field and carrier velocity should be rearranged. Thirdly electron moves through polymer bulk with repeating band conduction along a chain or can hop to another chain alternatively. [17,23]

Higher electrostatic resistivity is desirable for polymers used in charged filter media. However, absorption of the moisture from the atmosphere will reduce resistivity of filter media since water is highly conductive compare to most commercial polymers, and the presence of water absorbed by polymer will promote of discharge of electrostatic charge.

This is actually one of the strategies used in antistatic additive design[52]. Therefore, when one select polymer used for charged filter media, not only resistivity of polymer but also its moisture regain should be considered. In this aspect, polypropylene (PP) is a good candidate due to its good electrical resistivity (> 10^{16} Ω cm) and low moisture regain (0% at 65% RH).[53]

Other than natural phenomena acting on charge decay of electret, some other factors will be effective in the discharge of electret filters. Brown conducted loss of electrostatic capture efficiency to the following[9,10]:

- Neutralization due to sharing charges with captured particles
- Chemical disruption of fiber by aerosol
- Screening of fiber's charge by formed layer of screen.

2.4 Methods for Producing Electret Filters

For high filtration efficiency there should be high electric field within webs that will give rise to electrostatic forces on particles. After the invention of Hansen filter in 1930s, various systems were developed to produce more efficient electret filters. Electret filters can be classified according to charging mechanism: Corona discharge, triboelectrification via carding or hydroentanglement and liquid contact. Electrospinning may also be added[54–57], even though it has been investigated in very recent studies. According to charging mechanism web composition will change, ie triboelectrification generally needs more than one component. On the other hand they were also classified as space charge electrets that possess an injected or imbedded charge as in corona treated PP webs or dipolar electrets that are formed by the orientation of dipoles[58].

2.4.1 Corona Discharge

Corona discharge occurs when a sufficiently high potential difference exists between electrodes having asymmetric shapes such as a fine wire or point and a surface. Because of the high electric field near the emitting electrode, the air which is normally an insulator becomes ionized. The ions are driven towards the low electric field electrode. Charging can be either positive or negative. This is the polarity of the voltage on the emitting electrode [59].

Negative and positive air ions are different from each other. In a positive corona the electron avalanche accelerates toward the electrode so that fully formed primary positive ions are repelled into atmosphere. Mostly hydronium ion $H^+(H_2O)_n$ is produced. In a negative corona the electrons are generated at the electrode by the photoelectric action of photons striking its surface. Produced electrons will strike the neutral gas molecules to form primary negative ions which have a structure based on O_2^- . (6 ref) Those can be hydrates such as $O_2^-(H_2O)_n$ in a humidified environment and secondary chemical species such as $CO_4^-(H_2O)n$, $NO^-(H_2O)n$ and $NO_2^-(H_2O)n$. Primary ions are able to grow in size as they collide with neutral molecules and aerosol particles[60].

Rader et al [61] investigated the effect of electronegative gases in corona medium. Such gases like those containing oxygen deenhance the resulting corona. But when low corona current is desired with high electric field, this medium could be useful. Electronegative gases in the medium will drop the ionization efficiency and system will require higher voltage to produce corona. Authors mentioned that the corona in a nonelectronegative medium will be more intense by a factor of at least 10 and uniform. So most of the energy spent for corona will be used for ionization and polarization of these species in the medium. That is why in most of the industrial applications inert gases such as He, Ne, Ar or propane is used

It is well known that charging distance, time, temperature and humidity affect charge density and stability. According to Warburg law the distance between corona electrode and sample will determine the charge uniformity over the sample, which can be expressed as

$$I(x) = I(0)\frac{\cos^5\theta}{2d^2}$$ Equation 1.17

In Figure 1.10 charging current and charge distribution according to Warburg law were illustrated.

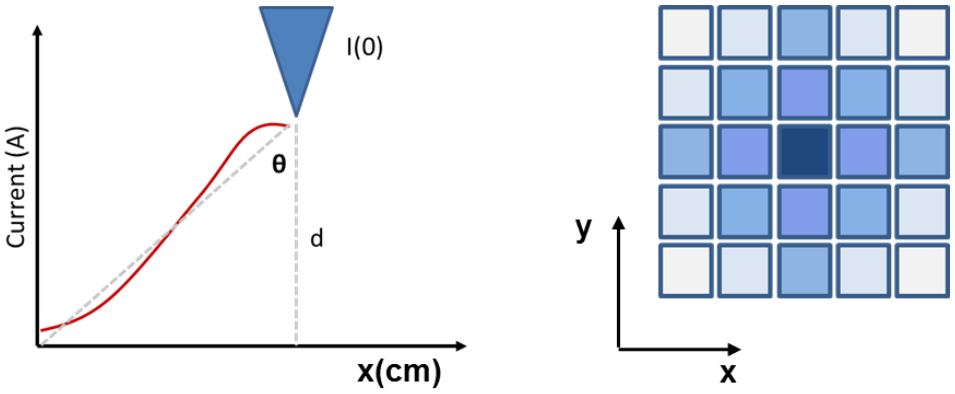

Figure 1.10 Current distribution on corona region and sample

On the other hand the distance between corona needle and ground electrode is divided into two: drift and ionization regions. So called regions have different thermodynamics. In the drift region ions and electrons drift and react with neutrals, but with too low energy to ionize and too low density to react with other ionized particles [62]. During corona a thin layer of electrons and ions of same charge will be formed very close to sample surface. This sheath layer will act on recently formed charge carriers. The penetration depth of excited charge

carriers depends on surface morphology and carrier type and energy, which is generally only a few nanometers. Surface charges can move into the bulk and be retrapped at depths of several microns, which will be dependent on bulk properties[58]. After a certain charging time, the reason behind charge saturation may be explained with the formation of carrier sheath layer and its interaction with polymer [63]. So for the corona discharged webs an optimization will be obligatory.

Corona discharge process is space charge limited, because ions of one polarity will be accumulated in the interelectrode space. Increases in current will need higher electric field to drive onto other electrode. It involves either ions produced or energetic electrons that produces plasma. Ionic identity depends on polarity if discharge. Ionic corona occupies a small fraction of medium, whereas electronic plasma covers a large area. Volumetric filling factor for ionic plasma is lower. Negative corona generally propagates by impact ionization of gas molecules, whereas positive corona depends more on photoionization [64]. Wang et al observed longer stability for positively charged porous PP films, compared to negatively charged films [65]. On the other hand XPS studies revealed that the oxygen content on negative-corona-charged samples is approximately 2.4 times higher than that in positive corona- charged samples[66].

One of the disadvantages of corona discharge is oxidation that occurs due highly energetic charge carriers. This will increase the hydrophilicity of fibers, which results in adsorption of water film, which causes surface conductivitiy. However methods other than

corona doesnot allow polarization in polar electrets or polar additive containing electrets. This will be discussed in detail in part 2.5.3 with effect of oxidation and antioxidants on electret properties.

To improve the efficiency, charging temperature is increased during corona. Even for some cases charging is done in molten state. The electric field is switched off after solidification of molten electret. Those are called thermoelectrets. They mostly have better charge density and stability compared to ones that are prepared at lower temperatures[67].

Van Turnhout found a drawback for direct corona discharge on fibrous webs. At high voltages he observed arcing through open pores; thus suggested covering the charging electrodes with poorly conductive sheet[68]. In another patent he proposed "charged film fibrillation method" which produced even better electret properties[69]. Both corona discharge and triboelectrification would be seen in split fiber webs. The initially corona discharged film is split and stretched to form filaments with a ribbon-like structure. The ribbon-like filaments are then carded into a filter web[58].

Tsai et al investigated the charging and filtration properties of meltblown webs that are polarized at various points during meltblowing. Webs charged in molten state did not hold enough charges, which was conducted to high conductivity at this state. However fibers charged at the die exit exhibited highest potential. Both negative and positive wire ionizer were mounted in the system. Webs having the highest monopolar charges, and opposite

charges on the face and screen showed the largest filtration efficiency, close to ULPA filters[70].

Another interesting improvement is found with simultaneous application of radiation and electric field. Electret is exposed to penetrating high energy radiations such as gama, beta, or x-ray to a dose about 10^6 rads in the presence of an external polarization field. The charging is produced in the dielectric due to the electron-hole pairs created by the ionizing radiation, which drift in the applied electric field towards the electrodes and trapped inside the material[67].

2.4.2 Triboelectrification

High energy electron injection is the main reason for producing functional, unsaturated groups and broken chains. Those of the groups may increase the charge mobility on the surface layer, thus giving rise to decay rate. So instead of injection methods, such as corona discharge or electron beam; triboelectrification is advantageous for charging stable electret filters[71–74].

When two insulating materials are rubbed, the surfaces acquire a net electric charge; one becoming negative and the other positive. To transfer charge, it is sufficient to touch the surfaces together, and then separate them. Most frictionally charged surfaces have both positive and negatively charges areas, but one polarity predominates and determines the net

charge on the surface can be formed. Even contact and separation is enough for charging of materials. Tribolectrification involves both contact of two solids and their motion under friction. Details of contact, such as contact area, sliding, rolling, normal forces will be effective in triboelectrification[75].

When surfaces of different materials are triboelectrically charged, it is possible to determine which one of the pair becomes positively and which becomes negatively charged from triboelectric series. In this series, the materials are ranked according to their tendency to generate a positive or negative charge [76]. The triboelectric series is arranged according to electron accepting or donating characteristic of materials[58]. There are some controversies with the published data, which were thought to be due to asymmetric rubbing or different surface composition[77]. In Figure 1.11 triboelectric series for various materials were summarized[78]. In general nonpolar polymers are on the most negative side, and polar polymers are on the most positive.

Figure 1.11 Triboelectric series of common materials [Adapted from [78]]

To produce largest electric field within webs, triboelelectrification is applied on more than one component webs, ie one from most negative, one from most positive side.

Triboelectrification phenomena is explained with kinetic and equilibrium components. Energy dissipated during rubbing will determine kinetic phenomena. Frictional heating at the area of contact is thought to be related with charge transfer between the materials. The equilibrium component is also known as contact electrification[58]. A deep

understanding on triboelectrification would be achieved if chemical composition of surface is investigated. A good correlation was found between electron pair acceptor/ donor parameters, (α and β) and measured surface charge. Surface polarity was found to be effective on the rate of charging[79].

Previous explanation is based on electron transfer between polymer surfaces. This would be more possible for metal-polymer interaction since the work function required for electron transfer between polymers is too large. Taking nylon/PE surface as an example, triboelectrification will result in positive charging of nylon and negative charging of PE. Electron transfer between these materials will require removal of an electron from nylon (cost of several eV), separation of charge across the interface (cost of below 1 eV, depending on the distance) and addition of electron to polyethylene (again endothermic process) So it was calculated electron transfer would be possible with and endothermic process of 5-10eV, which is significantly larger than the thermal energy (kT=0.026eV at room temperature). This explanation on the impossibility of electron transfer satisfies for polymer in perfect structure. However all polymers have shallow traps, resulting from conformational disorders. Those of the defects have depths below 1eV, which is still larger than thermal energy but at least closer[18].

A second mechanism is based on the exchange of ionic species on the surface. This is accepted and proven in recent articles[75,78]. During separation ions within the interface will be shared according to their electron donor/acceptor parameters. The transfer of mobile ions

at interfaces will be facilitated by adsorbed water. However surfaces will share the aqueous ion (H^+, OH^-) unequally, which is experimentaly shown in triboelectric series.

In this regard water has important properties that are effective on triboelectrification. Its high bulk dielectric constant (ε=78 at 298 K) will reduce the strength of all electrostatic interactions by that factor. Secondly mobile ions (H+, OH-, and other electrolyte ions) within aqueous solutions will screen electrostatic charges on any surface. This is particularly important since some of the additives will act on hydrophilicity, which is undesirable for electrets. A thin film of water is deposited on nearly all surfaces from the atmospheric air. It was reported that even hydrophobic surfaces such as PTFE adsorb water from the air on PTFE (around 2 monolayers of water at 80% RH)[80] However water on those surface will form islands instead forming layers that cause conducitivity.

One other proof for ion exchange during triboelectrification is the observations of Diaz et al. Very less electrification was observed at 0%RH, maximum around 30%RH, and a decrease in contact electrification above 40%RH [81]. The decrease in contact electrification at high humidity was condected to increased surface conductivity, whereas decrease in contact electrification at 0%RH was concluded as necessity of water for the transfer of ions during contact electrification[75].

For triboelectrification of nonionic polymers, mechanism proposed by Diaz was thought to be explanatory. Again the thin water film on surface is effective. Upon adsorption

of water there are two layers created with different electrostatic properties. These are an immobile layer (the Stern layer) close to the surface of the solid and an ion atmosphere with remaining ions which is called Gouy–Chapman layer—that extends into the electrolyte solution. Hydroxide ions accumulate in immobile Stern layer, whereas hydronium remains solvated. Contact between the two surfaces results in rapid equilibration of hydroxide and hydronium ions. The polymer with a greater affinity for hydroxide accumulates a greater concentration of hydroxide in the Stern layer near its surface, so it will be charged negatively (Figure 1.12). This explains the position of PP and PE in triboelectric series. Due to that reason it was shown that basic environment works better for contact electrification of PP[75].

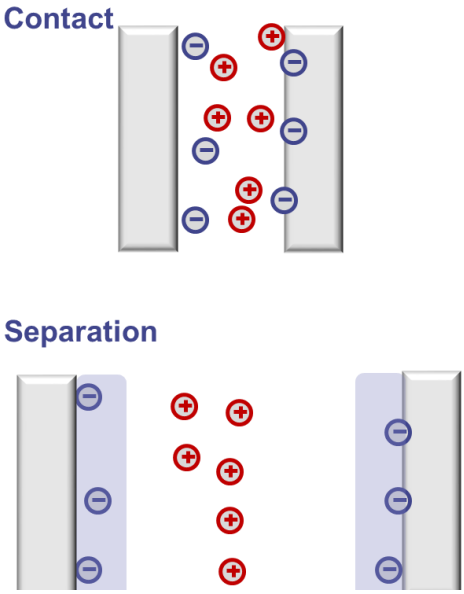

Figure 1.12 Hydroxide adsorption model for nonionic polymers [adapted from [75]]

These are important concepts to understand the triboelectrification. Incorporation of additives would probably change the surface composition and properties of PP, and therefore hydroxide affinity. There are various studies concentrated on triboelectrified webs. Resin-wool filters are first examples of triboelectrified filter media. Upon carding resin particles will be negatively charged, whereas relatively conductive wool will be positively. The low conductivity of the resin will stabilise the charge on the filter and wool will develop image charges to reduce the electrostatic energy of the system to a minimum[10].

Brown et al studied on PP filter media mixed with various fibers including nylon, modacrylic, cellulose diacetate, stainless steel. Significant improvement was obtained in filtration efficiency particularly with modacrylic and steel fibers[77].

Various patents were issued on electret filters that were charged via hydroentanglement[82,83] Fluorinated webs will be more available for triboelectrically charging via hydroentanglement, since nonfluorinated PP webs will be more hydrophilic comparatively. Those of the webs could be charged by water jets or stream of water droplets, since a subsequent drying process in not necessary. In the literature hydroentanglement at a water pressure of 10-500 psi was utilized for charging samples. Charge density and stability was not mentioned, instead filtration properties were discussed[84].

Oxidation as in corona will not be a problem when triboelectrification is prefered. One other advantage will be the distribution of charges. The field outwards filter will be very

strong if all fibers are charged at same sign; however this will not contribute to total filtration efficiency. Due to that reason bipolarly charged carded will be advantageous. This means both positively and negatively charged fibers are present[77]. However frictional charging is difficult to predict and cannot be controlled easily, so when charging in a controlled manner is desired, corona discharge may be preferred[85].

2.4.3 Liquid Contact

Liquid contact charging of polymer films via electrophoresis was discussed in an early patent. As shown in Figure 1.13 film is passing over a capstan under wetted sponge-electrode-air blower. Here a dielectric liquid should be used to wet the film. They utilized from a composition methyl alcohol, ethyl alcohol and acetone. The later acts as penetrator. As the films passes under the field, very little amount of liquid leaves the tip. This is called electophoresis, which is found to be more effective in electret charging compared to physical contact with sponge. Mixture was observed to be capable of charging films to potential approximately to be applied. Liquid is completely dried under blower at room temperature[86].

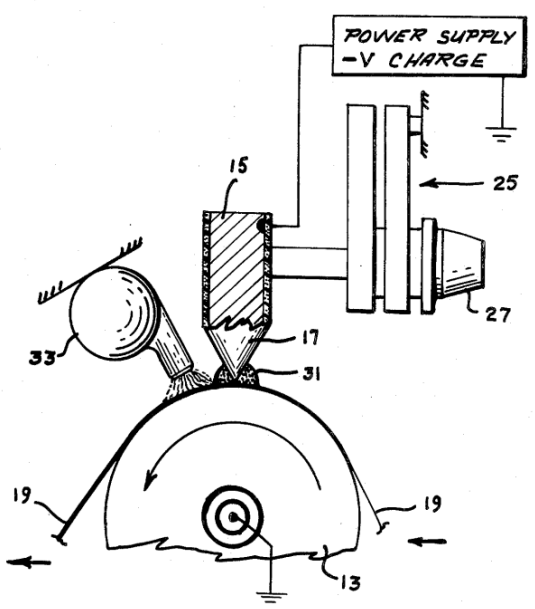

Figure 1.13 Electret charge technique from [86]

Eitzman et al used same phenomena to charge fibrous webs. Nonaqeous polar liquids were found to be obligatory for their ease of drying and higher wetting ability. After wetting the web is substantially dried to create electret filter web. The method is better than corona that it doesnot needs high voltages, and cause changes on polymer surface. The liquids should have a dipole moment of at least 1Debye and a dielectric constant between 30 and 40. Low vapour pressure will cause ease and completeness of drying. This method when applied to flurochemical coated PP media, resulted in very high quality factors values, which are at least 0.6. Some of the samples exhibited quality factor of above 1.1. In Table 1.3 preferred liquids and their properties were given[87].

Table 1.3 Liquids for contact electrification[87]

Liquid	Dipole moment (D)	Dielectric constant (-)
Acetone	2.88	20.7
Acetonitrile	3.92	37.5
DMF	3.82	36.71
Dimethyl Sulfoxide	3.96	46.6
Ethylene glycol	2.28	37
IPA	1.66	18.3
Methanol	1.7	32.6

In summary we can say that main mechanisms for all methods are explained so far. However due to its ease of application, corona discharge was preferred in this study as charging method. On the other hand other methods are not capable of polarizing dipolar species which is desired for some of the additives.

2.4.4 Electrospinning

Electrospinning is a versatile method for producing fibers having nanometer scale diameters. Studies on electrospun electret webs is comparatively less than other methods. Ignatova et al investigated charging properties of electrospun PET webs. Stability of

electrospun and corona treated webs were found to be longer than that of PET mat. However measured surface potential was normalized according to mass which is irrelevant and inaccurate. As a result of normalization lower weight nanofiber webs was found to exhibit high initial potential[88].

Yeom et al investigated boehmite nanoparticles incorporated into Nylon-6 (PA6) nanofiber webs as an electrostatic charging agent. Processed and corona charged PA6 nanofiber web showed significant improvement in aerosol capture efficiency compared to the discharged nanofiber web. Boehmite addition was found to be strongly effective on the electret performance of the web which was shown with bot potential measurement and filtration tests[89].

2.5 Additives for Improving Electret Properties of PP

There are various additives mentioned to be effective to enhance electret properties of PP films and webs. Some of them are soluble such as antioxidants, light stabilizers; whereas some are insoluble such as barium titanate, NA11 nucleating agents. Rather than classification under miscibility their traditional place in additive industry is based on where most pronounced effect was observed. For instance some of the antioxidants may have nucleating ability[90], however their antioxidant role is more dominant and required. There is not a special class of additive that is intentionally designed for electret purposes. However

according to requirement for electret purposes, one or more additive would be selected from several additive classes. In the literature electret additives were very much selected from inorganic ceramic ferroelectrics [91,92], nucleating agents [35,93–96], antioxidants including light stabilizers [90,97,98] and fluorochemicals [99–101]. In this study additives that can be processed via reactive extrusion were selected. Fluorochemicals were not preferred due to environmental issues.

2.5.1 High Dielectric Constant Inorganic Additives

Inorganic additives may be divided into two groups: Linear and nonlinear dielectrics. For the case of linear dielectrics dependency of polarization to applied field is linear. It means polarization continues until all dipoles are aligned. For nonlinear dielectrics, also called "ferroelectrics" there is not a similar linear relation between polarization and electric field[102].

2.5.1.1 Linear Dielectrics

The charge storage of a typical linear dielectric materials is between 10^{-12} and 10^{-6} C , and most of them has a dielectric constant between 5 and 10. Al_2O_3, SiO_2, MgO, BaO are common linear dielectrics that may be useful as electret additives [41]. Nifuku et al found maximum surface charge density 45μC/m^2 in case of PP, 10μC/m^2 for PTFE nonwovens.

Those webs had a filtration efficiency of above 99% upon charging. Effect of SiO_2, TiO_2, Al powders addition at concentrations of 0.1, 0.5, 1.0%wt were investigated. At lower concentrations SiO_2 and TiO_2 gave slight increase to surface charge. However surface charge density dropped upon mixing at a ratio of 5% and 10%. The effect of aluminum mixing on the surface charge density was found fluctuating [103].

2.5.1.2 Nonlinear Dielectrics

It is not as easy to explain the dielectric properties of nonlinear dielectrics. Second mechanism of dipolar polarization is predominant: Rotation of dipoles between two equivalent equilibrium positions. The spontaneous alignment of dipoles is so strong that it can cause crystallographic phase transformations at a critical temperature, which is called Curie temperature. The Curie temperature in piezoelectric materials is used to describe the temperature above which the material loses its spontaneous polarization and piezoelectric characteristics. In lead zirconate titanate (PZT), the material is tetragonal below T_c and the unit cell contains a displaced central cation and hence a net dipole moment. Above T_c, the material is cubic and the central cation is no longer displaced from the centre of the unit cell. Hence, there is no net dipole moment and no spontaneous polarization[41]

The electric dipoles which are parallel to each other within the crystal region are called domains. When an electric field is applied the domains can turn from one direction of

spontaneous alignment to opposite. This is the reason of very large changes in polarization and dielectric constants (ε >1000). Those of the materials are widely used in pressure transducers, ultrasonic cleaner, loudspeakers where electro-mechanical coupling is needed [41].

Polymer dielectrics have the advantage of flexibility, whereas its ceramic counterparts superior due to absence from creep, absence from deformation under stress at room temperature, resistance to environmental changes, high temperature and oxidation [41]. Also it should be noted processability of plastic materials is easier when compared to ceramics. Both advantages would be gained since polymer/inorganic ceramic dielectric composites will be prepared in this study. Table 1.4 summarizes dielectric properties of some nonlinear dielectrics.

Table 1.4 Dielectric properties of ABO_3 perovskite structures [41]

	Curie Temperature (°C)	**Spontaneous polarization ($\mu C/cm^2$)**	**κ at T_c**
$BaTiO_3$	120, 5,90	26 [at 23 ℃]	1600
$PbTiO_3$	490	750[23]	-
$KNbO_3$	415,225,-10	30	4200, 2000, 900

As nonlinear dielectric (also called ferroelectric ceramic) barium titanate was selected. High dielectric constant of barium titanate is probably what makes it one of the most used materials for capacitor and electromechanical coupling applications.

Barium titanate has a ABO_3 type mixed oxide structure. Crystal structure consists of a regular array of corner sharing oxygen octahedra with smaller Ti (IV) cations occupying the central octahedral B site and barium (II) cations filling the interstices between octahedral [Figure 2.13]. The high polarizability is a result of more space for small Ti ions within the oxygen octahedra. The Ti atoms of $BaTiO_3$ are surrounded by 6 O ions. All crystals having the TiO_6 configuration exhibit high dielectric constant. A net permanent moment of the octahedron can result only by a unilateral displacement of the positively charged Ti^{+4} ion against its negatively charged O^{-2} surrounding. Ferroelectricity requires the coupling of such displacements and dipole moments associated with displacements [41,42].

At a high temperature Ti atoms in the center will move randomly from one position to another and will develop a large dipole moment in applied field (Figure 1.14). When the temperature is reduced below so called Curie point, the octahedral structure changes from a paraelectric cubic to tetragonal symmetry with an off-centered Ti ion which causes permanent dipole. Above T_c $BaTiO_3$ is isotropic. In the absence of external field the isotropic crystals are nonpolar [44,104].

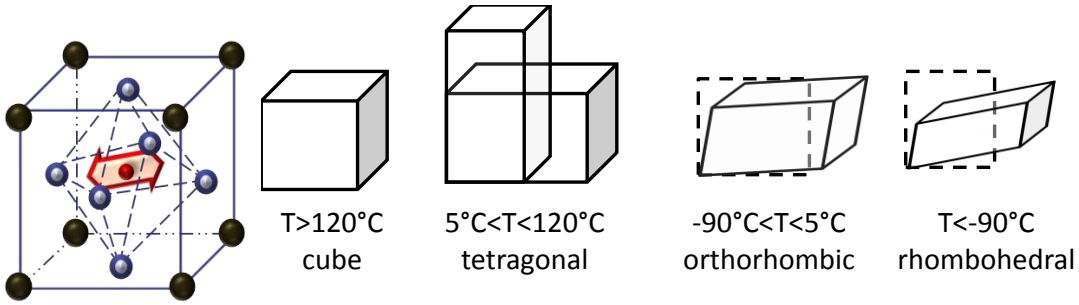

Figure 1.14 Atomic structure of $BaTiO_3$ crystal and crystal structures under various temperatures

Its dielectric properties can be controlled within a wide range by means of composition, mixed crystal formation and particle size[104,105]. Figure 1.15 shows the changes in dielectric constant upon change in particle size. , it was observed that dielectric constant is enhanced in samples down to grain size of 0.7μm and dropped again at 0,28μm. However for lower grain sizes dielectric constant at Curie temperature stays low, whereas peaks were obtained for samples having grain sizes larger than 0.7 μm[106]. Uncontrollable particle size within extruded polymer may give complicated responses on electrets properties of $BaTiO_3$/PP composites. However even in the worse conditions one can expect higher dielectric constant for $BaTiO_3$ and increase in polarization of PP.

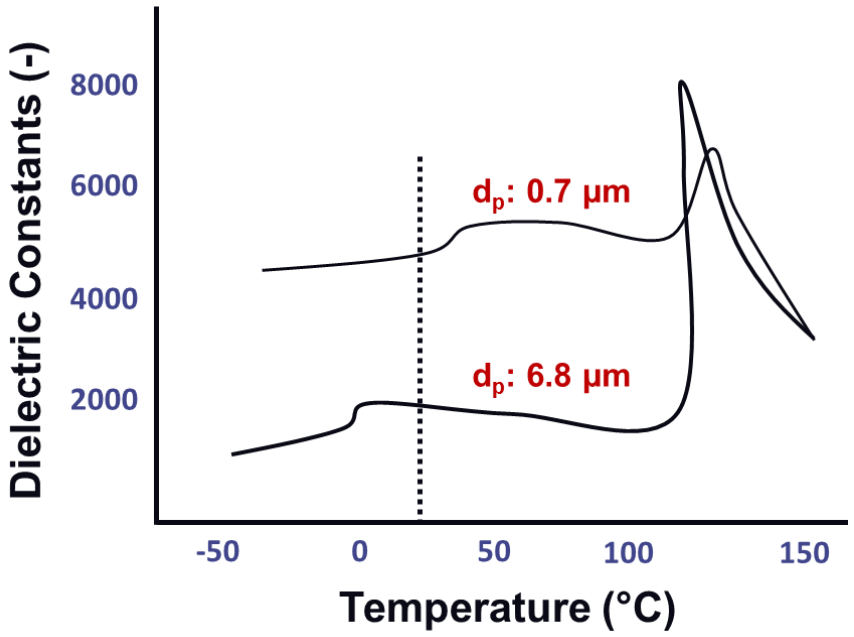

Figure 1.15 Dielectric constant of barium titanate depending on grain size and temperature

At high T ($T>T_c$) the thermal energy is sufficient to allow moving of Ti atoms from one position to another. So there is no fixed asymmetry. Octahedral site allows the Ti atom to develop a large dipole moment in an applied field, but no spontaneous alignment of dipoles. In this symmetric configuration the material is paraelectric (no net dipole moment, E=0). The magnitude of displacement of the Ti in its O coordination octahedron is 0.12 A and the O displacements are 0.03 A. Thus a net dipole moment has been produced in the octahedron by the permanent displacement of the Ti ion against its surrounding O_2 ions. When the T is lowered below T_c, the position of the Ti ion and the octahedral structure changes from cubic

to tetragonal symmetry with the Ti ion in an off-center position corresponding to a permanent dipole. These dipoles are ordered giving a domain structure with a net spontaneous polarization within domains. Below T_c there is a very large spontaneous polarization, giving rise to a large dielectric constant [44,104]

It was also observed that barium titanate obey the Curie-Weiss law (given in Equation 2.18) above Curie temperature[107].

$$\varepsilon' / \varepsilon_0 = \frac{C}{T - T_C} \qquad \text{Equation 1.18}$$

where ε_0 is permittivity of free space, C is constant T is temperature and Tc is Curie temperature. So it will be critical to apply thermal charging at exact Curie temperature to polarize particles effectively.

Since the nonlinearity in dielectric properties exhibit itself with a change in crystal structure, other than dielectric spectroscopy XRD would be used to estimate dielectric behaivious. Muralidhar et al observed elimination and suppression of some of the peaks of PVDF and shifting of some of the BaTiO3 peaks in BaTiO3/PVDF composites. They contributed these changes to the internal stresses [108].

Reference PVDF doesnot have any peak at 101.1° whereas a (400) tetragonal peak at 101.16° with pseudocubic form was obtained for $BaTiO_3$ which corresponds ultrafine particle sizes. In some concentrations there was a deviation from pseudocubic form. At 70%

BT concentration samples have a high pyroelectric coefficient and a high dielectric constant. There is a change in pseudocubic form and also internal stresses at this concentration is believed to be effective.

Another tetragonal form of $BaTiO_3$ at the (004) position is almost absent around 99.6° in $BaTiO_3$ itself because of its ultra-fine particle size. 31.7° peak is another identifier of the tetragonal form of $BaTiO_3$ which is present in all composites except PVDF. This peak is shifted to 31.6° in 70% and 31.5° in 90% weight fractions of $BaTiO_3$ composites. All these changes are conducted with internal stresses developed in the composites[108].

Quantification of crystal structure using XRD was found to be difficult. For instance theoretically 100% tetragonal barium titanate has two separate peaks between theta 44 and 47° corresponding to (200) and (002) crystals, whereas complete cubic barium titanate shows just one peak (Figure 1.16). A mixture of these two crystal forms (tetragonal and cubic barium titanate) will have intermediate forms between one and two peaks. Due to that reason Baeten et al investigated properties of $BaTiO_3$ via DSC. They conclude two factors having effect on Curie temperature: Barium to titanium ratio and mechanical stress introduced by milling. Differential scanning calorimetry (DSC) can measure the energy difference for the tetragonal to cubic transition; it can give the amount of tetragonality as well as the Curie temperature on the as prepared powder. Mechanical distortion of the barium titanate agglomerates has two effects: decrease of tetragonality and increase of the Curie temperature.

So after milling Curie temperature increased significantly. Probably in our case mechanical stresses and high temperature may change the Curie temperature and dielectric properties[109].

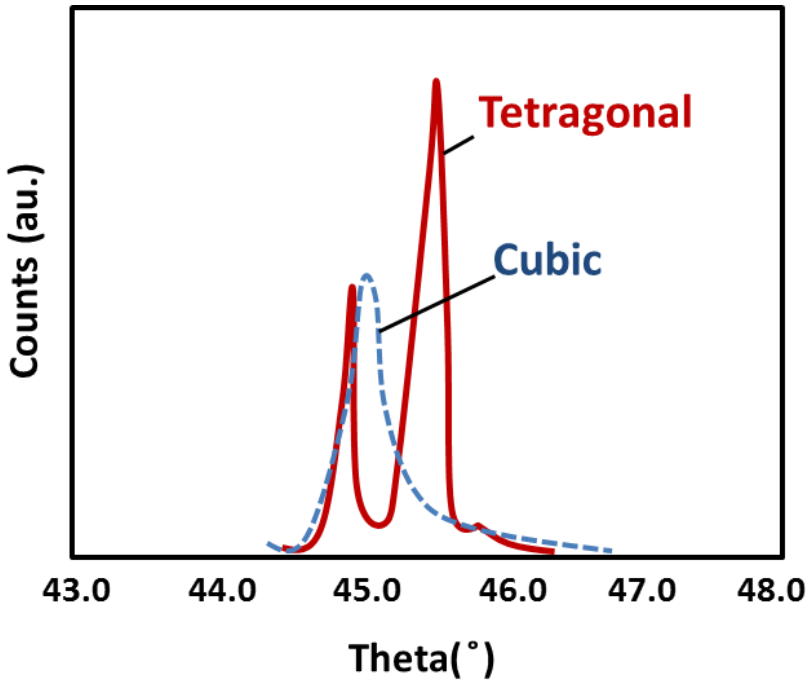

Figure 1.16 Crystal forms within 43-48° diffraction angles [109]

2.5.2 Nucleating Agents

Polymer crystallization is a process from a disordered to lower energy order structure. Crystallization involves two steps: Nucleation and crystal growth[110].

Nucleation can be described as formation of short range ordered polymer aggregations in a melt which act as growth centers for crytallization. Pritchard describes nucleating agents as chemicals which promotes or controls the formation of spherulites in crystallizable polymers[111]. As shown in Figure 1.17 leading to several small spherulites, rather than a few large ones, they enhance mechanical properties and provide consistent optical properties. Clarity will improve since the size of the spherulites will be smaller than wavelength of the light. On the other hand the need of industry is apparent, because increased solidification temperature will allow higher production rates. Among the very first nucleating agents were talc and carboxylate salts (e.g. sodium benzoate, NaOBz) and they are still widely used today. In 1980's, sorbitol acetals penetrate into market. More recently high performance phosphate ester salts were introduced [112].

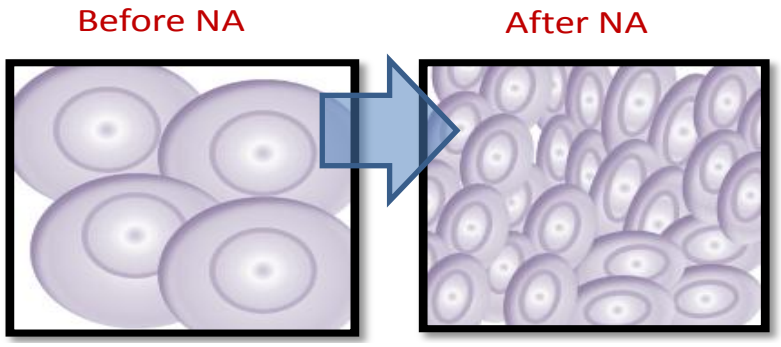

Figure 1.17 Crystal structure before and after nucleating agent

If one modifies the polymer with some kind of nucleating agents this is called *heterogenous nucleation.* Nucleating agents provide nuclei for heterogenous crytallization, raises the crytallization rate and temperature. On the other hand spontaneous nucleation of a polymer is called *homogenous nucleation*. The polymer itself produces growth centers for crytallization in a form of partly 3-D ordered short segments of the macromolecular chain [113].

Efficiency of polymer modification is generally based on chemical and thermal parameters. When nucleation is considered crystallization temperature and crystallite size and shape will be responses. For improving these properties, chemical and thermal factors should be controlled at a sensitive manner. The difference between melting and crystallization temperature ($\Delta T=T_m-T_c$) is a representative data for the efficiency of nucleation. If melting point and crystallization temperature get closer, it means modification is achieved[113] For a quantitative analysis Equation 2.19 can be used.

$$NE=(T_{C,NA}-T_{C,1})(T_{C2,max}-T_{C,1})*100\% \qquad \text{Equation 1.19}$$

where $T_{C,NA}$ corresponds crystallization temperature of nucleated polymer; $T_{C,1}$,crystallization temperature of blank polymer; $T_{C2,max}$, crystallization temperature of self-nucleated polymer[114].

Also one can compare the crystallization halftimes, which is measured via cooling a polymer melt quickly to a certain temperature and recording heat flows as a function of time. Crystallization half time is the time needed to attain 50% crystallinity. Other than those

thermodynamic methods, optical properties such as clarity, haze may be measured as explained elsewhere. In Figure 1.18 those changes were illustrated [114].

For certain highly active nucleating agents, the structure is controlled by nucleating agent, not process conditions. Nucleating agents are mostly insoluble in polymer. Melting point of nucleating agents should be higher than that of polymer. Efficiency of nucleating agents can also be understood from nucleation density, which is the number of nuclei where crystal growth is initiated per unit volume. It needs to be between 10^3-10^{12} cm^{-3}. The most efficient nucleating agents have a structure in both polar and nonpolar parts coexist, the latter will be in contact with polymer. In most cases a very small amount of additive, 10-10^2 ppm concentration is needed. The concentration does not exceed 5.10^3 ppm[111,113].However relationship between polymer and the physical and chemical characteristics of nucleating agents has not been clarified yet. It is known that a good matching between nucleating agent crystal and chain structure of polymer[116].

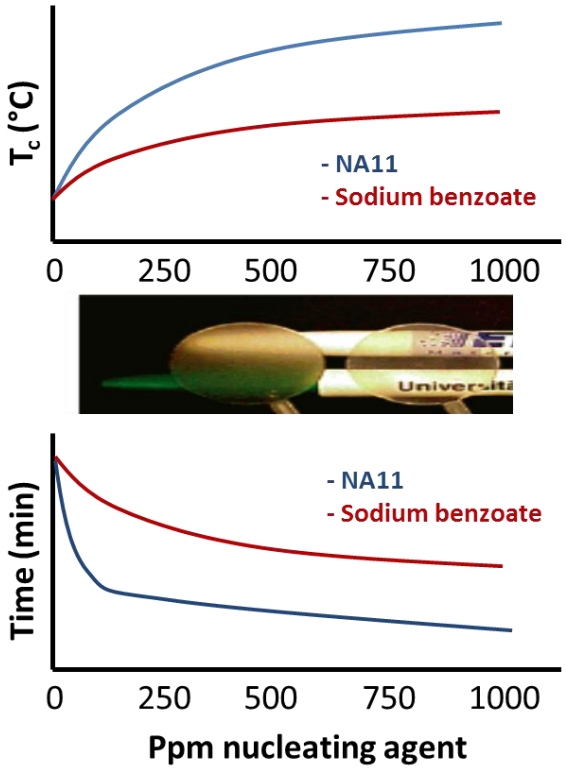

Figure 1.18 Changes in crystallization temperature, clarity and crystallization half-time [adapted from[112,115]]

2.5.2.1 Crystallization during Fiber Formation

Being a first-order phase transition during crystallization an ordered, crystalline structure is formed from a disordered, coiled state in the melt. In general a two phase morphology which is composed of plate-like lamellar crystals and amorphous regions is observed in semicrystalline polymers[110].

Both kinetic and thermodynamic argument during spinline crystallization will result in many orders of magnitude more rapid transformation than in quiescent state. Therefore crystallization will be governed by two driving forces in spinning line: Super cooling and stress[117]

Both crystal structure and crystallization kinetics will be different compared to quiescent crystallization. For instance flow induced chain orientation will reduce kinetic barriers against crystallization. The spherulitic morphology that is observed under low shear rate will be distorted into more fibrillar along orientation axis. Transformation of an oriented melt to crystalline solid will need lower enthropy decrease than does crystallization of unoriented melt and therefore a larger free energy change. With increase in shear rate, the level of orientation increases. On the other hand very high cooling rates -upto 3,000-4,000K/sec- is observed in fiber formation processes[117,118]. Lagasse and Maxwell stated that flow induced crystallization dominated after a critical shear rate, at lower shear values crystallization is governed by added nucleating agent[12]. It was stated that in shear thinning region polymer coil conformations are significantly distorted from their equilibrium isotropic state, and crystallize directly from this distorted state.

At such a high spinning speed and cooling rate one of the major questions will be nucleus size that approaches to crystal unit dimensions. It leads people to the question whether it is just nucleation and no crystal growth. George assumes the phenomena as collapsive nucleation instead of nucleated growth[117].

Modified models for crystallization in flow fields are criticized to be insufficient. Among them are Avrami-type models as functions of deformation history, or Flory like approach relating the decrease in enthropy, Hoffman's kinetic model based on modified crystal growth rate. Avrami type model do not consider molecular behaviors between flow and crystallization whereas the crystal growth geometry is not incorporated in the Flory-type approach. An important factor during fiber formation, the effect of reduced kinetic barriers for crystallization due to flow-induced orientation of chains is also another ignored point[118].

Jinan et al proposed two mechanisms for crystallization at various speeds. For lower spinning velocity if the effect of shear is low, crystallinity of as-spun filaments may decrease with increasing take-up velocity, because cooling rate will be dominant on the crystallization process. On the other hand, crystallinity of as-spun filament may increase with increasing take-up velocity. This is because of the increase in crystallization rate which is sufficiently high due to high spinning stress and high molecular orientation. At low take-up velocity, crystallization occurs at relatively high temperature because of low cooling rate, and monoclinic crystals are formed. With increasing take-up velocity, cooling rate increases, and crystallization temperature decreases. Consequently, pseudohexagonal (mesomorphic) crystals are formed. With further increase of take-up velocity, crystallization rate increases because of significant molecular orientation[119].

The presence of polymer chain in more than one crystal structure is the distinguishing character of polymer when compared to small chains[118]. Due to that reason, polymers have

different crystallization and melting temperatures[114]. Use of nucleating agent makes crystallization and melting temperature closer. Some other factors such as presence of comonomers, large spatial extent of chains and chain-chain entanglement lowers molecular mobility and act against nucleation[118]. Secondary and tertiary nucleations refer to crystallization of chain on the surface of a flat polymer crystal and on the edge of crystal respectively. Heterogenous nucleation makes use of a foreign preexisting surface the reduce free energy opposing primary nucleation[114].

2.5.2.2 Types of Nucleating Agents

PP crystallize into 4 crystal forms: α-, β-, γ- and smectic forms. Currently there are nucleating agents for α-, β- crystals. However smectic form and γ-crystals depends on spinning conditions, rather than additives.

Nucleating agents can be classified into two: Inorganic and organic. Carbon black, kaolin and talc are mentioned to be effective as nucleators. Also in the literature various mineral materials, such as TiO_2 are reported to have nucleating effects on PP. However in general they do not have a good fame as a nucleating agent [52].

Alkali metals and Al salts of aromatic alicyclic carboxylic acids like Al, Na, K, Li benzoate, Na beta naphtalate, Al tert butyl benzoate are defined in this group. Al, Na

benzoate changes the crystallization temperatures significantly and provides smaller spherulites, but need to be dispersed as finely as possible[111,114,120].

Derivatives of sorbitols are most widely used ones in industry. They are the products of condensation of aromatic aldehyde and sorbitol. 1,3,2,4-di benzylidene sorbitol (DBS) ; 1,3,2,4-di para methyl benzylidene sorbitol (MDBS) and 1,3,2,4-di para ethyl benzylidene sorbitol (EDBS) are the kinds of sorbitol based nucleating agents. DBS is not preferred too much due to problems during processing… ie, odour. Sorbitol derivatives have a high degree of dispersion in PP, and even at very less concentrations (0,25%) gives the best clarity of matrix. They dissolve in molten PP, upon cooling a fibrous network of clarifying agent is formed. The fibrous network (fiber diameter 10nm) increases dispersion of the nucleating agent, which results in high nucleating efficiency [111,120].

When compared to benzoates sorbitols are better nucleating agents. As a quantitave result, modified iPP films with NaBz show 10 times spherulite size reduction, while iPP films modified with sorbitol derivatives have 50 times reduction in spherulite size. Upon modification with those crystallization temperatures is in the order: DMBDS>MDBS>DBS>NaBz[111,120]. The sorbitol derivatives differ from other nucleating agents with dissolving and recrystallization capability in the molten polymer. By the way formation of a well-dispersed, large surface area, tridimensional nanofibrillar network will be allowed[121].

2.5.2.3 Nucleating Agents as Electret Additives

So far many studies were also conducted to improve charging properties of polypropylene with nucleating agents. Bisamides[122], trisamides[32], sodium 2,2'-methylene-bis(4,6-di-tertbutylphenyl)- phosphate (NA11)[123,124], N,N'-dicyclo-hexyl- 2,6-naphthalene-dicarbox-amide (NU100) [93], trisamides derivatives [121] are a few of them. It seems studies not only on nucleating agent containing electret materials, almost all studies on nucleating agents are focused on films. This can be conducted to inessentiality of advantages provided from those additives on filament properties. Only in a recent study a 30% increase in tensile modulus was reported for DMDBS/PP filament at low spinning speeds. Kristiansen et al investigated phase behavior of DMDBS/PP composites and a simple binary monotectic was advanced. Increased DMDBS concentration resulted in an adverse effect not only on crystallization, but also clarity and haze. They observed the maximum crystallization between 0,2-1wt%. More than 2% DMDBS concentration gave phase separation and thus a high haze value [115]. Clarification of polymeric films depends on the size of crystal structures, which are already too small in filaments. There is no need to shorten processing time such as in plastic part production, since a solid fiber formation is also achieved very rapidly.

Behrendt et al used two commercial nucleating agents, sodium 2,2'-methylene-bis(4,6-di-tertbutylphenyl)-phosphate (NA11) and N,N'-dicyclo-hexyl-2,6-naphthalene-dicarbox-amide (NU100) at lower concentrations below 0.5% percent. For NU100, the charge decay was found to proceed faster in comparison to the pure i-PP reference, which is

conducted with charge drift pathways generated by H bonds through the volume of films. So the decay mechanism is much more chemistry related, than microstructure. Intermolecular hydrogen bonds provide pathways for the charges through the volume of the film due to the formation of fibrillar three-dimensional network structures of the additive. On the other hand NA 11 exhibits a significant improvement when biaxially stretched. Upon stretching there is a significant change in electret properties. The reason behind the improvement is not explained by better crystalline-amorphous distrubition provided upon nucleation, instead nonsoluble NA11 particles caused elongated, regular cavities due to weak interfacial bondings. So as shown in Figure 1.19 NA11 particles acted as stress concentrators and lead to local microvoids during drawing. Adhesion between NA11 as an organic phosphorous salt and polypropylene would be very low due to strong differences in the chemistry[93,125]. Same group also investigated efficiency of NA11 at higher concentration values. Decay rate was significantly reduced at a concentration of 10%, which was also proved in TSD measurement. The peak discharge temperature nearly reached to melting temperature of PP. The improvement was attributed to barrier effect of generated cavities upon NA11 addition. Charge stability was reduced at lower concentration due to generation of shallow traps upon nucleation; while at high concentrations it was improved due to larger number of voids generated by a larger number of additive particles hindering the drift by lengthening the path of the carriers[123].

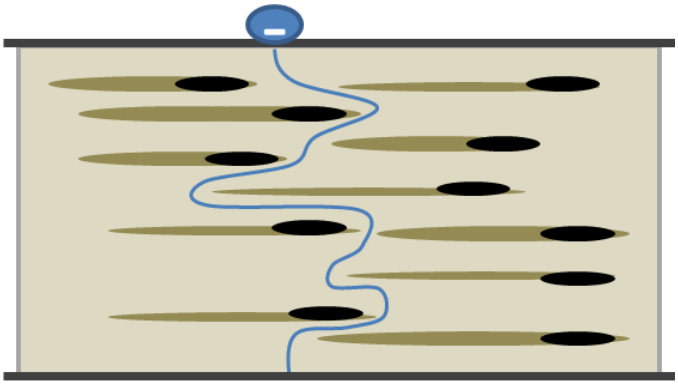

Figure 1.19 Elongated cavities formed upon modification with NA11 [adapted from[93]]

Complete solubility of nucleating agent is advantageous for homogenous distribution and efficient nucleation [111,114,120]. Due to that reason Mohmeyer et al synthesized triphenylamine-based trisamide derivatives as nucleating agents for PP. As a result of increased solubility, fibrillar crystals were observed instead of spherulites. Onset of crystallization temperature, which is an indicator for nucleation efficiency, was found to increase largely even at additive concentrations of 0.2%. Interestingly they obtained rapid charge decay in the range of concentrations that efficient nucleation takes place, which was attributed to the presence of the three dimensional network structure of the nucleating agent, providing conductive, nanometer-sized path ways within the bulk of the sample through which the charge can drift. This phenomena, called as percolation concentration is illustrated in Figure 1.20. At higher concentrations ie higher than 0.2 %, a three-dimensional network

structure and non-dissolved additive crystals were observed which resulted in deeper traps within the material[35,96].

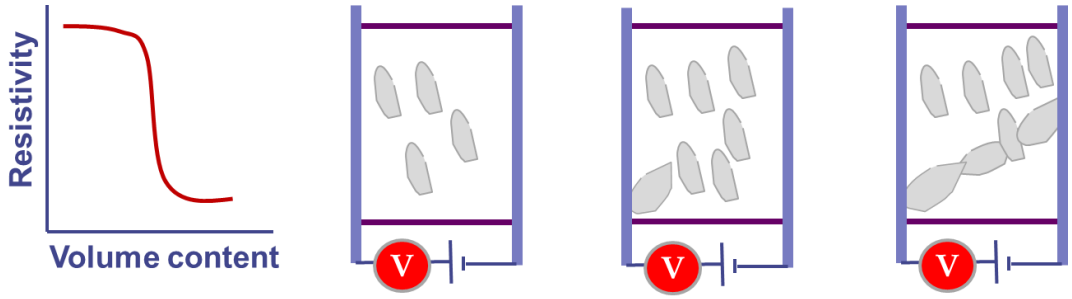

Figure 1.20 Schematics for percolation concentration

Another finding is that formation of isolated nanostructures having dipolar structures strongly affects electrets properties. Nucleating agents having dipole groups will be buried into highly frozen crystal regions. Decay tests on trisamide based nucleating agents showed that additives with three secondary amide groups enhances charge stability whereas surface potential of samples with cyclohexyl substituents rapidly decays. If they are not separated charges may find a path to accumulate. For trisamide based nucleating agents it was percolation and the formation of a three-dimensional network was obtained which promotes charge drift. So use of soluble nucleating agents at very high concentrations is not suitable. The formation of nano aggregates and three dimensional structures may be dictated by

thermal history. At elevated temperatures those structures will have the mobility to become together resulting in a higher conductivity. On the other hand replacing hydrogens with phenolic groups also resulted in complete change in charge stability. For this specific case benzene groups on those sides increased conductivity[121]. Results were given in Table 1.5.

Table 1.5 Electret properties of trisamide based nucleating agents containing PP films[117]

– Range III: a heterogeneous system where the additive is not completely soluble in the polymer melt at the processing temperature of 260 ◦C, leading to non-dissolved additive particles. – Range II: Optimum concentration for nucleation. The additive is completely dissolved and, upon cooling, rod-like nanostructures are formed. In this range the surface potential reveals a minimum because the percolating network of the rod-like nanostructures provides pathways which allow the charges to drift. – Range I: Surface potential increases considerably. The rod-like nanostructures are not in contact instead isolated additive nano-domains arise that act as charge traps	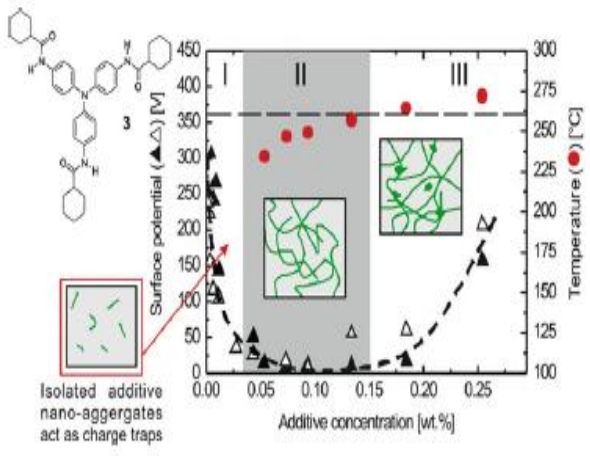 Remaining potentials upon keeping 50μm thick additive containing films at 90 °C for 12h Red dots indicate dissolution temperature of nucleating agent.

Tani et al utilized from fatty acid metal salts and organic nucleating agents to enhance the electrostatic filtration properties of split fiber webs. The additive containing and probably nucleated 25-50 μm films were split into yarns by stretching or cutting. After stretching at a ratio of 1:15 film begins to break into fibers. The additives were aluminum laurate as fatty acid metal salt and pentaerithrityktetrakis [2-(3,5d-t-butyl-4-hydoxyphenyl) propionate] as nucleating agent at concentrations between 0.1-5%. After two seconds of corona charging, each sample was split into fibers by a film splitter having four circular blades. Filtration efficiency of 97,4% was achieved at reasonably low pressure drop about 0.24mmWater[126].

In summary there are two reasons for the use of nucleating agents as electret additives:

i. Smaller crystallites will lead to larger crystal-amorphous boundaries, which results with efficient Maxwell-Wagner type polarization[36,127]
ii. Nucleating agents are designed to locate in the center of crystal regions. Rather than exclusion through amorphous regions as observed in many additives[114], nucleating agents will be buried into crystallites [111,114,120,121]. This means any kind of polarizable groups will be buried into crystal region. They will enhance polarizability in a stable regime. However this will strictly depend on concentration, since at a level of so called percolation, those of the high carrier concentrated species will combine and increase charge mobility.

The mechanism of sorbitol based additives can be summarized as gelation and formation of a 3d network within the molten PP during cooling, which act as nucleating centers. Due to its large surface area, an efficient nucleation occurs. DMDBS is a chiral amphiphilic molecule which possesses hydrophobic benzene wings and an sorbitol hydrophilic center which is capable of forming hydrogen bonds. Network formation originates from these hydroxyl groups which are involved in intermolecular hydrogen bonding. Also π interactions between the phenyl groups of the same chirality are thought to be contributing to the formation of the network[128,129]

Yoshimoto et al investigated the nucleation mechanism of NA11 in PP. Crystallographic data obtained from DMF/NA11 solution-PP film and molten PP-NA11 crsytals revealed that epitaxial crystallization takes place preferentially. It was concluded that a lattice matching occurs between the pitch of PP helix which is comparable to the interval of tertiary butyl groups in the b-axis of NA-11 crystals[130].

2.5.3 Antioxidants

Antioxidants are probably the largest family in polymer additives. Those are compounds that prevent or inhibit chemical oxidation process, which produces oxygen containing compounds such as carbonyl (C=O) groups. They have different acting mechanisms, so as chemistry and composition. Prior to explaining antioxidation mechanism,

it would be better to understand polymer oxidation, which is also effective on electret properties. So this chapter will deal on effects of oxidation and antioxidants on electret properties. However it will be challenging since both products coming from oxidation, antioxidants-oxidized species interaction and unreacted antioxidants will change the chemical composition.

2.5.3.1 Oxidation of Polypropylene

Oxidative degradation is thought to be occurring predominantly in amorphous regions since crystalline regions are impermeable to oxygen[131,132] However as explained in chapter 2.5.2, crystallization is so rapid in fiber formation which is a shear induced nonisothermal process. It causes significant difference in crystallization kinetics, which results in crystal sizes significantly smaller than that of spherulites. So we would expect a more uniform oxidation within fibers, compared to films.

PP is highly susceptible to oxidation due to presence of the tertiary H on the C atom bonded to the pendant methyl group. Its dissociation energy is the lowest compared to primary and secondary bonds. Oxidative chain scisson can occur under normal processing conditions if the resin is not stabilized. PP more readily goes to oxidation than PE[133]. Rather than crosslinkage as shown in Figure 1.21 which need the loss of primary H within pendant methyl group chain scissoning dominates in PP.

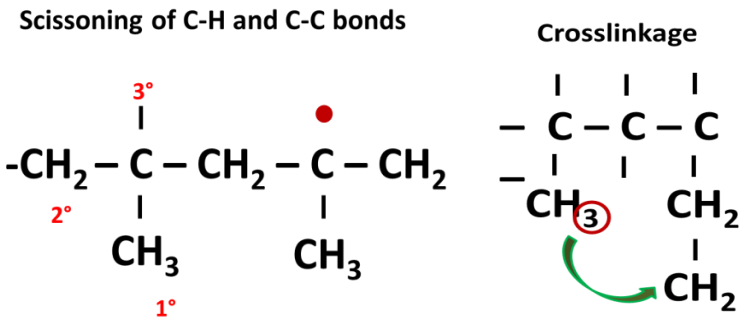

Figure 1.21 Loss of tertiary H and crosslinkage in PP

Oxidation occurs in a free radical chain reaction, which has initiation, propagation and termination processes. As shown in Figure 1.22 a self-propagating, fast oxidation occurs through the main chain or side chain cleavage from shear. Thermal instabilities in the system, attack of atmospheric oxygen or any other radicals may cause the loss of H [134].

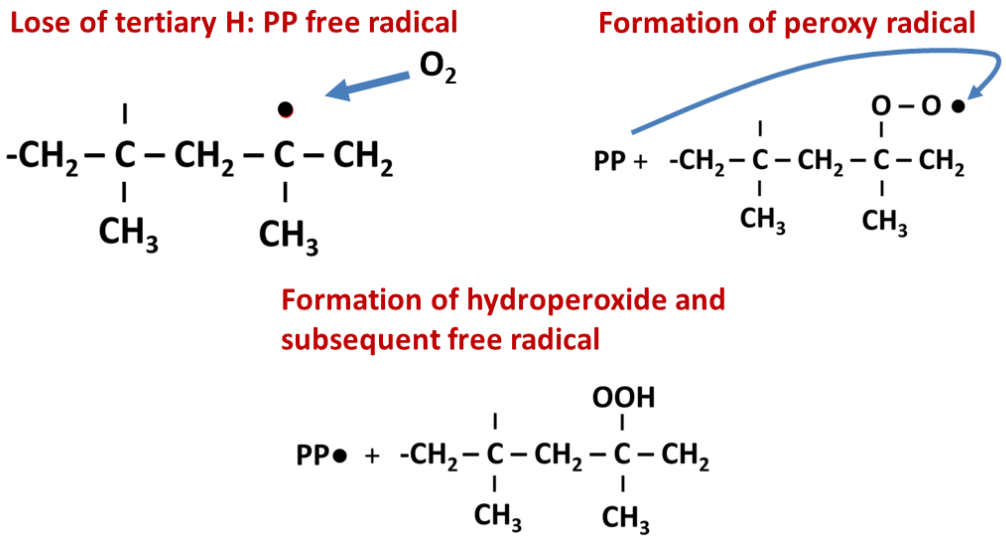

Figure 1.22 Initiation of oxidation reaction for PP[134]

As shown in Figure 1.23 formation of hydroperoxides is the critical reaction during oxidation, because hydroperoxides are the source of further radicals. Generated water as indicated in the seventh reaction is a prodegredant in some of the polymers. Besides the effect of heat or UV, hydroperoxide decomposition can be catalyzed by a number of transition metals, such as Fe, Cu, Ni, Ti, Co, V (Reactions 9-11).[134]

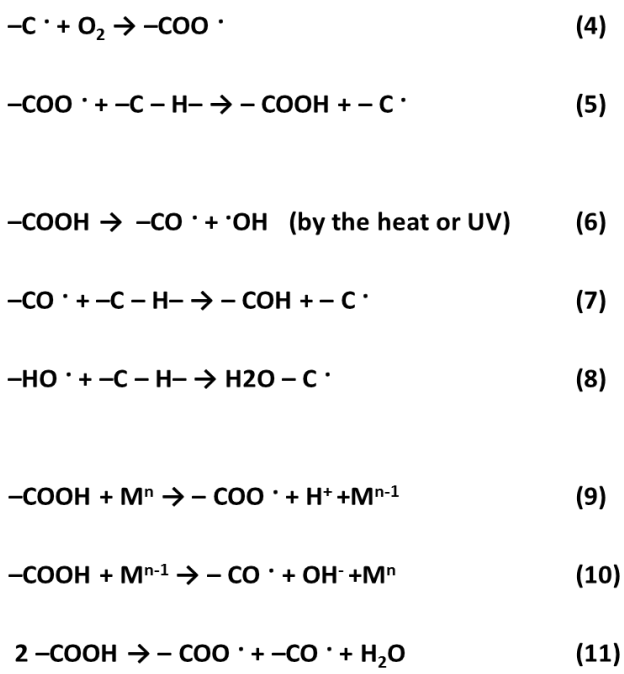

Figure 1.23 Possible propagation mechanisms during the oxidation of PP[134]

Looking at termination of free radical reactions that occur during oxidations, it is quite possible that recombination can occur (Figure 1.24). However the case is not the reversal of experiment (1), since two separated radicals are combined. If it occurs within chains, crosslinking may be obtained. Secondly, fragments of radical can be generated which results in alternating structures. Every other C can form a secondary radical in PP, if reaction 12 is favoured over 11. Primary C atoms favour crosslinkage over fragmentation in PE. Thirdly chain scission can take place, where oxygen containing radicals are generated, which

results in rapid lowering of molecular weight. Weak points can be observed on the oxidized sites[134].

$$– C^{\cdot} + – C^{\cdot} \rightarrow – C – C – \qquad (12)$$

$$– C – C – C^{\cdot} \rightarrow – C = C + – C – \qquad (13)$$

$$R – CO^{\cdot} \rightarrow R^{\cdot} + C=O \qquad (14)$$

$$H – C – C = O \rightarrow {}^{\cdot}C – C = O \qquad (15)$$

Figure 1.24 Termination processes upon oxidation[134]

In summary oxidation products are mostly macroalkyl radicals through homolysis of C-C or C-H bonds, having functional groups such as aldehydes, ketones, carboxylic acids, esters, γ- lactones and volatile (water)[135].

There are two types of oxidation that should be mentioned for corona discharged PP electrets. Possible initial oxidation will occur during masterbatch production and meltspinning processes which are originated from shear and thermal conditions. Secondly high energetic corona ions will induce surface oxidation. Both surface and bulk oxidation will be effective on electret properties.

Oxidized species located as separate polar species will give rise to polarity of PP, hence electret properties. Kravtsov et al charged meltblown PP produced at 380°C and stated ionization of macromolecules were accompanied by ejection of electrons. Charge carriers can be located in the gaps between macromolecules with such defects. For instance ions formed during corona might be captured in the depth of several molecular layers from the surface whereas electrons penetrate more deeply[136]. On the other hand energetic corona ions caused macromolecular breakages which are ionic species within nonpolar PP. They were contributed with a higher TSD peak temperature for oxidized PP than non-oxidized. It was concluded that oxidation products such as carbonyl acted as deep traps[137]. Products resulting from oxidation process may function variously:

- A high-energy electron can self-localize in the bulk of the material upon spontaneously forming a defect in the structure, which plays the role of a trap [138],
- Thermal-oxidative destruction of the polymer may cause formation of polar functional groups and charged fragments of macromolecules,
- Ozone, atomic oxygen, and nitrogen oxides in the air gap under the influence of the electric field and their oxidative action on the macromolecules will form polar groups, and
- Whenever heterolytic rupture of chemical bonds occurs within the polymer, macromolecules break down into charged fragments[139].

On the other side corona treatment is used for improving wettability, printability, laminability of PP surfaces[140–142]. Oxidation is a result of excited gas molecules which induce the cleavage of chemical bonds and formation of polar groups[141,143] Those of the oxidized groups can be C=O, C-O and COH. Atomic oxygen generated during corona treatment reacts with polymer chain, thus forms oxidized polar groups. Those are low molecular weight oxidized materials (LMWOM) having a molecular weight of approximately 400 D and produced by the random cleavage of the PP chain into oligomers containing oxidized groups such as –COOH, -CHO, CH_2OH. Even washing water for 1 min in ultrasonic bath is enough for removal functional groups, but some oxidized species stayed there, which are thought to be due to intermediate size of products. Increasing charging time will cause more chain scission. Oxidation can even change the surface morphology of films. Morphological changes on surface was observed via AFM in various studies, which is dependent on applied electric field, charging time, enviromental conditions such as humidity and temperature. [144,145]. However oxidation will be strictly dependent on power of corona system. Suzer et al couldnot obtain similar changes on surface morphology, which was conducted to power of corona process and oxidation it produced[140].

As a result of oxidation products on surface, corona discharge increases the wettability of inert PP[141,142,144]. Depending on the power of instrument and humidity, even charging times of a few seconds may result in a decrease from 110° to 54° in advancing contact angle. The XPS and contact angle results obtained by Strobel et al is shown in Table

1.6. A hydrophilic layer will cause liquid film formation on surface thus ease of accumulation of charges. This is proven in various papers by XPS, contact angle and AFM analysis[141,144,145]. According to our knowledge there is no special antioxidant, that is useful against that sort of surface modification, instead they prohibit oxidation due to production and using conditions.

Table 1.6 Change in O/C ratio on surface and contact angle upon corona discharge[146]

	O/C ratio on surface	**θ_a (lowest advancing contact angle)**	**θ_r(lowest receding contact angle)**
None	0	110	83
Corona ($0.17j/cm^2$)	0.08	91	54
Corona ($1.7j/cm^2$)	0.12	75	50
Corona ($17j/cm^2$)	0.23	54	31

During corona discharge, atomic oxygen rapidly causes scission of the PP chains and widespread chain scission results in the formation of polar LMWOM which are soluble in water and other polar solvents. Strobel and Lyons found that LMWOM contents enhanced the adhesion of the ink and acrylate-based materials onto PP fibres, which was initially

highly nonpolar[147]. LMWOM amount is related with relative humidity other than energy input during corona and. Increased electrode power causes more LMWOM contents, whereas it decreases at higher humidity values [144]. In this regard we think that at high relative humidity values ions will be functional just for charging and they cannot hit the fiber surface as strong as electrons.

Mizutani et al obtained significant differences between charging properties of pure and oxidized PE. Interestingly pure gave a long peak in TSC tests, whereas surface potential was lower (Figure 1.25). Carbonyl groups introduced during oxidation were thought to be effective on deep trap formation[137].

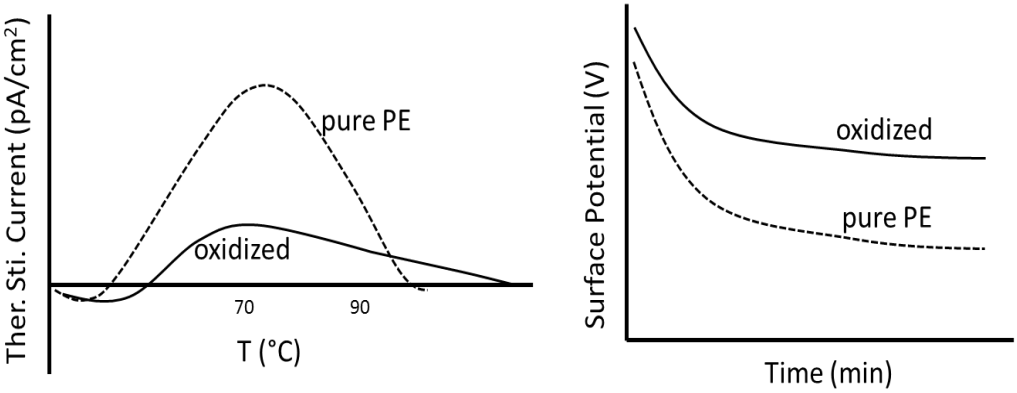

Figure 1.25 TSC and SPD test performed by [137]

It is difficult to compare the results obtained in the literature, since difference in charging conditions, polymer properties, processing condition, sample geometries. However in summary it can be concluded as;

- Oxidation work negatively by forming hydrophilic surface, which results in worse long term stability

-Oxidation again may work negatively by introducing conjugated groups that lower bandgap, and increase carrier mobility

-However oxidation introduces groups such as carbonyl acting as deep traps, which are effective in space charge formation

2.5.3.2 Antioxidants: Chemistry and Mechanism

As mentioned earlier both chemistry of antioxidant and products after antioxidant-oxidized radical will change the chemistry of pure PP filaments, so as electrostatic properties. Antioxidants assure protection against thermal and oxidative degradation during process or use. Some antioxidants work during processing, and some are more effective at room temperatures and used for improving service conditions [148]. To prevent any type of oxidation, various solutions were proposed. These are based on:

- Activation energy: To contemplate processing at the lowest possible temperature with the minimum shear rate. So the result will be lower output.

- Activation enthropy: The availability (or lack) of weak points on the polymer for oxidation
- Competing reactions: Preparing antioxidants that have more tendency to oxidation or UV light than species through the chain[148].

In Table 1.7 various types of antioxidant are tabulated. Primary antioxidants inhibit the propagation of oxidation by donating a proton. Common primary antioxidants, such as stearically hindered phenols, secondary aromatic amines, aminophenols inhibit chain breaking. Secondary antioxidants are used for preventive effects. Organic phosphates, sulfur containing acids are in this group. Also mixture of primary and secondary antioxidants will provide multifunctional effects as observed in hydroxylamines [5]. Other than those for long term purposes light stabilizers are used to protect PP.

Table 1.7 Antioxidants, general classification

Family	Type	Acting Mechanism
Primary antioxidants	Hindered Phenols Secondary Aromatic Amines Lactones Acrylated bisphenols	H donors
Secondary antioxidants	Organophosphorus compounds Thiosynergists	Hydroperoxide decomposers
Multifunctional antioxidants	Hydroxylamines	Both H donors and hydroperoxide decomposers
Radical Scavengers	Nitroxyl radicals produced by hydroxylamines and benzofuronane	Interrupt the oxidative chain reactions
Light stabilizers	UV absorbers Hindered amine light stabilizers Energy quenchers	Interfere with the absorption of flight Deactivate excited states
Metal deactivators		Chelating

Hindered phenolic antioxidants are common primary antioxidants. They simply act as H donors, reacts with peroxy radical to form hydroperoxides and prevent abstraction from polymer backbone. They are useful for both processing and long term use. The mechanism in vivo Tocopherol (vitamin E) is similar to hindered phenols. Secondary aromatic amines are

more effective H donors when compared to hindered phenols, because steric hindrance is less (Figure 1.26). Secondary aromatic amines of a great molecular weight variety would be designed, however discoloration is the problem with secondary aromatic amines[149]. This is an important fact for electret properties, since discoloration means there are some chromographic groups that gives conductivity at visible region. After adding antioxidant a chemical competition starts between oxygen and antioxidant to combine with radical.

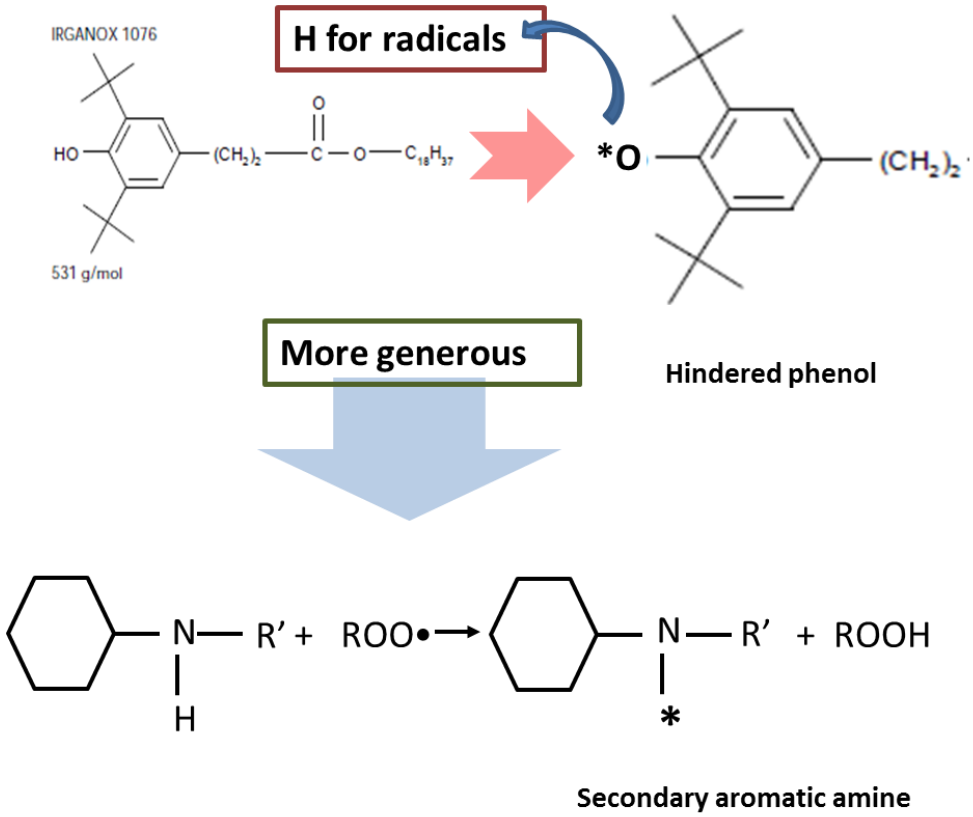

Figure 1.26 Primary antioxidants and H donoring mechanism

Secondary antioxidants are hydroperoxide decomposers. Hydroperoxides are the critical oxidation products that govern oxidation kinetics. Use of secondary antioxidants converts them into nonradical, nonreactive species. The hydroperoxide group is reduced to an alcohol group, ROH, whereas the hydroperoxide decomposer is oxidized in a stoichiometrical reaction. Hydroperoxide decomposers are usually used in combination with H-donors, e.g. phenols[149]. Secondary antioxidants include organophosphorous compounds and thiosynergists. Organophosphorus compounds are trivalent phosphorus compounds. They are effective stabilizers, especially when combined with primary antioxidants. Thiosynergists which are sulfur based hydroperoxide decomposers can be divided into three: Dialkyl dithiocarbomates, dithiophosphates and dithioalkyl propionates. They are effective for long term applications. All acidic species formed can decompose ROOH in an overstoichiometric manner[150].

Radical scavengers interrupt the oxidative chain reactions. Propagation would be totally prevented if all macromolecules P• were scavenged. Due to presence of O_2, POO• reactions are more favorable. So terminator should react with POO• and products must be inert. Due to extremely high reaction rate of oxygen with alkyl radicals, it is difficult to compete with this reaction.[135,149] Nitroxy radicals produced by HALS(hindered amine stabilizer) act also as alkyl radical scavengers even though reaction rate is slightly lower than alkyl radicals with oxygen. [151] Hydorxylamines and benzofuronane dereivatives are also

capable of producing nitroxyl radicals that act as radical scavengers[149]. Their acting mechanism can be summarized as following:

$P\bullet + O_2 \rightarrow POO\bullet$

$POO\bullet + PH \rightarrow POOH + P\bullet$

$P\bullet + CT \rightarrow$ Products (CT:Chain terminators)

$POO\bullet + CT \rightarrow$ Products

So far general antioxidants against oxidation due to thermal and mechanical conditions were summarized. Light stabilizers are also under antioxidants family, however have different acting mechanisms. Upon absorption of photon, chromophoric groups generate an excited state and the later can undergo various deactivation modes. It is electronic transitions that causes light absorption. The probability for such transition will increase if some constituent atoms - chromophoric groups - are arranged in special bonding positions. Figure 1.27 shows a few of them. Chemical deactivation generally results in free radicals, which are reactive and attack intact molecules. Particularly electronically formed ketonic carbonyl groups will cause reactions called Norrish I and II types. There are three strategies developed against light induced oxidation

- UV absorbers: Interfere with the absorption of light
- Energy quenchers: Deactivate excited states

– Radical scavengers: React with free radical directly, which are mentioned in previous section

UV absorbers have high absorption in UV region thus reducing the amount absorbed by polymer's chromophores. They transform the absorbed radiation energy into harmless thermal energy by way of photophysical processes involving the ground state and excited state of molecules. Benzotriazoles, benzophenone, 1,3,5 triazines, oxanilides are common UV absorbers.

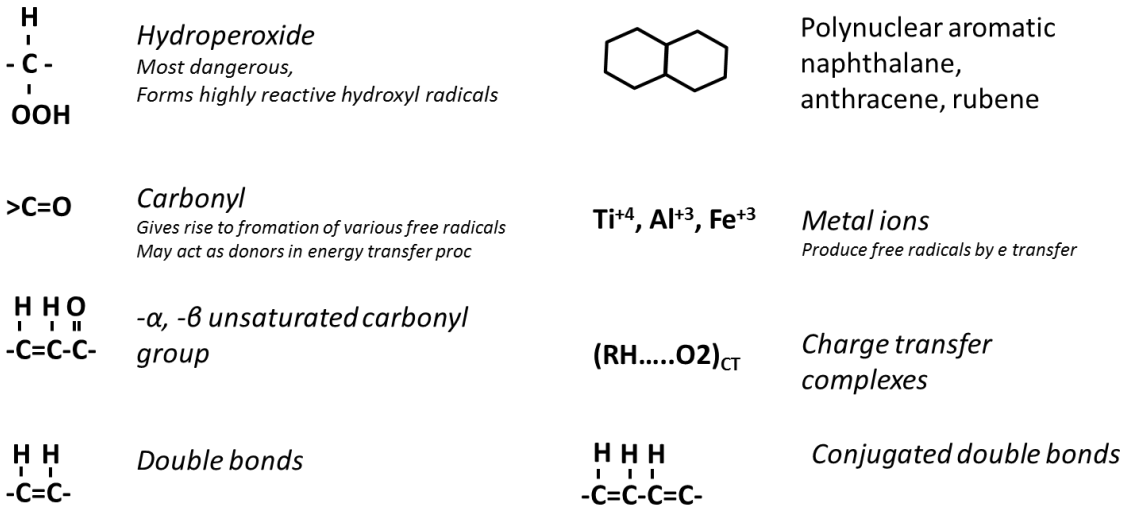

Figure 1.27 Functional groups that have chromophoric effects.

Hindered amine stabilizers are derivatives of piperidine [2,2',6,6' tetramethyl peperidine (TMP)]. Their advantage over UV absorbers is that no specific layer thickness or concentration requirement, since donot absorb UV, but act to inhibit photo-induced degradation. Tinuvin 111, 123, 494, 765, 770, NOR, XT, Chimasorb 2020, 944 are common HALS that are widely in use.

Energy quenchers accept energy of excited chromophores tethered to polymers. The energy of undesired chemical deactivation of excited chromophore through bond rupture (via Norrish I, II) or rearrangements is transferred to quenchers. So energy transfer from P* to Q is possible if the energy level of the excited state of the chromophore is higher than that of the quencher[135]. As shown in Figure 1.28 excited quencher is deactivated into grounded state by light emission or heat dissipation.

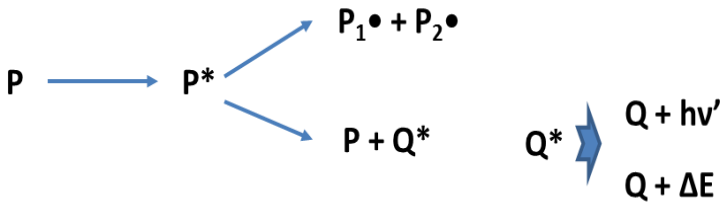

Figure 1.28 Mechanism of energy quenchers[135]

2.5.3.3 Selected Antioxidants

In this study Irgafos 168 which is a hydroperoxide decomposer and Tinuvin622LD which is a hindered amine light stabilizer were selected to examine as an electret additive. In Figure 1.29 Irgafos 168 and its acting mechanism is shown. Irgafos 168 has phosphite group in the center which acts as a trapping agent. Phosphite as a trapping agent has P atom in the center which has [Ne] $3s^2$ $3p^3$ electron distribution and joined to three O atoms which has electron distribution of $1s^2$ $2s^2$ $2p^4$. So two electrons of phosphorus will remain unbounded, which acts in trapping mechanism. These two electrons, increasing nucleophiliciry, are undoubtedly will be effective in charging characteristics. Those electrons will make a bond with oxygen in the carbonyl group and stops sequential reactions.

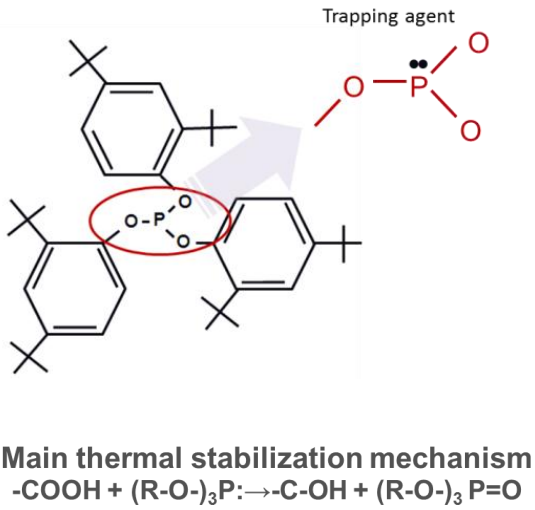

Main thermal stabilization mechanism

$-COOH + (R-O-)_3P: \rightarrow -C-OH + (R-O-)_3 P=O$

Figure 1.29 Chemical structure and acting mechanism of Irgafos168

Irgafos 168 is an effective additive at low concentrations. According to manufacturer data concentrations between 0.2 - 0.8% is sufficient for antioxidation against thermal stresses. So above 1% concentration, excess concentration will not act in stabilizing process and will remain for understanding its effect on electret properties.

Antioxidants, as process stabilizers are competitor with bonds for radical; whereas UV light stabilizers are competitor with bonds for quantum of light energy [152]. Due to difference in their use, they have significant differences in chemistries. In Figure 1.30 chemistry and acting mechanism of Tinuvin 622LD is shown. Peroxy radicals formed upon light induced oxidation will be converted into less reactive nitroxides in the presence of HALS. Complex set of reactions occur which yield not only simple nitroxides but varying products[134,153]. In our case HALS were used not for stabilization against photoinduced oxidation but as an electret additive. So the products will not be similar since the samples were not subjected to photoinduced oxidation.

It was also asserted that HALS amines and amino ethers are not effective alkyl radical scavengers, but are believed to be effective in pacifying the oxidative ability of peroxy radicals. The rate of scavenging of alkyl radicals depends on molecular diffusion of nitroxides.Peroxy radicals are known to be less reactive than alkyl radicals in the reactivity with nitroxides. More than peroxy scavenging alkyl radical scavenging is critical, the rate of which depends on molecular diffusion of nitroxides[153].

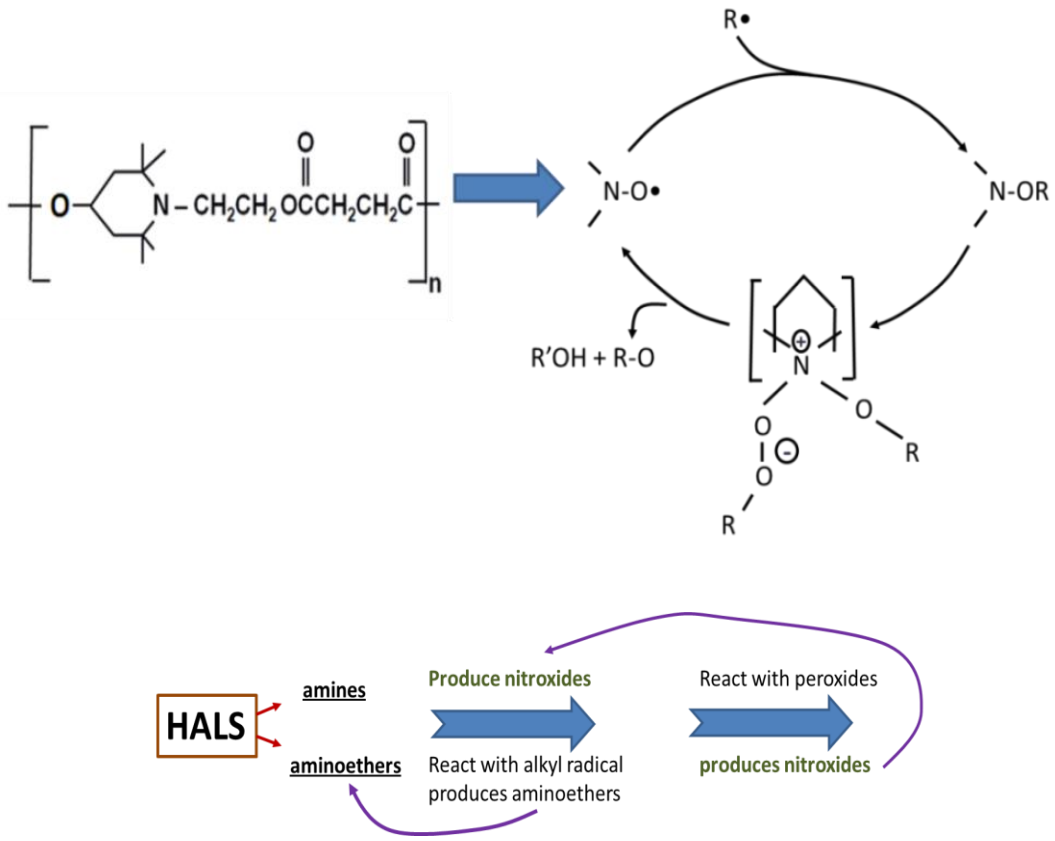

Figure 1.30 Chemical structure and acting mechanism of HALS[153]

As a conclusion remark, we know that solubility parameter of the additive and polymer need to be close enough for compatibility. The additive contains a group (usually a nonpolar tail) that has a very limited solubility in polymer. If the difference is very high, additive will act like filler or a plasticizer[134]. Antioxidants especially ones with an oligomeric structure (like Tinuvin) prefer to stay on lower energy surface. This is

advantageous since stabilization of light mostly will be needed on the surface. This may change surface structure abruptly, thus making it more conductive due to conjugated and cyclic species[154].

2.5.3.4 Electret Properties of Antioxidant/PP

High resistance of polymers leads to long retention of space charges; as charge carriers trapped within the bulk of the polymer. Space charges causes significant changes in the internal electric stress distribution, which eventually result in the premature failure (below the expected breakdown strength of the polymer). So most of the studies were concentrated on space charge formation due to its effect on breakdown properties[155–157]. Formation of carbonyl groups (C=O) also reduce the strength of insulation. To slow down carbonyl formation via oxidation, antioxidants are obligatory to the polymer, thus increasing the life expectancy.

Cartwright et al. studied on the effect of an antioxidant on morphology and space charge formation in LDPE (Low Density Polyethylene)[157]. They found significant changes in polymer morphology as a result of antioxidant addition which changed the ability of polymer to trap charge. They stated that reduction in carbonyl groups due to reduced oxidation in the chemically aged material may lessen the space charge as these groups are highly polar and act as charge trapping sites. Tanaka et observed that both space charge formation and decay

process changed remarkably. Large amount of negative charge accumulation was seen in LDPE-AO (antioxidant) at 50 °C and 70 °C while charge density values at room temperature was not affected by additive addition. Their explanation for temperature dependencies is the differences in morphology between LDPE and LDPE-AO, besides the addition of the antioxidant into the LDPE induces deep trap sites within the system[155].

Addition of antioxidant not only reduces oxidation but also have a significant effect on morphology. Morphological changes were found to have secondary effects on space formation and transportation. More than microstructure defect or impurity content is effective on space charge formation[155,157] An increase in conductivity of PE was observed due to increase in shallow trap density because of structural defects caused by the presence of antioxidant [155] The negative charge injection and the transport within the bulk were found more effective upon addition of antioxidant [155,156]. Antioxidants as an electret additive can act as deep charge traps[155], may change nucleation ability[155,157]. However antioxidants in total were found to increase the mobility of the charge carriers. On the other hand if antioxidants have ability to act like nucleating agents, they should locate in the center of crystal structures. The amount accumulated into intercrystalline regions is expected to play a significant role in charge trapping and transport[155].

Hindered amine light stabilizer (HALS) also affects charge holding capability of polymer. It has been reported that 1% addition of Tinuvin770 in PP lead better charge stability at high temperature, even it showed little impact at low temperatures (42 °C). It is

explained by that additive provides dipolar forces on PP film, which increases the charging capacity[158]. Nishuara et. al. claimed addition of very low concentration HALS impart thermal stability and high charge holding capability. Below 0.01% concentration partial consumption of stabilizer during use will reduce its additional electret effect. Polypropylene was initially modified with 0.03% 2,6-di-tert.-butyl-p-cresol, 0.1% calcium stearate as an halogen catcher. Then various mixtures of HALS, phenolic stabilizers, metal containing hindered phenol, sulfur type stabilizers were added at concentrations in the range 0.01-0.22. The most significant improvement was obtained for samples containing some amount of all additives, however samples containing only Tinuvin 770 at 0.04% concentration also exhibited high charge density.[159]

It seems charge retention of PP upon addition of antioxidants will be a complicated issue due to large changes in composition. In summary antioxidants

i) Can act like deep charge traps.

ii) Can prohibit the generation of ionic species within the material. Chain scisson, mostly observed in polypropylene, creates ionic species in the structure which has catalytic effect on charge transport.

iii) Can cause morphological changes in polymer, such as nucleating effect. Trap sites in the crystalline/amorphous boundaries will carry impure and defective material in the interspherulitic regions.

2.5.4 Oily Mist Resisting Agents

Surface morphology and composition are strongly effective on electrostatic properties of polymeric materials. Resultant water or liquid adsorption properties is particularly effective on charge stability. Water film on surfaces which can be analyzed via ellipsometry studies showed that even hydrophobic PS surface can adsorb a layer of 1nm water[160]. Water has a higher surface tension when compared to oily mist aerosols, meaning formation of oily film on polymer surface will be much easier. Oily mist resistant agents are capable of providing a surface layer with a very low surface tension that prevents formation of conductive liquid layer on charged fiber.

Jones et al described the use of fluorochemical additives to enhance oily mist resistance of the webs. Fluorochemical oxazolidinone, piperazine and perfluorinated alkanes were investigated (Figure 1.31). Specifically those additives have a molecular weight of 500-2500 and a melting temperature of at least 280°C. Those of the additives should be substantially free from mobile polar and/or ionic species. Those additives were designed to be used as melt additive. So they were mixed prior to extrusion and meltblown. After annealing procedure samples were discharged via corona. For some of the embodiements a quality factor of 0.87 was recorded. After loading with 100mg DOP samples lost significant amount of electrostatic filtration efficiency, however modified samples were still better than virgin PP webs[161].

A surface dominated by -CF_3 groups will have a lower surface tension than one dominated by -CF_2[162]. Most probably due to that reason Spartz et al for reasonable enhancement strictly emphasized CF_3:CF_2 ratio of at least 0.15 and a flurosaturation ratio greater than about 200. Fluorosaturation ratio is the atomic percent fluorine of a sample divided by its saturated/unsaturated ratio. It was also claimed high CF_3:CF_2 provides longer thermal stability[163]. In one of the earlier studies of the same group fluorosaturation ratio was less than 200, however fluorine ratio was greater than 40% and one or more heteroatoms were present on the web. Fluorine containing species within plasma were more complicated including SiF_4/C_3F_8, NF_3, BF_3 etc, resulting in various surface chemistries. Samples exhibited high efficiencies even after annealing at 100°C for 9h[164].

In general plasma treatment is utilized for this specific surface composition. Plasma treatment without using any chemical agent, results in various modifications. If enough energy is absorbed at the tertiary carbon site, this leads to chain scission and subsequent etching, while modification at the methyl side group results in functionalities being incorporated at the polymer surface[165]. However plasma medium is filled with various fluorine-containing gases that can react with functional groups and form olephobic surfaces. Elemental fluorine, fluorinated sulfur, fluorinated nitrogen and their combonations were found to be effective. The atmosphere should be free from oxygen and other undesired components (less than 0.1% in volume) since those species are highly active on surface. For achieving this conditions pressure in the atmosphere was reduced below 4Pa. Gas flow,

fluorinated gas concentration and exposure to plasma are another parameters that should be controlled strictly[163].

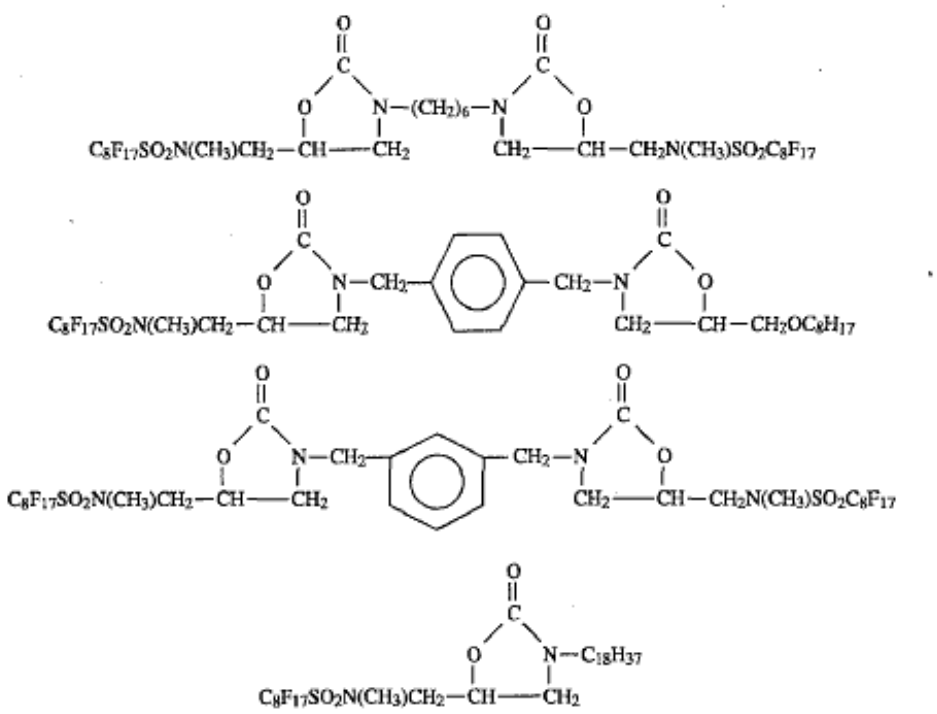

Figure 1.31 Fluorochemical oxazolidinones used in [161]

Having super hydrophobic surface those of the webs would be charged via hydroentanglement method as explained in [166]. Water will probably act like solid jet during the process and webs will be charged due to friction since optimum charging conditions were

provided over a limit pressure (70 to 3500Pa). A quality factor value of 2 was reported when hydrocharging was applied with corona discharge.

2.6 References

1. Gonzalez, C. & others Charge storage mechanisms in polymer electrets. (2006).
2. Bai, M. R., Chen, R.-L. & Wang, C.-J. Electroacoustic analysis of an electret loudspeaker using combined finite-element and lumped-parameter models. *J. Acoust. Soc. Am.* 125, 3632 (2009).
3. Sessler, G. Physical principles of electrets. *Electrets* 13–80 (1979).
4. Goel, M. Electret sensors, filters and MEMS devices: New challenges in materials research. *Curr Sci* 85, 443–453 (2003).
5. Hinds, W. C. *Aerosol technology: properties, behavior, and measurement of airborne particles*. (Wiley: 1999).
6. Sessler, G. M. Self-Biased Condenser Microphone with High Capacitance. *J. Acoust. Soc. Am.* 34, 1787 (1962).
7. Kestel′man, V. N., Pinchuk, L. S. & Gol′dade, V. A. *Electrets in engineering: fundamentals and applications*. (Springer: 2000).
8. Krucinska, I. The influence of technological parameters on the filtration efficiency of electret needled non-woven fabrics. *Journal of Electrostatics* 56, 143–153 (2002).

9. Brown, R. C. & Brown, R. C. *Air filtration: an integrated approach to the theory and applications of fibrous filters*. (Pergamon Press: 1993).

10. Brown, R. C. Electrically charged filter materials. *Engineering Science and Education Journal* 1, 71–79 (1992).

11. Brown, R. C. Capture of dust particles in filters by linedipole charged fibres. *Journal of Aerosol Science* 12, 349–356 (1981).

12. Kowalski, W. J., Bahnfleth, W. P. & Whittam, T. S. Filtration of airborne microorganisms: modeling and prediction. *ASHRAE TRANS* 105, 4–17 (1999).

13. Liu, B. Y. H. & Rubow, K. L. Efficiency, pressure drop and figure of merit of high efficiency fibrous and membrane filter media. *Proceedings of the 5th World Filtration Congress, Nice, Societe Francaise de Filtration, Paris* 3, 112–119 (1990).

14. Eitzman, P. D., Rousseau, A. D., Jones, M. E. & Angadjivand, S. A. *Method of making a fibrous electret web using a nonaqueous polar liquid*. (2002).

15. Brown, R. C. Capture of dust particles in filters by linedipole charged fibres. *Journal of Aerosol Science* 12, 349–356 (1981).

16. Lewis, T. J. Charge transport, charge injection and breakdown in polymeric insulators. *J. Phys. D: Appl. Phys.* 23, 1469–1478 (1990).

17. Teyssedre, G. Charge transport modeling in insulating polymers: from molecular to macroscopic scale. *Dielectrics and Electrical Insulation, IEEE Transactions on* 12, 857–875 (2005).

18. Meunier, M., Quirke, N. & Aslanides, A. Molecular modeling of electron traps in polymer insulators: Chemical defects and impurities. *The Journal of Chemical Physics* 115, 2876 (2001).

19. Meunier, M. & Quirke, N. Molecular modeling of electron trapping in polymer insulators. *The Journal of Chemical Physics* 113, 369 (2000).

20. Guarrotxena, N., Millán, J., Sessler, G. & Hess, G. Charge decay properties of poly (propylene) samples (PP) with various stereochemical compositions. *Macromolecular rapid communications* 21, 691–696 (2000).

21. Nath, R. & Perlman, M. M. Effect of crystallinity on charge storage in polypropylene and polyethylene. *Electrical Insulation, IEEE Transactions on* 24, 409–412 (1989).

22. Ikezaki, K., Kaneko, T. & Sakakibara, T. Effect of crystallinity on electrical conduction in polypropylene. *Japanese Journal of Applied Physics* 20, 609–615 (1981).

23. Ieda, M. Electrical conduction and carrier traps in polymeric materials. *Electrical Insulation, IEEE Transactions on* 162–178 (1984).

24. Xie, H., Wu, X., Peng, Z. & Zhang, H. The energy criterion for breaking chemical bonds in electrical breakdown process of polymers. *Properties and Applications of Dielectric Materials, 1994., Proceedings of the 4th International Conference on* 1, 39–41

25. Ryan, T., Calvert, P. & Billingham, N. The Distribution of Additives and Impurities in Isotactic Polypropylene. *Stabilization and degradation of polymers: based on a*

symposium sponsored by the Division of Polymer Chemistry at the 173rd meeting of the American Chemical Society, New Orleans, Louisiana, March 21-25, 1977 261 (1978).

26. Maier, C. & Calafut, T. *Polypropylene: the definitive user's guide and databook*. (William Andrew: 1998).

27. Stournara, M. E. & Ramprasad, R. A first principles investigation of isotactic polypropylene. *Journal of materials science* 45, 443–447 (2010).

28. Strobel, M. *et al.* Low-molecular-weight materials on corona-treated polypropylene. *Journal of adhesion science and technology* 3, 321–335 (1989).

29. Zhang, Y., Lewiner, J., Alquie, C. & Hampton, N. Evidence of strong correlation between space-charge buildup and breakdown in cable insulation. *Dielectrics and Electrical Insulation, IEEE Transactions on* 3, 778–783 (1996).

30. Stein, R. S. & Powers, J. *Topics in polymer physics*. (Imperial College Press: 2006).

31. Blythe, A. R. & Bloor, D. *Electrical properties of polymers*. (Cambridge University Press: 2005).

32. Mohmeyer, N. *et al.* Additives to improve the electret properties of isotactic polypropylene. *Polymer* 48, 1612–1619 (2007).

33. Kravtsov, A. G., Brünig, H. & Zhandarov, S. F. Analysis of the polarization state of melt-spun polypropylene fibers. *Journal of Materials Processing Technology* 124, 160–165 (2002).

34. Gilbert, R., Crine, J. P., Noirhomme, B. & Pelissou, S. Measurement of organic and inorganic ions in cable insulation and shields. *Electrical Insulation and Dielectric Phenomena, 1989. Annual Report., Conference on* 235–240

35. Ikezaki, K., Yagishita, A. & Yamanouchi, H. Charge trapping sites in spherulitic polypropylene. *Electrets, 1994.(ISE 8), 8th International Symposium on* 428–433 (1994).

36. Arita, Y., Sha Shiratori, S. & Ikezaki, K. A method for detection and visualization of charge trapping sites in amorphous parts in crystalline polymers* 1. *Journal of electrostatics* 57, 263–271 (2003).

37. Mishra, A. Studies of polymer electrets. I. Factors governing the stabilities of homoelectrets obtained from poly (1-olefin) s. *Journal of Applied Polymer Science* 27, 381–395 (1982).

38. Kravtsov, A. G. & Gol'dade, V. A. Optimization of the Electret State of Polymer Fibres. *Fibre Chemistry* 33, 189–192 (2001).

39. Kravtsov, A. G., Zotov, S. V. & Brunig, H. Peculiarities of the electret state of melt-spun and melt-blown fibrous polypropylene materials. *Mechanics of composite materials* 36, 491–496 (2000).

40. Sessler, G. H., Sessler, G. M., Broadhurst, M. G. & Gerhard-multhaupt, R. (CON) *Electrets*. (Laplacian Press: 2000).

41. Hench, L. L. & West, J. K. *Principles of electronic ceramics*. (Wiley: 1990).

42. Kingery, W. D., Bowen, H. K. & Uhlmann, D. R. *Introduction to ceramics*. (Wiley: 1976).

43. Kasap, S. O. *Principles of electrical engineering materials and devices*. (McGraw Hill: 2000).

44. Guarrotxena, N. & Millán, J. On a novel molecular microstructure based approach to the extrinsic space charges releasing in polypropylene (PP). *Polymer Bulletin* 39, 639–646 (1997).

45. Meunier, M., Quirke, N. & Aslanides, A. Molecular modeling of electron traps in polymer insulators: Chemical defects and impurities. *J. Chem. Phys.* 115, 2876 (2001).

46. Behrendt, N. *et al.* Charge storage behavior of isotropic and biaxially-oriented polypropylene films containing α-and β-nucleating agents. *Journal of applied polymer science* 99, 650–658 (2006).

47. Dakin, T. W. Conduction and polarization mechanisms and trends in dielectric. *Electrical Insulation Magazine, IEEE* 22, 11–28 (2006).

48. Zweifel, H., Maier, R. D. & Schiller, M. *Plastics Additives Handbook*. (Hanser Verlag: 2009).

49. Maier, C. & Calafut, T. *Polypropylene: the definitive user's guide and databook*. (William Andrew: 1998).

50. Lovera, D., Bilbao, C., Altst\ädt, V., Schmidt, H. W. & Giesa, R. Electrospun Nanofibers of High Performance Electret Polymers. *Microscopy and Microanalysis* 13, 444–445 (2007).

51. Tsai, P. P., Schreuder-Gibson, H. & Gibson, P. Different electrostatic methods for making electret filters. *Journal of Electrostatics* 54, 333–341 (2002).

52. Lovera, D. *et al.* Charge storage of electrospun fiber mats of poly (phenylene ether)/polystyrene blends. *Polymer Engineering & Science* 49, 2430–2439 (2009).

53. Yeom, B. Y., Shim, E. & Pourdeyhimi, B. Boehmite nanoparticles incorporated electrospun nylon-6 nanofiber web for new electret filter media. *Macromolecular Research* 18, 884–890 (2010).

54. Myers, D. L. & Arnold, B. D. Electret media for HVAC filtration applications. *INJ Winter* 43–54 (2003).

55. Giacometti, J. & Oliveira, O. Corona charging of polymers. *IEEE transactions on electrical insulation* 27, 924–943 (1992).

56. Fletcher, L. A., Noakes, C. J., Sleigh, P. A., Beggs, C. B. & Shepherd, S. J. Air ion behavior in ventilated rooms. *Indoor and Built Environment* 17, 173 (2008).

57. Rader, M. S., Alexeff, I., Tsai, P. P. & Wadsworth, L. C. *Electrostatic charging apparatus and method*. (Google Patents: 1997).

58. Goldman, M., Goldman, A. & Sigmond, R. S. The corona discharge, its properties and specific uses. *Pure & Appl. Chem* 57, 1353–1362 (1985).

59. Shishoo, R., (Manchester, T. I. & England) *Plasma technologies for textiles*. (Woodhead: 2007).

60. Kowalski, W. J., Bahnfleth, W. P. & Whittam, T. S. Filtration of airborne microorganisms: modeling and prediction. *ASHRAE TRANS* 105, 4–17 (1999).

61. Wang, X., Zhang, X., Pan, D., Cao, G. & Xia, Z. Charge storage capability of cross-linked polypropylene electret films. *Properties and Applications of Dielectric Materials, 2009. ICPADM 2009. IEEE 9th International Conference on the* 926–929

62. Yovcheva, T. A., Avramova, I. A., Mekishev, G. A. & Marinova, T. S. Corona-charged polypropylene electrets analyzed by XPS. *Journal of Electrostatics* 65, 667–671 (2007).

63. Nalwa, H. S. *Ferroelectric polymers: chemistry, physics, and applications*. (CRC Press: 1995).

64. *Device For Forming Electrets*. (Google Patents: 1971).

65. Van Turnhout, J. *Method for the manufacture of an electret fibrous filter*. (Google Patents: 1976).

66. Peter Ping-yi Tsai, Guo-wei Qin and Charles Hassenboehler Comparison of Electrostatic Charging At Different Locations In The Melt Blowing Process. *International Nonwovens Journal* 9, (2000).

67. Süzer, S., Argun, A., Vatansever, O. & Aral, O. XPS and water contact angle measurements on aged and corona-treated PP. *Journal of applied polymer science* 74, 1846–1850 (1999).

68. Sellin, N. & Campos, J. S. . Surface composition analysis of PP films treated by corona discharge. *Materials Research* 6, 163–166 (2003).

69. Matsuda, Y., Saito, Y. & Tasaka, S. Dipole polarization formed on surface of polypropylene electrets. *Dielectrics and Electrical Insulation, IEEE Transactions on* 17, 1015–1020 (2010).

70. Briggs, D., Kendall, C. R., Blythe, A. R. & Wootton, A. B. Electrical discharge treatment of polypropylene film. *Polymer* 24, 47–52 (1983).

71. McCarty, L. S. & Whitesides, G. M. Electrostatic Charging Due to Separation of Ions at Interfaces: Contact Electrification of Ionic Electrets. *Angewandte Chemie International Edition* 47, 2188–2207 (2008).

72. Slade, P. E. *Handbook of fiber finish technology*. (CRC Press: 1998).

73. Smith, P. A., East, G. C., Brown, R. C. & Wake, D. Generation of triboelectric charge in textile fibre mixtures, and their use as air filters. *Journal of Electrostatics* 21, 81–98 (1988).

74. Diaz, A. F. & Felix-Navarro, R. M. A semi-quantitative tribo-electric series for polymeric materials: the influence of chemical structure and properties. *Journal of Electrostatics* 62, 277–290 (2004).

75. Németh, E., Albrecht, V., Schubert, G. & Simon, F. Polymer tribo-electric charging: dependence on thermodynamic surface properties and relative humidity. *Journal of electrostatics* 58, 3–16 (2003).

76. Awakuni, Y. & Calderwood, J. H. Water vapour adsorption and surface conductivity in solids. *J. Phys. D: Appl. Phys.* 5, 1038–1045 (1972).

77. Pence, S., Novotny, V. J. & Diaz, A. F. Effect of Surface Moisture on Contact Charge of Polymers Containing Ions. *Langmuir* 10, 592–596 (1994).

78. Angadjivand, S. A., Schwartz, M. G., Eitzman, P. D. & Jones, M. E. *Method and apparatus for making a nonwoven fibrous electret web from free-fiber and polar liquid*. (Google Patents: 2002).

79. Haskett, T. E. *Method for forming an electrostatic fibrous filter web*. (Google Patents: 1998).

80. Rousseau, A. D., Jones, M. E. & Angadjivand, S. A. *Electret filter media containing filtration enhancing additives*. (Google Patents: 1999).

81. Giacometti, J. A. & Oliveira Jr, O. N. Corona charging of polymers. *Electrical Insulation, IEEE Transactions on* 27, 924–943 (1992).

82. Garbett, M. G. *Electret charge technique*. (Google Patents: 1980).

83. Eitzman, P. D., Rousseau, A. D., Jones, M. E. & Angadjivand, S. A. *Method of making a fibrous electret web using a nonaqueous polar liquid*. (Google Patents: 2002).

84. Ignatova, M. *et al.* Study of charge storage in the nanofibrous poly(ethylene terephthalate) electrets prepared by electrospinning or by corona discharge method. *European Polymer Journal* 44, 1962–1967 (2008).

85. Yeom, B. Y., Shim, E. & Pourdeyhimi, B. Boehmite nanoparticles incorporated electrospun nylon-6 nanofiber web for new electret filter media. *Macromolecular Research* 18, 884–890 (2010).

86. Cartwright, G. A., Davies, A. E., Swingler, S. G. & Vaughan, A. S. Effect of an antioxidant additive on morphology and space-charge characteristics of low-density polyethylene. *Science, Measurement and Technology, IEE Proceedings*- 143, 26–34 (1996).

87. Tani, Y. & Takase, S. *Electret sheet and a method for the production of the same*. (Google Patents: 1992).

88. Turkevich, L. A. & Myers, D. L. *Ferroelectric fibers and applications therefor*. (Google Patents: 2000).

89. Behrendt, N. *et al.* Charge storage behavior of isotropic and biaxially-oriented polypropylene films containing α-and β-nucleating agents. *Journal of applied polymer science* 99, 650–658 (2006).

90. Behrendt, N., Altstadt, V., Schmidt, H. W., Zhang, X. & Sessler, G. M. Development of porous polypropylene blends with NA11 particles and glass hollow spheres by biaxial

stretching for electret applications. *Dielectrics and Electrical Insulation, IEEE Transactions on* 13, 992–1000 (2006).

91. Hillenbrand, J., Behrendt, N., Altst\ädt, V., Schmidt, H. W. & Sessler, G. M. Electret properties of biaxially stretched polypropylene films containing various additives. *Journal of Physics D: Applied Physics* 39, 535 (2006).

92. Mohmeyer, N. *et al.* Nucleation of isotactic polypropylene by triphenylamine-based trisamide derivatives and their influence on charge-storage properties. *Polymer* 45, 6655–6663 (2004).

93. Haskett, T. E. *Electrostatic fibrous filter web*. (Google Patents: 1998).

94. Tanaka, Y. *et al.* Effect of additives on morphology and space charge accumulation in low density polyethylene. *Dielectrics and Electrical Insulation, IEEE Transactions on* 10, 148–154 (2003).

95. Rousseau, A. D., Jones, M. E. & Angadjivand, S. A. *Electret filter media containing filtration enhancing additives*. (Google Patents: 1999).

96. Lifshutz, N., Gahan, R. E. & Stevens, G. C. *Charge stabilized electret filter media*. (Google Patents: 1997).

97. Jones, M. E. & Rousseau, A. D. *Oily mist resistant electret filter media*. (Google Patents: 1995).

98. Askeland, D. R. & Phulé, P. P. *The science and engineering of materials*. (Cengage Learning: 2006).

99. Nifuku, M., Zhou, Y., Kisiel, A., Kobayashi, T. & Katoh, H. Charging characteristics for electret filter materials. *Journal of Electrostatics* 51-52, 200–205 (2001).

100. Arlt, G. & Hennings, D. Dielectric properties of fine-grained barium titanate ceramics. *Journal of Applied Physics* 58, 1619–1625 (1985).

101. Kinoshita, K. & Yamaji, A. Grain-size effects on dielectric properties in barium titanate ceramics. *Journal of Applied Physics* 47, 371–373 (1976).

102. Gachigi, K. W. ., Kumar, U. & Dougherty, J. P. Grain size effects in barium titanate. *Ferroelectrics* 143, 229–238 (1993).

103. Roberts, S. Dielectric and Piezoelectric Properties of Barium Titanate. *Phys. Rev.* 71, 890 (1947).

104. Muralidhar, C. & Pillai, P. K. C. XRD studies on barium titanate (BaTiO3)/polyvinylidene fluoride (PVDF) composites. *Journal of Materials Science* 23, 410–414 (1988).

105. Baeten, F., Derks, B., Coppens, W. & van Kleef, E. Barium titanate characterization by differential scanning calorimetry. *Journal of the European Ceramic Society* 26, 589–592 (2006).

106. Mandelkern, L. *Crystallization of polymers*. (McGraw-Hill: 1964).

107. Pritchard, G. *Plastics additives: an A-Z reference*. (Springer: 1998).

108. Botkin, J. H., Dunski, N. & Maeder, D. Improving Molding Productivity And Enhancing Mechanical Properties Of Polypropylene With Nucleating Agents. *Ciba Specialty Chemicals*

109. Brostow, W. *Performance of plastics*. (Hanser Verlag: 2000).

110. Zweifel, H., Maier, R. D. & Schiller, M. *Plastics Additives Handbook*. (Hanser Verlag: 2009).

111. Kristiansen, M. *et al.* The binary system isotactic polypropylene/bis (3, 4-dimethylbenzylidene) sorbitol: phase behavior, nucleation, and optical properties. *Macromolecules* 36, 5150–5156 (2003).

112. Balzano, L., Rastogi, S. & Peters, G. W. . Flow induced crystallization in isotactic polypropylene-1, 3: 2, 4-bis (3, 4-dimethylbenzylidene) sorbitol blends: implications on morphology of shear and phase separation. *Macromolecules* 41, 399–408 (2008).

113. George, H. H. Spinline crystallization of polyethylene terephthalate. *High-speed fiber spinning: science and engineering aspects* 271 (1985).

114. Kumaraswamy, G. Crystallization of Polymers from Stressed Melts. 45, 375 (2005).

115. Jinan, C., Kikutani, T., Takaku, A. & Shimizu, J. Nonisothermal orientation-induced crystallization in melt spinning of polypropylene. *Journal of Applied Polymer Science* 37, 2683–2697 (1989).

116. Gächter, R., Müller, H. & Andreas, H. *Plastics additives handbook: stabilizers, processing aids, plasticizers, fillers, reinforcements, colorants for thermoplastics*. (Hanser: 1985).

117. Erhard, D. *et al.* Recent Advances in the Improvement of Polymer Electret Films. *Advances in Polymer Science,* 1–53 (2010).

118. Mohmeyer, N., Schmidt, H. W., Kristiansen, P. M. & Altst\ädt, V. Influence of chemical structure and solubility of bisamide additives on the nucleation of isotactic polypropylene and the improvement of its charge storage properties. *Macromolecules* 39, 5760–5767 (2006).

119. Hillenbrand, J., Behrendt, N., Altst\ädt, V., Schmidt, H. W. & Sessler, G. M. Electret properties of biaxially stretched polypropylene films containing various additives. *Journal of Physics D: Applied Physics* 39, 535 (2006).

120. Hillenbrand, J. *et al.* Charge retention in biaxially-oriented polypropylene films containing various additives. *Electrets, 2005. ISE-12. 2005 12th International Symposium on* 276–279 (2005).

121. Behrendt, N., Altstadt, V., Schmidt, H. W., Zhang, X. & Sessler, G. M. Development of porous polypropylene blends with NA11 particles and glass hollow spheres by biaxial stretching for electret applications. *Dielectrics and Electrical Insulation, IEEE Transactions on* 13, 992–1000 (2006).

122. Tani, Y. & Tokuda, S. *Electret Filter*. (Google Patents: 1995).

123. Influence of quenching on the charge stability of polymer electrets. 543–547 (1988).doi:10.1109/ISE.1988.38622

124. Libster, D., Aserin, A. & Garti, N. Advanced nucleating agents for polypropylene. *Polymers for Advanced Technologies* 18, 685–695 (2007).

125. Thierry, A., Straupé, C., Wittmann, J. C. & Lotz, B. Organogelators and Polymer Crystallisation. *Macromolecular Symposia* 241, 103–110 (2006).

126. Yoshimoto, S. *et al.* Epitaxial act of sodium 2,2'-methylene-bis-(4,6-di-t-butylphenylene)phosphate on isotactic polypropylene. *Polymer* 42, 9627–9631 (2001).

127. Hawkins, W. L. & Chemistry, A. C. S. D. of P. *Stabilization and degradation of polymers: based on a symposium sponsored by the Division of Polymer Chemistry at the 173rd meeting of the American Chemical Society, New Orleans, Louisiana, March 21-25, 1977*. (American Chemical Society: 1978).

128. Hawkins, W. L., Matreyek, W. & Winslow, F. H. The morphology of semicrystalline polymers. Part I. The effect of temperature on the oxidation of polyolefins. *Journal of Polymer Science* 41, 1–11 (1959).

129. Maier, C. & Calafut, T. *Polypropylene: the definitive user's guide and databook*. (William Andrew: 1998).

130. Lutz, J. T. & Grossman, R. F. *Polymer modifiers and additives*. (CRC Press: 2001).

131. Schnabel, W. *Polymers and light: fundamentals and technical applications*. (Wiley-VCH: 2007).

132. Kravtsov, A. G. & Gol'dade, V. A. Optimization of the Electret State of Polymer Fibres. *Fibre Chemistry* 33, 189–192 (2001).

133. Mizutani, T. & Ieda, M. TSC from corona-charged high-density polyethylene and the effects of oxidation. *Journal of Physics D: Applied Physics* 11, 185 (1978).

134. Sessler, G. H., Sessler, G. M., Broadhurst, M. G. & Gerhard-multhaupt, R. (CON) *Electrets*. (Laplacian Press: 2000).

135. Kravtsov, A. G., Zotov, S. V. & Brunig, H. Peculiarities of the electret state of melt-spun and melt-blown fibrous polypropylene materials. *Mechanics of composite materials* 36, 491–496 (2000).

136. S\üzer, S., Argun, A., Vatansever, O. & Aral, O. XPS and water contact angle measurements on aged and corona-treated PP. *Journal of applied polymer science* 74, 1846–1850 (1999).

137. Noeli, S. Surface composition analysis of PP films treated by corona discharge. (2003).

138. Briggs, D., Kendall, C. R., Blythe, A. R. & Wootton, A. B. Electrical discharge treatment of polypropylene film. *Polymer* 24, 47–52 (1983).

139. Dipole polarization formed on surface of polypropylene electrets. *Dielectrics and Electrical Insulation, IEEE Transactions on* 17, 1015–1020 (2010).

140. Strobel, M. *et al.* Low-molecular-weight materials on corona-treated polypropylene. *Journal of adhesion science and technology* 3, 321–335 (1989).

141. Jones, V., Strobel, M. & Prokosch, M. J. Development of poly (propylene) surface topography during corona treatment. *Plasma Processes and Polymers* 2, 547–553 (2005).

142. Strobel, M. *et al.* A comparison of corona-treated and flame-treated polypropylene films. *Plasmas and polymers* 8, 61–95 (2003).

143. Strobel, M. & Lyons, C. S. The role of low-molecular-weight oxidized materials in the adhesion properties of corona-treated polypropylene film. *Journal of adhesion science and technology* 17, 15–23 (2003).

144. Vasile, C. *Handbook of polyolefins*. (CRC Press: 2000).

145. Zweifel, H., Maier, R. D. & Schiller, M. *Plastics Additives Handbook*. (Hanser Verlag: 2009).

146. Zweifel, H. *Stabilization of Polymeric Materials State-Of-The-Art, Scope and Limitations*. (Heidelberg: Springer: 1998).

147. Beckwith, A. L. J., Bowry, V. W. & Ingold, K. U. Kinetics of nitroxide radical trapping. 1. Solvent effects. *Journal of the American Chemical Society* 114, 4983–4992 (1992).

148. Lutz, J. T. & Grossman, R. F. *Polymer modifiers and additives*. (CRC Press: 2001).

149. Step, E. N., Turro, N. J., Gande, M. E. & Klemchuk, P. P. Mechanism of Polymer Stabilization by Hindered-Amine Light Stabilizers (HALS). Model Investigations of the Interaction of Peroxy Radicals with HALS Amines and Amino Ethers. *Macromolecules* 27, 2529–2539 (1994).

150. Schlotter, N. E. & Furlan, P. Y. A review of small molecule diffusion in polyolefins. *Polymer* 33, 3323–3342 (1992).

151. Tanaka, Y. *et al.* Effect of additives on morphology and space charge accumulation in low density polyethylene. *Dielectrics and Electrical Insulation, IEEE Transactions on* 10, 148–154 (2003).

152. Tebani, M., Boudou, L. & Guastavino, J. Thermally stimulated depolarization current and space charge measurements on low-density polyethylene: Influence of the presence of antioxidant. *Journal of Applied Polymer Science* 109, 2768–2773 (2008).

153. Cartwright, G. A., Davies, A. E., Swingler, S. G. & Vaughan, A. S. Effect of an antioxidant additive on morphology and space-charge characteristics of low-density polyethylene. *Science, Measurement and Technology, IEE Proceedings*- 143, 26–34 (1996).

154. Albini, A., Degli Esposti, G., Guastavino, F. & Tommasini, D. Charging phenomena in polypropylene films. *Conduction and Breakdown in Solid Dielectrics, 1989., Proceedings of the 3rd International Conference on* 148–152

155. Nishiura, E. & Ando, K. *Electret materials and the method for preparing the electret materials*. (Google Patents: 1991).

156. Németh, E., Albrecht, V., Schubert, G. & Simon, F. Polymer tribo-electric charging: dependence on thermodynamic surface properties and relative humidity. *Journal of Electrostatics* 58, 3–16 (2003).

157. Jones, M. E. & Rousseau, A. D. *Oily mist resistant electret filter media*. (Patents: 1995).

158. Berg, J. C. *Wettability*. (M. Dekker,: New York, c1993.

159. Spartz, G. R. *et al. Electret article having high fluorosaturation ratio*. (Google Patents: 2007).

160. Kirk, S. M., Spartz, G. R., Jones, M. E., Pachuta, S. J. & Huberty, J. S. *Electret Article Having Heteroatoms And Low Fluorosaturation Ratio*. (Google Patents: 2007).

161. France, R. M. & Short, R. D. Plasma Treatment of Polymers: The Effects of Energy Transfer from an Argon Plasma on the Surface Chemistry of Polystyrene, and Polypropylene. A High-Energy Resolution X-ray Photoelectron Spectroscopy Study. *Langmuir* 14, 4827–4835 (1998).

162. Angadjivand, S. A., Jones, M. E. & Meyer, D. E. *Electret filter media*. (Google Patents: 2000).

CHAPTER 3

3 Optimizing Charging Properties of $BaTiO_3$/Polypropylene Composite Filaments

Abstract

Mostly being an undesired property, charge retention of polymeric fibers is critical for electrostatic filtration process. To improve long term charge holding properties of fibers, additives such as nucleating agents, antioxidants, fluorochemicals and high dielectric inorganics were used in the previous studies. In this work charging properties of polypropylene (PP) filaments were investigated upon blending with barium titanate ($BaTiO_3$). Maleic anhydride grafted polypropylene (MA-g-PP) was added to enhance miscibility. It was shown that both initial potential values and charge retention stability were improved after modification. Samples were treated with corona discharge for different timings to find optimum conditions at which saturation in terms of charge holding capability was reached. Isothermal potential decay method was modified to compare long term electrostatic behavior of filaments. Important microstructural factors acting on electret properties such as crystal structure and chain orientation were also investigated via Differential Scanning Calorimetry (DSC), Wide Angle X-ray Diffractometry (WAXD) and Interference Microscopy.

3.1 Introduction

Electret filters, holding quasipermanent electrostatic property are of particular interest due to their high filtration efficiency without increase in resistance to airflow. Submicron size particle capture by mechanical means involves three mechanisms: diffusion, interception, and inertial impaction which are basically dependent on fiber diameter and solidity [167]. In electret filters, electrostatic attraction as a fourth mechanism will be effective on particle capture. For high capture efficiency, charge density should be at a level and conserved during filtration.

Polypropylene with a large band gap and tailorability with additives is a widely investigated and used polymer for electret filter applications. Having very low dielectric constant, its electret property is mostly related with inherent and injected charges[168]. To reach high and stable filtration efficiency, charge density and stability of PP fibers are important and charging properties are related with various properties either at molecular or morphological scale. To improve such properties, various additives were investigated as "electret additive". These additives provide various functionalities from the aspect of electrostatics. For instance by adding nucleating agents smaller spherulites are reported whose boundaries are traps for space charges[169,170]. For nonsoluble nucleating agents such as NA11, microvoids were obtained upon stretching which prohibit charge migration [171]. By adding polar additives dielectric constant of the system could be increased. Some recent studies deal with fluorochemicals as oil mist resistant agents to improve oleophobicity, thus

prohibits the formation of conductive film during oily aerosol filtration[172–176]. It can be said that each additive brings a different solution to fulfill complicated electrostatic requirements.

In this study one of the most widely investigated ferroelectric, barium titanate was selected as an electret additive. Barium titanate has an ABO_3 type mixed oxide structure. Smaller Ti cations occupy the central octahedral B site and barium cations fill the interstices between octahedra. The high polarizability is a result of more space for small Ti ions between the oxygen ions. A net permanent dipole moment of the octahedron can result only by a unilateral displacement of the positively charged Ti^{+4} against its negatively charged O^{-2} surrounding, thus giving a high dielectric constant[67,47]. Maleic anhydride grafted PP, as a coupling agent between inorganic $BaTiO_3$ powder and PP was used to enhance miscibility. MA-g-PP has a potential to cause polarity, however as Van Turnhout stated its fairly low dipolar relaxation temperature will result in easy depolarization at even room temperature [13].

Not only additives, but also microstructure will affect the charge retention. Karanja and Nath [14] compared commercial BOPP (biaxially oriented PP) and unoriented PP films in which crystallinity values were determined 66.5% and 34% respectively. They observed the half-life period of the charge-decay temperature increased with crystallinity. From the aspect of morphological characteristics, it can be said that the charges buried in solid crystalline regions cannot escape easily. Myslinski et al[15] showed reduction in charge retention ability upon annealing which destroy effective crystal defects. Upon increasing annealing temperature to 130°C, defect concentration dropped significantly and charge density and

depth of energetic traps reduced. On the other hand if crystal size is reduced somehow, space charge retention would be more efficient. Therefore nucleating agents are utilized for providing smaller crystals and modifying crystal and amorphous boundaries[16–18]. However from thermally stimulated discharge analysis, Kravtsov et al showed that such space charges are rapidly lost at low temperatures for PP filaments [19].

Even several studies[16–18,20–22] have reported electret properties on films, these results cannot be directly applied to fibrous filter media since fibrous materials and films poses significant morphological differences. Therefore we invesitated electret properties of filaments directly since we are dealing with fibrous filter media. For charging fibrous webs several methods such as corona discharge, liquid contact, triboelectrification, induction were described in the literature[23]. Corona discharge is generally preferred due to ease of operation and low cost[20]. Isothermal surface potential decay (ISPD) method was used to analyze charged fibrous samples. To do that filaments were aligned in a specific fashion, thus enormous deviations observed in measurements of previous studies[24] were reduced significantly.

3.2 Materials & Methods

Materials. PP resin of 34 MFR value (10 min at 230°C) was kindly provided from Sunoco Chemicals. PP resin had a number average molecular weight of ~55,000g/mole,

whereas weight average molecular weight is ~180,000g/mole. Barium titanate in powder form was purchased from Ferro Electronics, OH. 90% of the particles have diameters smaller than 2.1μm and 10% of them were smaller than 0.8 μm according to manufacturer data. A dielectric constant of 2300 was reported for the powder. Maleic anhydride grafted PP (Exxelor PO 1020) manufactured by Exxon Chemicals was used.

Electret filters are produced in the nonwoven form of either meltblown[25], spunbond[26], resin impregnated needled[27] or split from films[26]. Due to the end use in the form of nonwoven, rather than films, electret properties should be investigated on filaments. Before spinning the composite filaments, masterbatch at 20% concentration was prepared [Techmer PM, TN] to enhance the homogeneity. Then control and modified PP filaments containing $BaTiO_3$ at 1%, 3%, 5% concentrations and MA-g-PP at 4% concentration were produced. Samples were melt-spun in the Hills multifilament spinning line in the Nonwovens Institute (single- screw extruder with L: D ratio 1:24, the number of holes in spinhead is 72) in which the spinning speed was 2000 m/min and the throughput was 0.58 g/h/min. Temperature of spin head was fixed at 235°C.

Multifilament samples were washed with deionized water at 45°C for 6h to remove spinfinish applied during melt spinning process. The washing fluid was replaced every 2h. Use of any detergent or surface active was not preferred; since samples might be contaminated with the chemicals even after rinsing. Yarns wounded on washing tubes were dried overnight.

Charging and Characterization of Charging Property. After drying, yarns were aligned parallel on aluminum sample holders with a given spacing (10 yarns/cm) as shown in Figure 3.1. It was observed that any fiber protruding from specimen caused significant variations on measured value, so to fix protruding fibers perpendicular yarns were aligned at a distance of 0.7cm from each other. The filaments were fixed carefully by using conductive tape and epoxy.

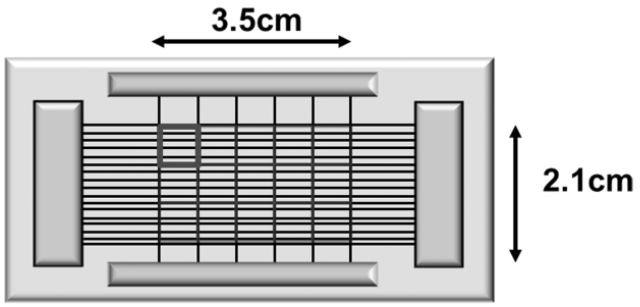

Figure 3.1 Specimen for ISPD test and surface potential detection points

Charging of the samples was carried out with a negative corona discharger (Mystic Marvels, Model NIP-7E) and the applied voltage was fixed at 9kV where maximum output direct current of the emitter needle was about 160 μA. Charging was done at laboratory conditions in which relative humidity was kept fixed between 54-58% RH at 22-23°C temperature. Samples were charged for 3 different timings: 10 seconds, 1, and 10 minutes.

The surface potential was measured with Monroe 244 Model electrostatic voltmeter. Three specimen were prepared from each samples and average values and standard deviations were calculated thereof. 15 specific points per sample across the sample surface was used for evaluation. The initial measurements (V_0) were taken directly after charging. All following measurements for surface potential decay test were carried out after fixed annealing times at 80°C. The periods in the oven were 0.5h, 1h, 2h, 4h, 8h, 12h, 16h, and 24h. Due to the nature of decay, periods kept shorter initially. Samples after annealing were cooled for 10 minutes in a desiccator to prohibit the effect of atmosphere.

Fiber microstructure. Optical microscopy images were taken randomly to understand the distribution of $BaTiO_3$ particles inside PP filament. Zeiss optical microscope with an objective of 40X was used and images of filament samples were captured with Nikon high-definition color camera- DS-Fi1.

Melting and crystallization behavior of the composite filaments was analyzed using Perkin-Elmer differential scanning calorimeter (DSC). $BaTiO_3$/MA-g-PP/PP samples (4.0 ±0.5 mg) were heated in a nitrogen atmosphere from 25°C to 190°C at a rate of 20°C/min and allowed to stand for 4 minutes at 190°C and then cooled from 190°C to 25°C at a rate of 20°C/min. The crystallinity of the samples was calculated using the following formula:

$$\%Crystallinity = \frac{\Delta H}{\Delta H_{PP}^{0}} \times 100 \qquad \text{Equation 3.1}$$

where, ΔH is the enthalpy of fusion of the sample (J/g) and ΔH_{PP}^{0} is the enthalpy of fusion of completely crystalline PP (~ 207 J/g) [28].

Crystal structures of the samples were calculated using Omni Instrumental X-ray diffractometer. The diffractometer is equipped with Be-filtered Cu-Kα radiation with a wavelength of 1.54 Å generated at 35 kV and 25 mA. The samples were scanned from 2Θ range from 5° to 40° at an increment of 0.5°. The crystal sizes of the samples were calculated using the Scherrer's equation [29]:

$$t = \frac{0.9 \times \lambda}{B \times \cos \theta_B} \qquad \text{Equation 3.2}$$

where t is crystal size (Å), λ is wavelength of X-ray (1.54 Å), B is full width at half maximum (radian), and Θ_B is Bragg angle (degree).

Birefringence of the samples was measured using Aus Jena Interference microscopy. The wavelength of the polarized light used was 546 nm. The refractive indices of fibers parallel and perpendicular to fiber axis were calculated from the interference fringe shift and the birefringence of the samples were calculated using the following formula:

$$\Delta n = \left| n_{\parallel} - n_{\perp} \right| \qquad \text{Equation 3.3}$$

where $n_{\parallel}$ and $n_{\perp}$ indicate refractive index of the samples parallel and perpendicular to fiber axis respectively.

3.3 Results and Discussion

3.3.1 Microstructure

From the optical micrographs given in Figure 3.2, it is seen that $BaTiO_3$ particles were not agglomerated.

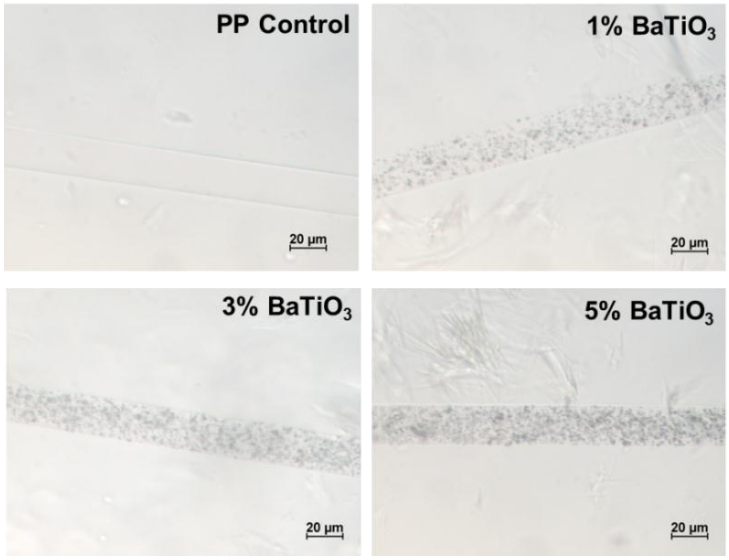

Figure 3.2 Optical micrographs of the samples

As seen on Figure 3.3 single DSC curves were obtained from PP/$BaTiO_3$/MA-g-PP compositions which means a high compatibility was achieved. Two consecutive peaks were observed in heating thermograms. Probable reasons for double melting peaks were

mentioned to be due to more than one type of crystals formed, reorganization during heating, and segregation of highly defective molecules [30,31]. When $BaTiO_3$ concentration increases, the second peak becomes invisible.

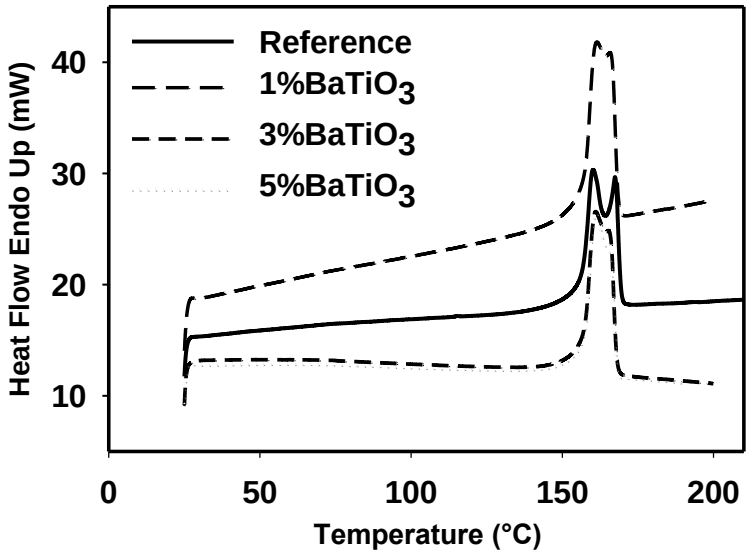

Figure 3.3 DSC melting thermograms for samples.

As shown in Table 3.1 crystallinity of PP filaments decreases upon modification with $BaTiO_3$ and MA-g-PP. Width of the endotherm (ΔW) for modified filaments got narrower with increasing $BaTiO_3$ concentration, which indicates uniform crystal size distribution.

Table 3.1 DSC analysis of reference and modified samples

Sample	Crystallinity (%)	Melt Onset Temperature (°C)	Melt End Temperature (°C)	Width of Endotherm(ΔW)
PP Cont.	43.9	156.4	169.4	13.0
1%$BaTiO_3$	42.9	156.9	168.5	11.6
3%$BaTiO_3$	42.6	156.9	167.9	11.0
5%$BaTiO_3$	39.9	157.2	168.0	10.9

WAXD analysis revealed addition of $BaTiO_3$ and MA-g-PP alters crystalline structure of fibers. As shown in Figure 3.4, crystalline peaks were detected at about 2θ=14.8°, 17.4° and 19.3° which correspond to (110), (040) and (130) planes in the PP[32,33]. $BaTiO_3$ addition did not affect crystalline d-spacings, where peaks were found at almost identical position, except slight shift to 2θ= 17.7° (d = 5.0 Å) in $BaTiO_3$ containing samples from 17.4° (d=5.1 Å) in PP control filaments.

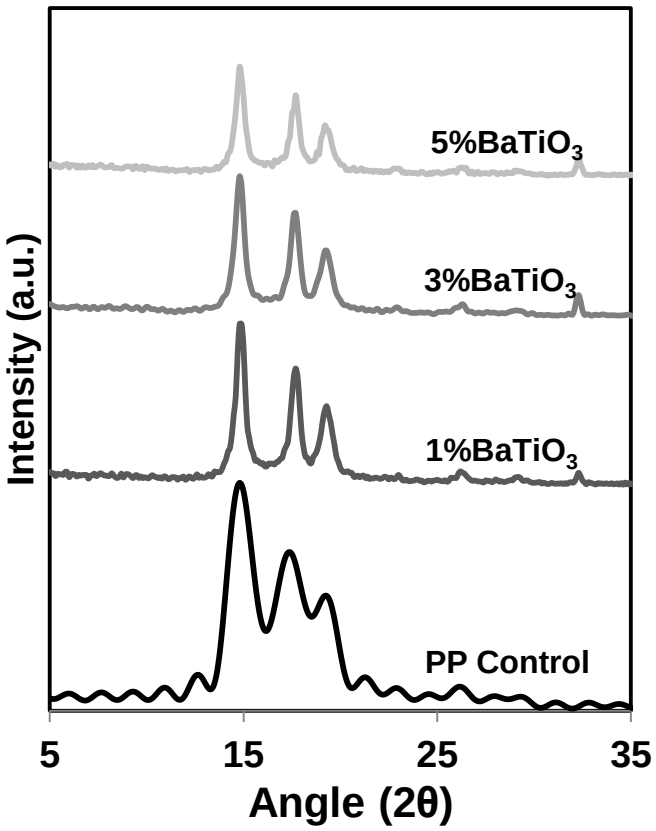

Figure 3.4 WAXD spectra for reference and modified PP filaments. The spectra were recorded at angles covering three major characteristic diffraction peaks of the PP.

Diffraction peaks which become sharper and more distinct after $BaTiO_3$ indicate larger crystals upon modification. When crystal sizes were calculated according to Scherrer equation (Figure 3.5), significant increase were observed after modification with $BaTiO_3$ and MA-g-PP. Thermodynamic interactions between $BaTiO_3$ particles and PP may result in

larger crystals. Interfaces between barium titanate particles and polymer will have higher energy, which may initiate lamellar growth earlier at higher temperature and cause them to be thicker. Modified samples have similar crystal sizes, which is drastically different from that of reference sample. Especially thickness corresponding to (040) plane increases significantly.

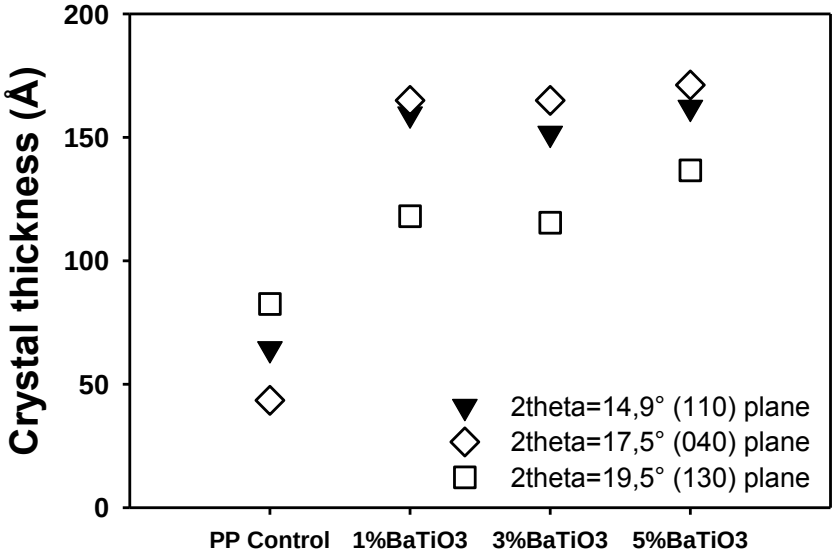

Figure 3.5 Crystal sizes calculated according to Schrerrer equation

Addition of $BaTiO_3$ resulted in a drop in birefringence of PP filaments which indicates lower molecular orientation; even the spinning conditions used were identical

[Figure 3.6]. It is presumably can be said that molecular motions in a more oriented structure will be lower due to better packaging. Jain et al[21] observed higher charge density and activation energy on highly stretched virgin PP films. According to their approach stretching deforms the crystalline–amorphous structure in various ways such as affecting the strength of physical bonds between the molecules due to compression forces between the polymer chains and thus modifying the trap structure. Increase in charge density was attributed to new deep traps, which were created at the amorphous-crystalline interface by stretching[6,4,14,21]. On the other hand it is known higher drawing ratio will result in higher molecular orientation. Kravtsov et al[19] charged meltspun PP fibers during extrusion at different stages. They obtained better results for filaments drawn at 2000m/min, than that of at 3000m/min. However rather than molecular orientation this improvement may also be attributed to the fact filaments passing through at 2000 m/min will be charged for longer time at molten state. For any semicrystalline polymer, chain mobility will be higher in amorphous regions, which will be destructive for the stability of accumulated charges and polarized species. And this was observed after $BaTiO_3$ addition.

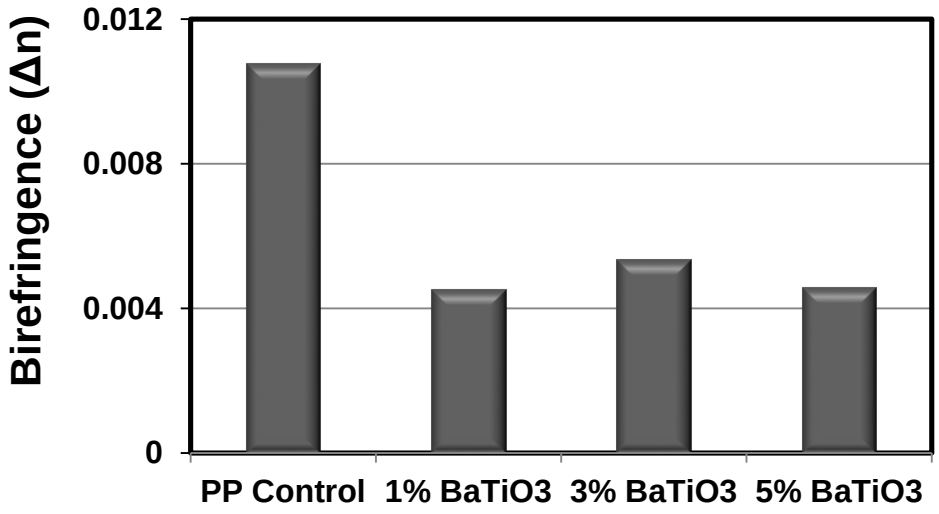

Figure 3.6 Birefringence value for $BaTiO_3$ containing filaments

3.3.2 Surface Potential Decay Tests

Yarns were aligned uniformly on metal plates like a film structure. This configuration reduced average CV values of potential measurements between 3 specimens below 20%, which is reasonable and even inevitable due to varying fiber chemistry and microstructure. Similar to films[169,170,180], exponential decay curves were observed for fibers charged for 1 min as shown in Figure 3.8.

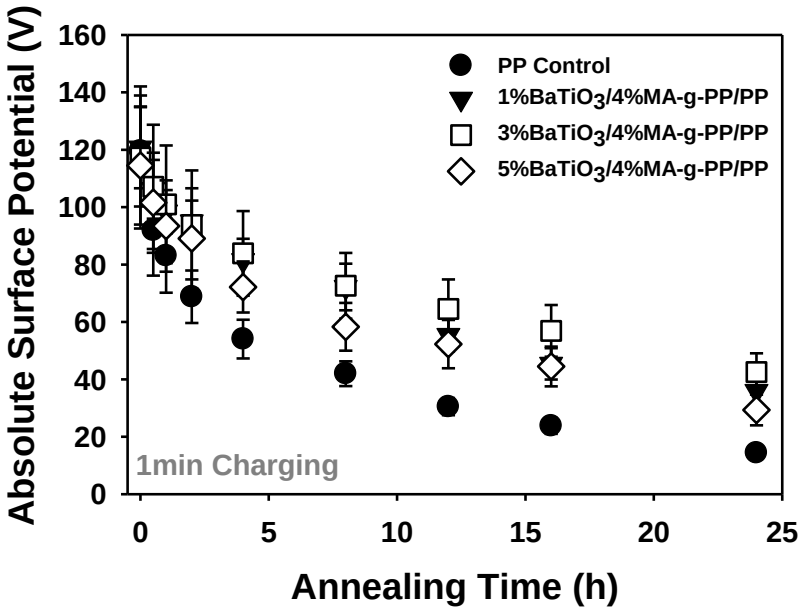

Figure 3.7 Surface potential decay after charging for 1min

As discussed earlier for the case of electret filters initial potential will indicate initial electrostatic filtration performance, where stability of the potential will show durability of the filter performance. In Figure 3.8 potentials after various charging times were compared.

Charged sample surface and corona drift region will reach to an equilibrium state and no further charge trapping or polarization was expected after saturation time. It can be said that 10 seconds charging time is not enough for saturation. The initial potentials increased approximately 10-20% after 1min charging. Longer charging time did not resulted in an increase in the potential, which shows 1min charging is optimum.

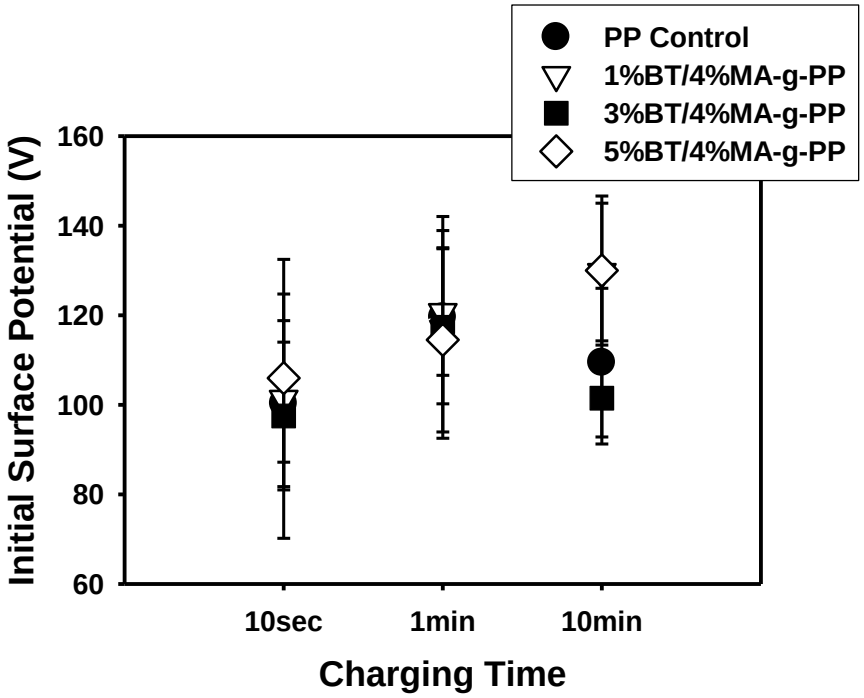

Figure 3.8 Initial surface potentials after charging for various times

For comparing potential stability, exponential decay curves can be analyzed with simple relaxation time equation:

$$V = V_0 * \exp\left(-t/\tau\right) \qquad \text{Equation 3.4}$$

where V denotes potential at a given time; V_0, initial surface potential; τ, relaxation time. Thus τ values indicate the time where remaining potential was reduced to 1/e th of initial. In Figure 3.9 calculated relaxation times were compared. Longer charging time did not resulted in longer charge stability either, which is probably due to increased oxidation [34]. As a result 1

and 3% $BaTiO_3$/ 4% MA-g-PP/ PP at 1 min charging time can be considered as the most superior system from the aspect of charge stability, which still had about 30% of initial potential after annealing for 24 h.

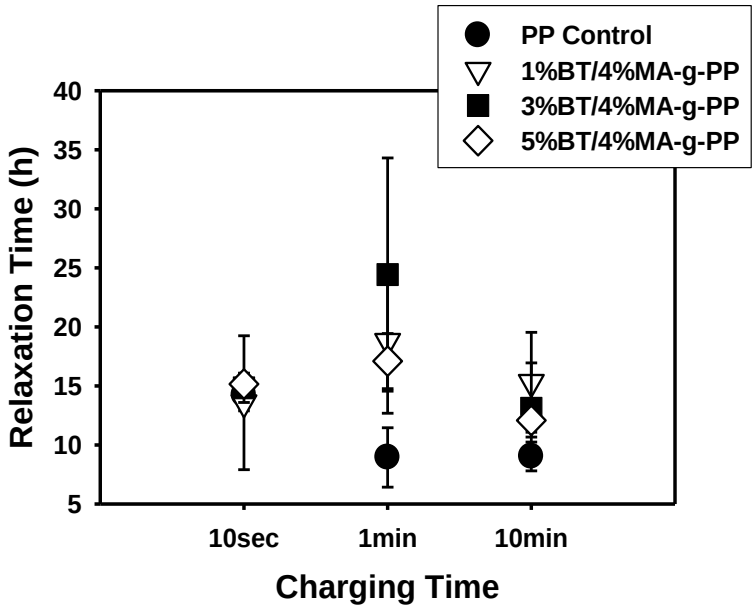

Figure 3.9 Relaxation times for various charging times

For inorganic additive/polymer composites Maxwell-Wagner polarization may be expected to be occurred not only between crystal-amorphous interfaces but also within polymer-particle boundaries [35]. As a result comparatively a higher initial potential was observed for modified samples. Decay followed the typical exponential trend which

consisted of two parts: (1) initial fast decay zone and (2) slow decay zone. Based on the findings of Kravtsov et al initial fast decay zone can be conducted to instant loss of Maxwell-Wagner type polarization for PP at low temperatures[168]. The surface potential decreases with an initial stiff slope within an hour of annealing time. Figure 3.10 shows the potential loss rate vs time curve for samples charged for 1min. This graph shows that initial potential loss in control sample is significantly larger than that of modified samples. Probably polarized $BaTiO_3$ particles reduced the instant loss of space charges. At the end of the day potential decay rate becomes similar for all samples.

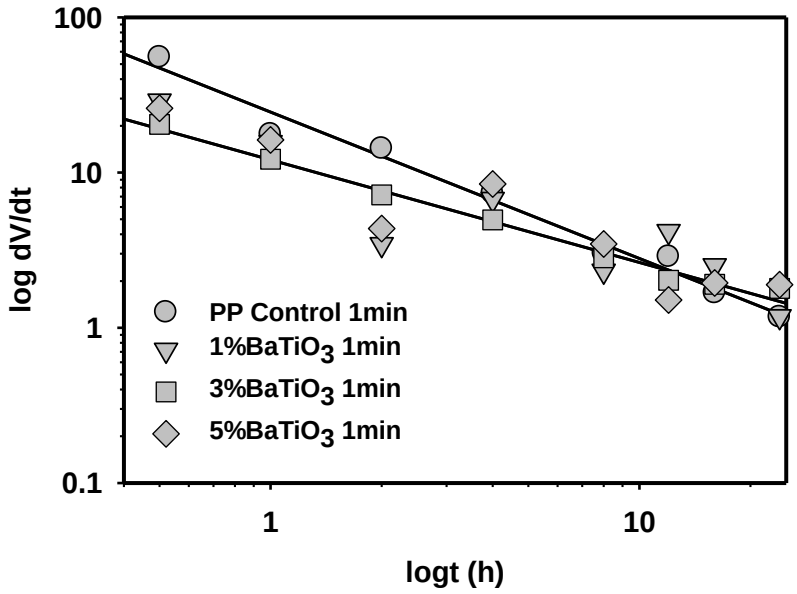

Figure 3.10 log dV/dt vs log t curves

3.4 Conclusion

A reliable technique is explained for measuring surface potential of filaments which are unit structures of nonwoven webs. Variations were thought to be limited to varying composition and microstructure in a definite length and minimized significantly. A significant increase in charge stability upon charging 1min was obtained for barium titanate and maleic anhydride containing PP filaments. According to microstructure analysis, there is a significant change in crystal sizes and molecular orientation. Despite those negative changes, improvement in electret properties after additive addition shows $BaTiO_3$ would be a good candidate as an electret additive for PP. It was also shown longer charging times are not proper for charge retention probably due to oxidation of filament surface.

3.5 References

1. Brown, R. C. & Brown, R. C. *Air filtration: an integrated approach to the theory and applications of fibrous filters*. (Pergamon Press: 1993).
2. Kravtsov, A., Brünig, H., Zhandarov, S. & Beyreuther, R. The electret effect in polypropylene fibers treated in a corona discharge. *Advances in Polymer Technology* 19, 312–316 (2000).

3. Mohmeyer, N. *et al.* Additives to improve the electret properties of isotactic polypropylene. *Polymer* 48, 1612–1619 (2007).

4. Mohmeyer, N., Schmidt, H. W., Kristiansen, P. M. & Altstadt, V. Influence of Chemical Structure and Solubility of Bisamide Additives on the Nucleation of Isotactic Polypropylene and the Improvement of Its Charge Storage Properties†. *Macromolecules* 39, 5760–5767 (2006).

5. Behrendt, N. *et al.* Charge storage behavior of isotropic and biaxially-oriented polypropylene films containing alpha- and beta-nucleating agents. *Journal of Applied Polymer Science* 99, 650–658 (2006).

6. Rousseau, A. D., Jones, M. E. & Mei, B. Z. Electret articles and filters with increased oily mist resistance. (2001).

7. Rousseau, A. D., Jones, M. E. & Mei, B. Z. Method of making electret articles and filters with increased oily mist resistance. (2000).

8. Jones, M. E., Rousseau, A. D. & others *Oily mist resistant electret filter media*. (Google Patents: 1995).

9. Jones, M. E., Rousseau, A. D. & others *Oily mist resistant electret filter media and method for filtering*. (Google Patents: 1995).

10. Huberty, J. S. *Oily-mist resistant filter that has nondecreasing efficiency*. (Google Patents: 2003).

11. Kao, K.-C. *Dielectric phenomena in solids: with emphasis on physical concepts of electronic processes*. (Academic Press: 2004).

12. Nalwa, H. S. *Ferroelectric polymers: chemistry, physics, and applications*. (CRC Press: 1995).

13. Van Turnhout, J., Droppert, P. J. & Wubbenhorst, M. PP-based blends for electret filters-an appraisal. *Electrets, 1994.(ISE 8), 8th International Symposium on* 961–966 (1994).

14. Karanja, P. & Nath, R. Study of charge storage properties in biaxially oriented polypropylene.

15. Mysacute; Linacuteski, P. & Kryszewski, M. The effect of crystalline structure on the thermally stimulated discharge current of isotactic polypropylene. *Acta Polymerica* 38, 253–258 (1987).

16. Behrendt, N. *et al.* Charge storage behavior of isotropic and biaxially-oriented polypropylene films containing α-and β-nucleating agents. *Journal of Applied Polymer Science* 99, 650–658 (2005).

17. Mohmeyer, N. *et al.* Additives to improve the electret properties of isotactic polypropylene. *Polymer* 48, 1612–1619 (2007).

18. Mohmeyer, N. *et al.* Nucleation of isotactic polypropylene by triphenylamine-based trisamide derivatives and their influence on charge-storage properties. *Polymer* 45, 6655–6663 (2004).

19. Kravtsov, A. G., Brünig, H. & Zhandarov, S. F. Analysis of the polarization state of melt-spun polypropylene fibers. *Journal of Materials Processing Technology* 124, 160–165 (2002).

20. Erhard, D. *et al.* Recent Advances in the Improvement of Polymer Electret Films. *Complex Macromolecular Systems II* 155–207 (2010).at <http://dx.doi.org/10.1007/12_2009_45>

21. Jain, V. & Mittal, A. Charge storage studies of unstretched and stretched polypropylene film electrets using short circuit TSDC technique. *Journal of Materials Science Letters* 19, 1991–1994 (2000).

22. Hillenbrand, J., Behrendt, N., Altst\ädt, V., Schmidt, H. W. & Sessler, G. M. Electret properties of biaxially stretched polypropylene films. *Journal of Physics D: Applied Physics* 39, 535–540 (2006).

23. Myers, D. L. & Arnold, B. D. Electret media for HVAC filtration applications. *INJ Winter* 43–54 (2003).

24. Tsai, P. P., Schreuder-Gibson, H. & Gibson, P. Different electrostatic methods for making electret filters. *Journal of Electrostatics* 54, 333–341 (2002).

25. Kubik, D. A. & Davis, C. I. *Melt-blown fibrous electrets*. (Google Patents: 1980).

26. Myers, D. L., Lassig, J. J., Turkevich, L. A. & Midkiff, D. G. *Stable electret polymeric articles*. (Google Patents: 2003).

27. Kim, J. C., Otani, Y., Noto, D., Namiki, N. & Kimura, K. Initial collection performance of resin wool filters and estimation of charge density. *Aerosol science and technology* 39, 501–508 (2005).

28. Mark, J. *et al. Physical Properties of Polymers*. (Cambridge University Press: 2004).

29. Grum, J. *D. R. Salem: Structure formation in polymeric fibers, Munich, Hanser, 2001*.

30. Li, J., Shanks, R. A. & Long, Y. Miscibility and crystallization of metallocene polyethylene blends with polypropylene. *Journal of Applied Polymer Science* 87, 1179–1189 (2003).

31. Rabello M.S. & White J.R.[1] Crystallization and melting behaviour of photodegraded polypropylene - II. Re-crystallization of degraded molecules. *Polymer* 38, 6389–6399 (1997).

32. Lafrance, C.-P. & Prud'homme, R. E. Characterization of the molecular orientation in highly oriented rolled polypropylene sheets by X-ray diffraction. *Polymer* 35, 3927–3935 (1994).

33. Wang, X. Y. & Gong, R. H. Morphology and Structure of Constituent Fibres in Thermally Bonded Nonwovens. *Macromolecular Materials and Engineering* 291, 499–509 (2006).

34. Strobel, M. [1] *et al.* Low-molecular-weight materials on corona-treated polypropylene. *Journal of Adhesion Science and Technology* 3, 321–335 (1989).

35. Ramesh, S., Huang, C., Shurong Liang & Giannelis, E. P. Integrated thin film capacitors: interfacial control and implications on fabrication and performance. *Electronic Components and Technology Conference, 1999. 1999 Proceedings. 49th* 99–104 (1999).doi:10.1109/ECTC.1999.776071

CHAPTER 4

4 Improving Electret Properties of PP Filaments with Barium Titanate

Abstract

Barium titanate ($BaTiO_3$) containing polypropylene (PP) composite filament fibers were produced by melt spinning process and their electrostatic charging characteristics were studied. Sample filaments containing $BaTiO_3$ at 0.01-10% concentration range were melt spun and charged/polarized at room temperature and 130°C -which corresponds to Curie point of $BaTiO_3$. $BaTiO_3$ exhibited effective polarization at high temperatures, thus significant enhancement obtained when compared to results obtained from samples charged at room temperatures. Due to observed negligible changes in filament microstructures, it is possible to conduct enhancement in charging properties to the outstanding dielectric properties of $BaTiO_3$ and interfacial polarization between host polymer and additive. Surface potential decay method was followed to analyze charging properties. Distribution of $BaTiO_3$ particles within filaments was investigated via optical and scanning electron microscopy, whereas changes in crystal structure were examined by X-ray Diffraction (XRD) analysis.

4.1 Introduction

Electrets have a long history in material sciences. Long term charge retention or

polarization ability of those dielectrics makes them useful for various applications such as filtration units, transducers and radiation sensors [1,23]. Among those, electret filters gained significant interest in recent decades as high efficiency filtration has been recognized as an effective and energy efficient tool to control air pollution. Increases in the number of pandemic cases, environmental pollution and strict clean room and operation room requirements force high growth rates in filtration industry. There are two main approaches to improve filter efficiency. One approach is the use of finer fibers, thus increasing the efficiencies of capture mechanisms such as diffusion and interception. However, this will also result in high pressure drop, which is unfavorable for filtration. A second approach is imparting electrostatic charge on filtration medium without changing web structure. Those are called as "electret filters" or "electrostatic filters"[4]. Uncharged fibrous filters capture submicron size particles only by mechanical means such as Brownian diffusion, direct interception and inertial impaction. However, electrostatic attraction as a fourth mechanism will be effective on particle capture [5,6]. Electret filters are advantageous over mechanical filters due to their low air resistance and their high dust collection performance. Their high collection efficiency on submicron size aerosol filtration without increasing pressure drop can lead to low energy expenditure. In facemasks use of charged webs with higher air permeability improves breathe comfort.

Undoubtedly, the electric field generated within the fibrous web should be over a limit value to capture particles, since electrostatic filtration is highly dependent on air velocity. On

the other hand stability of charging property is important, since in case electrostatic property is lost somehow, their open structure will lead to a drastic drop in efficiency. Hence, charge density and stability will be important factors that determine not only filtration efficiency, but also reliability of those filters.

So the question arising at that point is: "How are those of the polymeric structures charged and how do they keep charges quasi-permanently?" An oversimplified approach explains polymers as insulating materials, thanks to their large bandgap, however localized defective structures such as impurities and crystal-amorphous boundaries are found to be acting as charge traps and adding polarizability to nonpolar polymer structures [7,8]. Polymers already have those of the inevitable impurities which are originated from polymerization and process conditions. However for improving charge retention capacity and stability further, especially commodity polymers are required to be modified with additives. A huge patent literature [9–13] concerning with various additive based modifications could be found, however there are few academic works which are mostly concentrated on films[7,14,15]. Nucleating agents, antioxidants, oil mist resisting agents and some inorganic additives were mentioned to be effective. Nucleating agents either provide smaller spherulites whose boundaries are traps for space charges, or generate microvoids that prohibit charge migration [15]. Antioxidants may act as nucleating agents and also are able to provide deep traps [16], whereas flurochemicals improve surface properties, particularly via prohibiting the formation of thin conductive film during filtration [9].

In this study PP filaments were modified with one of the most widely used nonlinear dielectric, barium titanate ($BaTiO_3$) to enhance charging properties. Researches on polarization properties of barium titanate go back to 1940s[17]. Lattice transformation from tetragonal to a paralectric cubic form was shown to occur at Curie point which depends on crystal size and composition[27]. During this transformation spontaneous alignment of dipoles in one of the equilibrium position gives rise to polarization. Thus very high dielectric constants, i.e. 10^4 or more would be measured. As shown in figure 1 smaller Ti [atomic radius of 176pm] cation occupies the central octahedral B site and barium cations (atomic radius of 253pm) fill the interstices between octahedra. The high polarizability is a result of more space for Ti ions within the oxygen ions. A net permanent dipole moment of the octahedron can result only by a unilateral displacement of the positively charged Ti^{+4} ion against its negatively charged O^{-2} surrounding, thus giving a high dielectric constant[18].

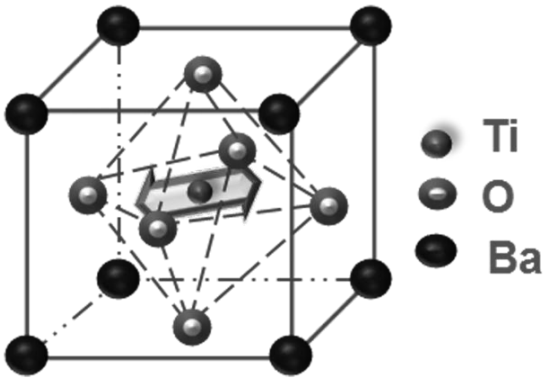

Figure 4.1 Arrangement of titanium, barium, and oxygen ions within $BaTiO_3$ crystal

The reason that we selected $BaTiO_3$ is that it could be a good candidate to improve localized polarizability within PP with its high dielectric constant. Besides, composites obtained from polymer-nonlinear dielectric mixtures could be expected to have superior properties, due to additional interfacial polarization between host polymer and ceramic particles [19]. Expected differences in charge storage and decay between films and filaments led our studies to be conducted on filaments. This is important since larger surface area of the later will make it more prone to decay by ionic attacks from the air and for filament production resin selection according to molecular weight and polydispersity will be much more limited. Therefore to find the best composition as a candidate for filter applications, charging and polarization property should be investigated on fibrous structures.

4.2 Materials & Methods

4.2.1 Material and Filament Preparation

PP resin (grade CP36OH, T_m=160°C, ρ= 0.91g.cm^{-3}, Melt flow index = 34dg.min^{-1}), having weight average molecular weight of 180,000g/mol and polydispersity of 3.3 was supplied from Sunoco Chemicals, PA. Barium titanate (219-6A) in powder form was provided from Ferro Electronics, OH. 90% of the particles have diameters smaller than 2.1μm and 10% of them was smaller than 0.8 μm according to manufacturer data. A dielectric constant of 2300 was reported for the powder. To provide better uniformity,

initially PP masterbatch pellets at a concentration of 20%(w/w) $BaTiO_3$ were prepared by Techmer PM (Clinton, TN). Then, masterbatch was re-extruded with pure PP resin to produce $BaTiO_3$/PP composite fibers with concentrations of 0.01%, 0.1%, 1%, 10% (w/w). Hill's multifilament spinning line located in the Nonwovens Institute (North Carolina State University, Raleigh, NC) was used to produce filaments. Spinning speed was 2000m/min and the throughput was maintained at 0.58 g $hole^{-1}$ min^{-1}. Temperature of the spin head was fixed at 235°C. As a control, PP without $BaTiO_3$ was melt extruded under the same conditions. Each yarn had 72 filaments whose diameter was about 20μm.

After spinning multifilament samples were washed with deionized water at 45°C for 6h to remove impurities and spinfinish applied during melt spinning process. The washing fluid was replaced every 2h. Yarns wounded on washing tubes were dried overnight.

4.2.2 Charging and Characterization of Charging Property

After drying, yarns were aligned parallel on aluminum sample holders with a definite spacing (10 yarns/cm) as shown in Figure 4.2. It was observed that any fiber protruding from specimen caused significant variations on measured potential value. In order to fix protruding fibers perpendicular yarns were aligned at a distance of 0.7cm from each other. The filaments were fixed carefully by using conductive tape and epoxy to prevent errors that can occur due to position changes during charging and decay tests.

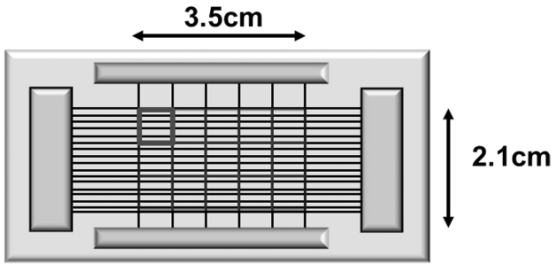

Figure 4.2 Specimen for SPD test and surface potential detection points

A lab scale negative corona discharger (Mystic Marvels, Model NIP-7E) was used to charge/polarize samples. Applied voltage was fixed at 9kV where maximum output direct current of the emitter needle was about 160 μA. Charging was kept 1 minute as it was determined as an optimized value from our previous works. All testing procedure was performed at laboratory conditions in which relative humidity was kept fixed between 54-58% RH at 22-23°C temperature for cold charging. Thermal charging procedure for fibrous electrets was explained in an early work by Thomas[20]. The fibrous material under high electric field is heated to soften and cooled in the presence of the field. For thermal charging samples were heated to 130°C, which took approximately 15sec, then polarized for 1 min and cooled to room temperature in approximately 2min.

The surface potential was measured with Monroe 244A noncontact electrostatic voltmeter. Three specimen were prepared from each samples and surface potential of 15 specific points across the each specimen was measured (Figure 4.2). Then average values and

standard error of total 45 points per sample were reported. average values and standard deviations were calculated thereof. The initial surface potentials (V_0) were measured directly after charging. Stability of charge was evaluated with isothermal surface potential decay (SPD) test. Since dissipation of charges or depolarization of the polymer electrets is long process and can takes several years[13]. Therefore, we performed decay at the elevated temperature to accelerate charge decay. Charged samples placed in the oven at 80°C and surface potential of were measured after 0.5h, 1h, 2h, 4h, 8h, 12h, 16h, and 24h decay time. Due to the nature of decay, periods kept shorter initially. Samples after annealing were cooled for 10 minutes in a desiccator to prohibit the effect of atmosphere.

4.2.3 Fiber Structure

Optical Microscopy. Optical microscopy images were taken randomly to understand the distribution of $BaTiO_3$ particles within PP filaments. Zeiss optical microscope with an objective of 40X and 0.08µm/scale resolution was used. To capture the images Nikon high-definition color camera head, DS-Fi1 was mounted on the microscope.

Scanning Electron Microscopy (SEM). To show radial distribution of $BaTiO_3$ within filaments, cross-section of $BaTiO_3$/PP filaments were analyzed with a Hitachi S-3200 Variable Pressure Scanning Electron Microscope. A non-conductive specimen maybe inserted directly into the VPSEM and observed without any coatings. A tungsten filament

was used to create the beam. The reported resolution was 35Angstroms with a 30kV beam. A 30μm diameter objective aperture, and a 25mm working distance were used for imaging, and with a 70 condenser lens setting and appropriate aperture for x-ray analysis to maintain suitable dead times. A 4Pi Isis EDS system is also attached to the instrument where elemental composition analyses were carried out. To avoid any damage on cross-section, sample filaments were cut with blade inside liquid nitrogen which is below glass transition of PP.

Wide-Angle X-ray Diffraction (WAXD). Crystal structure was investigated using Rigaku SmartLab® X-ray diffractometer which is equipped with a rotating anode Cu source in line focus geometry, thus producing Cu-Kα radiation having a wavelength of 1.5418 Å generated at 40 kV and 44 mA. Samples were equatorially scanned from 2θ range =10 - 35° at an increment of 0.1°. The crystal sizes of the corresponding peaks were deduced using the Scherrer's equation [21]:

$$t = \frac{0.9 \times \lambda}{B \times \cos \theta_B} \qquad \text{Equation 4.1}$$

where t is crystal size (Å), λ is wavelength of X-ray (1.54 Å), B is full width at half maximum (radian), and Θ_B is Bragg angle (degree).

Using diffraction curves crystallinity was also calculated, which is ratio between the area of the crystal peaks over total area under the scattering curve[22]. PDXL software was used for further crystal analysis.

4.3 Results and Discussions

4.3.1 Fiber Structure

Optical Microscopy. The optical micrographs of $BaTiO_3$/PP filaments [Figure 4.3] showed $BaTiO_3$ particle distribution within fibers. In all concentrations, very little agglomeration was observed even at 10% concentration which indicates particles were well distributed in PP. At 0.01% concentration particles were hardly observed due to low concentration, but as concentration increased, presence and distribution of $BaTiO_3$ particles in filaments became more visible. Even at 10% concentration, filaments were apparently filled with $BaTiO_3$ uniformly.

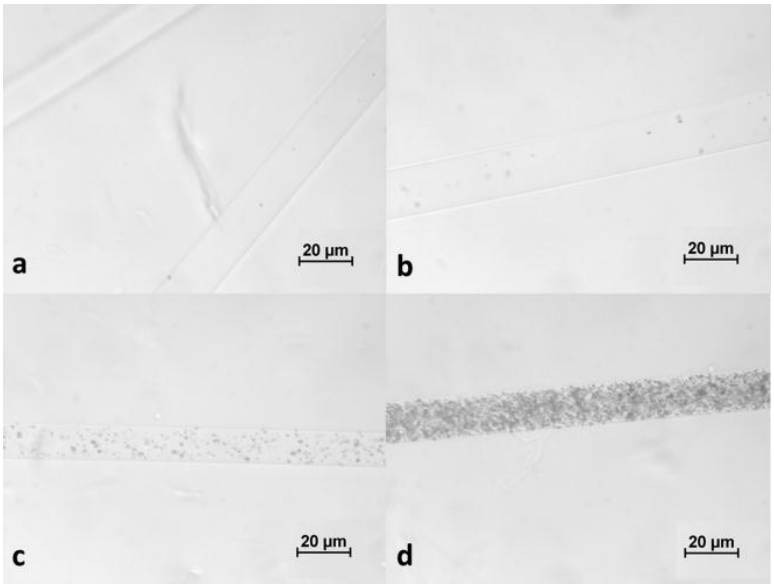

Figure 4.3 Optical micrographs of the samples with the indicated $BaTiO_3$ content

SEM-EDS analyses. Cross-sections of 10% $BaTiO_3$/PP filaments were observed with SEM (Figure 4.4) to investigate radial distribution of particles. Bright spots were found throughout fiber cross-sections. EDS spectra of these bright spots, given in Figure 4.5, exhibits strong peaks at 4.5 keV and 4.8keV corresponding to Ti and Ba elements, and indicates these bright spots are $BaTiO_3$ particles imbedded in PP filaments. These images further confirm $BaTiO_3$ particles are not agglomerated as the sizes of these spots are less than 2μm. In addition, particles are present both inside and close to surface of filaments, and no preferential distribution on surface or inside were observed. As shown was not an agglomeration issue even for 10%$BaTiO_3$ containing PP filaments. The bright and dark regions are components of composite filament observed under electron beam at 20kV. Elemental analysis upon further focusing showed those of the bright regions corresponds $BaTiO_3$ particles [Figure 4.5]. A noisy peak at x-ray energy of 1.5keV was obtained which is produced due to Al sample holder.

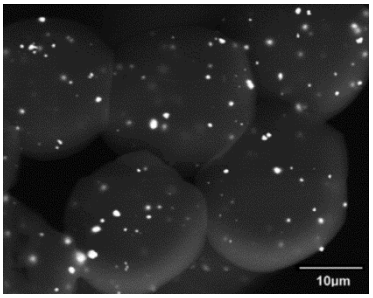

Figure 4.4 SEM images from the cross-section of 10% $BaTiO_3$/PP filament

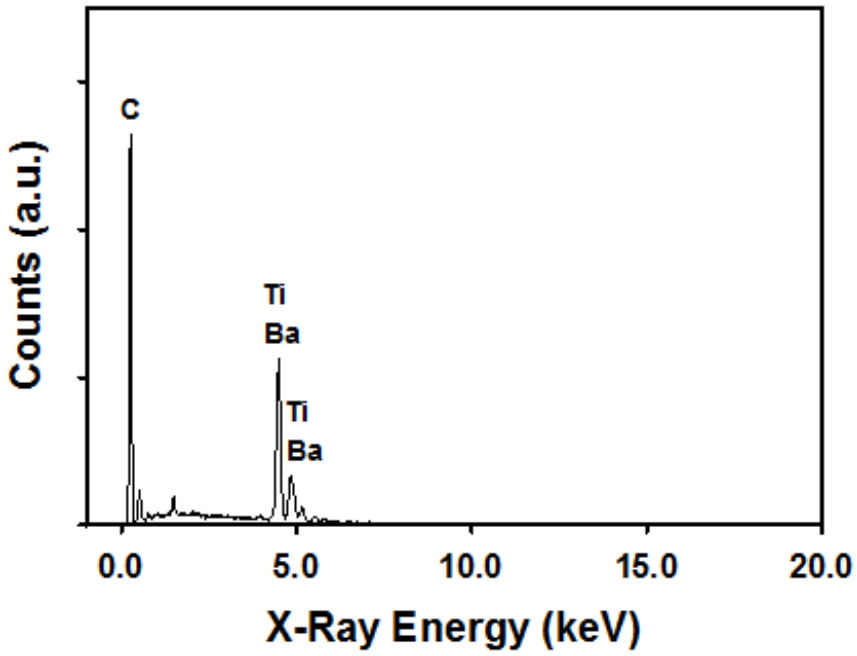

Figure 4.5 EDS mapping micrographs and elemental analysis of same specimen

X-ray diffraction. Addition of $BaTiO_3$ can accompany changes in microstructure of filaments. Not only from $BaTiO_3$ addition, but also double-processed PP resin that was used for masterbatch production might have resulted with some changes. $BaTiO_3$ particles would act as nucleating agent, since many inorganics may show such effect[23]. X-ray diffractogram of a control PP filament shows distinct peaks at 2θ=14.13°, 17.01°, and 18.56 [24,25]. As shown in Figure 4.6 overall X-ray diffractogram reveals addition of $BaTiO_3$ slightly alters crystalline structures of filaments. Addition of $BaTiO_3$ particles have not affected d-spacing of PP-

crystal as positions of peaks changed little. α-PP peak intensities for 10% $BaTiO_3$ containing filament is lower than other samples. Filaments with BaTiO3 concentration higher than 1% also exhibit peaks at around 31.5° which is corresponding to (1,1,0) plane of $BaTiO_3$ crystal (PXLD software).

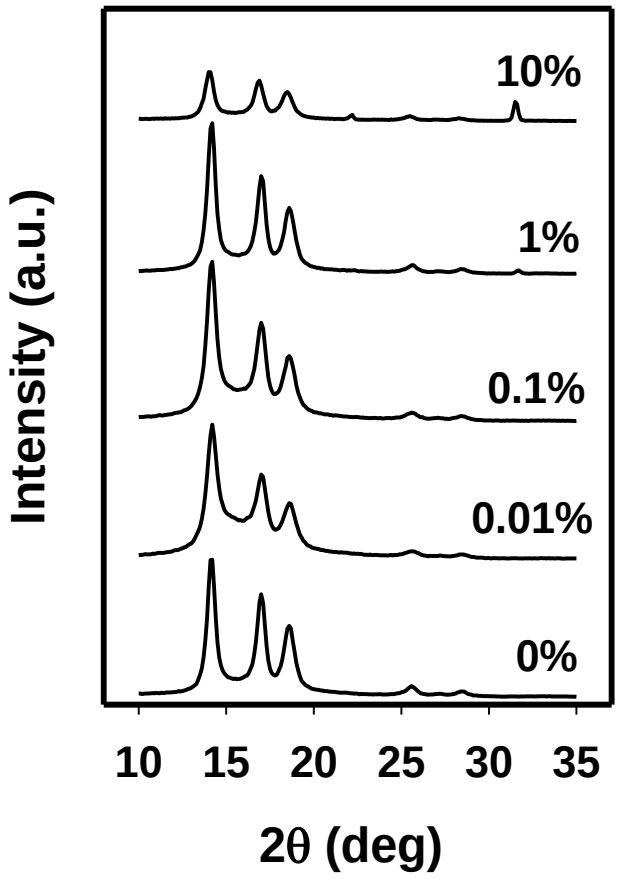

Figure 4.6 X-ray diffraction diagram $BaTiO_3$ containing filaments (detailed peak analysis was given in Table 4.1)

A detailed analysis of crystal structure was given in Table 1. Interestingly at 0.01 and 0.1% concentration drop in crystal sizes is apparent. Crystal sizes, calculated according to Scherrer equation revealed crystal thickness for (110) plane dropped significantly at 0.01 and 0.1% $BaTiO_3$ concentration, whereas at 1 and 10% sizes are similar. It seems supercooling and high shear rates during meltspinning would have dominated on crystal structure.

Table 4.1 Detailed crystal analyses for various $BaTiO_3$ concentrations. (Since $BaTiO_3$ peaks for 0.01%, 0.1% concentrations were not clear, they were not included)

$BaTiO_3$ Conc. (%)	2theta(°)	d (Å)	Size (Å)	Possible crystal
0	14.13	6.26	151.34	α-Polypropylene(1,1,0)
	17.01	5.21	148.53	α-Polypropylene(0,4,0)
	18.56	4.78	120.71	α-Polypropylene(1,3,0)
	25.53	3.49	129.05	α-Polypropylene(1,5,0)
	28.36	3.14	106.43	α-Polypropylene(1,5,-1)
1	14.16	6.25	151.59	α-Polypropylene(1,1,0)
	17.01	5.21	146.76	α-Polypropylene(0,4,0)
	18.57	4.77	117.17	α-Polypropylene(1,3,0)
	25.60	3.48	107.58	α-Polypropylene(1,5,0)
	27.15	3.28	104.66	α-Polypropylene(1,4,1)
	28.40	3.14	108.28	α-Polypropylene(1,5,-1)
	31.65	2.82	321.59	$BaTiO_3$(1,1,0)
10	14.07	6.29	137.73	α-Polypropylene(1,1,0)
	16.85	5.26	145.75	α-Polypropylene(0,4,0)
	18.46	4.80	111.15	α-Polypropylene(1,3,0)
	22.21	4.00	309.98	α-Polypropylene(1,2,1);
	25.45	3.50	116.22	$BaTiO_3$(1,0,0)
	28.26	3.16	95.56	α-Polypropylene(1,5,0)
	31.52	2.84	330.39	α-Polypropylene(1,5,-1)
				$BaTiO_3$ (1,1,0)

Since the samples were thermally charged at 130°C for 1min, possible changes in crystal structure would be expected. As seen in Figure 4.7 reference and 10% $BaTiO_3$/PP sample, holding at 130°C for did not change crystal structure abruptly, which is probably time dependent nature of crystallization process. Therefore microstructural changes played minimal roles in enhancing charging properties induced by thermal charging, discussed in following section.

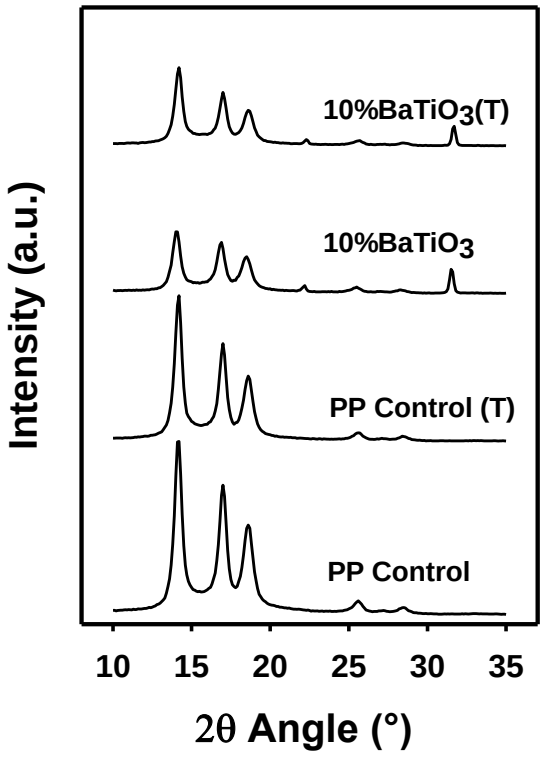

Figure 4.7 WAXD graphs after thermal charging. (T) indicates thermal treatment at 130°C

While crystal d-spacing little changed, $BaTiO_3$ addition affected the amounts of crystalline in the filaments. Using the same diffraction graphs crystallinity of the filaments was calculated [22]. The lowest crystallinity was found at 1% $BaTiO_3$ concentration (Figure 4.8), where crystal dimensions were similar to control sample. Crystallinity of filaments, calculated using the same x-ray diffraction graphs crystallinity of the filaments was calculated [21]. High loading of $BaTiO_3$ lowers crystallinity of filaments. At 1% $BaTiO_3$ addition, crystallinity of samples are about 40%, more than 10% reduction compared to PP filament spun at the same condition.

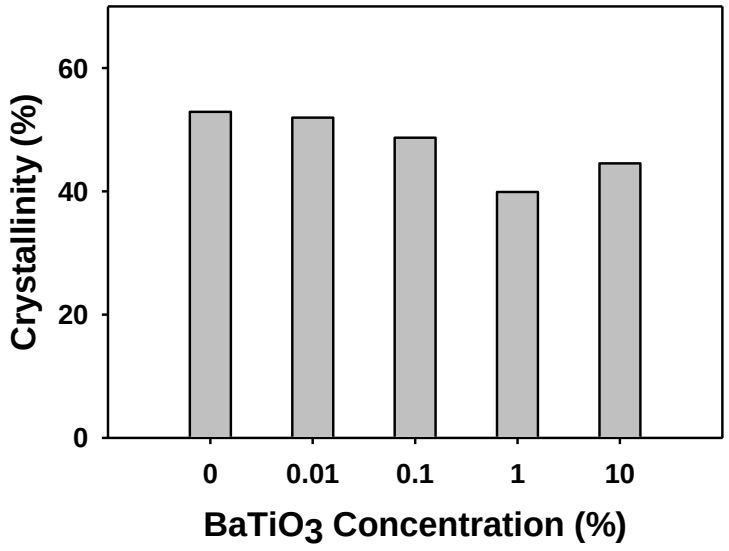

Figure 4.8 Crystallinity of $BaTiO_3$/PP filaments

4.3.2 Electret Properties of Barium Titanate Containing PP Filaments

Surface potential decay curves (illustrated in Figure 4.9) demonstrate charging and its decay behavior of samples. Initial surface potential is a measure of charge density imparted to the samples during charging process and reduction of surface potential with decay represent stability of charges. Corona discharge surface charges on all filament samples as initial surface potential reached to over 80-300V. Since these charges were not stable, samples experienced almost immediate charge decay. Both addition of $BaTiO_3$ and charging temperature have affected initial potential and their decay behavior. In particular, thermal charging greatly improved both charging and charge stability in all samples while BaTiO3 incorporation effects are more complicated.

It appears $BaTiO_3$ addition improved initial potential little when they are cold charged. Cold corona discharge resulted with very similar potential decay curves for control and modified samples. There is a slight increase in initial potential of sample containing $BaTiO_3$ at 0.1% concentration. However, initial potential of cold charged PP filaments tends to drop to 80-90V at high $BaTiO_3$ concentration from about 120V in PP control filaments (Figure 4.10).

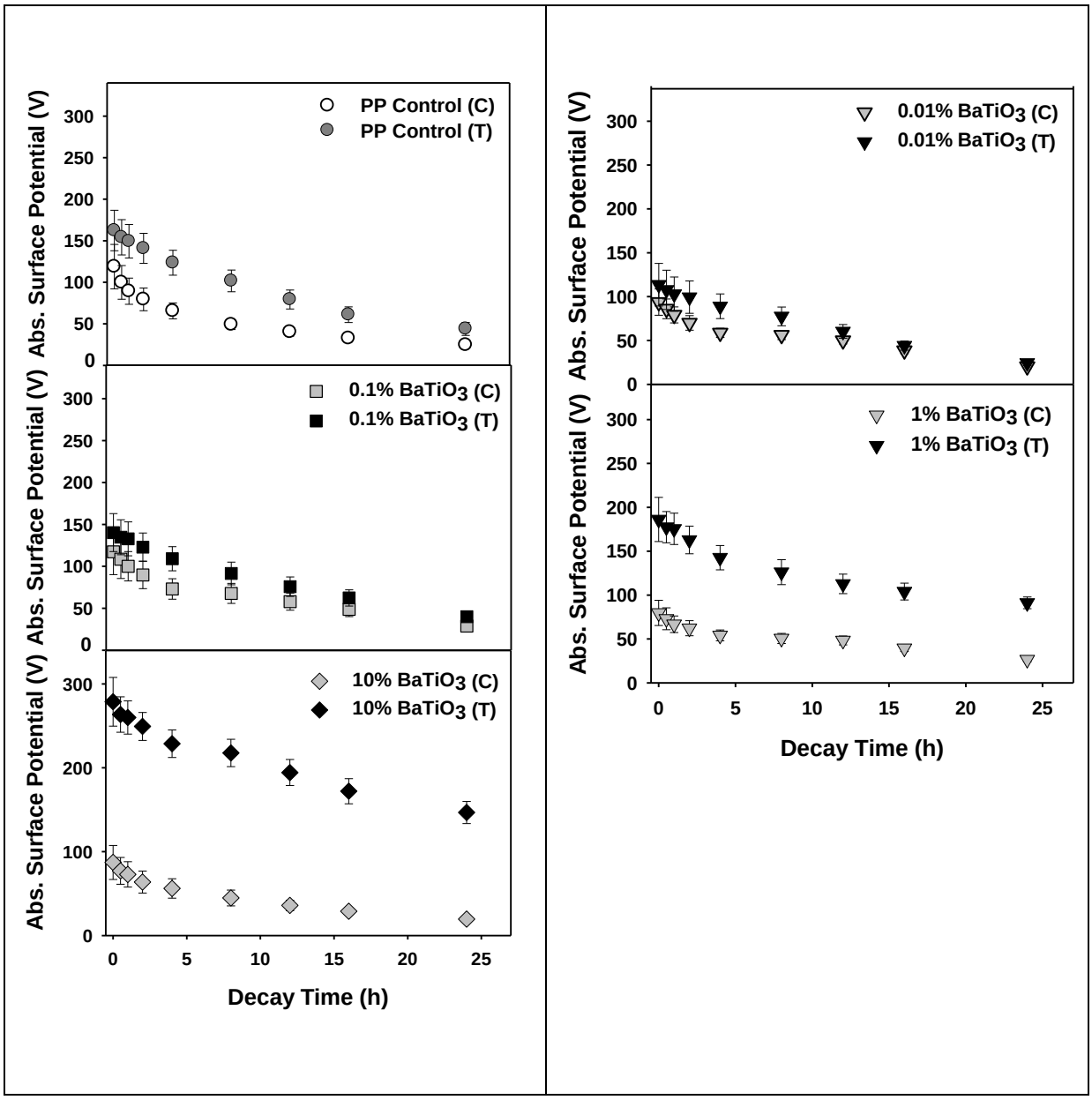

Figure 4.9 SPD curves for $BaTiO_3$/PP filaments.

On the other hand, when samples were thermally charged, significant enhancement was found for samples having $BaTiO_3$ concentration above 1%. 0.01% BaTiO3 addition did not show a significant improvement, which is probably due to very low amount of additive which did not contribute charging effectively. It is clear that thermal charging is more effective to impart charges to the samples than cold charge. Even in PP control filaments, surface potential reaches 162V, about 37% improvement compare to that of cold charging. Increase was more notable for $BaTiO_3$ incorporated filaments than control sample. Initial surface potential of thermal charged PP filament with Particularly at 10% $BaTiO_3$ concentration potential values were nearly tripled compared to that of cold charged one.

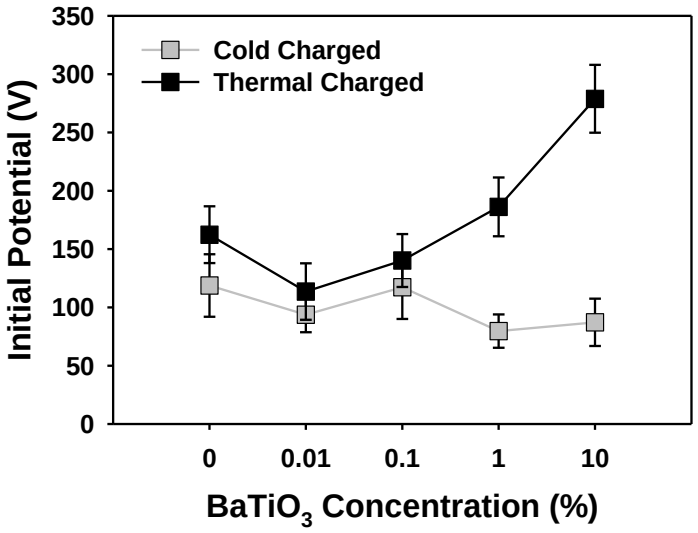

Figure 4.10 Comparison of initial potential values of cold and thermally charged samples

As previously mentioned, these initial charges are not stable and decay over time. Figure 4.11 summarizes initial potentials and remaining potential after isothermal decay test. Most probable concentrations that $BaTiO_3$ acts effectively is between 1-10% concentration. When cold charged 10%$BaTiO_3$ exhibited low initial potential, even remaining potential was almost nulled. However enhancement is remarkable after thermal charging.

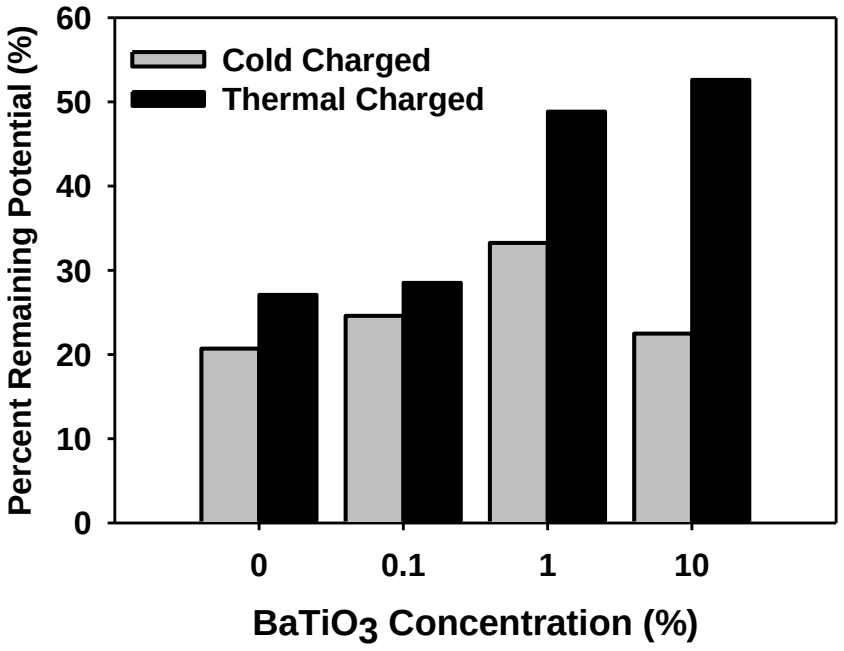

Figure 4.11 Remaining potential percentages after keeping at 80°C for 24h

To understand charging and charge decay properties of composite filament produced, we have analyze SPD curves further. Relaxation times which correspond 1/e th value of initial potential were calculated. Other than 1% $BaTiO_3$ containing samples, relaxation times for modified and cold charged samples were close to the reference PP, however clearly it doubles relaxation time at 1% concentration. When samples were thermally charged relaxation times were increased in all concentrations. Increase was more notable for $BaTiO_3$ incorporated filaments than control sample. 0.01% $BaTiO_3$ addition did not show a significant improvement, which is probably due to very low amount of additive which did not contribute charging effectively. However $BaTiO_3$ between 1 and 10% concentration range seems to act as good candidate as an electret additive for PP. Rather than enhancement in initial potential, cold charging resulted with an increase in charge stability for all concentrations, however thermal charging acted on both initial charge density and charge stability, particularly at high concentration.

4.4 Discussions

Barium titanate has a high dielectric constant already at room temperature [26], however there is a distinct increase at so called Curie temperature, which resulted in larger charge density and stability within PP filaments. Thermal charging also induced improvement in charging properties of PP control filaments, but enhancement is not as high as $BaTiO_3$

containing samples. As a result polarization of $BaTiO_3$ should be credited for the improvement in electret properties. $BaTiO_3$ particles will transform into paraelectic crystal structure when the temperature is above Curie point. If sample is under electric field during such heat induced crystal structure transformation, paraelectric cubic crystal will orient inversely with applied electric field and transform into tetragonal structure when temperature is lowered. Then produced electrostatic stress will attract negative charge carriers efficiently[47]. So what expected from this modification is nonpolar PP will have polarizable regions after addition of high dielectric constant $BaTiO_3$. Thus injected charges will be more stable around those of the polarized species.

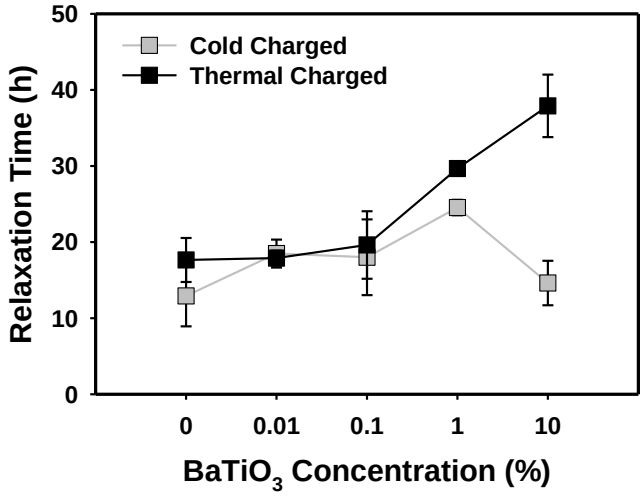

Figure 4.12 Comparison of calculated relaxation times of cold and thermally charged samples (after keeping 24h at 80°C)

It is already known electrets prepared at high temperatures even after melting are mostly stronger when compared to ones charged at low temperatures [67]. However charging PP filaments in molten state would be impossible since they will lose the shape and convert into a film. Fortunately polarization requirements of barium titanate are compatible with thermal behaviors of PP, which allow effective charging without melting filaments. On the other hand charging just after extrusion would be an option. However the time under the electric field will not be sufficient for this case, since the speed of molten polymer is already very high (about 3m/sec even under spinneret). This means filaments will stay under a 10cm electric field region just for 0.03second. Kravtsov et al also observed lower charging efficiency during extrusion [29]. As a result charging should be performed as an after treatment.

Crystal-amorphous boundaries would be inversely proportional with calculated crystal sizes, meaning smaller crystals would be expected to provide larger interfaces in total. In this regard samples at 0.01% concentration have the lowest crystal sizes, giving more interfacial area per unit volume of material. According to literature higher initial potential for samples having lower crystal sizes [35,47] would be expected. It did not occur; probably crystal size difference was not so broad in our case. Change in crystallinity was also not found to be so significant to act on electret properties.

4.5 Conclusion

Electret properties of $BaTiO_3$ containing PP filaments were investigated. Charging at 130°C -which is also known as Curie temperature- resulted in the highest initial potential and longest stability. The effect of $BaTiO_3$ was apparent for concentrations above 1%. High dielectric constant of barium titanate at that point, softening of the polymer and improved corona conditions are thought to be the reasons behind enhancement. Cold charged samples exhibited poor properties when compared to thermal charged ones.

4.6 References

1. Goel, M.*Current science* 85, 443–453 (2003).
2. Kestel′man, V. N., Pinchuk, L. S. & Goldade, V. A. *Electrets in engineering: fundamentals and applications*. (Springer: 2000).
3. Sessler, G. M. (Gerhard M. & Broadhurst, M. G. (Martin G. *Electrets / edited by G.M. Sessler ; with contributions by M.G. Broadhurst ... [et al]*. (Springer-Verlag: Berlin ; New York :, Berlin ; New York : Springer-Verlag, c1987.).
4. Klaase, P. T. . & Van Turnhout, J. *Method for manufacturing an electret filter medium*. (Google Patents: 1986).

5. Brown, R. C. & Brown, R. C. *Air filtration: an integrated approach to the theory and applications of fibrous filters*. (Pergamon Press: 1993).

6. Brown, R. C. Electrically charged filter materials. *Engineering Science and Education Journal* 1, 71–79 (1992).

7. Behrendt, N. *et al.* Charge storage behavior of isotropic and biaxially-oriented polypropylene films containing α-and β-nucleating agents. *Journal of Applied Polymer Science* 99, 650–658 (2005).

8. Yamashita, T. & Ikezaki, K. A method for correlating charge traps of polypropylene to its morphology. *Journal of Electrostatics* 63, 559–564 (2005).

9. Jones, M. E., Rousseau, A. D. & others Oily mist resistant electret filter media. (1995).

10. Cox, S. T. & Healey, D. T. *Melt blown composite HEPA filter media and vacuum bag*. (Google Patents: 2001).

11. Rousseau, A. D. & Miller, J. W. *Electret fibers and filter webs having a low level of extractable hydrocarbons*. (Google Patents: 2001).

12. Tani, Y. & Tokuda, S. Electret Filter. (1995).

13. Groh, W., Macholdt, H. T., Gibson, B. D., Walden, J. R. & Felton, C. D. Polymer electrets with improved charge stability. (1996).

14. Mohmeyer, N., Altstadt, V., Sessler, G. M. & Schmidt, H. W. Additives to improve the electret performance of polypropylene. *Electrets, 2008. ISE-13. 13th International Symposium on* C222 (2009).

15. Mohmeyer, N. *et al.* Additives to improve the electret properties of isotactic polypropylene. *Polymer* 48, 1612–1619 (2007).

16. Cartwright, G. A., Davies, A. E., Swingler, S. G. & Vaughan, A. S. Effect of an antioxidant additive on morphology and space-charge characteristics of low-density polyethylene. *IEE Proceedings-Science, Measurement and Technology* 143, 26 (1996).

17. Roberts, S. Dielectric and Piezoelectric Properties of Barium Titanate. *Phys. Rev.* 71, 890 (1947).

18. L. L. Hench *Principles of electronic ceramics*. (Wiley: (New York), 1990).at <http://openlibrary.org/b/OL2208624M/Principles_of_electronic_ceramics>

19. Blythe, A. R. & Bloor, D. *Electrical properties of polymers*. (Cambridge University Press: 2005).

20. Thomas, A. G. *Electrically charged material*. (1956).

21. Grum, J. *D. R. Salem: Structure formation in polymeric fibers, Munich, Hanser, 2001*.

22. Lima, M. F. S., Vasconcellos, M. A. Z. & Samios, D. Crystallinity changes in plastically deformed isotactic polypropylene evaluated by x-ray diffraction and differential scanning calorimetry methods. *Journal of Polymer Science Part B: Polymer Physics* 40, 896–903 (2002).

23. Pritchard, G. *Plastics additives: an A-Z reference*. (Springer: 1998).

24. Lafrance, C.-P. & Prud'homme, R. E. Characterization of the molecular orientation in highly oriented rolled polypropylene sheets by X-ray diffraction. *Polymer* 35, 3927–3935 (1994).

25. Wang, X. Y. & Gong, R. H. Morphology and structure of constituent fibres in thermally bonded nonwovens. *Macromolecular Materials and Engineering* 291, 499–509 (2006).

26. Strumpler, R., Rhyner, J., Greuter, F. & Kluge-Weiss, P. Nonlinear dielectric composites. *Smart Materials and Structures* 4, 215 (1995).

27. Kao, K.-C. *Dielectric phenomena in solids: with emphasis on physical concepts of electronic processes*. (Academic Press: 2004).

28. Nalwa, H. S. *Ferroelectric polymers: chemistry, physics, and applications*. (CRC Press: 1995).

29. Kravtsov, A. G., Zotov, S. V. & Brunig, H. Peculiarities of the electret state of melt-spun and melt-blown fibrous polypropylene materials. *Mechanics of composite materials* 36, 491–496 (2000).

30. Mohmeyer, N. *et al.* Additives to improve the electret properties of isotactic polypropylene. *Polymer* 48, 1612–1619 (2007).

CHAPTER 5

5 Filtration Properties of $BaTiO_3$ Containing Meltblown Electret Filters

Abstract

Performance of an electret filter mainly stands on the strength of created electric field within webs, whereas the stability of charges determines their long term behavior. To enhance both properties various additives including nucleating agents, inorganic ceramic dielectrics, light stabilizers, antioxidants and oil mist resisting agents were used so far. In the previous chapters we had demonstrated barium titanate ($BaTiO_3$) would be a useful additive for improving electrostatic properties of polypropylene (PP) filaments. In this study same was investigated on meltblown PP webs by analyzing both filtration and surface potential properties. Samples were corona discharged under two thermal regimes: At room temperature and 130°C, which corresponds to Curie temperature of $BaTiO_3$. Results indicated that barium titanate with its high dielectric constant would enhance electrostatic charging and filtration properties meltblown PP webs.

5.1 Introduction

Electret filters gained significant importance in filtration and personal protective equipment (PPE) market over the past few decades. Those of the filters exhibit high efficiency without sacrificing pressure drop, thus providing high quality air at a lower expense. They owe a significant ratio of capture efficiency to electrostatic properties of fibers, whereas for uncharged filters, to provide high efficiency, one needs to manipulate basic web properties such as fiber diameter or solidity, which mostly results in high airflow resistance. As an example, mechanical filter composed of glass fibers can possess a high collection efficiency (> 99%) for submicron particles, however also too high resistance (25 - 40 mmH_2O). This pressure range is unacceptable for fans in most apartment units [1]. Contrariwise to densely packed mechanical filters, more open structure of electret filters will lead to lower pressure drop values (3-6 mmH_2O) for the same efficiency [2]. Low flow resistance is also one of the critical metrics in PPE design, since this will directly affect breath comfort.

On the other hand in a particular diameter range, mechanical filtration efficiency coming from either Brownian diffusion or interception drops significantly in conventional filters. As shown in efficiency-particle diameter graph (Figure 5.1), well in this range is quiet deep. Unfortunately diameter of several pathogenic microorganisms was reported to be in this range [3]. For charged filter media the efficiency is significantly high in this range and most penetrating particle size (MPPS) shifts through Brownian regime [4,5,6,7].

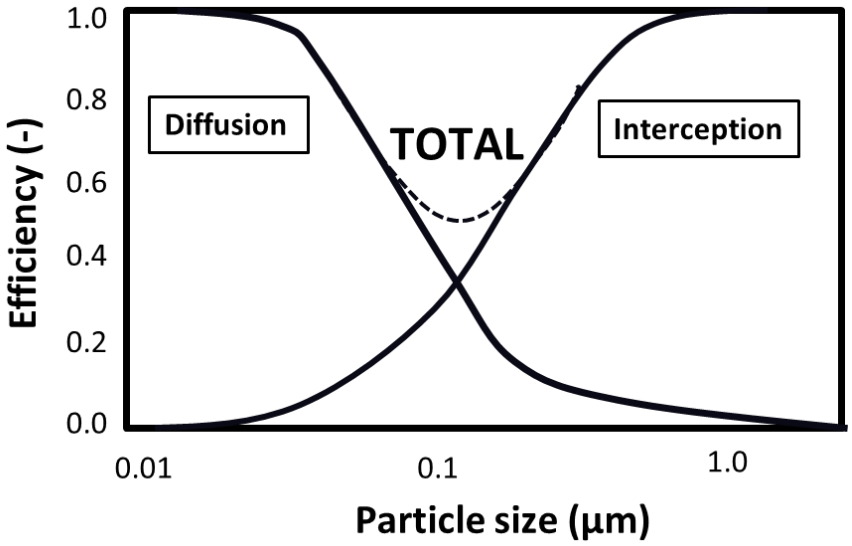

Figure 5.1 Particle capture efficiency for conventional filters[3]

For those of the filters efficiency drops significantly at high face velocities. Kim [8,9] and Boskovic [8,9] conducted reduction to shorter residence time within the web. Such low initial efficiency might also be due to insufficient strength of the electric field acting on particles[10]. Other than initial efficiency, several studies were concentrated on improving electrostatic stability[11–16] since decay of charges will convert them into loosely-constructed mechanical filters.

One of the mostly addressed solutions for such problems is modification of polymeric webs with melt additives. So far nucleating agents, antioxidants, light stabilizers, inorganic additives and fluorochemicals as oil mist resisting agents were utilized to improve electret

properties of polymeric materials. Nucleating agents either provide smaller spherulites whose boundaries are traps for space charges, or generate microvoids that prohibit charge migration[17–19]. Antioxidants and light stabilizers can act as nucleators and also deep charge traps [11,20] whereas flurochemicals improve surface properties, particularly by prohibiting the formation of conductive liquid film during filtration[16,21]. In this regard barium titanate has some distinct behaviors that are needed to be considered. It is a nonlinear dielectric which owes high polarizability to the rotation of central Ti atoms between two equivalent equilibrium positions. Thus transformation of tetragonal unit cell into cubic paraelectric at the so called Curie temperature causes dielectric constants of 10^4 or more [22,23]. Effects of grain size and composition on its dielectric properties were largely discussed in the literature[24,25].

In Chapter 4, it was shown that charge density and stability of PP filaments were improved significantly after addition of $BaTiO_3$. Surface potential of thermally charged 10% $BaTiO_3$ containing sample was nearly tripled when compared to the reference. Hence in this study the same enhancement was investigated on meltblown PP webs, which was expected to be observed also in filtration properties. Using a lab scale corona discharge instrument samples were charged at room conditions and 130°C for 10min. Surface potential properties and filtration efficiencies of cold charged and thermally charged webs were compared. To analyze electrostatic stability, samples were annealed at 80°C for 24h. After 24h filtration

tests were repeated on decayed samples and compared. Possible changes in microstructural properties were analyzed via Wide Angle X-ray Diffraction.

5.2 Materials & Methods

5.2.1 Materials

Achieve 6936G1 PP resin with a melt flow rate of 1550 was kindly provided from ExxonMobil. Barium titanate in powder form was purchased from Ferro Electronics, OH. 90% of the particles have diameters below 2.1μm and 10% of them were smaller than 0.8μm according to manufacturer data. A dielectric constant of 2300 was reported for the as received powder. To provide better uniformity, initially PP masterbatch pellet at 10%(w/w) $BaTiO_3$ concentration was prepared by Techmer PM (Clinton, TN). Then, masterbatch was re-extruded with pure PP to produce $BaTiO_3$/PP composite webs with concentration of 0.01%, 0.1%, 1%, and 10%(w/w).

5.2.2 Methods

Web preparation. Meltblown (MB) webs were produced with mini-Meltblown line in the Nonwovens Institute (North Carolina State University, Raleigh). MB line had a 6-inches die which has 120 holes, each of which is 0.15 mm in diameter (i.e ~25 holes/inch). Polymer pellets were melted and pressurized using a 1 1/4" C.W. Brabender extruder, mounted

horizontally. The heating in the extruder involves four zone temperature controls. The die was manufactured by the Reifenhäuser REICOFIL GmbH&Co. KG. The air plate angle is 60° with the air gap of 0.3 mm and the die tip is outset the die face by 1 mm. The temperature profile was tabulated in Table 5.1.

Table 5.1 Temperature profile of MB process

	Z1	**Z2**	**Z3**	**Z4**	**Pump**
Temp. [°C]	190	220	230	250	248
	Transfer	**Turning**	**Die**	**Air Fed**	**Air measured**
Temp. [°C]	250	250	250	339	260-270

Since attenuation is provided by air drag rather than a forwarding force, meltblowing is not a controllable process compared to melt spinning. By changing process conditions such as die/air temperature, polymer throughput, air pressure, die-collector distance, belt velocity we can produce samples having different fiber diameter distributions and solidity [26–28]. Initial studies were conducted to optimize the process conditions. Some of the process parameters such as die-collector distance, zone temperatures were kept constant. Belt speed and throughput was arranged such that basis weight values of the samples were resulted similar. The most defect free and uniform webs were found to be produced at a throughput around 0.2-0.25 g/hole/min and air pressure of 20-30 psi. So meltblown webs containing barium

titanate at various concentrations (0.01%, 0.1%, 1%, and 10%) were produced within this range.

Basic Web Properties. Basis weight was calculated from the average of 5 randomly cut specimen. According to ASTM D 5729, the thickness testing gage (AMES, BG1110-04) with a presser foot diameter of 25.4 mm at an applied force of 4.14 kPa was used to measure web thickness. From measured basis weight and thickness, solidity was calculated according to Equation 5.1:

$$solidity = \frac{basis\,weight}{thickness * density} \qquad \text{Equation 5.1}$$

To analyze fiber diameter and distribution Phenom FEI scanning electron microscope (SEM) was used. 100 measurements were taken from 15 pictures and averages and standard deviations were calculated thereof.

Charging and Surface Potential Analysis. Charging of the samples was carried out with a single needle corona discharger (Mystic Marvels, Model NIP-7E). The voltage was fixed at 9kV. Various charging distances and timings were tried to optimize charging conditions. Samples are charged at two different temperatures – cold charging at room temperature and thermal charging at 130°C. The fibrous material under high electric field is heated to soften and cooled in the presence of the field. Samples were heated to 130°C, which took approximately 1 minute, then polarized for 10 min and cooled to room temperature instantly.

The surface potential was measured with noncontact electrostatic voltmeter (Monroe 244 Model with 1017AE electrostatic voltage probe) immediately after charging. The initial measurements (V_0) were taken directly after charging at room temperature. As shown in Figure 5.2 potential on 16 specific points were measured on 5cmx5cm cut samples. Not only potential of face of the fabrics, but also back side were measured. Potential maps obtained from 3 samples were drawn. After that absolute difference between face and back values were calculated since this will be close to electric field that particles will be subjected to.

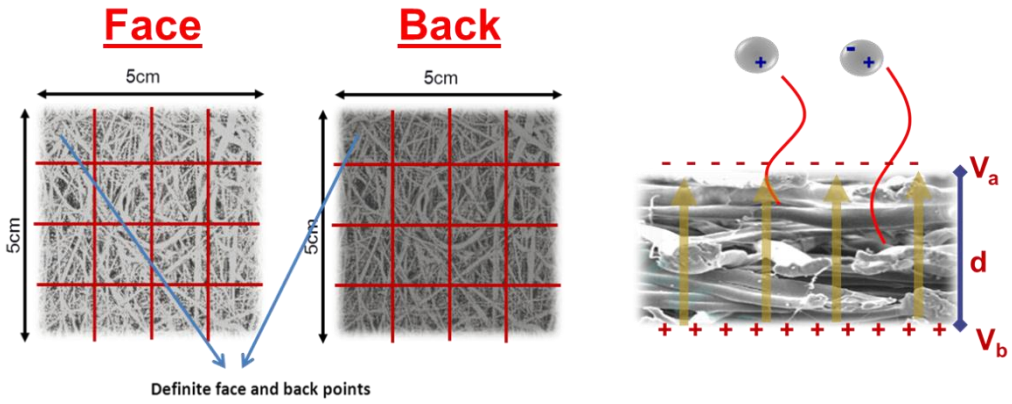

Figure 5.2 Surface potential measurement of MB webs

Filtration Properties. Filtration properties of meltblown webs were evaluated with monodisperse DOP(dioctyl phthalate) particles having diameter of 0.3µm at a face velocity of 5.3cm/s. A full scan was also performed in 0.02-0.3µm range. DOP aerosols were

generated by a collision type atomizer and then evaporated through a membrane dryer. Monodisperse aerosols were selected in a long differential mobility analyzer (DMA, TSI Model 3081, MN, USA) and neutralized by a Kr-85 radioactive source. The neutralized DOP aerosols were fed into a filter holder with 25.81cm^2 of effective area and their number concentrations at upstream and downstream positions were measured by using two condensation particle counters (CPCs, TSI Model 3760A, MN, USA). The flow rate and the resistance were measured by a mass flow meter (TSI Model 4043, MN, USA) and an electronic manometer (TSI Model 220, MN, USA). Quality factor ($QF=-\ln P/\Delta p$) which relates aerosol capture efficiency by the pressure drop across the media was also calculated from the slope of penetration vs pressure drop of 1, 2, 3 and 4 layers of webs.

After measuring the initial filtration efficiencies, samples were kept in the oven at 80°C for 24h and same filter testing protocol was applied again. Accelerated decay test would be useful especially for storage conditions.

Crystal Structure. Crystal structure was investigated using Omni Instrumental X-ray diffractometer. The diffractometer was equipped with Be-filtered CuK_α radiation with a wavelength of 1.54 Å generated at 35 kV and 25 mA. The samples were scanned from 2Θ range from 10° to 60° at an increment of 0.1°.

5.3 Results and Discussions

5.3.1 Basic Web Properties

Barium titanate is an insoluble additive inside PP. Previous works on filaments showed $BaTiO_3$ particles were uniformly distributed within PP without use of compatibilizer. Agglomeration of particles was not observed within meltblown webs. At 1 and 10% concentrations particles are easily seen on the surface of the fibers. On the other hand though the diameter distribution of barium titanate is comparable to meltblown fiber diameter, ones on the fiber surfaces were relatively small when compared to particle size values provided by the manufacturer company. The shear forces during both masterbatch production and meltblowing might have a grinding effect and reduce the particle sizes. SEM images of selected samples were given in Figure 5.3.

PP Control	0.01% $BaTiO_3$	0.1% $BaTiO_3$	1% $BaTiO_3$	10% $BaTiO_3$
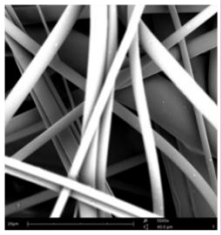	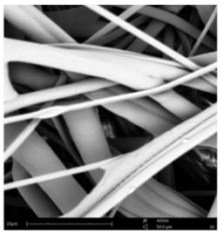	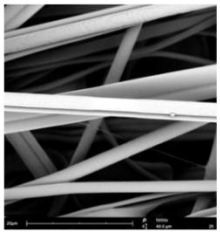	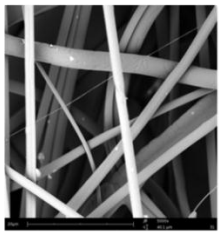	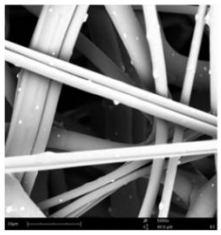
0.25ghm, 25psi	0.25ghm, 25psi	0.25ghm, 25psi	0.20ghm, 25psi	0.25ghm, 25psi

Figure 5.3 SEM images of $BaTiO_3$ containing MB webs

Fiber diameters and their distributions were found very similar [Figure 5.4]. For comparing the change in electrostatic filtration properties, it was an intention of the study to produce webs having similar basic structures, which gives similar mechanical filtration properties. So the contribution of the additives would be subtracted from total filtration efficiency. Looking at solidity of selected samples, as shown in Figure 5.4 at higher concentrations due to increased fiber density the value of solidity was calculated as nearly 30% lower than control sample. Meltblown web production process was performed as weight feed base, meaning at a given time same amount of resin was fed during process. So less volume of feed was sent per unit time for high concentrations since the density of barium titanate is approximately six times the density of polypropylene[29]. If there is a significant change in mechanical filtration properties of virgin and modified web, based on the definition of solidity, pressing the samples one can reduce the thickness of higher concentration samples to increase their solidity.

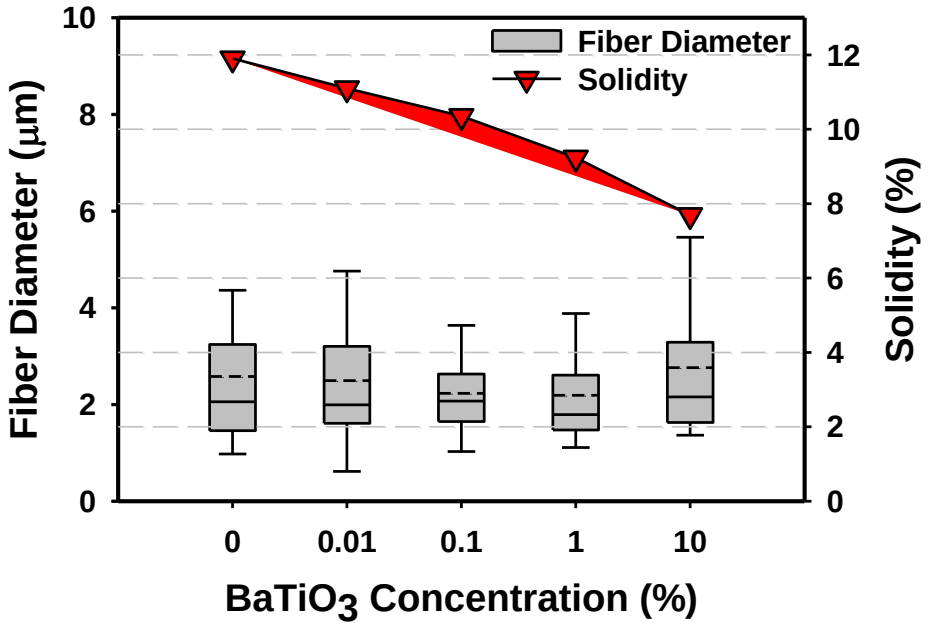

Figure 5.4 Fiber diameter and solidity of selected MB webs (box boundaries indicate upper and lower hinges, whereas dashed line stands for average fiber diameter, solid for median)

5.3.2 Surface Potential and Filtration Properties

Charging of $BaTiO_3$ containing meltblown web enhance filtration efficiency both in cold charging and thermal charging (Figure 5.5). This is because $BaTiO_3$ has very high dielectric constant. Even at room temperatures $BaTiO_3$ has very high dielectric constant [30] that enables web to hold electrostatic charges. However as explained in previous chapters for polarizing barium titanate within composite fibers at a larger extend, samples should be

heated to Curie point and charged for various timings to find optimized the charging/polarization conditions. As shown in Figure 5.5 effective polarization at high temperatures lead to better charging of web, thus higher filtration efficiency in 1% $BaTiO_3$ containing webs. Charging for 10min was sufficient to reach a saturation point.

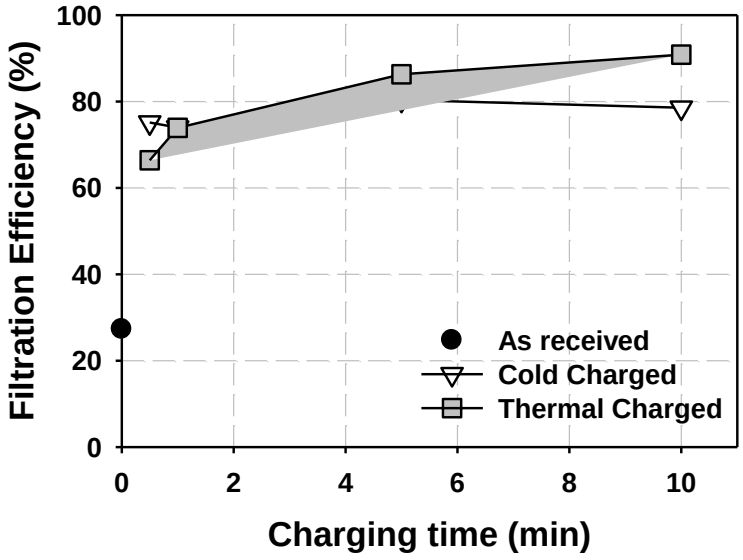

Figure 5.5 The effects of charging time and temperature on filtration efficiency

Moreover the surface potential of webs was measured and surface potential distributions of meltblown webs were mapped. As shown in Figure 5.6-5.8 thermally charged samples exhibited a high uniform potential on both face and back. Hence the potential

difference through webs, which is roughly related with the electric field on aerosol particles, is significantly high and uniform compared to cold charged sample. Weakly charged regions on cold charged sample would act as defective regions for electrostatic filtration process. The efficiency of 10min thermally charged 1% $BaTiO_3$/PP sample was observed as 90.8%, whereas it was 78.9% for cold charged sample which is thought to be due to more uniform and effective charging as shown in Figure 5.7. Interestingly for PP control sample, back of the sample also exhibited negative surface potential, whereas it was positive for $BaTiO_3$ containing webs.

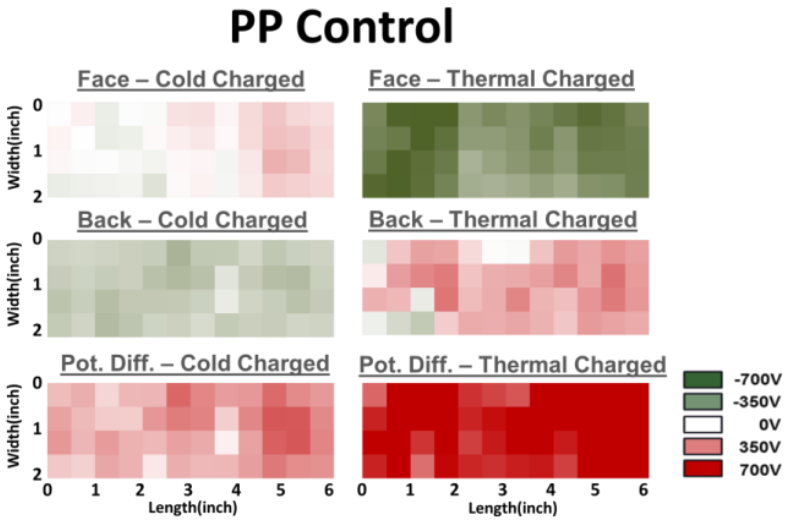

Figure 5.6 Potential map for cold charged and thermal charged control webs

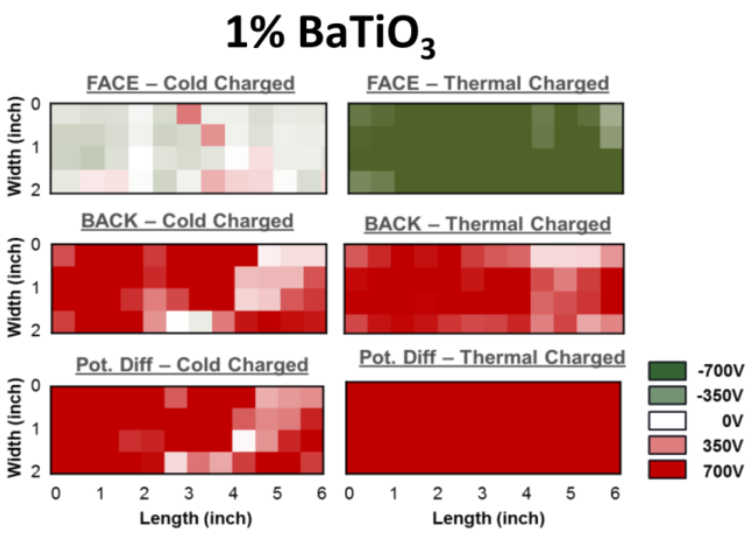

Figure 5.7 Potential map for cold charged and thermal charged 1% $BaTiO_3$/PP web

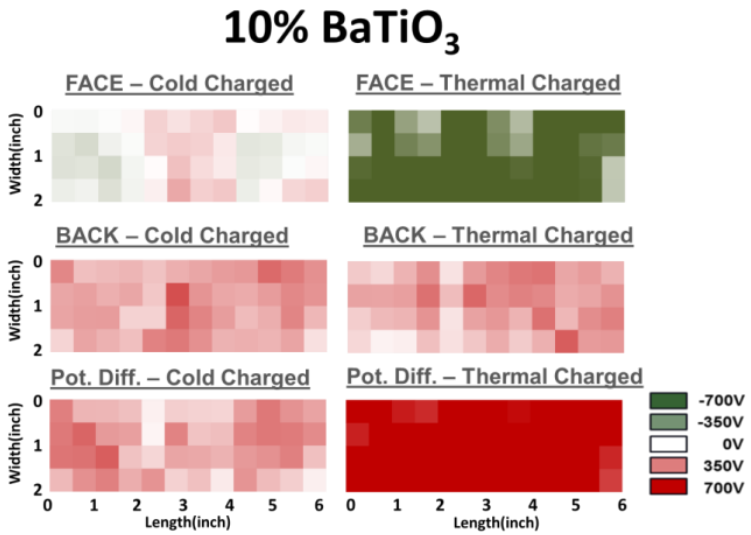

Figure 5.8 Potential map for cold charged and thermal charged 10% $BaTiO_3$/PP web

Control, 0.1, 1 and 10% $BaTiO_3$ containing samples were charged/polarized under the same conditions. Initial collection efficiencies of those samples were measured and HEPA level efficiency which is 99.97% for 0.3 μm particle size was found to be reached at an expense of 100Pa resistance. In Figure 5.9 results for as received, cold charged and thermally charged samples were shown. Again charging enhances filtration efficiency dramatically regardless of $BaTiO_3$ concentrations. Thermally charged samples poses best filtration performances. Mechanical filtration efficiencies were quite similar, hence electrostatic filtration efficiencies depending on additive presence and its concentrations would be compared.

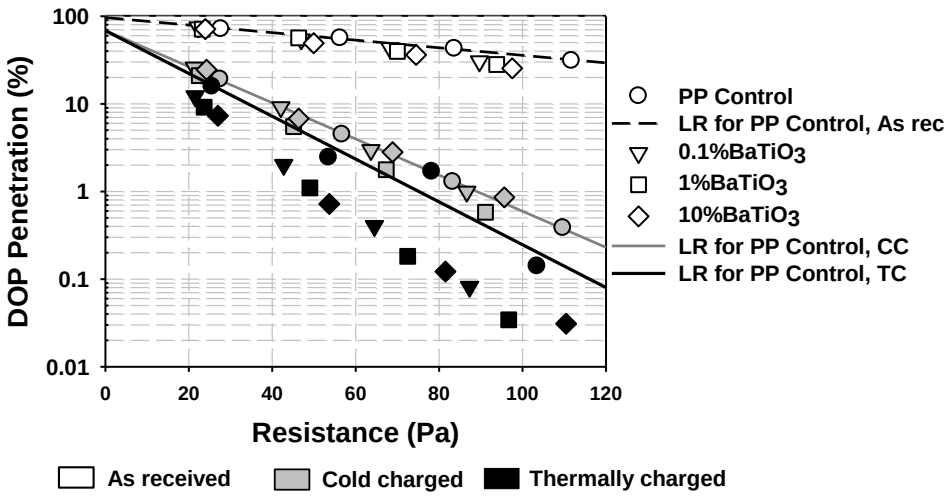

Figure 5.9 Penetration vs resistance curves of samples (d_p: 0.3μm, u:5.3cm/sec) LR indicates linear regression on semilog plot, whereas CC cold charged; TC thermal charged

Figure 5.10 summarizes the quality factor values after cold and thermally charging. The increase for $BaTiO_3$ containing samples is larger due to added polarization. Reference samples also exhibited a significant improvement upon charging at high temperatures. This was explained with accumulation of charges through deep traps[31]. So initial charge density of such samples would be expected to be higher. Also polarization of dipoles coming from any kind of impurities such as catalyst, extrusion residues and stabilizers within PP will be more effectively polarized at high temperatures because of high molecular mobility. Addition of BaTiO3 increased the concentration of polarizable species within the fibers. So when polarized against applied electric field, field produced by $BaTiO_3$ particles most probably attracted and fixed accumulated charges.

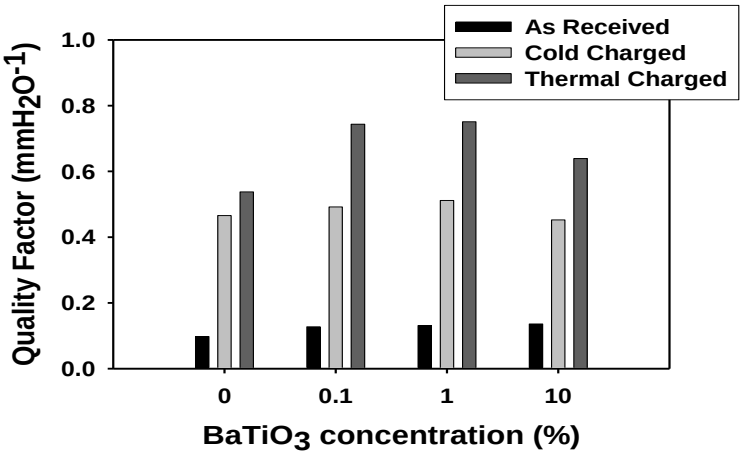

Figure 5.10 Quality factors calculated for 0.3μm DOP filtration at a face velocity of 5.3cm/sec

As shown in Figure 5.11 for uncharged media MPPS was obtained 0.3µm, whereas it shifted to 0.05µm for same media when thermally charged. For high efficiency electret filter media it is known that maximum penetrating particle size shifts to lower diameters[4]. We can conclude induction of uncharged aerosol particles was more efficient within thermally charged webs, thus they were captured at high efficiency.

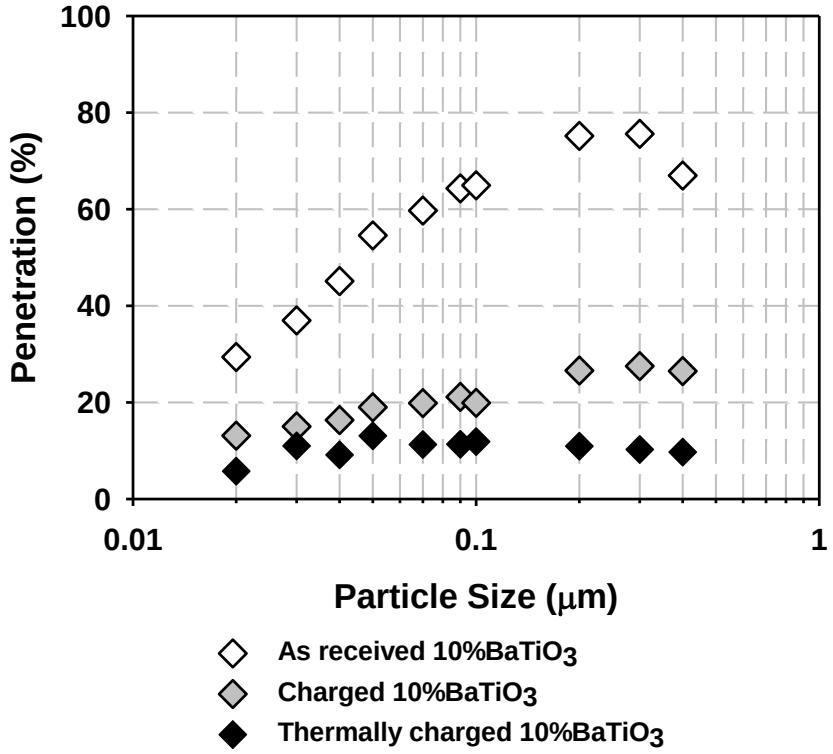

Figure 5.11 DOP penetration through 10% $BaTiO_3$/PP web for various particle diameter

5.3.3 Filtration Properties after Isothermal Potential Decay

One other concern on electret filters is the stability of charges and the resultant filtration properties. For this purpose there is no standard test method, so we designed a simple accelerated decay method at elevated temperatures for analyzing filtration stability. At higher temperatures molecular motions will lead to ease of decay. Charge decay is thought to be due to three mechanisms: Firstly even for highly insulators charged/polarized species will have temperature dependent mobility within bulk and over surface. Secondly ionic species in the air will lead to contamination [32] And thirdly captured DOP particles in the initial test will lead to neutralization or screening of charged surface[33] However it should be noted that contamination with air ions in the oven may not be as high as during filtration. When compared to real situation the decaying effect caused by captured particles will be relatively small since the samples were loaded for a few minutes during tests. Figure 10 shows results on the thermally charged samples. The increase in penetration is apparent especially for the case of reference sample. At 1 and 10 % concentration filtration efficiency did not drop so significantly which means charges/polarization is more stable.

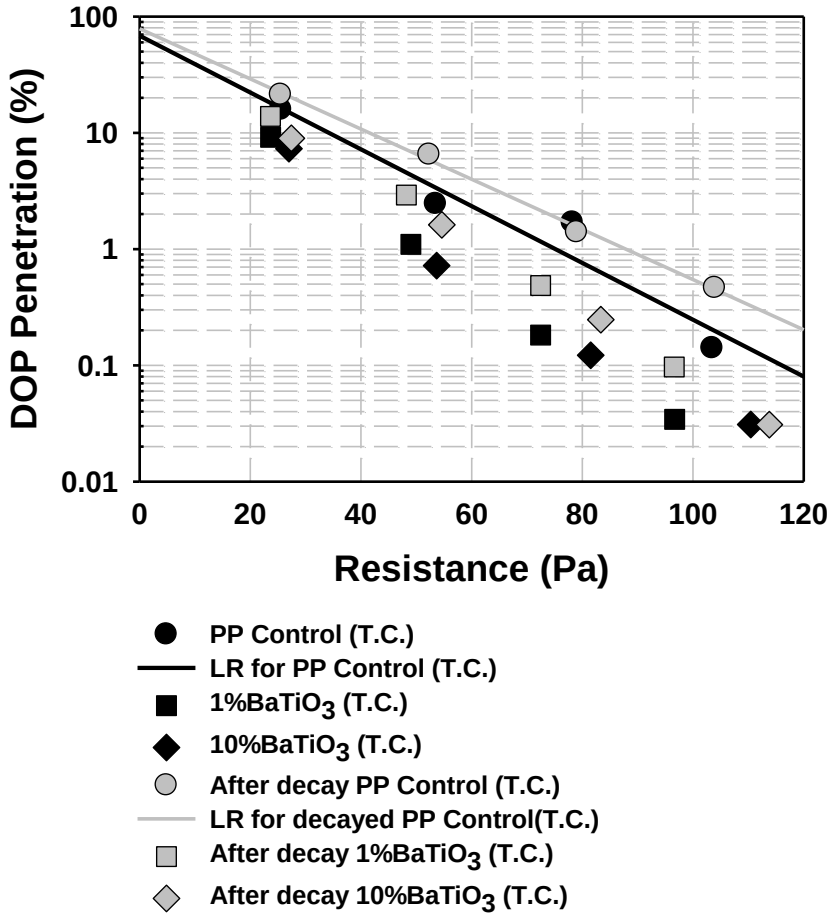

Figure 5.12 Filtration properties of thermally charged samples before and after accelerated decay test

5.3.4 Microstructural Properties of $BaTiO_3$/PP Webs

X-ray diffraction analysis showed that there is a significant change in morphology upon thermally charging [Figure 5.13]. 10%$BaTiO_3$ containing sample had a mesomorphic structure initially, however both reference and barium titanate containing samples α-form crystals became more clear exhibiting diffraction peaks at 110, 040, 130, 111, 041. However corresponding angles are a little higher when compared to data in literature[34], which indicates a small increase in d-spacing between atomic layers. Broad peaks at 2θ=15° and 21° indicates mesomorphic structures[35] for 10% $BaTiO_3$ containing sample which may be due to changes in temperature profile of solidifying molten jet. $BaTiO_3$ content might have caused ease of solidification, due to its higher heat transfer coefficient than that of PP[36,37]. Peaks shown between 30-60° correspond mostly ones diffracted by perovskite barium titanate crystals[38,39]. Apparently change in $BaTiO_3$ structure was much less. Improved crystallinity is effective on charge stability of the webs, which was seen on filtration tests upon isothermal potential decay test.

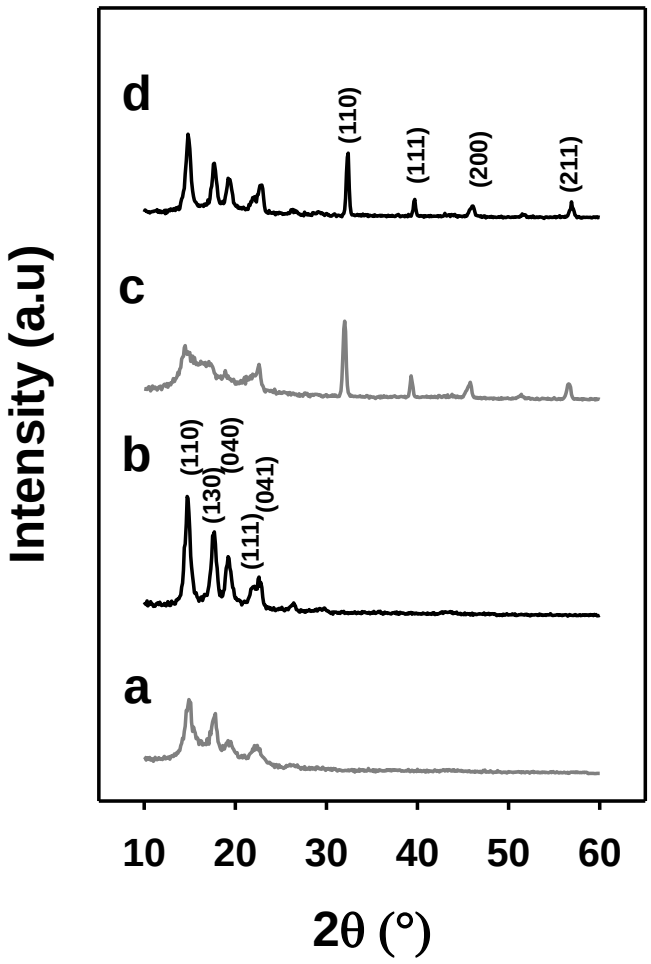

Figure 5.13 X-ray diffraction patterns of samples (a)PP Control, as received, (b)PP Control, after thermal charging, (c)10%$BaTiO_3$/PP, as received, (d)10%$BaTiO_3$/PP, after thermal charging (The samples for WAXD analysis were taken from ones used in filtration)

5.4 Conclusion

Thermal charging enhances electret properties of high dielectric constant inorganic additive containing webs significantly. For those of the composites containing nonlinear dielectrics charging at Curie temperature should be taken into account and charging/polarization temperature should be kept high. Higher potentials on the face and back of the fabric and large absolute difference led to higher filtration efficiency for thermally charged webs. Accelerated decay test was applied to filter webs, which would be useful for analyzing charge stability. Samples having uniform and high potential values exhibited best filtration performances. Even for high loading modified samples efficiency and stability of filtration was significantly enhanced after thermal charging. Results showed that barium titanate is solely an effective electret additive, since the resultant crystal structure did not change a lot.

5.5 References

1. Raynor, P. *et al.* Collection of biological and non-biological particles by new and used filters made from glass and electrostatically charged synthetic fibers. *Indoor air* 18, 51–62 (2008).

2. Barrett, L. W. & Rousseau, A. D. Aerosol loading performance of electret filter media. *American Industrial Hygiene Association Journal* 59, 532–539 (1998).

3. Kowalski, W. J., Bahnfleth, W. P. & Whittam, T. S. Filtration of airborne microorganisms: modeling and prediction. *ASHRAE TRANS* 105, 4–17 (1999).

4. Bałazy, A. *et al.* Manikin-Based Performance Evaluation of N95 Filtering-Facepiece Respirators Challenged with Nanoparticles. *Annals of Occupational Hygiene* 50, 259 –269 (2006).

5. Wang, C.-S. Electrostatic forces in fibrous filters--a review. *Powder Technology* 118, 166–170 (2001).

6. Huang, S.-H., Chen, C.-W., Chang, C.-P., Lai, C.-Y. & Chen, C.-C. Penetration of 4.5nm to aerosol particles through fibrous filters. *Journal of Aerosol Science* 38, 719–727 (2007).

7. Martin Jr, S. B. & Moyer, E. S. Electrostatic respirator filter media: filter efficiency and most penetrating particle size effects. *Applied Occupational and Environmental Hygiene* 15, 609–617 (2000).

8. Kim, S. C., Harrington, M. S. & Pui, D. Y. H. Experimental study of nanoparticles penetration through commercial filter media. *Nanotechnology and Occupational Health* 117–125at <http://www.springerlink.com/content/lm1w710937127427/>

9. Boskovic, L., Agranovski, I. E., Altman, I. S. & Braddock, R. D. Filter efficiency as a function of nanoparticle velocity and shape. *Journal of Aerosol Science* 39, 635–644 (2008).

10. Lee, M., Otani, Y., Namiki, N. & Emi, H. Prediction of collection efficiency of high-performance electret filters. *Journal of chemical engineering of Japan* 35, 57–62 (2002).

11. Rousseau, A. D., Jones, M. E. & Angadjivand, S. A. Fibrous Webs Having Enhanced Electret Properties. (2003).at <http://www.freepatentsonline.com/EP0845058.html>

12. Rousseau, A. D., Jones, M. E. & Angadjivand, S. A. *Fibrous webs useful for making electret filter media*. (Google Patents: 1999).

13. Angadjivand, S. A., Jones, M. E. & Meyer, D. E. *Method of charging electret filter media*. (Google Patents: 1996).

14. Eitzman, P. D. & Rousseau, A. D. *Method and apparatus for making a fibrous electret web using a wetting liquid and an aqueous polar liquid*. (Google Patents: 2002).

15. Jones, M. E. & Rousseau, A. D. *Oily mist resistant electret filter media*. (Google Patents: 1995).

16. Jones, M. E. & Rousseau, A. D. *Oily mist resistant electret filter media and method for filtering*. (Google Patents: 1995).

17. Mohmeyer, N. *et al.* Additives to improve the electret properties of isotactic polypropylene. *Polymer* 48, 1612–1619 (2007).

18. Behrendt, N. *et al.* Charge storage behavior of isotropic and biaxially-oriented polypropylene films containing α-and β-nucleating agents. *Journal of applied polymer science* 99, 650–658 (2006).

19. Mohmeyer, N., Schmidt, H. W., Kristiansen, P. M. & Altst\ädt, V. Influence of chemical structure and solubility of bisamide additives on the nucleation of isotactic polypropylene and the improvement of its charge storage properties. *Macromolecules* 39, 5760–5767 (2006).

20. Cartwright, G. A., Davies, A. E., Swingler, S. G. & Vaughan, A. S. Effect of an antioxidant additive on morphology and space-charge characteristics of low-density polyethylene. *Science, Measurement and Technology, IEE Proceedings*- 143, 26–34 (1996).

21. Jones, M. E. & Rousseau, A. D. *Oily mist resistant electret filter media*. (Google Patents: 1995).

22. McNeal, M. P., Jang, S.-J. & Newnham, R. E. Size effects on the dielectric properties of barium titanate (BaTiO3) at microwave frequencies. *Ferroelectrics* 211, 153 (1998).

23. Hench, L. L. & West, J. K. *Principles of electronic ceramics*. (Wiley: 1990).

24. Hennings, D. Barium titanate based ceramic materials for dielectric use. *International Journal of High Technology Ceramics* 3, 91–111 (1987).

25. Arlt, G., Hennings, D. & de With, G. Dielectric properties of fine-grained barium titanate ceramics. *Journal of Applied Physics* (1985).at <10.1063/1.336051>

26. Wang, X. & Ke, Q. Experimental investigation of adhesive meltblown web production using accessory air. *Polym. Eng. Sci.* 46, 1–7 (2006).

27. Shambaugh, R. L. A macroscopic view of the melt-blowing process for producing microfibers. *Industrial & Engineering Chemistry Research* 27, 2363–2372 (1988).

28. Milligan, M. W., Lu, F., Buntin, R. R. & Wadsworth, L. C. The use of crossflow to improve nonwoven melt-blown fibers. *J. Appl. Polym. Sci.* 44, 279–288 (1992).

29. Hennings, D. F. K., Metzmacher, C. & Schreinemacher, B. S. Defect Chemistry and Microstructure of Hydrothermal Barium Titanate. *Journal of the American Ceramic Society* 84, 179–182 (2001).

30. Hennings, D. Barium titanate based ceramic materials for dielectric use. *International Journal of High Technology Ceramics* 3, 91–111 (1987).

31. Zhong-Fu Xia, Guo-Mao Yang & Xi-Min Sun Charge dynamics in Mylar films corona-charged at various temperatures. *Electrical Insulation, IEEE Transactions on* 27, 702–707 (1992).

32. Jonassen, N. *Electrostatics*. (Springer: 2002).

33. Brown, R. C., Wake, D., Gray, R., Blackford, D. B. & Bostock, G. J. Effect of Industrial Aerosols on the Performance of Electrically Charged Filter Material. *Annals of Occupational Hygiene* 32, 271 –294 (1988).

34. Lee, Y. & Wadsworth, L. C. Effects of melt-blowing process conditions on morphological and mechanical properties of polypropylene webs. *Polymer* 33, 1200–1209 (1992).

35. Yan, R. J., Li, W., Li, G. & Jiang, B. Structure of mesomorphic form of isotactic polypropylene. *J. of Macromolecular Sc., Part B* 32, 15–31 (1993).

36. He, Y. Heat capacity, thermal conductivity, and thermal expansion of barium titanate-based ceramics. *Thermochimica acta* 419, 135–141 (2004).

37. Weidenfeller, B., Höfer, M. & Schilling, F. R. Thermal conductivity, thermal diffusivity, and specific heat capacity of particle filled polypropylene. *Composites Part A: Applied Science and Manufacturing* 35, 423–429 (2004).

38. Wang, M.-C., Hsiao, F.-Y., Hsi, C.-S. & Wu, N.-C. Crystal structure and ferroelectricity of nanocrystalline barium titanate thin films. *Journal of Crystal Growth* 246, 78–84 (2002).

39. Yuh, J., Nino, J. C. & Sigmund, W. M. Synthesis of barium titanate (BaTiO3) nanofibers via electrospinning. *Materials Letters* 59, 3645–3647 (2005).

CHAPTER 6

6 Effect of Nucleating Agents on Electret Properties of Polypropylene Filaments

Abstract

A comparative study on the effects of two different nucleating agents -DMDBS (3:2, 4-bis(3,4-dimethyldibenzylidene) sorbitol) and NA11 (sodium 2,2'-methylene-bis(4,6-di-tertbutylphenyl)-phosphate)- on morphological and electret properties of polypropylene (PP) filaments is reported. Fiber microstructure was examined via X-ray Diffraction (XRD) and Differential Scanning Calorimetry (DSC). Rather than reducing the crystal sizes, X-Ray diffractograms revealed that crystal sizes increased upon nucleating agent addition. For nonsoluble NA11 containing filaments elongated cavities were observed from microscopy images. Charging properties were analyzed via isothermal surface potential decay technique (ISPD) at 80°C. NA11 was found to be more efficient as an electret additive with a 50% increase in charge stability. However, DMDBS containing filament exhibited more rapid decay. Interestingly further studies on thermal charging showed both additives were effectively enhanced charge density and stability of the fibrous samples.

6.1 Introduction

Due to their quasipermanent charging property, electret materials are useful in various applications. Sessler and West used metalized fluoropolymer electrets to develop microphones[2]. Instruments were designed to analyze concentration of energetic ions that spread from radioactive sources[3]. Besides those of the transducer and sensor practices, during last decades electret filters attracted significant attention due their high efficiency at low pressure drop. Since electrostatic attraction is responsible for particle capture, more open webs composed of coarser fibers would be designed. However our initial studies on commercial electret filters showed that filter efficiency may not be as high as expected everytime, which would be due to weak electrostatic properties. As shown in Figure 6.1 filtration efficiency was not found so high for Filter 3 even at a relatively low face velocity, 5.3cm/sec. Another work by Raynor et al[4] in operating HVAC systems at a hospital, showed that for those of the filters, electrostatic capture performance may not be so stable, particularly during use in harsh conditions.

Nonwoven production and bonding methods such as meltblowing, spunbonding, needlepunching and hydroentanglement produce already triboelectrically charged webs at a level; however charges on those webs are not so stable and strong for long term filtration applications. As a result two step procedure; modification of webs with additives and a subsequent charging process is generally followed. So far various polymer additives were investigated as “electret additives”. For instance addition of high dielectric constant additives

provided polarizability to nonpolar polymers, such as PP[5]. Fluorochemicals were used as oil mist resistant agents to improve oleophobicity, thus reducing the formation of a destructive conductive film during filtration[172–176]. Other than those, nucleating agents were found to be useful to improve electret properties of PP films[11–18]. By adding nucleating agents smaller spherulites were observed in films whose boundaries are traps for space charges[12]. For the case of nonsoluble nucleating agents microvoids were observed upon stretching which prohibit charge migration [171].

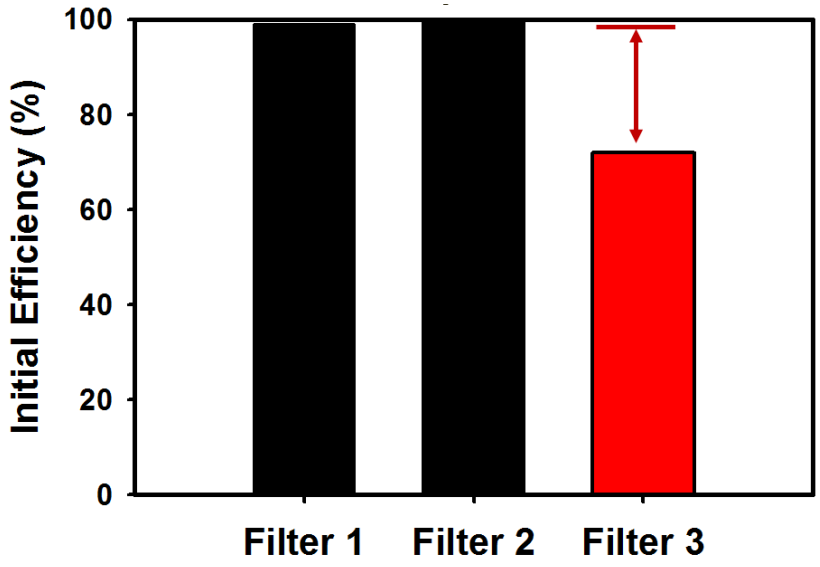

Figure 6.1 Filtration test on commercial filter media. 0.3μm NaCl particles at u=5.3cm/sec

Bisamides[16], trisamides [1218], sodium 2,2'-methylene-bis(4,6-di-tertbutylphenyl)-phosphate (NA11) [13,15], N,N'-dicyclo-hexyl- 2,6-naphthalene-dicarbox-amide (NU100) [14] were investigated so far. Effect of isomery and length of alkyl chain was examined on low molecular weight 1,4 phenylene bisamides as β-crystal nucleators with different substituents. Bisamides containing long aliphatic side chains disturbed the nucleation ability so as charge stability of PP films. Varying the symmetry of the additive molecules also resulted in changes in electret properties, but more than symmetry, concentration acted on charge stability. Comparing according to remaining potential after annealing at 90°C for 24h, approximately 20% improvement was achieved for iPP films containing bisamide additives at concentrations below 0.05wt%. At higher concentrations electret properties dropped, not because of network formation, but due to percolation of insoluble additive aggregates in the system[16].

Similarly addition of triphenylamine based trisamides at larger concentrations (0.04 wt%) introduced charge carriers at sufficient quantities to cause noticeable conductivity [12]. Comparison of trisamides comprising amide groups and cyclohexyl substituents showed that presence of -NH groups results in self-assembly, thus formed macrodipoles which gave rise to charge retention. Trisamides without those amide groups exhibited worse stability than even pure films. However larger 3D network structures were observed at higher concentrations which correspond to percolation concentration. Higher initial potentials could be reached at those concentrations, but decays rapidly [18].

On the other hand NA11 and some conventional nucleating agents do not dissolve in PP. Their electret characteristics were thought to be depending on formation of elongated voids which act as charge barriers against decay. Upon stretching effect of formed cavities becomes more dominant for NA11 containing films which resulted in longer stability. [13,15]

Almost all electret studies on nucleating agents were focused on improving properties of PP films.In this study the effect of nucleating agents on morphological properties and electret characteristics was investigated directly on PP filaments, thus their possible effect on electrostatic filtration properties will be enlightened. Two different nucleating agents, soluble sorbitol based DMDBS and non-soluble organophosphorous compound, NA11 were compared.

6.2 Experimental

6.2.1 Sample preparation

34 MFR iPP resin, having M_n~55,000g/mole, M_w~180,000g/mole molecular weight, kindly provided from Sunoco Chemicals (TX) was used as host polymer. DMDBS and NA11 in powder form were donated by Milliken Company (SC) and BASF respectively. Molecular structures of the additives were given in Figure 6.2.

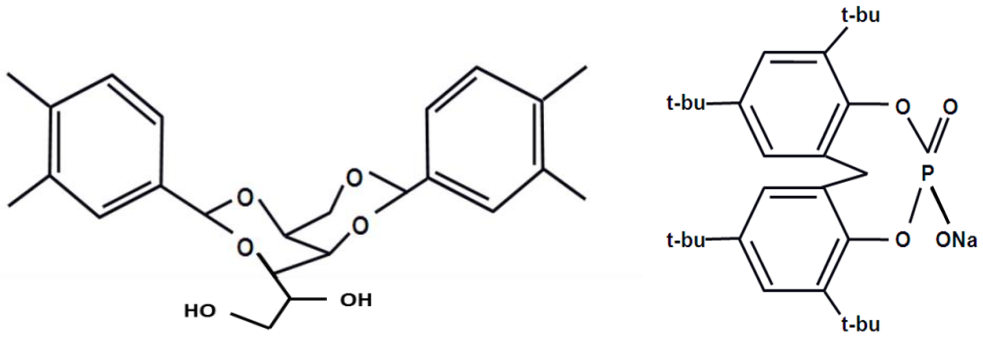

Figure 6.2 Chemistry of DMDBS (left) and NA11 (right)

Masterbatch at 20%w concentration was prepared by Techmer PM (TN), prior to filament extrusion. Then PP filaments containing additives at 0.1, 0.5, 1, 5% concentrations were melt-spun in Hills multifilament spinning line in the Nonwovens Institute (single screw extruder with an L:D ratio of 24:1). Spinning speed was fixed at 2000m/min and throughput was 0.58ghole^{-1}min^{-1}. Diameters of the filaments were kept 20μm for all samples. Temperature of spin head with 72 holes was fixed at 235°C.

Multifilament samples were washed with deionized water at 45°C for 6h to remove impurities and spinfinish applied during melt spinning process. The washing fluid was replaced every 2h. Use of any detergent or surface active was not preferred; since samples might be contaminated with those of the chemicals even after rinsing. Yarns wounded on washing tubes were dried overnight.

6.2.2 Charging and Characterization of Charging Property

After drying, yarns were aligned parallel on aluminum sample holders with a definite spacing (10 yarns/cm) as shown in Figure 6.3. It was observed that any fiber protruding from specimen caused significant variations on measured potential value. In order to fix any protruding fiber, perpendicular yarns were aligned at a distance of 0.7cm from each other. The filaments were fixed carefully by using conductive tape and epoxy to prevent errors that can occur due to position changes during charging and decay tests.

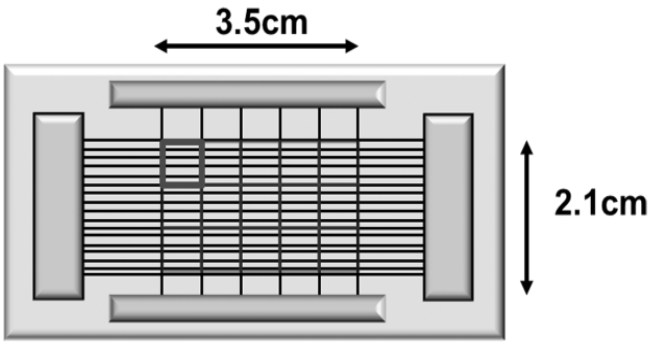

Figure 6.3 Specimen for SPD test and surface potential detection points

Charging of the samples was carried out with a point-to-plate negative corona discharger (Mystic Marvels, Model NIP-7E). Applied voltage was fixed at 9kV where maximum output direct current of the emitter needle was about 160μA. Samples were charged for 1 minute as it was determined as an optimized value (Chapter4). All testing

procedure was performed at laboratory conditions in which relative humidity was kept fixed between 54-59% RH at 22-23°C temperature.

The surface potential was measured with Monroe Modeal244A noncontact electrostatic voltmeter. Three specimen were prepared from each samples and average values and standard deviations were calculated thereof. Across the surface 15 specific points per sample were used for evaluation. The initial measurements (V_0) were taken directly after charging. All following measurements for surface potential decay test were carried out after fixed annealing times at 80°C. The periods in the oven were 0.5h, 1h, 2h, 4h, 8h, 12h, 16h, and 24h. Due to the nature of decay, periods kept shorter initially. Samples after annealing were cooled for 10 minutes in a desiccator to prohibit the effect of atmosphere.

6.2.3 Fiber microstructure

Microscopy. Optical microscopy images were taken randomly to understand the distribution of additives inside PP filament. Zeiss optical microscope with an objective of 40X was used and images were captured with Nikon high-definition color camera head DS-Fi1. To confirm optical micrographs and show distribution within filament cross-section SEM analyses were performed on a Hitachi S-3200 Scanning Electron Microscope.

Differential Scanning Calorimetry (DSC). Melting and crystallization behavior of the composite was analyzed using Perkin-Elmer differential scanning calorimeter. Samples

weighing 4.0±0.5 mg were heated in a nitrogen atmosphere from 25°C to 190°C at a rate of 20°C/min. During each run the sample was kept for 4 min at the highest temperature prior to cooling in order to ensure complete melting of the polymer and delete thermal history. Crystallization and melting temperatures reported here correspond to the peak temperatures in the DSC thermograms. Also crystallinity of the samples was calculated using the following formula:

$$\%Crystallinity = \frac{\Delta H}{\Delta H^{0}_{PP}} \times 100 \qquad \text{Equation 6.1}$$

where, ΔH is the enthalpy of fusion of the sample (J/g) and ΔH^{0}_{PP} is the enthalpy of fusion of completely crystalline PP (~ 207 J/g) [20].

Wide Angle X-ray Diffraction (WAXD). Crystal sizes of the samples were calculated using Omni Instrumental X-ray diffractometer. The diffractometer was equipped with Be-filtered Cu-K_α radiation with a wavelength of 1.54Å generated at 35kV and 25mA. Filament samples were wounded on the sample holder and the placed in the sample holder. The samples were scanned from 2Θ range from 10° to 30° at an increment of 0.1°. The crystal size of the samples was calculated using Scherer equation[21].

$$t = \frac{0.9 * \lambda}{B * \cos \theta_B}$$

Equation 6.2

where, t: Crystal size (Å); λ:Wavelength of X-ray (1.54 Å); B:Full Width at Half Maximum (radian); Θ_B:Bragg angle (degree)

6.3 Results

6.3.1 Fiber microstructure

The distribution of additives was investigated via optical microscopy. For miscible DMDBS no varying phases were observed that can be detected via visible light, whereas solid NA11 particles produced elongated cavities. Optical images of 1 and 5% NA11 containing samples were given in Figure 6.4.

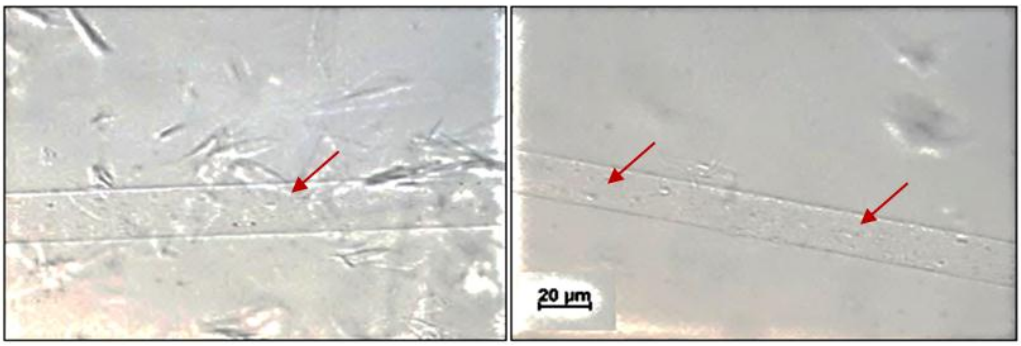

Figure 6.4 Optical micrographs for samples containing 1% NA11 (left), 5% NA11 (right)

Arrows indicate elongated cavities

Formation of cavities would be thought as another evidence for early solidification. In our previous study on nonsoluble $BaTiO_3$ containing PP filaments such cavities were not observed, however for the case of NA11, stretching resulted in elongated voids within solidified polymer threadline. As shown in Figure 6.5 other than cavities, surface became roughened after NA11 addition.

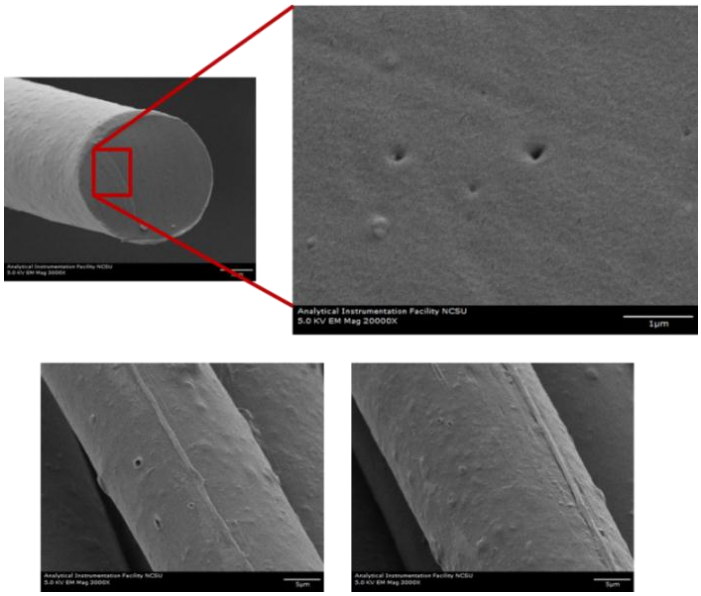

Figure 6.5 Cross-sectional image of 5% NA11 containing fibers obtained via SEM

Acting mainly on crystallization kinetics, nucleating agent addition may change resultant polymer microstructure, ie crystal forms and size [1]. Difference in melting (T_m) and crystallization temperatures (T_c) of DMDBS/PP and NA11/PP filaments were determined

from DSC cooling graph (Figure 6.6). For cooling rates at 20°C/min, there is a significant increase in crystallization temperature (T_c) as a result of nucleating agent incorporation, meaning that molten jet probably solidified earlier than PP control filaments. In this regard NA11 had nucleating ability even at 0.1% concentration, whereas T_c increase in DMDBS/PP started at 0.5% concentration. Increase in crystallization temperature for DMDBS containing filaments were 12-15°C and for NA11 12-17°C change was obtained.

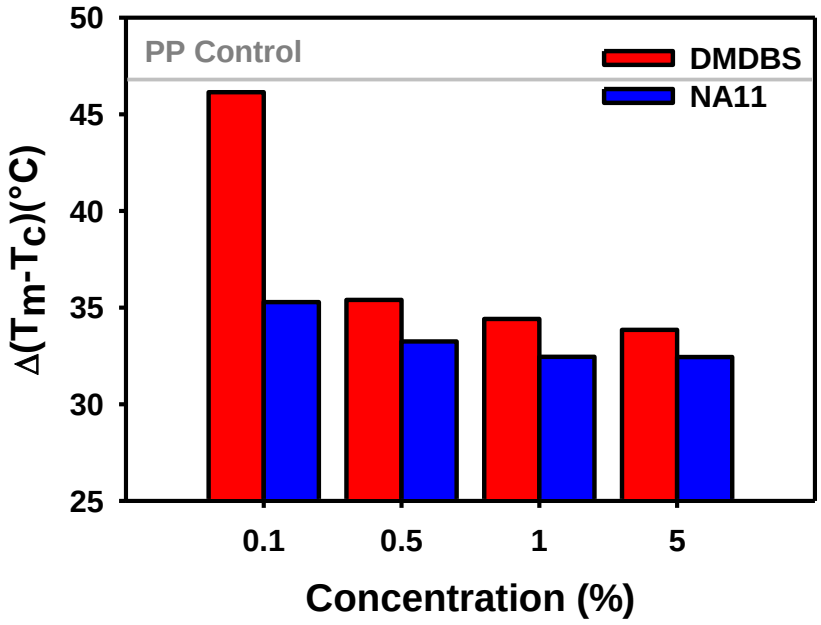

Figure 6.6 Difference between melting and crystallization temperatures, $\Delta(T_m-T_c)$ of nucleating agent containing filaments

From WAXD analysis a significant increase in crystal sizes was observed. Though being a very rapid process, as revealed from DSC studies nucleating agent addition caused earlier crystallization, which provided more time for crystal growth. Change in crystal sizes on (110) plane was summarized in Figure 6.7. Largest crystals were obtained at 1% concentration of nucleating agents, where most efficient nucleation in films was obtained in previous studies[1].

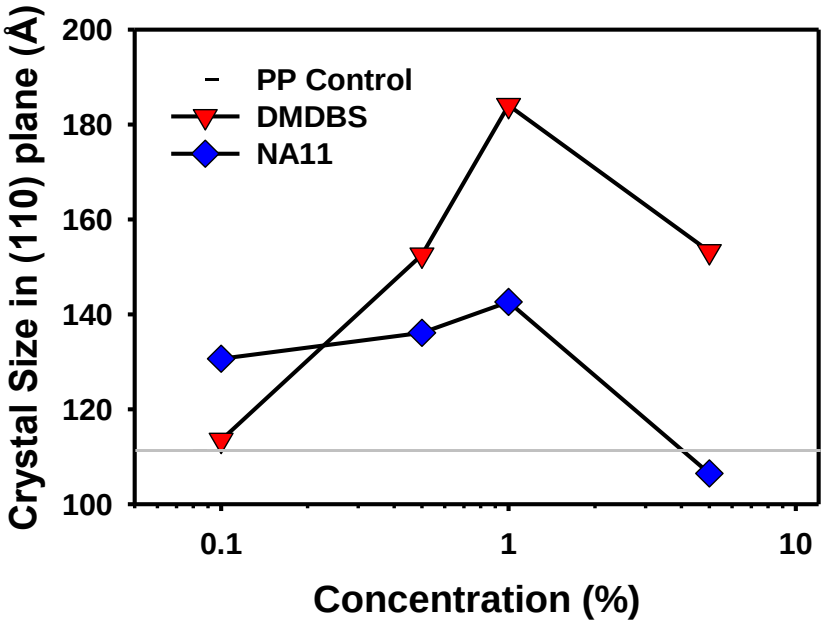

Figure 6.7 Crystal size in (110) planes of nucleating agent/PP filaments

Table 6.1 Detailed WAXD analysis for various nucleating agent concentrations

Additive Conc. (%)	2theta(°)	Size (Å)	Possible crystal
0	14.99	111.2	α-Polypropylene(1,1,0)
	17.73	144.8	α-Polypropylene(0,4,0)
	19.40	112.0	α-Polypropylene(1,3,0)
0.1% DMDBS	14.88	113.5	α-Polypropylene(1,1,0)
	17.65	114.6	α-Polypropylene(0,4,0)
	19.32	124.6	α-Polypropylene(1,3,0)
0.5%DMDBS	14.60	152.5	α-Polypropylene(1,1,0)
	17.46	155.0	α-Polypropylene(0,4,0)
	19.06	124.1	α-Polypropylene(1,3,0)
1%DMDBS	14.66	184.0	α-Polypropylene(1,1,0)
	17.48	210.9	α-Polypropylene(0,4,0)
	19.12	131.4	α-Polypropylene(1,3,0)
5%DMDBS	15.07	153.3	α-Polypropylene(1,1,0)
	17.88	208.1	α-Polypropylene(0,4,0)
	19.51	125.8	α-Polypropylene(1,3,0)
0.1%NA11	15.43	130.6	α-Polypropylene(1,1,0)
	17.80	144.0	α-Polypropylene(0,4,0)
	19.46	120.6	α-Polypropylene(1,3,0)
0.5%NA11	14.96	136.1	α-Polypropylene(1,1,0)
	17.74	138.5	α-Polypropylene(0,4,0)
	19.39	119.9	α-Polypropylene(1,3,0)
1%NA11	14.96	142.6	α-Polypropylene(1,1,0)
	17.75	127.6	α-Polypropylene(0,4,0)
	19.40	115.2	α-Polypropylene(1,3,0)
5%NA11	15.01	106.5	α-Polypropylene(1,1,0)
	17.76	130.2	α-Polypropylene(0,4,0)
	19.41	105.9	α-Polypropylene(1,3,0)

From the DSC thermograms, crystallinity of the filaments was calculated (Figure 6.8). For both of the additives below 1% concentration, crystallinity values were very similar

with control samples. 5%DMDBS addition reduced crystallinity, whereas an increase was observed with NA11 content at this concentration.

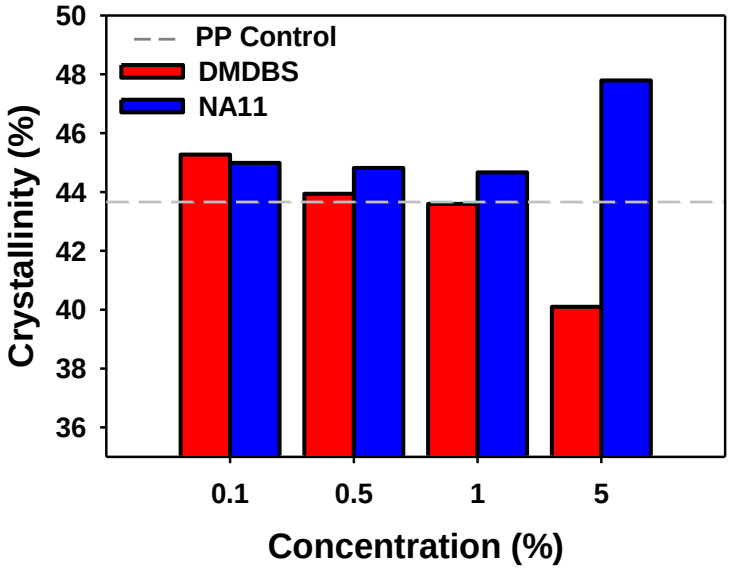

Figure 6.8 Crystallinity values of nucleating agent/PP filaments calculated from DSC thermograms

6.3.2 Charging Properties

As shown in isothermal potential decay graphs (Figure 6.9) DMDBS containing samples exhibited more rapid decay, compared to control samples at all concentration range between 0.1-5%. At 0.1% concentration the initial surface potential was high, but

accompanied with rapid charge decay. On the other hand NA11 containing samples exhibited better charging properties when compared to control PP. Particularly at 5% concentration increase in initial potential and charge stability was found to be significant.

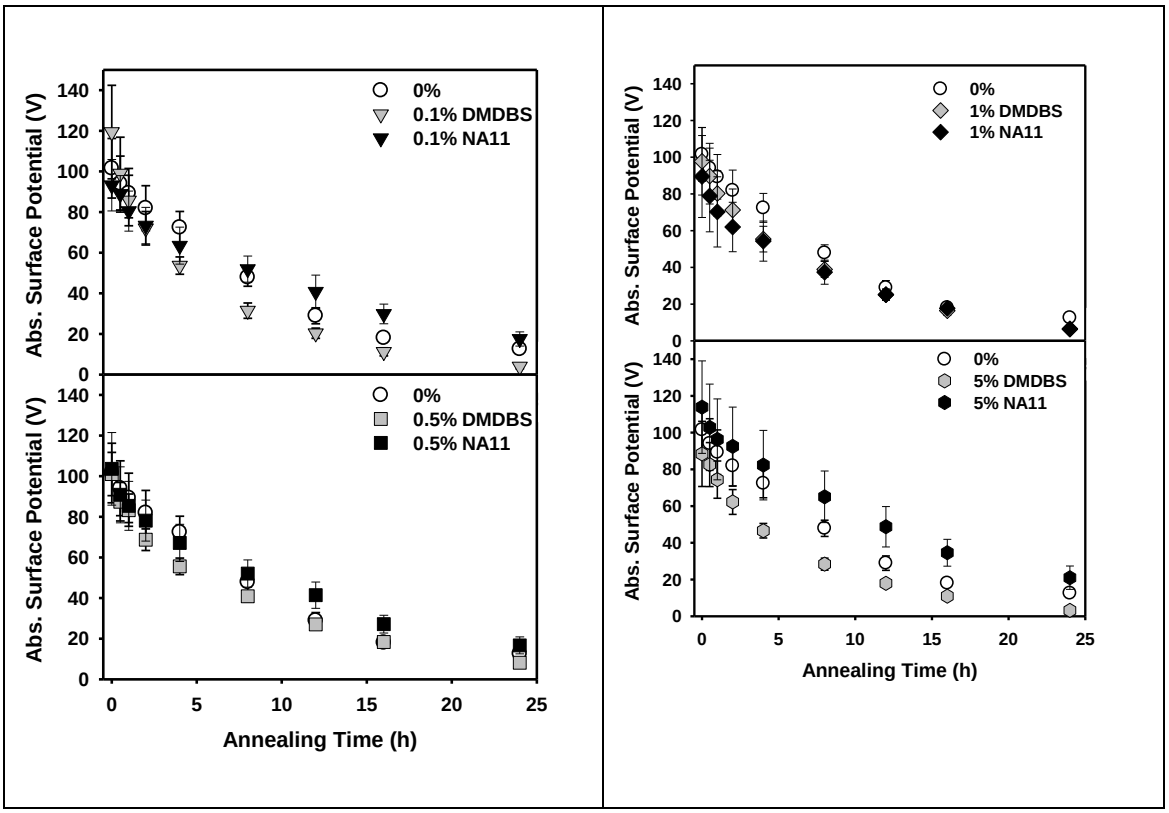

Figure 6.9 Isothermal surface potential decay on DMDBS/PP and NA11/PP filaments

Relaxation time which corresponds to 1/e th value of initial potential would be calculated to compare stability of the samples. Figure 6.10 shows initial absolute potential

and relaxation times of corresponding samples. Charge decay in DMDBS containing samples is significantly fast, which exhibited 20-40% reduction in relaxation times. On the other hand relaxation time increased 30-50% upon addition of NA11. Interestingly both initial potential and charge stability of 1% NA11 containing sample are significantly low. Same was also observed by Hillenbrand et al [15]. However the effect was not so destructive on their studies on films.

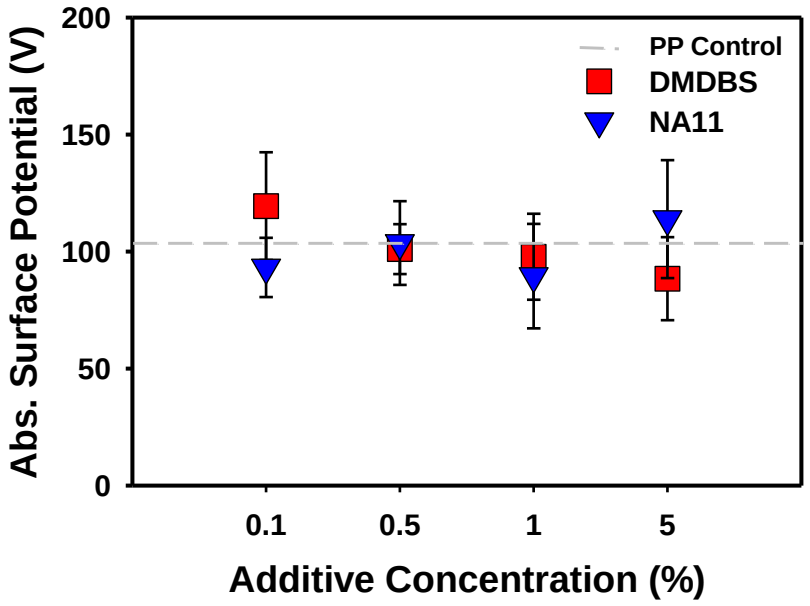

Figure 6.10 Initial potentials of the nucleating agent containing samples (after charging 1min under 4.5kV/cm corona discharger)

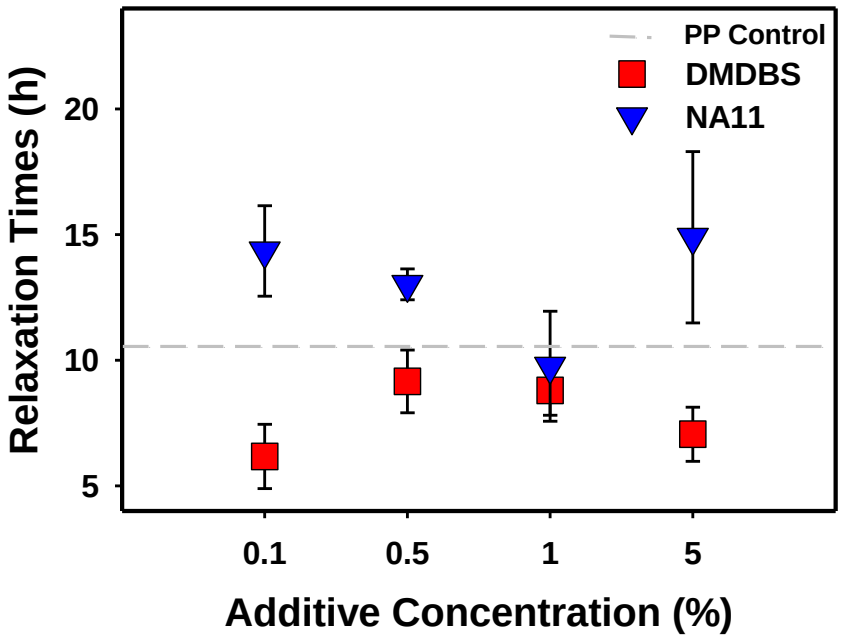

Figure 6.11 Relaxation times of the nucleating agent containing samples

Combining microstructural data evolved from WAXD and DSC studies with isothermal potential decay studies, we know that interfacial polarization takes place in heterophase systems where there are boundaries between phases of different conductivity and permittivity [22]. Thus polarizability of the samples would be enhanced when crystal size was smaller because for such systems smaller crystals will produce comparatively larger interfaces in total, where space charges are located. For filaments, addition of nucleating agent mostly resulted in larger crystal sizes, which would be due to early initiation of

crystallization process that gave more time for crystal growth. However for the case of nonsoluble NA11, interfaces between polymer and additive would be created and play role in charge holding capacity.

It is already known that more stable electrets would be observed via thermal charging. Softening of the polymer, improved corona conditions and activation of polarizable species due to enhanced charge carrier mobility at elevated temperatures would be reason behind this phenomenon [23,24]. We have charged the samples for 1min at 130°C, which is maximum temperature we can achieve without damaging filaments in our system. Resultant electret properties of both DMDBS and NA11 containing samples were different from that we obtained in cold charged samples (Figure 6.12).

Thermally charged samples containing NA11 at 0.5 and 5% concentration exhibited longer charge stability when compared to DMDBS. Interestingly DMDBS containing samples at 5% was found to be more stable and highly charged, whereas electret properties were close to reference sample at 0.5% concentration.

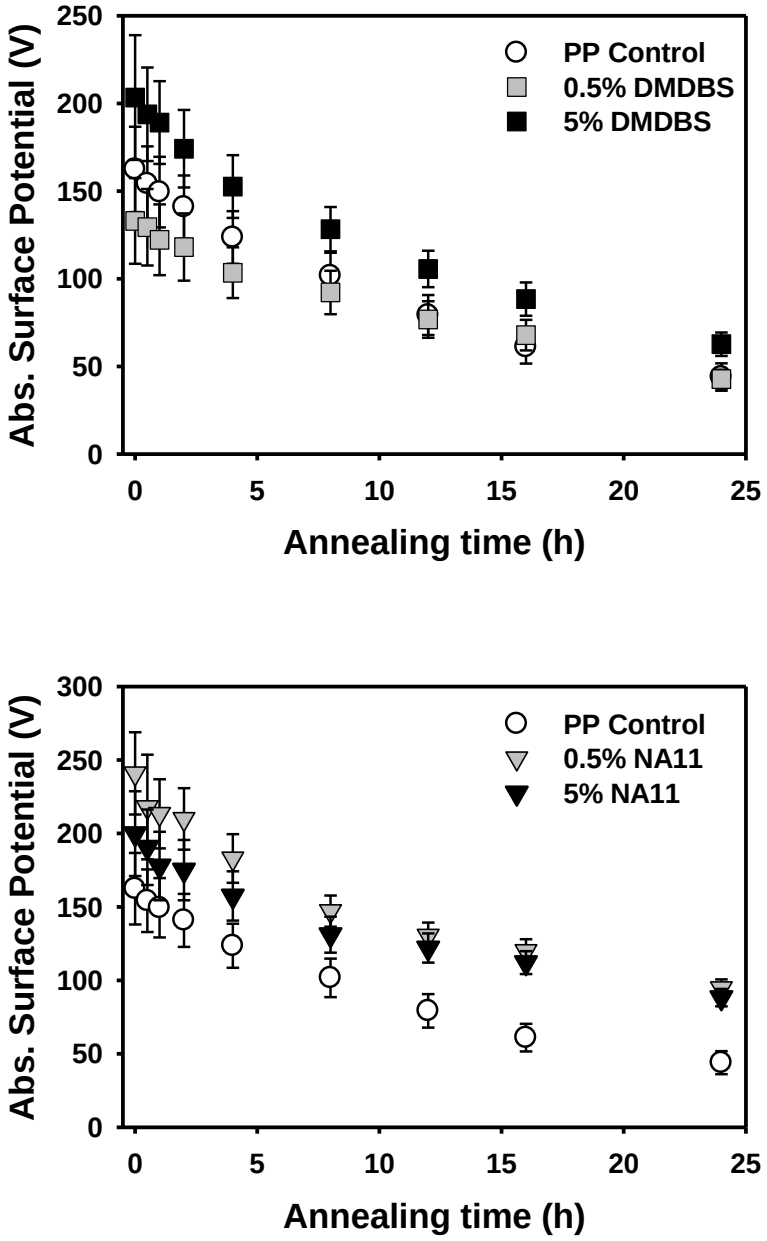

Figure 6.12 Isothermal surface potential decay test on thermally charged DMDBS/PP filaments and NA11/filaments

Initial surface potentials and relaxation times of all samples are summarized in Figure 6.13. Initial surface potential of cold charged samples were similar, whereas it was almost doubled for thermally charged NA11 containing samples. However calculated relaxation times were higher for all modified samples.

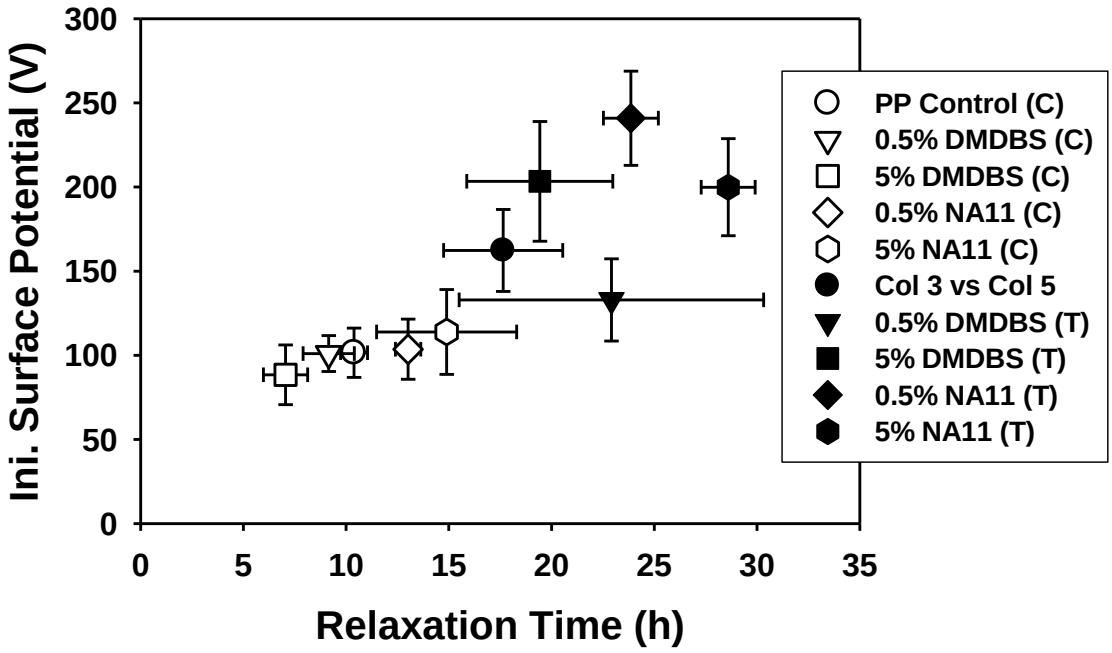

Figure 6.13 Initial potentials and relaxation times of thermally charged samples. (C) indicates cold charged, whereas (T) indicates thermally charged

6.4 Discussion

DMDBS containing samples did not improve charge stability at any concentration upon cold charging. However even at 5% concentration both additives had significantly longer stability when thermally charged. Like bisamides and trisamides, which are forming conductive aggregates, stability of DMDBS containing samples was expected to get worse due to percolation concentration resulting from H-bond formation[16–18]. Probably high shear rates during extrusion did not allow such drift pathways and distribute DMDBS aggregates uniformly within filaments.

For NA11 containing films, elongated voids are thought to be acting as barrier against charge drift[11] through electrodes. However filament electrets are nonmetallized dielectrics with a circular cross-section. Due to that reason barrier effect is not thought to be dominant.

Polar groups were incorporated into nonpolar PP with nucleating agents. DMDBS contains –OH groups, whereas NA11 contains more polar –ONa group. Those species should have given rise to total polarizability of modified samples, which was observed clearly in thermal charging tests. Due to nature of orientational polarization, high temperature would lead to higher molecular mobility, thus high initial potential were obtained at %5DMDBS and 0.5 and 5% NA11 containing filaments. Cold charging resulted with similar initial potentials which will probably result in similar electrostatic filtration properties if studied on webs.

On the other hand polar group containing polymers have the problem of having more hydrophilic surface which is not good for filtration in high humidity conditions particularly at high oily aerosol concentrations. Nevertheless according to general spirit of nucleating agents, polar groups coming from nucleants would be expected to be buried within crystal structures, whereas most of the other additives are located in lower density amorphous regions. Another interesting finding was that charge decay within filaments is found to be more rapid than that of nucleated films investigated in the literature[11–13,16,18]. Besides charge migration through bulk, charge decay within filaments might be surface dependent.

6.5 Conclusion

Morphological and electrostatic behaviors of PP filaments containing nucleating agents were examined. Initial potentials of cold charged modified samples were not enhanced significantly, whereas DMDBS also disturbed charge stability. Interestingly thermal charging improved electret properties which would be because of softening of the polymer, improved corona conditions and activation of polarizable species due to enhanced charge carrier mobility at elevated temperatures. One other possibility for enhancement would be orientational polarization of additive which is temperature dependent. This will be investigated in a future study. Due to those possibilities, not only additive incorporation, but also required charging conditions should be modified to obtain better electret properties.

6.6 References

1. Kristiansen, M. *et al.* The Binary System Isotactic Polypropylene/Bis(3,4-dimethylbenzylidene)sorbitol: Phase Behavior, Nucleation, and Optical Properties. *Macromolecules* 36, 5150–5156 (2003).

2. Sessler, G. M. & West, J. E. Electret transducers: a review. *J. Acoust. Soc. Am.* 53, 1589–1600 (1973).

3. Silva, M. D., Bandeira, I. N. & Miranda, L. C. M. Open-cell photoacoustic radiation detector. *Journal of Physics E: Scientific Instruments* 20, 1476 (1987).

4. Raynor, P. C. *et al.* Collection of biological and non-biological particles by new and used filters made from glass and electrostatically charged synthetic fibers. *Indoor Air* 18, 51–62 (2008).

5. Turkevich, L. A. & Myers, D. L. *Ferroelectric fibers and applications therefor*. (Google Patents: 2000).

6. Rousseau, A. D., Jones, M. E. & Mei, B. Z. Electret articles and filters with increased oily mist resistance. (2001).

7. Rousseau, A. D., Jones, M. E. & Mei, B. Z. Method of making electret articles and filters with increased oily mist resistance. (2000).

8. Jones, M. E., Rousseau, A. D. & others *Oily mist resistant electret filter media*. (Google Patents: 1995).

9. Jones, M. E., Rousseau, A. D. & others *Oily mist resistant electret filter media and method for filtering*. (Google Patents: 1995).

10. Huberty, J. S. *Oily-mist resistant filter that has nondecreasing efficiency*. (Google Patents: 2003).

11. Behrendt, N., Altstadt, V., Schmidt, H. W., Zhang, X. & Sessler, G. M. Development of porous polypropylene blends with NA11 particles and glass hollow spheres by biaxial stretching for electret applications. *Dielectrics and Electrical Insulation, IEEE Transactions on* 13, 992–1000 (2006).

12. Mohmeyer, N. *et al.* Additives to improve the electret properties of isotactic polypropylene. *Polymer* 48, 1612–1619 (2007).

13. Hillenbrand, J. *et al.* Charge retention in biaxially-oriented polypropylene films containing various additives. *Electrets, 2005. ISE-12. 2005 12th International Symposium on* 276–279 (2005).

14. Behrendt, N. *et al.* Charge storage behavior of isotropic and biaxially-oriented polypropylene films containing α-and β-nucleating agents. *Journal of applied polymer science* 99, 650–658 (2006).

15. Hillenbrand, J., Behrendt, N., Altst\ädt, V., Schmidt, H. W. & Sessler, G. M. Electret properties of biaxially stretched polypropylene films containing various additives. *Journal of Physics D: Applied Physics* 39, 535 (2006).

16. Mohmeyer, N., Schmidt, H. W., Kristiansen, P. M. & Altst\ädt, V. Influence of chemical structure and solubility of bisamide additives on the nucleation of isotactic polypropylene and the improvement of its charge storage properties. *Macromolecules* 39, 5760–5767 (2006).

17. Mohmeyer, N. *et al.* Nucleation of isotactic polypropylene by triphenylamine-based trisamide derivatives and their influence on charge-storage properties. *Polymer* 45, 6655–6663 (2004).

18. Erhard, D. *et al.* Recent Advances in the Improvement of Polymer Electret Films. *[Advances in Polymer Science]* 1–53 (2010).

19. Behrendt, N. *et al.* Charge storage behavior of isotropic and biaxially-oriented polypropylene films containing alpha- and beta-nucleating agents. *Journal of Applied Polymer Science* 99, 650–658 (2006).

20. Mark, J. *et al. Physical Properties of Polymers*. (Cambridge University Press: 2004).

21. Salem, D. R. *Structure formation in polymeric fibers*. (Hanser Verlag: 2001).

22. Lilaonitkul, A. & Cooper, S. L. Dielectric Relaxation Studies of Segmented Polyesters. *Macromolecules* 12, 1146–1156 (1979).

23. Klaase, P. T. . & Van Turnhout, J. *Method for manufacturing an electret filter medium*. (Google Patents: 1986).

24. Nalwa, H. S. *Ferroelectric polymers: chemistry, physics, and applications*. (CRC Press: 1995).

CHAPTER 7

7 Effects of Stabilizers on Charging of PP Filaments

Abstract

Other than protection against oxidation, stabilizers with their different electronic structure may be useful as charge enhancing additives for polymeric fibers. To investigate this relation polypropylene (PP) filaments were blended with Irgafos 168 -Tris(2,4-di-*tert*-butylphenyl)phosphite and Tinuvin 622LD -Poly(4-hydroxy-2,2,6,6-tetramethyl-1-piperidine ethanol-alt-1,4-butanedioic acid). In conventional use the former acts as hydroperoxide decomposer, whereas the later is a hindered amine type ligth stabilizer. In experimental additive concentration was kept in 0.1-5% range. Charging properties were analyzed via isothermal surface potential decay technique (ISPD) at 80°C. Results on corona charged samples showed that Irgafos 168 at 0.1-0.5% concentrations led to 50% increase on charge stability, whereas Tinuvin622 addition barely enhanced charge holding properties at 1% concentration. Decay tendency was more rapid for other concentrations. Fiber microstructure was examined via X-ray Diffraction (XRD). Though there is a significant reduction in crystallinity of Tinuvin containing samples, interestingly charge stability did not drop as expected.

7.1 Introduction

Charge retention properties of polymers are related with either molecular or morphologic scale defective structures within those high band gap materials. Those defects may act as deep and shallow traps according to electronic structure within polymer structure. Former can be due to any kind of impurity, such as catalysts, antioxidants or oxidized species, whereas space charges are accumulated within amorphous-crystalline boundaries[1,2]. Thus resulting *electret* property is important for various applications since a considerable electric field is produced without need of a power source. For instance within fibrous electrets created electric field is sufficient to capture aerosol particles, which resulted with one of the most common electret applications. Fibrous electret webs have superior particle capture efficiency when compared to conventional uncharged filters. Rather than mechanical capture mechanisms, such as inertial impaction, interception and diffusion; electrostatic forces will also take part in the filtration process, hence their efficiency gets higher for particles having diameter around 0.3μm, where maximum particle penetration occurs in uncharged filters [3].

It is well known that various polymer properties would be manipulated by using additives. In this regard if charge holding is undesirable external and internal antistatic agents are applied on filaments. One of the common approach is creation of a hydrophilic surface, which induces charge accumulation by water adsorption[4]. On the contrary for electret filters, larger charge density and longer stability is required to reach high, reliable filtration

performance. So far nucleating agents, antioxidants, light stabilizers, inorganic additives and fluorochemicals were utilized to improve electret properties. Nucleating agents either provide smaller spherulites whose boundaries are traps for space charges, or generate microvoids that prohibit charge migration[5–7]. Flurochemicals improve surface properties, particularly via prohibiting formation of conductive liquid film layer during filtration [8,9]. Some other studies on films showed that antioxidants and light stabilizers may act as nucleators and deep charge traps [10,11].

So far stabilizer effect on charge holding properties of polymers have been performed on composite films designed for high voltage cable applications. Cartwright et al. studied effect of an antioxidant on morphology and space charge formation of low density polyethylene (LDPE)[157]. Charge trapping ability of polymer was conducted with changes in polymer morphology as a consequence of antioxidant addition. They stated that reduction in carbonyl groups due to reduced oxidation might have lessened the space charge as these groups are highly polar and act as charge trapping sites. Tanaka et al[155] observed that both space charge formation and decay process changed remarkably. Significant negative charge accumulation was obtained in LDPE-antioxidant at 50°C and 70°C, while charge density values at room temperature was not affected by additive addition. Those foreign molecules were found to be acting as deep traps within the system, however an increase in conductivity of PE was observed due to high shallow trap density caused by the presence of antioxidant. The negative charge injection and the transport within the bulk were found to be more rapid

upon addition of antioxidant[155,156]. TSDC studies by Ronarch and Haridoss[15] showed increase in the intensity of discharging peak upon antioxidant addition at 0.45 to 1% concentration. Improved charging behaviors directly affected electrostatic filtration performance. In a recent patent hydrocharged Irgafos 168 containing PP webs exhibited a quality factor around $1.83 mm H_2O^{-1}$ for 0.3μm DOP particles at a face velocity of 6.9cm/sec, which is significantly high compared to commercial products[16].

Hindered Amine Light Stabilizers (HALS) also affect charge holding capability of polymers. It has been reported that 1% addition of Tinuvin770 into PP led better charge stability at high temperatures. Dipolar structures introduced into PP film were thought to be effective in enhancing charging capacity [158]. Nishuara et al. found HALS addition at very low concentrations was sufficient to impart thermal stability. However below 0.01% concentration partial consumption of stabilizer during use was found to be reducing its additional electret effect. Polypropylene was initially modified with 0.03% 2,6-di-tert.-butyl-p-cresol, 0.1% calcium stearate as an halogen catcher. Then various mixtures of HALS, phenolic stabilizers, metal containing hindered phenol, sulfur type stabilizers were added at concentrations in the range 0.01-0.22%. The most significant improvement was obtained for samples containing some amount of all additives [159].

In this study we analyzed effect of a commercial antioxidant and light stabilizer on charging of PP filaments. PP is one of the mostly used polymers in electret filters. Analyzing effect of stabilizers on charging properties will be challenging since complex chemical

interactions is another point under question. Both products coming from oxidation, antioxidants-oxidized species interaction and unreacted antioxidants will change the chemical composition. Morphological changes were also expected as reported in the literature[155,157]. Irgafos 168 which is a hydroperoxide decomposer and Tinuvin 622LD which is a hindered amine light stabilizer were selected to examine as an electret additive. Figure 7.1 illustrates Irgafos 168 and its antioxidation mechanism. Phosphite group in the center acts as a trapping agent for excited species. Unbounded electrons of phosphorus will make the molecule vulnerable to oxidized groups. Those electrons will make a bond with oxygen in the carbonyl group and stop sequential reactions, which might be expected.

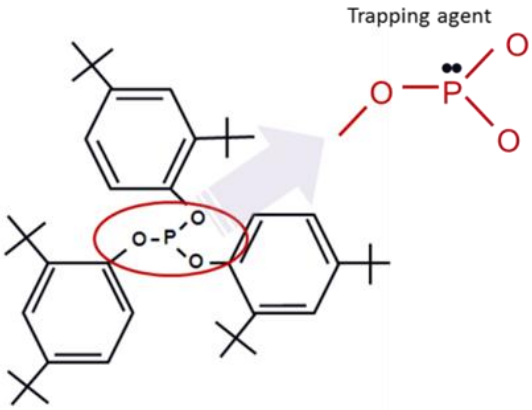

$$\text{-COOH} + (\text{R-O-})_3\text{P:} \rightarrow \text{-C-OH} + (\text{R-O-})_3\,\text{P=O}$$

Figure 7.1 Chemical structure and acting mechanism of Irgafos168

Process stabilizers are competitor of polymer bonds for radical capture; whereas UV light stabilizers are competitor of bonds for quantum of light energy [152]. Due to difference in their use, they have significant differences in chemistry. Structure and acting mechanism of Tinuvin 622LD is given in Figure 7.2. Peroxy radicals formed upon light induced oxidation will be converted into less reactive nitroxides in the presence of HALS. Complex set of reactions occur which yield not only simple nitroxides, but various products[134,153].

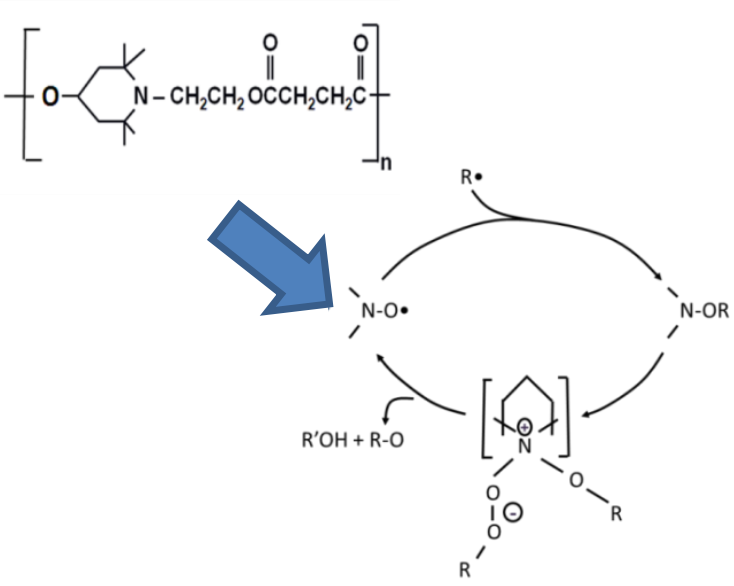

Figure 7.2 Chemical structure and acting mechanism of HALS [153]

7.2 Materials & Methods

7.2.1 Material and Filament Preparation

PP resin, having weight average molecular weight of 180,000 g/mole and polydispersity of 3.3 was kindly supplied from Sunoco Chemicals. Both antioxidant Irgafos168 and light stabilizer Tinuvin 622LD was donated by BASF Inc.

To provide better uniformity, initially PP masterbatch pellets at a concentration of 20% (w/w) stabilizers were prepared by Techmer PM (Clinton, TN). Then, masterbatch was re-extruded with pure PP resin to produce composite fibers with concentrations of 0.1%, 0.5%, 1%, 5% (w/w). Hill's multifilament spinning line located in the Nonwovens Institute (North Carolina State University, Raleigh, NC) was used to produce filaments. Spinning speed was 2000 m/min and the throughput was maintained at 0.58 g $hole^{-1}$ min^{-1}. Temperature of spin head was fixed at 235°C. Control sample was also melt extruded under the same conditions. Each yarn had 72 filaments whose diameter was fixed at 20μm.

Multifilament samples were washed with deionized water at 45°C for 6h to remove impurities and spinfinish applied during melt spinning process. Washing fluid was replaced every 2h. Use of any detergent or surface active was not preferred; since samples might be contaminated with those of the chemicals even after rinsing. Yarns wounded on washing tubes were dried overnight.

7.2.2 Fiber Microstructure

The XRD tests were carried out in Omni X-ray diffractometer. The diffractometer is equipped with Be-filtered Cu-K_α radiation (λ=1.5184 Å) 35 kV, 25 mA. Melting and crystallization behavior of the composite was analyzed in Perkin-Elmer differential scanning calorimeter (DSC). Samples weighing 4.0±0.5 mg were heated in a nitrogen atmosphere from 25°C to 190°C at a rate of 20°C/min, kept at this temperature for 1min and then cooled to room temperature at a rate of 20°C/min. From exothermic curves crystallinity of the samples was calculated using the following formula:

$$\%Crystallinity = \frac{\Delta H}{\Delta H_{PP}^{0}} \times 100 \qquad \text{Equation 7.1}$$

where ΔH is the enthalpy of fusion of the sample (J/g) and ΔH_{PP}^{0} is the enthalpy of fusion of completely crystalline PP (~ 207 J/g)[22].

7.2.3 Charging and Characterization of Charging Property

After drying, yarns were aligned parallel on aluminum sample holders with a definite spacing (10 yarns/cm) as shown in Figure 7.3. It was observed that any fiber protruding from specimen caused significant variations on measured potential value. In order to fix protruding fibers perpendicular yarns were aligned at a distance of 0.7cm from each other. The filaments

were fixed carefully by using conductive tape and epoxy to prevent errors that can occur due to position changes during charging and decay tests.

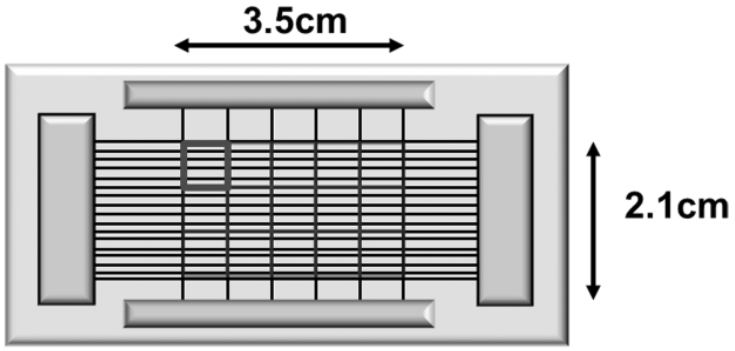

Figure 7.3 Specimen for SPD test and surface potential detection points

Charging of the samples was carried out with a lab scale negative corona discharger (Mystic Marvels, Model NIP-7E). Applied voltage was fixed at 9kV where maximum output direct current of the emitter needle was 160μA. Samples were charged for 1 minute as it was determined as an optimized value according to our previous work [Chapter 3]. All testing procedure was performed at laboratory conditions in which relative humidity was kept fixed between 57±3% RH at 22-23°C temperature.

The surface potential was measured with Monroe 244 Model electrostatic voltmeter. Potential over 15 specific points across the sample surface was used for evaluation. Three

samples were prepared from each filaments, and average values and standard deviations were calculated thereof. The initial measurements (V_0) were taken directly after charging. All following measurements for surface potential decay test were carried out after fixed annealing times at 80°C. The periods in the oven were 0.5h, 1h, 2h, 4h, 8h, 12h, 16h, and 24h. Due to the nature of decay, periods kept shorter initially. Samples after annealing were cooled for 10 minutes in a desiccator to prohibit the effect of atmosphere.

7.3 Results

7.3.1 Fiber Microstructure

XRD analysis revealed for both control and stabilizer containing filaments, crystal structure was dominated by α-monoclinic, exhibiting 2θ peaks at 14.3°, 17.0°, and 18.7° which correspond to (110), (040) and (130) planes respectively[23]. Irgafos content at high concentrations resulted with narrower peaks which indicate larger crystal sizes. Such increase in crystal size might be due to nucleation effect. For melt spinning conditions due to high shear rate and rapid cooling; any increase in crystallization temperature will provide more time for crystal growth, thus rather than reducing, crystal sizes may increase upon nucleating agent incorporation. However looking at crystallization temperatures there is not an abrupt change upon addition of either of the stabilizers [Figure 7.5]. In our previous study an increase about 12-17°C was obtained in NA11/PP filaments.

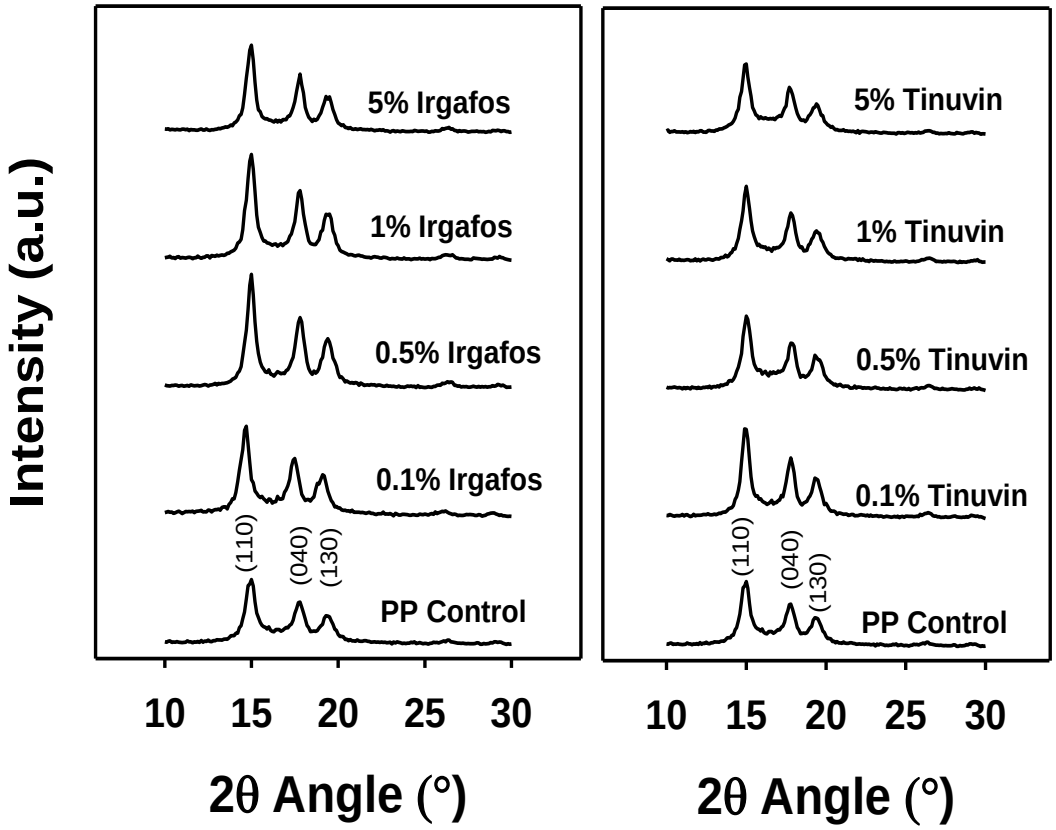

Figure 7.4 XRD spectra for reference and additive containing PP filaments. The spectra were recorded at angles covering three major characteristic diffraction peaks of the PP.

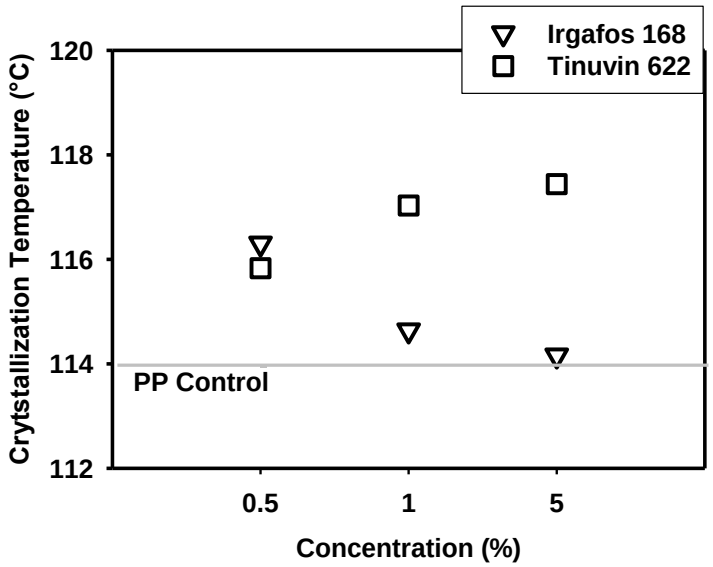

Figure 7.5 Changes in crystallization temperature upon addition of stabilizers

On the other hand according to DSC analyses, a significant reduction in crystallinity of Tinuvin/PP filaments was observed (Figure 7.6). Tinuvin has an oligomeric structure, which probably inhibited crystal formation by locating within PP chains. Since there is not a significant change in crystal structure, apparently order of chains was disturbed by long Tinuvin chains containing carboxyl groups. Irgafos containing samples had closer crystallinity to reference samples.

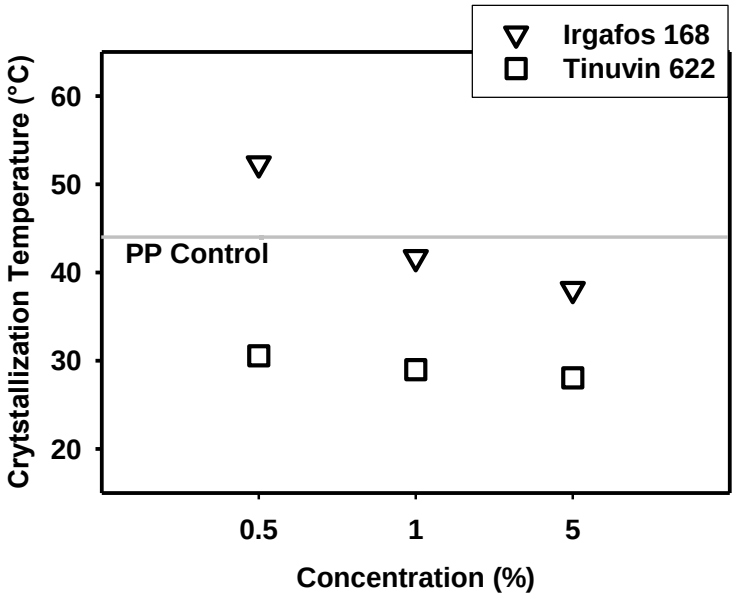

Figure 7.6 Crystallinity of the samples calculated from endothermic DSC curve

7.3.2 Charging Properties

As illustrated in Figure 7.7 generally an exponential decay curve is obtained from surface potential decay test. From these curves initial potential and stability of the potential are two important concerns for electret materials. According to our approach measured initial potential will be indicative for initial electrostatic filtration efficiency, whereas stability will indicate reliability of filtration performance. Relaxation times which corresponds to time where potential drops to 1/e th of initial value (approximately 37%) would be calculated to compare stability of the samples..

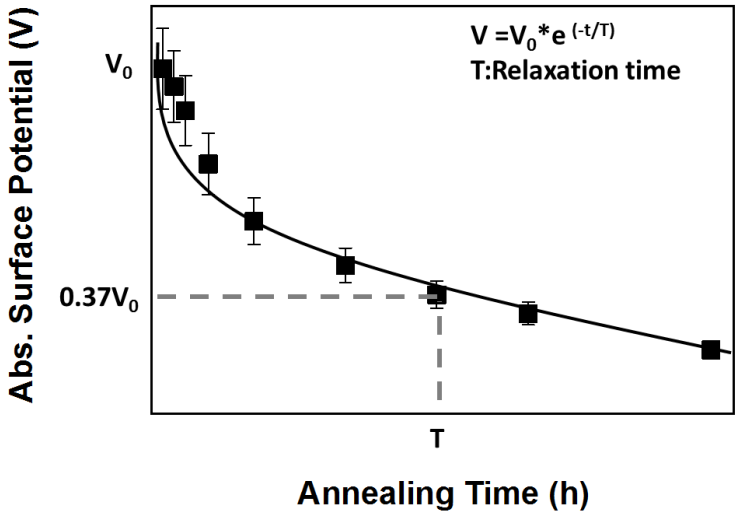

Figure 7.7 Isothermal surface potential decay curve at elevated temperatures [Real data from charged PP filaments]

Measured initial potentials were summarized in Figure 7.8, and calculated relaxation times were given in Figure 7.9. Both initial potential and stability of Irgafos/PP filaments were found higher at low concentrations. Effect of Tinuvin on potential stability was more apparent at 1% concentration. Tinuvin has a molecular weight around 3100-4000g/mole, which is nearly 5 times that of Irgafos. Since blends were prepared with a weight based fashion, stoichiometric ratio of produced traps will not be same

At high concentrations samples containing either of the additives discharged as rapid as pure PP sample. However additive incorporation even at 5% was not so destructive on

charging to be named as antistatic agent. 0.1% Tinuvin containing sample showed very close properties with reference sample from aspects of both of initial potential and relaxation time, which shows probable consumption of additive during extrusion.

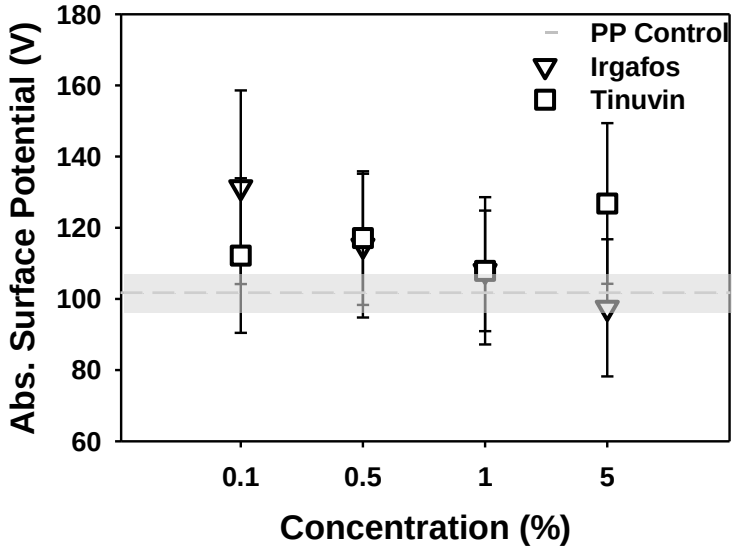

Figure 7.8 Initial surface potential vs additive concentrations after 1min charging at 23°C. Filaments were arranged as shown in Figure 7.3. Shadowed region corresponds to deviation for PP Control sample.

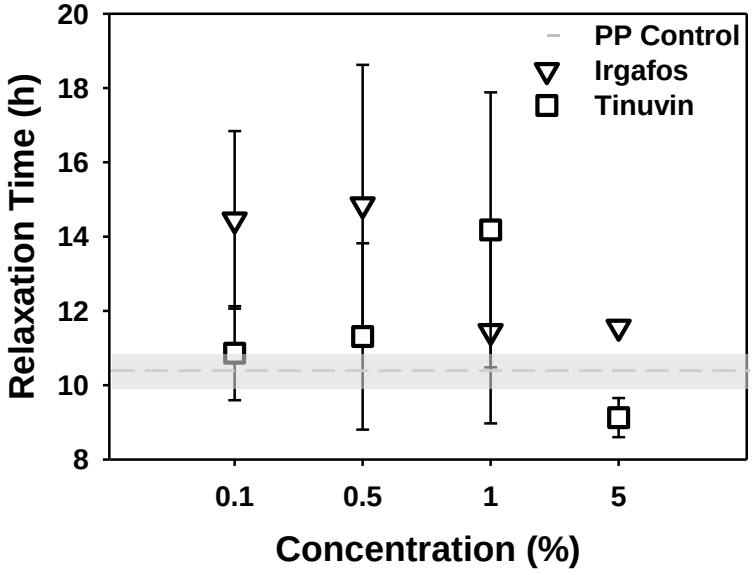

Figure 7.9 Relaxation times after accelerated potential decay at 80°C. Shadowed region corresponds to deviation for PP Control sample.

Apparently antioxidants and light stabilizers changed both chemical and morphological composition of PP at a degree. From the aspect of chemistry according to manufacturer data adding at concentrations between 0.2-0.8% is sufficient for protecting polymer. So above 1% concentration, excess concentration will probably not act in stabilizing process and will remain unreacted. For the case of HALS, unreacted proportion would be expected, since it was not tested for stabilization against photoinduced oxidation.

Irgafos did not contribute to crystal structure significantly. This would be due to exclusion of such low molecular weight additives during crystallization. Antioxidants and oxidized species are mostly located in amorphous parts and amorphous-crystalline boundaries[24],[131,132]. Tinuvin addition resulted with significant drop in crystallinity, which would be one of the reasons behind weak even disturbing effect stability.

It is already known that oxidized species located as separate polar species will give rise to polarity of PP, hence its electret properties. Kravtsov et al charged meltblown PP produced at very high temperatures to increase concentration of such species [136]. Concentration of oxidation products acting as deep traps would get lower upon antioxidant addition above 1%[137]. Probably most of those excited species were converted into stable, low energy phosphate compounds, nitroxide radicals and alcohols upon reacting with Irgafos and Tinuvin, which reduced their polarization ability and excess charges.

7.4 Conclusion

The rationale behind this study was to examine effect of possible chemical and morphological changes on charging properties of PP filaments. Up to 0.5% concentration Irgafos/PP filaments exhibited 40% longer charge stability, whereas the increase was just 10% at higher concentrations. Interestingly Tinuvin enhanced charge stability only at 1 % concentration, whereas for other concentrations similar decay tendency was observed. For

both additives decay was more rapid at excess concentrations. Selected stabilizers did not contribute to initial surface potential significantly. When combined with antioxidants and light stabilizers oxidized species probably produced various low energy products, that do not contribute charging properties so significantly.

7.5 References

1. Behrendt, N. *et al.* Charge storage behavior of isotropic and biaxially-oriented polypropylene films containing α-and β-nucleating agents. *Journal of applied polymer science* 99, 650–658 (2006).

2. Jain, V. & Mittal, A. Charge storage studies of unstretched and stretched polypropylene film electrets using short circuit TSDC technique. *Journal of materials science letters* 19, 1991–1994 (2000).

3. Brown, R. C. & Brown, R. C. *Air filtration: an integrated approach to the theory and applications of fibrous filters*. (Pergamon Press: 1993).

4. Bart, J. C. J. *Additives in polymers: industrial analysis and applications*. (John Wiley: 2005).

5. Mohmeyer, N. *et al.* Additives to improve the electret properties of isotactic polypropylene. *Polymer* 48, 1612–1619 (2007).

6. Behrendt, N. *et al.* Charge storage behavior of isotropic and biaxially-oriented polypropylene films containing α-and β-nucleating agents. *Journal of applied polymer science* 99, 650–658 (2006).

7. Mohmeyer, N., Schmidt, H. W., Kristiansen, P. M. & Altst\ädt, V. Influence of chemical structure and solubility of bisamide additives on the nucleation of isotactic polypropylene and the improvement of its charge storage properties. *Macromolecules* 39, 5760–5767 (2006).

8. Jones, M. E. & Rousseau, A. D. *Oily mist resistant electret filter media*. (Google Patents: 1995).

9. Jones, M. E. & Rousseau, A. D. *Oily mist resistant electret filter media and method for filtering*. (Google Patents: 1995).

10. Rousseau, A. D., Jones, M. E. & Angadjivand, S. A. Fibrous Webs Having Enhanced Electret Properties. (2003).at <http://www.freepatentsonline.com/ EP0845058.html>

11. Cartwright, G. A., Davies, A. E., Swingler, S. G. & Vaughan, A. S. Effect of an antioxidant additive on morphology and space-charge characteristics of low-density polyethylene. *Science, Measurement and Technology, IEE Proceedings*- 143, 26–34 (1996).

12. Cartwright, G. A., Davies, A. E., Swingler, S. G. & Vaughan, A. S. Effect of an antioxidant additive on morphology and space-charge characteristics of low-density

polyethylene. *Science, Measurement and Technology, IEE Proceedings*- 143, 26–34 (1996).

13. Tanaka, Y. *et al.* Effect of additives on morphology and space charge accumulation in low density polyethylene. *Dielectrics and Electrical Insulation, IEEE Transactions on* 10, 148–154 (2003).

14. Tebani, M., Boudou, L. & Guastavino, J. Thermally stimulated depolarization current and space charge measurements on low-density polyethylene: Influence of the presence of antioxidant. *Journal of Applied Polymer Science* 109, 2768–2773 (2008).

15. Ronarc'h, D. & Haridoss, S. Depolarization-current study of low-density polyethylene containing an antioxidant. *Journal of Applied Physics* 52, 5916–5920 (1981).

16. Sebastian, J. M. *et al. Method of making electret articles based on zeta potential*. (Google Patents: 2010).

17. Albini, A., Degli Esposti, G., Guastavino, F. & Tommasini, D. Charging phenomena in polypropylene films. *Conduction and Breakdown in Solid Dielectrics, 1989., Proceedings of the 3rd International Conference on* 148–152

18. Nishiura, E. & Ando, K. *Electret materials and the method for preparing the electret materials*. (Google Patents: 1991).

19. Lutz, J. T. & Grossman, R. F. *Polymer modifiers and additives*. (CRC Press: 2001).

20. Lutz, J. T. & Grossman, R. F. *Polymer modifiers and additives*. (CRC Press: 2001).

21. Step, E. N., Turro, N. J., Gande, M. E. & Klemchuk, P. P. Mechanism of Polymer Stabilization by Hindered-Amine Light Stabilizers (HALS). Model Investigations of the Interaction of Peroxy Radicals with HALS Amines and Amino Ethers. *Macromolecules* 27, 2529–2539 (1994).

22. Mark, J. *et al. Physical Properties of Polymers*. (Cambridge University Press: 2004).

23. Lafrance, C.-P. & Prud'homme, R. E. Characterization of the molecular orientation in highly oriented rolled polypropylene sheets by X-ray diffraction. *Polymer* 35, 3927–3935 (1994).

24. Ryan, T., Calvert, P., Billingham, N., Allara, D. & Hawkins, W. L. The Distribution of Additives and Impurities in Isotactic Polypropylene. *Stabilization and degradation of polymers: based on a symposium sponsored by the Division of Polymer Chemistry at the 173rd meeting of the American Chemical Society, New Orleans, Louisiana, March 21-25, 1977* 261 (1978).

25. Hawkins, W. L. & Chemistry, A. C. S. D. of P. *Stabilization and degradation of polymers: based on a symposium sponsored by the Division of Polymer Chemistry at the 173rd meeting of the American Chemical Society, New Orleans, Louisiana, March 21-25, 1977*. (American Chemical Society: 1978).

26. Hawkins, W. L., Matreyek, W. & Winslow, F. H. The morphology of semicrystalline polymers. Part I. The effect of temperature on the oxidation of polyolefins. *Journal of Polymer Science* 41, 1–11 (1959).

27. Kravtsov, A. G. & Gol'dade, V. A. Optimization of the Electret State of Polymer Fibres. *Fibre Chemistry* 33, 189–192 (2001).

28. Mizutani, T. & Ieda, M. TSC from corona-charged high-density polyethylene and the effects of oxidation. *Journal of Physics D: Applied Physics* 11, 185 (1978).

CHAPTER 8

8 Effect of Heat Treatment on Charging Properties of Electret Fibers

Abstract

In the present work effect of heat treatment on charging and surface morphology of isotactic polypropylene (PP) filaments were reported. To enhance the surface crystallinity of the filaments, samples were kept at 70°C and 110°C for 12h. As expected, fiber surface crystallinity increased upon heat treatment which led more stable electret fibers, whereas change in initial surface potential was not so remarkable. Same trend was also observed in filaments containing a commercial nucleating agent, NA11(sodium2,2'-methylene-bis(4,6-di-tertbutylphenyl)-phosphate). Surface crystallinity was analyzed using intensity of specific peaks obtained from Attenuated Total Reflection Infrared Spectroscopy (ATR-FTIR) analysis, whereas surface potential decay test is modified to analyze charging properties of fibers.

8.1 Introduction

There are two well-known approaches to enhance efficiency of aerosol filters in submicron particle range. One approach is the use of finer fibers, thus increasing efficiency

via capture mechanisms such as diffusion and interception. A drawback behind this approach is high pressure drop, which causes high energy expenses and ease of clogging. A second approach is imparting electrostatic charge on filtration medium without changing web structure. Those of the filter media are known as "electret filters" or "electrostatic filters"[1]. Since particles are captured by means of electrostatic forces, more open fabric structures with coarser fibers would be used, which results in lower pressure drop. However for those filters charge density and stability will be concern, because loss of electrostatic property will change this active filter media into a passive (mechanical) media with significantly low efficiency.

Looking deep into phenomena, electret filters are generally composed of polymer fibers at micron scale. Electric field generated within web will depend on macro, micro and atomic scale properties. For instance electrostatic charging for Hansen filters is referred to triboelectrification between wool and resin particles [77]. Selection of fibers showing positive and negative triboelectric series will produce higher efficiency[3]. Smith et al published a comprehensive study on triboelectrification of webs with 11 different fiber composition[77]. Focusing in micro scale, morphological properties such as crystallinity, crystal sizes were shown to be effective in charging of polymer structures. Nath et al found significant improvement in charge stability upon heat treatment due to enhanced crystallinity and crystal size[4]. From the aspect of chemical composition generally high band gap polymers like polypropylene is preferred which has lower conduction. Other than conduction, species

causing charge transfer over surface or leading to a hydro/oleophilic surfaces will cause rapid decay of charges[5].

In this study we examined another parameter, the effect of surface crystallinity of PP fibers on charge density and stability. It could be expected that surface crystallinity should be more dominant for non-metallized fibrous electrets due to their high surface area.

There are several reasons that would be asserted behind the difference in surface and bulk crystallinity of polymer. Differences in thermal history, tendency to oxidative reactions and mechanical stresses will cause significant changes between surface and bulk layers. As indicated in various studies [6,7] during crystallization impurities, additives will be excluded through surface. Migration of defective structures through lower energy-surface will prohibit crystallization [8]. On the other hand looking at atomic scale the difference is also apparent from the aspect of coordination numbers. Say an atom in a face centered cubic crystal (FCC) has 12 nearest neighbors, whereas it has fewer than 12 on the surface. And it is well known, systems form bonds maximally to lower their energy. So less number of bonds will produce a different surface with a higher energy compared to bulk. OSVICD (organic solvent induced charge decay) and TSD (thermally stimulated discharge) works on charged films showed that rather than bulk crystallinity, surface crystallinity is important for the charge stability of film electrets[9,10].

From the aspect of electrostatic properties these structural and molecular differences will cause various results. Firstly impurities particularly located within amorphous regions will induce charge motions. For instance excluded oxidized species will lower hydrophobicity of the surface[11]. Due to reduced hydrophobicity either condensed water or collected oily aerosols will form a conductive liquid film on fibers which leads ease of charge decay. On the other hand particularly penetration of air ions or solvent vapors will be difficult through crystalline regions, however amorphous regions will be open to such decay mechanism. Thirdly molecular mobility within amorphous regions is higher which will induce charge decay and depolarization.

Other than factors related with polymer structure, penetration depth of charges are not so deep particularly for low electric field, room temperature corona discharge treatments. Using thermally stimulated discharge current method Cresswell and Perlman[12] measured depth of penetration of charge at most 5% of the 25.4 μm-thick corona charged Mylar films under 12kV/cm. Nordhage and Baekstrom found a lower penetration depth, -about 40 nm- which still indicates charges cannot penetrate into the bulk so deeply[13]. According to Laser Induced Pressure Pulsed (LIPP) studies on irradiated 36 μm thick PP films, charge penetration depth was found to be strongly dependent on energy of electrons. The depth of charges were found 1.5-2μm when electron energy was kept 10eV, whereas penetration through thickness was observed when electron energy increased to 50eV [14]. The results show

that morphological and molecular properties on uppermost surface layer will be important on charging.

Interestingly, there are a few studies on surface crystallinity of fibers properties, though as summarized this phenomenon is important for various chemical and electrical behaviors of polymers. Atomic Force Microscopy(AFM)[15–17], Grazing Angle Incident Xray Diffraction (GIXD)[8,18] and Attenuated Total Reflection IR Spectroscopy (ATR)[9,10,19–22] are techniques so far reported for surface crystallinity evaluation of polymeric films.

AFM is a high resolution method to investigate morphology and mechanical properties of polymer surfaces. The tip of the probe, which is theoretically constituted by one single atom size, scans the surface and forces between probe and surface are measured. By the way unique information about the common crystal structures of polymers such as spherulites, microfibrils and shish-kababs could be obtained[17]. However AFM doesnot give quantitative results.

GIXRD is based on the similar methodology with common XRD. However instead of bulk, in order to maximize the scattering from the surface, x-rays are incident at glancing angles to the surface. Angle of the incident X-ray reduced to 0.5° instead direct collision on sample. Even in this case, energetic x-rays will be scattered from deeper atomic layers which should be subtracted from total intensity curves to correct the obtained values [8,18]. Nishino et al [18] obtained lower crystallinity for the surface when compared with the bulk of the PP

film and the apparent crystal sizes were calculated lower for surface. Heat treatment at higher temperatures initially enhanced crystallinity both on surface and in bulk, however for longer heat treatment time surface oxidation was observed and this resulted in lower crystallinity on surface. Surface effect was obtained to be propagating on the order of microns into the bulk. From corresponding GIXRD studies we know that bulk and surface of films will possess almost same crystal structure. GIXRD can be applicable for flat surfaces, which makes test of filaments impossible.

When subjected to IR radiation, molecules having inherent vibrations will absorb radiations at specific wavelengths [23]. It is also known that at the same ranges polymer samples with different conformational and configurational properties exhibit distinguishing peaks from each other due to changes in molecular vibrations. For instance trans-conformation of glycol unit is a characteristic of crystalline PET [15]. Several works have also been done on absorbance characteristics of PP [19,21,22]. Quynn et al [20] have shown that the absorbance ratio at A_{997}/A_{972} is linearly related to polymer density and hence may be used to measure polymer crystallinity. One other study by Heinen[24] showed that the absorbance ratio A_{841}/A_{1168} have a similar relationship with crystallinity of PP. On the other hand FTIR and ATR-FTIR was stated to be more sensitive than GIXRD [25]. Since it is not possible to reach quantitative result from AFM, infrared spectroscopy seems best available option to analyze cyrstallinity of uppermost surface of filaments.

For attenuated total reflection spectroscopy, IR will penetrate into sample partially. That is why for surface crystallinity analysis; ATR is preferred instead of transmission infrared (T-IR) spectroscopy. Penetration depth is not the actual distance through which the electromagnetic wave travels. Instead it could be described as the depth that the field decays to a definite value, ie intensity where it decay to 1/e th of incident [19]. Depth of the penetration of IR radiation depends on various factors such as wavelength of IR peak under consideration (λ), refractive indexes of sample (n_s) and ATR element (n_c) and incident angle (θ). It is calculated via equation explained by Kortum[26]:

$$d_p = \frac{\lambda}{4\pi n_c \sqrt{\sin^2\theta - (n_s / n_c)^2}} \qquad \text{Equation 8.1}$$

where λ is the wavelength of the light and n_c and n_s are the refractive indexes.

The degree of surface crystallinity in PP filaments averaging in depth of about 0.33μm has been calculated from absorbance values in ATR spectroscopy. Deeper surface can be probed either at lower incidence angle or with a low refractive index crystal such as KRS-5 instead diamond.

8.2 Experimental

8.2.1 Materials and Filament Preparation

34 MFR iPP resin, having Mn~55,000g/mole, Mw~180,000g/mole molecular weight, kindly provided from Sunoco Chemicals (TX) was used as host polymer. NA11 in powder form was donated by BASF. Molecular structure of NA11 was given in Figure 8.1.

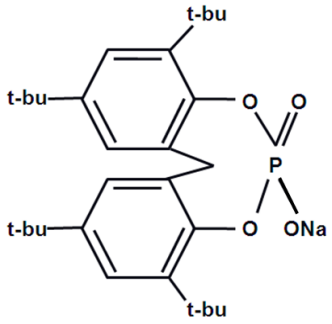

Figure 8.1 Chemistry of NA11

Masterbatch at 20%w/w concentration was prepared by Techmer PM (TN), prior to filament extrusion. Then PP filaments containing additives at 0.5, 5% concentrations were melt-spun in Hills multifilament spinning line in the Nonwovens Institute (single screw extruder with an L:D ratio of 24:1). Spinning speed was fixed at 2000m/min and throughput was 0.58ghole^{-1}min^{-1}. Diameters of the filaments were kept 20μm for all samples. Temperature of spin head with 72 holes was fixed at 235°C.

Multifilament samples were washed with deionized water at 45°C for 6h to remove impurities and spinfinish applied during melt spinning process. The washing fluid was replaced every 2h. Use of any detergent or surface active was not preferred; since samples might be contaminated with those of the chemicals even after rinsing. Yarns wounded on washing tubes were dried overnight.

8.2.2 Charging and Characterization of Charging Property

After drying, yarns were aligned parallel on aluminum sample holders with a definite spacing (10 yarns/cm) as shown in Figure 8.2. It was observed that any fiber protruding from specimen caused significant variations on measured potential value. In order to fix any protruding fiber, perpendicular yarns were aligned at a distance of 0.7cm from each other. The filaments were fixed carefully by using conductive tape and epoxy to prevent errors that can occur due to position changes during charging and decay tests.

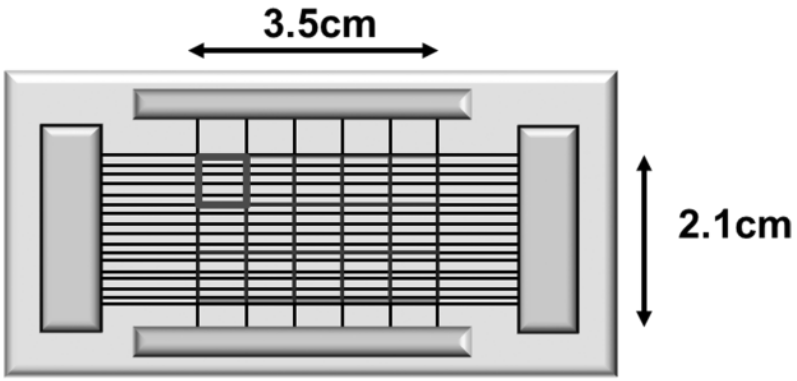

Figure 8.2 Specimen for SPD test and surface potential detection points

Charging of the samples was carried out with a point-to-plate negative corona discharger (Mystic Marvels, Model NIP-7E). Applied voltage was fixed at 9kV where maximum output direct current of the emitter needle was about 160μA. Samples were charged for 1 minute as it was determined as an optimized value for our system. All testing procedure was performed at laboratory conditions in which relative humidity was kept fixed between 57±3% RH at 22-23°C temperature.

The surface potential was measured with Monroe Modeal244A noncontact electrostatic voltmeter. Three specimen were prepared from each samples and average values and standard deviations were calculated thereof. 15 specific points across the sample surface was used for evaluation. The initial measurements (V_0) were taken directly after charging. All following measurements for surface potential decay test were carried out after fixed heat

treatment times at 80°C. The periods in the oven were 0.5h, 1h, 2h, 4h, 8h, 12h, 16h, and 24h. Due to the nature of decay, periods kept shorter initially. Samples after heat treatment were cooled for 10 minutes in a desiccator to prohibit the effect of atmosphere.

8.2.3 Surface Crystallinity Analysis

All ATR-FTIR measurements were carried at 23°C using a Nicolet Nexus 470 FTIR spectrometer equipped with a Ge crystal. Spectra were collected at a resolution of 4 cm^{-1} with 64 scans. Following the works of Quynn [20] data from attenuated total reflection (ATR) was used for calculating the surface crystallinity. The absorbance ratio was corrected according to absorbance intensity at 917 cm^{-1}.

$$Abs\,Ratio = \frac{A_{997} - A_{917}}{A_{972} - A_{917}} \qquad \text{Equation 8.2}$$

where indices indicate the wavenumber of peaks, and A is the absorption intensity.

After finding density, crystallinity could be calculated by simple density-crystallinity formula:

$$X_c = \frac{\rho - \rho_{amor}}{\rho_{crys} - \rho_{amor}} \qquad \text{Equation 8.3}$$

where X_c indicates crystallinity, and ρ's corresponds densities.

In this regard density of amorphous regions could be assumed as 0.853g/cm^3, whereas it is 0.935g/cm^3 for fully crystalline PP [19].

8.3 Results and Discussions

In Figure 8.1 the average surface potential decay of filaments containing 0%, 0.5%, and 5% of NA11 are shown. The reference filament and all NA11 containing filaments showed excellent charge stabilities after heat treatment for 12h. As an example, 5%NA11 containing heat treated filament still kept more than half of the potential after decay at 80°C for 1day. Without heat treatment the decay was much faster. Another interesting feature of the measurements in Figure 8.1 is that heat treatment at 70°C was already sufficient to enhance stability. Not only charge stability but also initial potential values were found slightly higher for control sample.

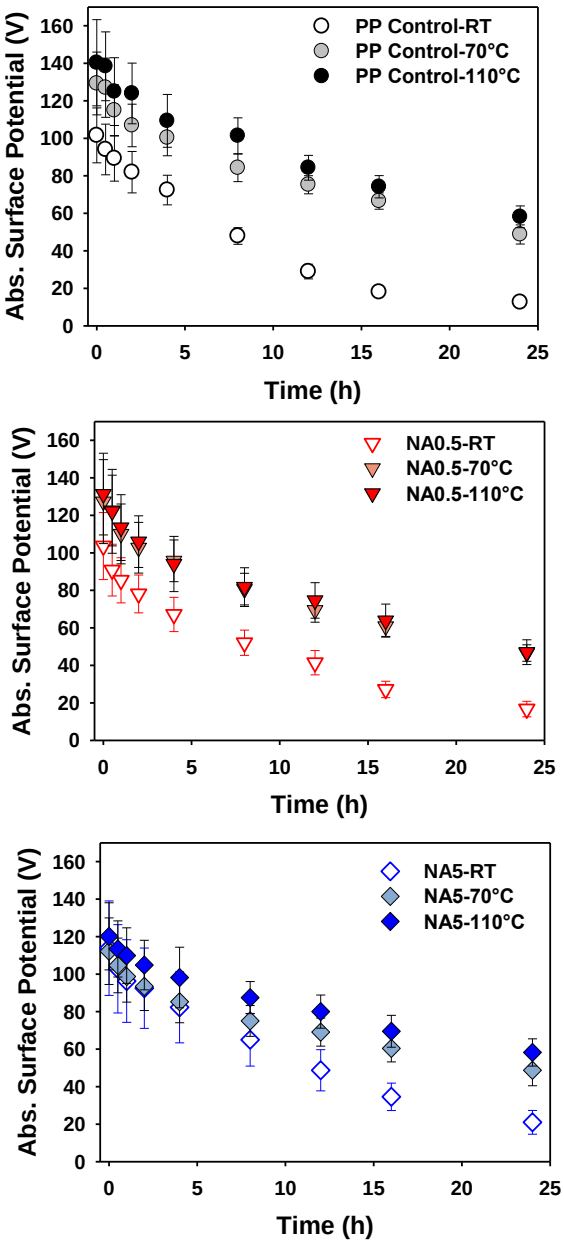

Figure 8.1 Isothermal surface potential decay at 80°C of heat treated PP filaments containing different concentrations NA11

Before performing FTIR tests for surface crystallinity measurement, NA11in powder form was analyzed solely to check if there is a particular peak at 950-1000cm^{-1} range which we will track crystallinity. As shown in Figure 8.2 NA11 donot have a peak at this range.

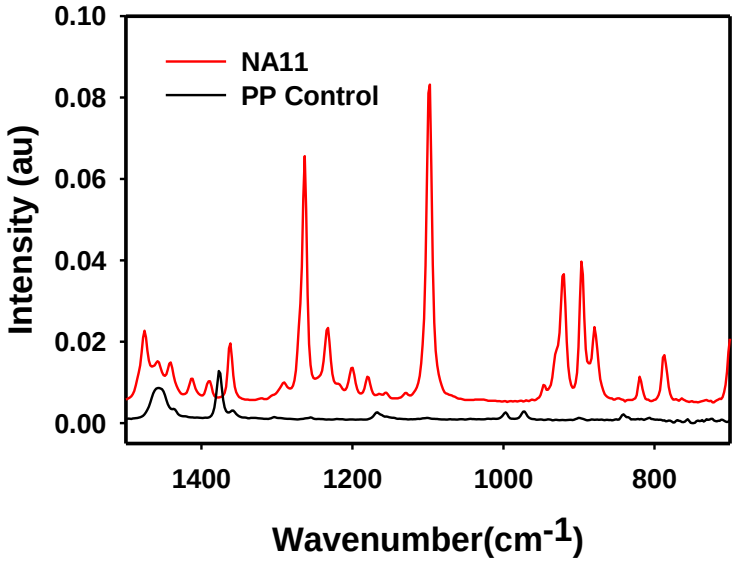

Figure 8.2 ATR analysis for PP filament and NA11 in powder form

Figure 8.3 shows change in surface cyrstallinity upon heat treatment. For NA11 containing samples increase in surface crystallinity is continuous, whereas surface crystallinity of PP Control and 0.5%NA11/PP sample heat treated at 110°C is only slightly lower than one treated at 70°C, though being significantly higher than untreated samples.

Improvement on surface order of 5% NA11 containing filaments is more significant compared to other samples.

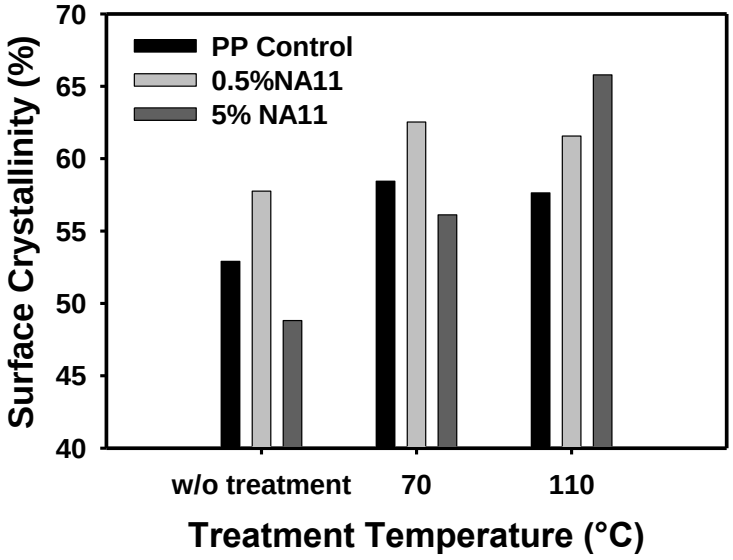

Figure 8.3 Measured FTIR-surface crystallinity values for heat treated NA11 containing filaments

In Figure 8.4 measured surface crystallinity was compared with electret properties of PP filaments. For analyzing exponential decay tests, we calculated relaxation times. Relaxation time is the value where potential value drops to 1/e th of the initial value. Neither additive concentration nor heat treatment influences initial potential values. However for

relaxation times, which indicate charge stability, there is a significant improvement. It was clearly shown that for such systems where polarization and charge injection occurs in upper surface layer, surface crystallinity is an important factor. The most significant change in charge stability was observed in 5%NA11, where relaxation time nearly tripled upon heat treatment at 110°C.

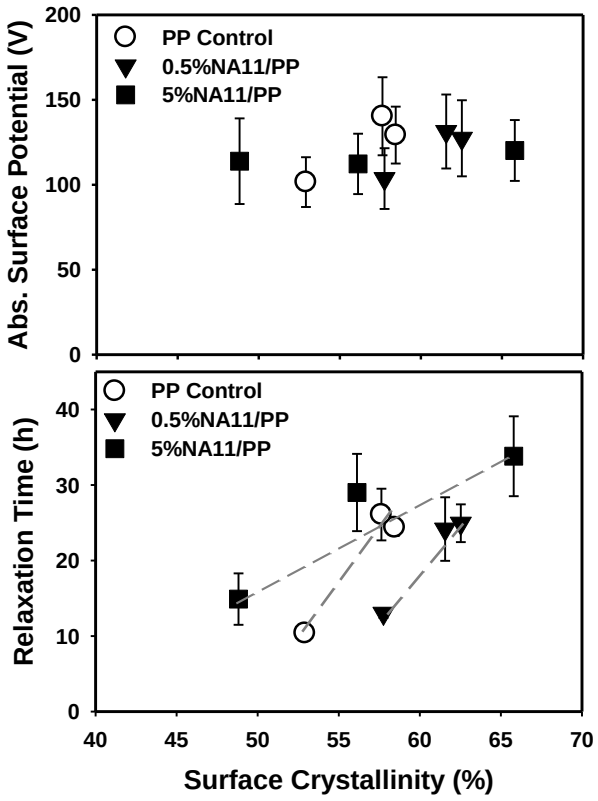

Figure 8.4 Surface crystallinity values compared to electret properties: Initial potential and relaxation time (Lines were given for ease of tracking)

Other than such chain motions, particular molecular groups would be excluded through surface or generated during heat treatment procedure. Due to that reason carbonyl index, which stands for concentration of carbonyl (>C=O) groups (ketones, acids, esters, etc) were calculated after normalizing peaks at 1700-1800cm^{-1} with peak at 2720cm^{-1} [27]. Though there is an increase in concentration of such oxidized species which induces surface conductivity, we observed an enhancement in charge stability which would be conducted with only changes in surface morphology.

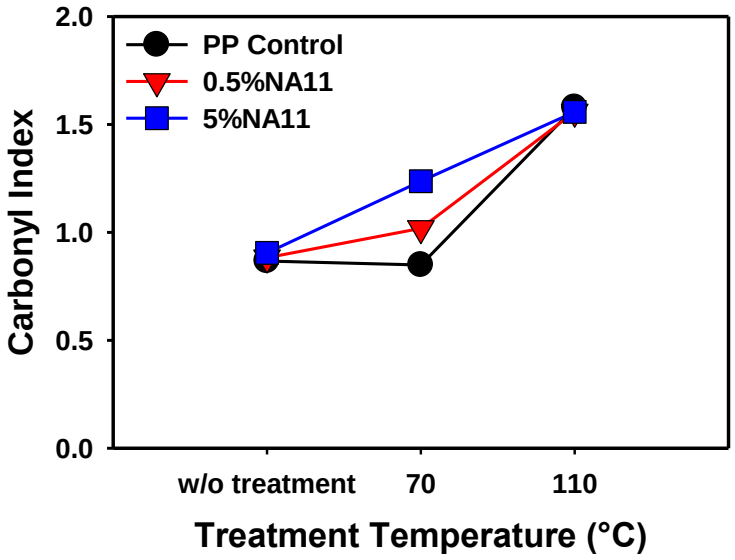

Figure 8.5 Change in carbonyl index upon heat treatment at 70 and 110°C

8.4 Conclusion

In this study we investigated the effect of heat treatment on surface morphology and charging properties of PP filaments. It was shown that for electret, particularly electret filter applications higher surface crystallinity induced by heat treatment leads to longer stability, whereas change in initial potentials were not so significant.

8.5 References

1. Klaase, P. T. . & Van Turnhout, J. *Method for manufacturing an electret filter medium*. (Google Patents: 1986).

2. Smith, P. A., East, G. C., Brown, R. C. & Wake, D. Generation of triboelectric charge in textile fibre mixtures, and their use as air filters. *Journal of Electrostatics* 21, 81–98 (1988).

3. Myers, D. L. & Arnold, B. D. Electret media for HVAC filtration applications. *INJ Winter* 43–54 (2003).

4. Nath, R. & Perlman, M. M. Effect of crystallinity on charge storage in polypropylene and polyethylene. *Electrical Insulation, IEEE Transactions on* 24, 409–412 (1989).

5. Rousseau, A. D., Jones, M. E. & Mei, B. Z. *Method of making electret articles and filters with increased oily mist resistance*. (Google Patents: 2000).

6. Lee, H. & Archer, L. A. Functionalizing polymer surfaces by field-induced migration of copolymer additives. 1. Role of surface energy gradients. *Macromolecules* 34, 4572–4579 (2001).

7. Spatafore, R. & Pearson, L. T. Migration and blooming of stabilizing antioxidants in polypropylene. *Polymer Engineering & Science* 31, 1610–1617 (1991).

8. Kawamoto, N. *et al.* Microstructural characterization of polypropene surfaces using grazing incidence X-ray diffraction. *Macromolecular Chemistry and Physics* 199, 261–266 (1998).

9. Yamashita, T. & Ikezaki, K. A method for correlating charge traps of polypropylene to its morphology. *Journal of Electrostatics* 63, 559–564 (2005).

10. Arita, Y., Sha Shiratori, S. & Ikezaki, K. A method for detection and visualization of charge trapping sites in amorphous parts in crystalline polymers* 1. *Journal of Electrostatics* 57, 263–271 (2003).

11. Strobel, M. *et al.* Low-molecular-weight materials on corona-treated polypropylene. *Journal of Adhesion Science and Technology* 3, 321–335 (1989).

12. Creswell, R. A. Thermal Currents from Corona Charged Mylar. *J. Appl. Phys.* 41, 2365 (1970).

13. Lowell, J. & Rose-Innes, A. C. Contact electrification. *Advances in Physics* 29, 947–1023 (1980).

14. Tingji, L. & Sessler, G. M. An experimental study of charge distributions in electron-beam irradiated polypropylene films. *Electrical Insulation, IEEE Transactions on* 26, 228–235 (1991).

15. De Cupere, V. M. & Rouxhet, P. G. Surface crystallization of poly(ethylene terephtalate) studied by atomic force microscopy. *Polymer* 43, 5571–5576 (2002).

16. Risnes, O. K., Mather, R. R., Neville, A. & Buckman, J. Comparing the surface and internal structure of polypropylene fibres using advanced microscopy techniques. *Journal of Materials Science* 38, 2161–2165 (2003).

17. De Rovère, A., Shambaugh, R. L. & Edgar, A. Investigation of gravity-spun, melt-spun, and melt-blown polypropylene fibers using atomic force microscopy. *Journal of Applied Polymer Science* 77, 1921–1937 (2000).

18. Nishino, T., Matsumoto, T. & Nakamae, K. Surface structure of isotactic polypropylene by X-ray diffraction. *Polymer Engineering & Science* 40, 336–343 (2000).

19. Hobbs, J. P., Sung, C. S. P., Krishnan, K. & Hill, S. Characterization of surface structure and orientation in polypropylene and poly(ethylene terephthalate) films by modified attenuated total reflection IR dichroism studies. *Macromolecules* 16, 193–199 (1983).

20. Quynn, R. G., Riley, J. L., Young, D. A. & Noether, H. D. Density, crystallinity, and heptane insolubility in isotactic polypropylene. *Journal of Applied Polymer Science* 2, 166–173 (1959).

21. Bonnerup, C. & Gatenholm, P. Physical modifications of propylene/ethylene-propylen-diene-monomer rubber surfaces. I. Determination of surface composition and surface order by fourier transform infrared-attenuated total reflectance. *Journal of Polymer Science Part B: Polymer Physics* 31, 1487–1494 (1993).

22. Sung, C. S. P. & Hobbs, J. P. Development - Of - Ft-Ir - Attenuated - Total - Internal - Reflection - Dichroism - Techniques - For - Structural - Characterization - Of - Polymer - Surfaces - PB - Taylor & Francis. *Chemical Engineering Communications* 30, 229 (1984).

23. Stuart, B. H. *Infrared spectroscopy: fundamentals and applications*. (John Wiley and Sons: 2004).

24. Heinen, W. Infrared determination of the crystallinity of polypropylene. *Journal of Polymer Science* 38, 545–547 (1959).

25. Kawamoto, N. *et al.* Microstructural characterization of polypropene surfaces using grazing incidence X-ray diffraction. *Macromol. Chem. Phys.* 199, 261–266 (1998).

26. Kortum, G. & Korta1/4m, G. *Reflectance Spectroscopy: Principles, Methods, Applications*. (Springer: 1969).

27. Rabello M.S. & White J.R.[1] Crystallization and melting behaviour of photodegraded polypropylene - II. Re-crystallization of degraded molecules. *Polymer* 38, 6389–6399 (1997).

CHAPTER 9

9 Aerosol Filtration Properties of Nucleating Agent Containing Electret Filters

Abstract

A study on the effects of nucleating agents on morphology, charging and electrostatic filtration performance of polypropylene meltblown webs is reported. Two commercial nucleating agents DMDBS (3:2, 4-bis(3,4-dimethyldibenzylidene) sorbitol) and NA11 (sodium 2,2'-methylene-bis(4,6-di-tertbutylphenyl)-phosphate) were used. Probable early solidification upon nucleating agent addition caused remarkable increase in fiber diameter and reduction in web solidity. Samples were not only cold, but also thermally charged. Upon thermal charging significant enhancement in electrostatic potential and filtration performance was observed. Particularly stability of electrostatic filtration performance was found to be promising with those additives. Results led us to analyze dielectric properties of modified webs which confirmed increase in orientational polarization after nucleating agents.

9.1 Introduction

Electret properties of polymers led several inventions such as microphones, radiation sensors and aerosol filters. So far nucleating agents were examined in various studies to

enhance electret properties of those devices[1–5]. Researhcers mostly concentrated on electret films, and possible results were expected for electret filters[2]. However due to larger surface area and more open structure of electret fibers charge density and charge stability significantly differs than that of films, which was shown in previous chapters.

Among the nucleating agents bisamides[5], trisamides[1], sodium 2,2'-methylene-bis(4,6-di-tertbutylphenyl)- phosphate (NA11)[2,6], N,N'-dicyclo-hexyl- 2,6-naphthalene-dicarbox-amide (NU100)[4], trisamides derivatives[3] were used so far. For films nucleating agents were found to be acting on electret properties in various ways. Behrendt et al[4,7] used two commercial nucleating agents, sodium 2,2'-methylene-bis(4,6-di-tertbutylphenyl)-phosphate (NA11) and N,N'-dicyclo-hexyl-2,6-naphthalene-dicarbox-amide (NU100) at lower concentrations below 0.5%. For NU100, the charge decay was found to proceed faster in comparison to the pure PP sample, which was conducted with intermolecular hydrogen bonds providing pathways for the charge carriers. Such H bonds formed three-dimensional network structure, which was verified with optical microscopy images. Hence decay mechanism was much more chemistry related rather than changes in microstructure. On the other hand NA11 containing films exhibited a significant improvement when biaxially stretched. Nonsoluble NA11 particles caused elongated, regular cavities due to weak interactions with PP. Those local microvoids acted as charge barriers and enhanced stability[4,7]. Same group also investigated efficiency of NA11 at higher concentration values. Decay rate was significantly reduced at a concentration of 10%, which was also proven via

TSD analysis. The peak discharge temperature nearly reached to melting temperature of PP, which was attributed to barrier effect of generated cavities at high concentrations. Interestingly charge stability decreased at lower concentrations due to generation of shallow traps upon nucleation[2].

Complete solubility of nucleating agent is advantageous for homogenous distribution and efficient nucleation[8–10]. Due to that reason triphenylamine-based trisamide derivatives were synthesized as nucleating agents for PP. As a result of increased solubility, fibrillar crystals were observed instead of spherulites. Onset of crystallization temperature, which is an indicator of nucleation, was found to increase largely even at additive concentrations of 0.2%. Charge decay was found more rapid in the range of concentrations that efficient nucleation takes place, which was attributed to the presence of three dimensional network which provides conductive pathways through film. Such concentration range where conductivity increases abruptly is called percolation concentration [1,11]. Another finding is that formation of isolated nanostructures having dipolar characteristics strongly enhances electret properties. Nucleating agents having dipole groups will be buried in frozen crystal regions. Most probably electron density is also important since decay tests on trisamide based nucleating agents showed that additives with three secondary amide groups enhance charge stability, whereas surface potential of samples containing additives with cyclohexyl substituents rapidly decays[3]

On the other hand nucleating agents containing films will be composed of smaller crystal structures. Thus it would be expected to produce larger crystal-amorphous boundaries, which results with efficient Maxwell-Wagner type polarization[12,13]. Nucleating agents are designed to act as center of crystal. Rather than exclusion through amorphous regions as observed in many additives[9], nucleating agents will be buried into crystallites [3,8–10]. This means any kind of polarizable groups will be buried into crystal region.

Those particular properties make several types of nucleating agents effective as electret additives. In this study we compared effect of two commercial additives on electrostatic filtration properties of corona charged meltblown PP webs. In the experimental part their efficiency was also analyzed by means of surface potential, electrostatic filtration and dielectric spectroscopy.

9.2 Experimental

Materials and Melt Blown Web Production. Achieve 6936G1 propylene polymer resin with a melt flow rate of 1550 was kindly provided from ExxonMobil. DMDBS was kindly donated by Milliken Company (SC); whereas NA11 by BASF. To provide better uniformity, initially PP masterbatch pellet at 10%(w/w) additive concentration was prepared by Techmer PM (Clinton, TN). Then, masterbatch was re-extruded with pure resin to produce additive/PP

composite webs with concentration of 0.01%, 0.1%, 1%(w/w). The chemical formulas of the additives were given in Figure 9.1.

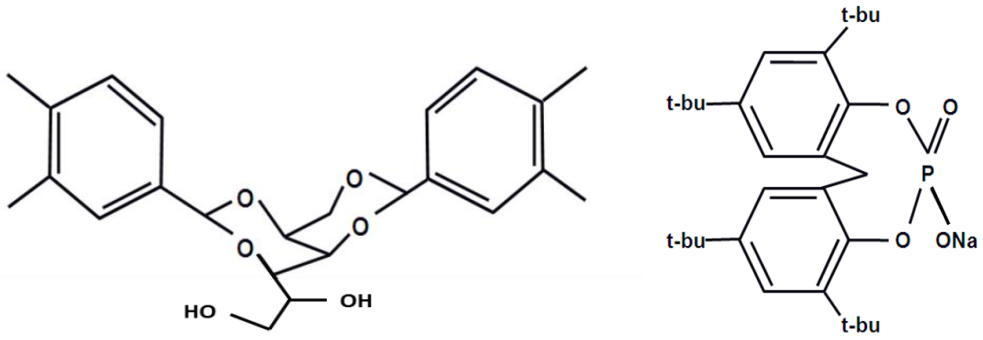

Figure 9.1 Chemistry of DMDBS and NA11

Small melt blowing line used in the web preparation had a 6-inches MB die which has 120 holes, each of which is 0.15mm in diameter (i.e ~ 25 holes/inch). Polymer pellets are melted and pressurized using a 1 1/4" C.W. Brabender extruder, mounted horizontally. The heating in the extruder involves four zone temperature controls. The die is manufactured by the Reifenhäuser Reicofil GmbH & Co. KG. The air plate angle is 60° with the air gap of 0.3 mm and the die tip is outset the die face by 1mm. The temperature profile is tabulated in Table 9.1.

Table 9.1 Temperature profile of MB process

	Z1	**Z2**	**Z3**	**Z4**	**Pump**
Temp. [°C]	190	220	230	250	248
	Transfer	**Turning**	**Die**	**Air Fed**	**Air measured**
Temp. [°C]	250	250	250	339	260-270

Meltblowing is not a specifically controllable process compared to melt spinning process. It means by changing process conditions such as die/air temperature, polymer throughput, air pressure, die-collector distance, belt velocity one can produce samples having different fiber diameter distributions and solidity [14–16]. Dominating melt blowing parameters, throughput value and air pressure were selected as 0.2-0.25ghm and 20-25psi respectively. Belt speed was changed according to desired basis weight. Important parameters for aerosol filtration such as basis weight, thickness, fiber diameter and distribution, solidity and air permeability were measured.

Basis weight measurements were done via weighing 5 specimen of $1dm^2$ area and averages were calculated thereof. Web thickness was measured according to ASTM D 5729 procedure where thickness testing gage (AMES, BG1110-04) with a presser foot diameter of 25.4 mm at pressure of 4.14kPa was used. From measured basis weight and thickness solidity of the webs were calculated from the following equation.

$$solidity = \frac{basisweight}{thickness * density} \qquad \text{Equation 9.1}$$

Fiber Diameter. SEM images of the meltblown samples were taken with a Phenom FEI scanning electron microscope. 100 measurements were taken from 15 pictures and average and standard deviations were calculated thereof.

Air Permeability. For air permeability test the method explained in ASTM D507 and D737 was used. A fixed area (38 cm^2) of sample was subjected to negative pressure of 125 Pa after sealing**.**

Charging. Charging of the samples was carried out with a corona discharger (Mystic Marvels, Model NIP-7E). Applied voltage was fixed at 9 kV, thus an electric field of 3kV/cm was produced within 3cm charging distance. For thermal charging, procedure described by our early work [Chapter 6] was followed. The fibrous material under high electric field is heated to soften and cooled in the presence of the field. Samples were heated to 130°C, which took approximately 1 minute, then polarized for 10 min and cooled to room temperature instantly.

Surface Potential Measurement. The surface potential was measured with electrostatic voltmeter (Monroe 244 Model with 1017AE electrostatic voltage probe) immediately after charging. The initial measurements (V_0) were taken directly after charging at room temperature. Potential maps were drawn after measurements at 16 different points across the sample surface. Not only potential of face of the webs, but also back were measured. After that absolute difference between face and back values were calculated since

total electric field that particles will be subjected to during filtration will be close to that value.

Dielectric Spectroscopy. Since meltblown webs are highly porous, a comparative study was done to analyze change in dielectric properties. Dielectric constants of the meltblown webs were measured in an Agilent 16451B dielectric test fixture equipped with an HP4284A LCR meter operated at 25°C over a frequency range of 1kHz to 1 MHz. Samples were initially cut about 4cm diameter and layered until reaching a thickness of 1.5±0.2mm. The thickness and solidity within electrodes were measured to normalize the measured capacitance values.

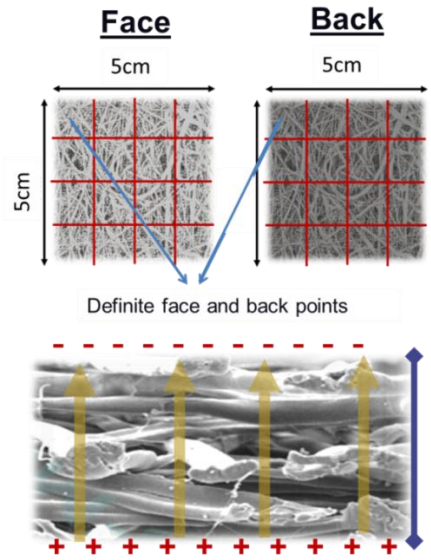

Figure 9.1 Surface potential measurement. 16 specific points were determined.

Analysis of Filtration Properties. Filtration properties of webs were evaluated at a face velocity of 5.3 cm/sec. DOP (dioctyl phthalate) aerosols were generated by a collision type atomizer and then evaporated through a membrane dryer, which were selected monodisperse aerosols of 0.3 μm in a long differential mobility analyzer (DMA, TSI, Model 3081, MN, USA) and then neutralized by a Kr-85 radioactive source. The neutralized DOP aerosols were feed into a filter holder with 25.81 cm^2 of effective area and measured their number concentrations at upstream and downstream positions by using two condensation particle counters (CPCs, TSI, Model 3760A, MN, USA). The flow rate and the resistance were measured by a mass flow meter (TSI, Model 4043, MN, USA) and an electronic manometer (TSI, Model 220, MN, USA).

9.3 Results and Discussions

9.3.1 Analysis of DMDBS/PP Meltblown Webs

Nucleating agents are chemicals that are used for ease of crystallization. Previous meltspinning studies showed that due to early solidification, filaments had larger crystal sizes upon nucleating agent incorporation. For meltblowing the early solidification resulted with comparatively larger fiber diameters and lower solidity as shown in Figure 9.2. Change in diameter and solidity resulted with higher air permeability for those webs. For that reason measured potential was normalized according to thickness and surface area of the webs,

whereas filtration data according to pressure drop, which is a well-known filter characteristic: quality factor (QF=(-lnP)/ΔP, where P corresponds penetration and ΔP, pressure drop.

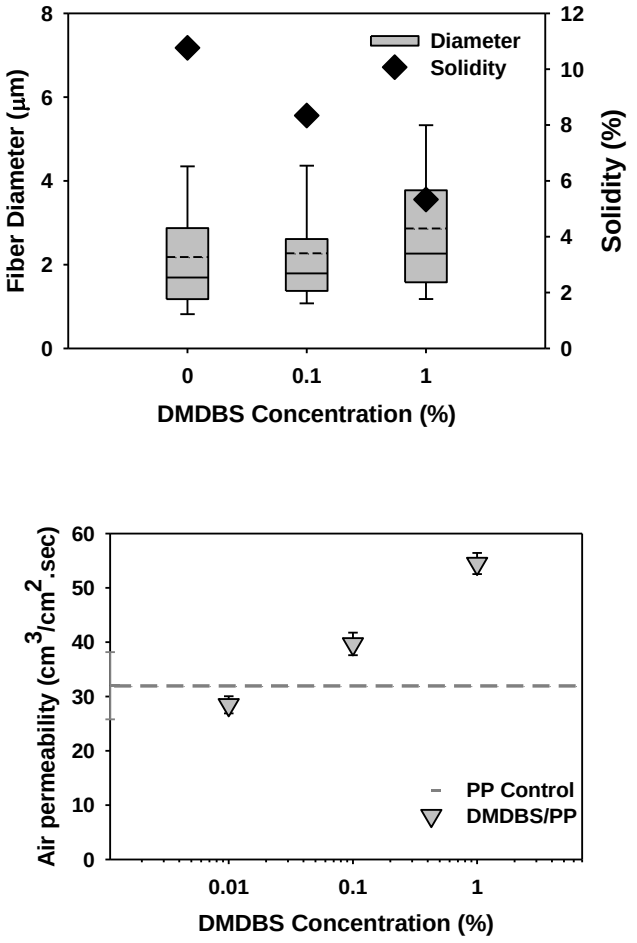

Figure 9.2 Fiber diameter, solidity and air permeability values for DMDBS containing webs (box boundaries indicate upper and lower hinges, whereas dashed line stands for average fiber diameter, solid line for median)

From the experience obtained from our previous studies on filaments [Chapter 6], it is known that thermal charging produces highly and stably charged electrets. Due to that reason samples were charged both in room conditions and high temperature conditions (130°C) for 10 min. As shown in Figure 9.3 particularly modified webs exhibited high efficiency after both cold and thermal charging. For instance 99.9% efficiency was observed at an expense of approximately 80Pa pressure drop for thermally charged 1%DMDBS webs, whereas it was found as 120Pa for unmodified reference sample.

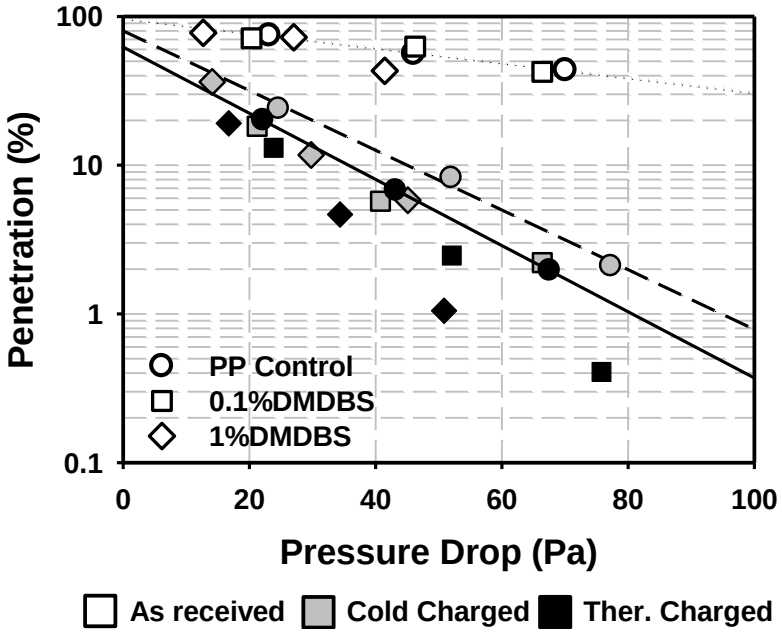

Figure 9.3 Filtration properties of cold and thermally charged DMDBS containing webs. Regression lines corresponds to PP Control sample for comparison

Due to mentioned differences in web properties quality factors were calculated (Figure 9.4). At 0.01% concentration the improvement was very similar to control sample, probably due to insufficient amount of the additive. Reaching to 0.83mmH_2O^{-1} quality factor at 1%DMDBS concentration, thermal charging enhanced even filtration properties of reference sample. This would be conducted to improved efficiency of corona discharge and changes in polymer properties at high temperatures.

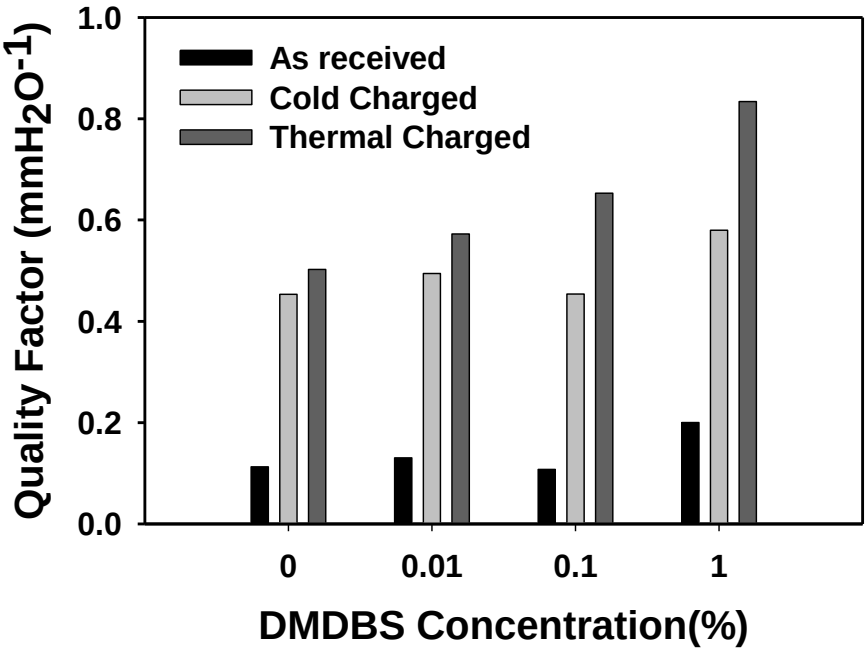

Figure 9.4 Quality factor vs concentration for DMDBS/PP webs (calculated from initial filtration and pressure drop values)

Due to H bonding and π-π interactions sorbitol based nucleating agents produces networks even below 1% concentration in polymers [17–19]. The network formation causes pathways for accumulation of charges and disturbs the stability. However we found the stability of thermal charged 1% DMDBS containing webs were still better when compared to lower additive concentrations even after holding samples 24h at 80°C. Relatively still longer stability might be due to high shear during meltblowing process, which prevented formation of such conductive 3-D networks.

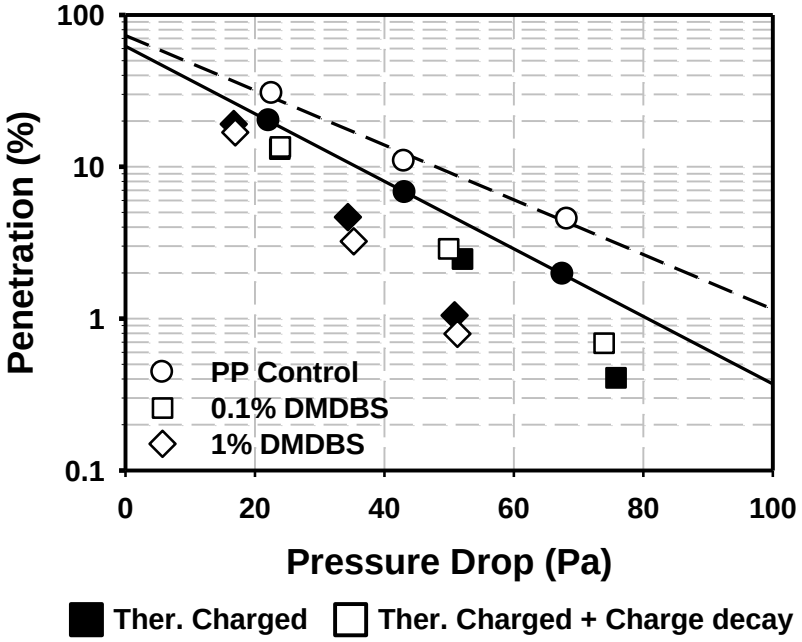

Figure 9.5 Filtration properties of thermally charged DMDBS containing webs after 24h charge decay at 80°C Regression lines corresponds to PP Control sample for comparison

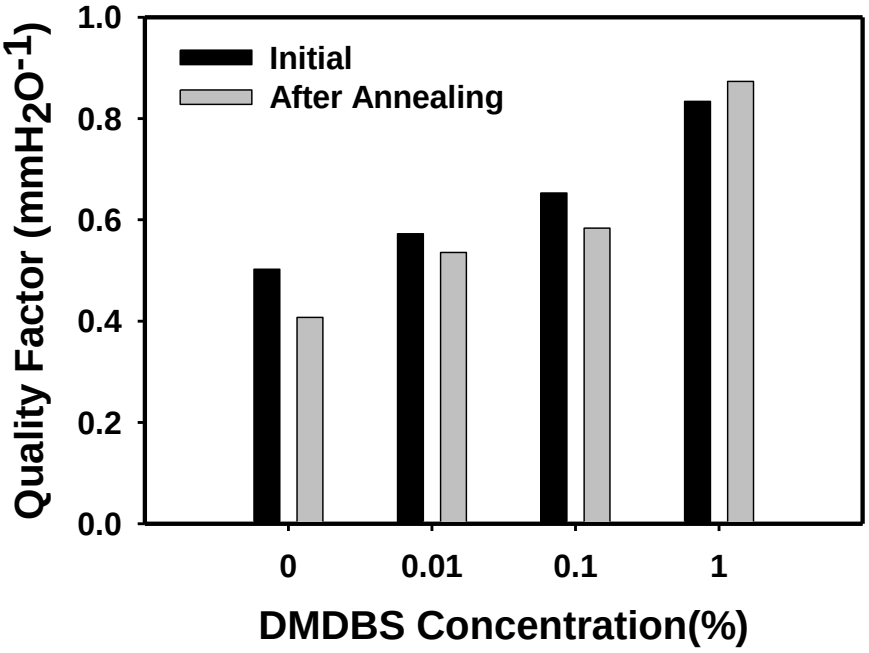

Figure 9.6 Quality factor vs concentration for thermally charged DMDBS/PP webs after annealing at 80°C for 24h

9.3.2 Analysis of NA11/PP Meltblown Webs

Fiber diameter and solidity of NA11 containing webs showed similar tendency with DMDBS containing webs. Increased fiber diameter and reduced solidity resulted with higher air permeability for NA11 containing webs as shown in Figure 9.7 .

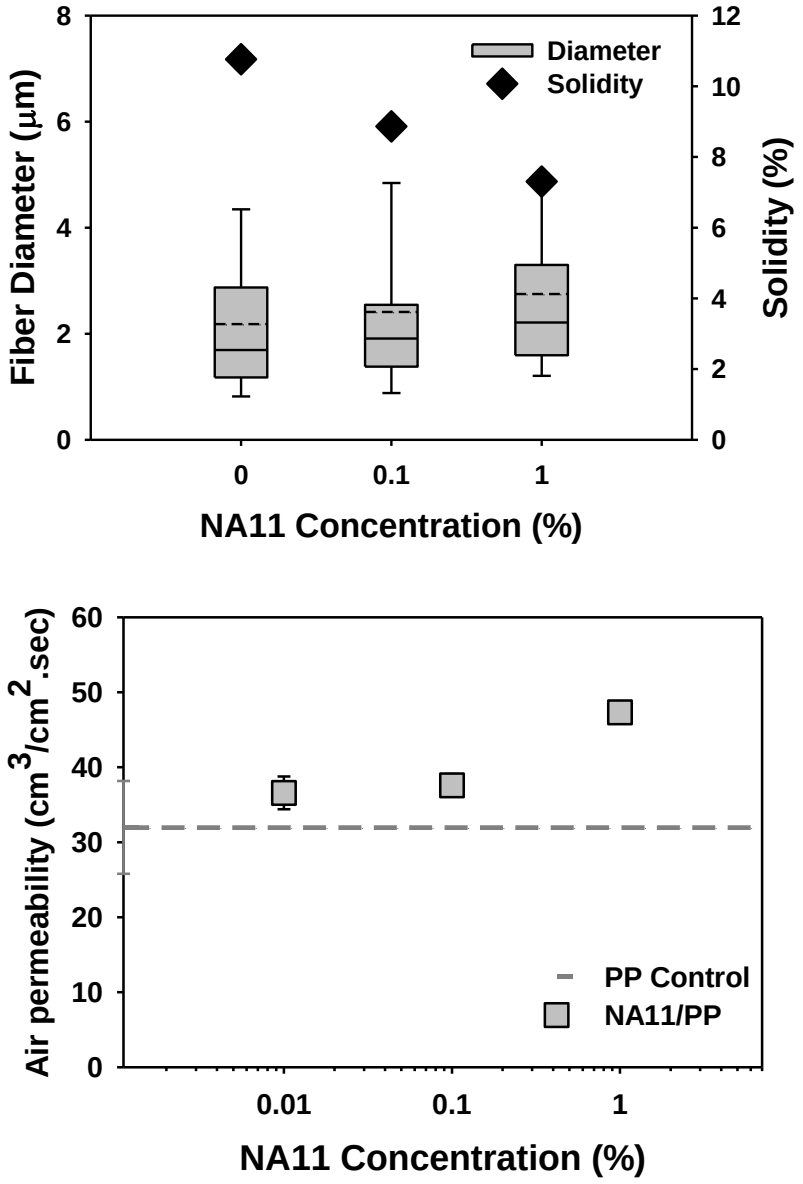

Figure 9.7 Fiber diameter, solidity and air permeability values for NA11 containing webs (box boundaries indicate upper and lower hinges, whereas dashed line stands for average fiber diameter, solid line for median)

The increase in filtration properties of NA11 is found to be similar to DMDBS containing webs. However even 0.1% NA11 concentration led to high increase in filtration efficiency. Interestingly filtration properties of cold and thermal charged samples do not show the same tendency. Upon thermal charging it enhanced enormously which might indicate that polarization occurred more effectively. Initial quality factor values were found similar around 0.6mmH_2O^{-1} for control and 0.01% concentration. Interestingly cold charged 0.1%NA11/PP webs exhibited weakly better initial filtration properties compared to cold charged ones (Figure 9.9).

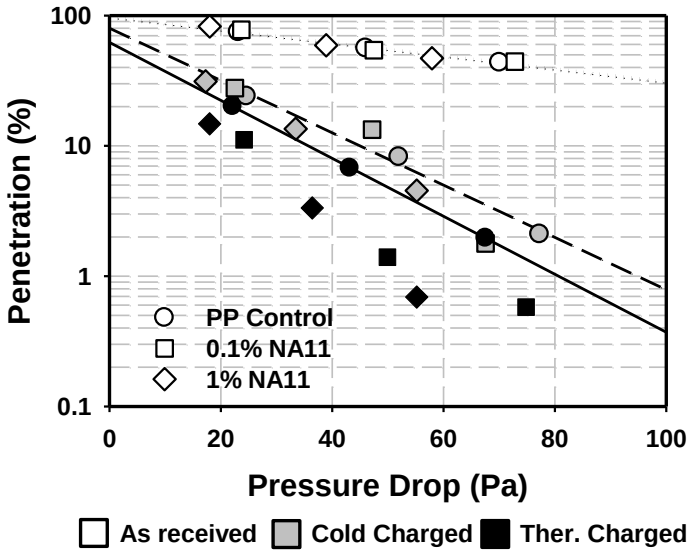

Figure 9.8 Filtration properties of cold and thermally charged DMDBS containing webs. Regression lines corresponds to PP Control sample for comparison

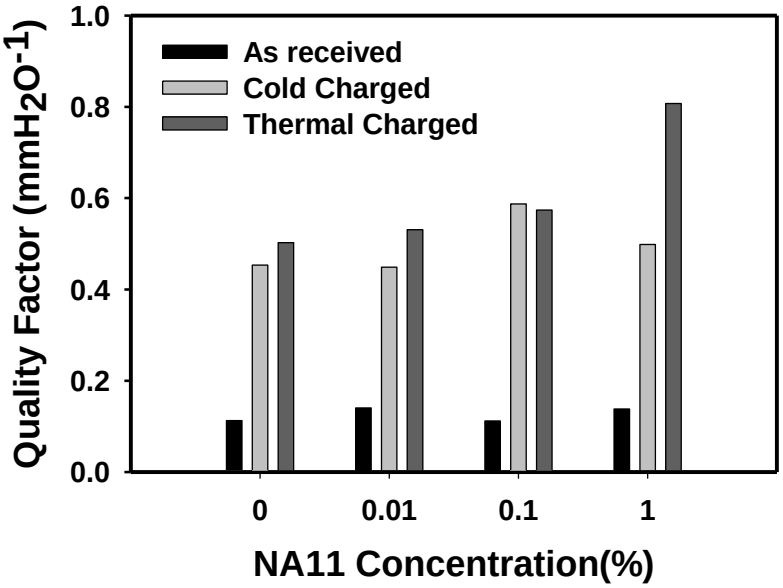

Figure 9.9 Quality factor vs concentration for NA11/PP webs (calculated from initial filtration and pressure drop values)

As shown in Figure 9.10 filtration stability for thermal charged samples is comparatively better than reference sample. Here again we observed at 1% sample has long stability which is important for stable electrostatic filtration.

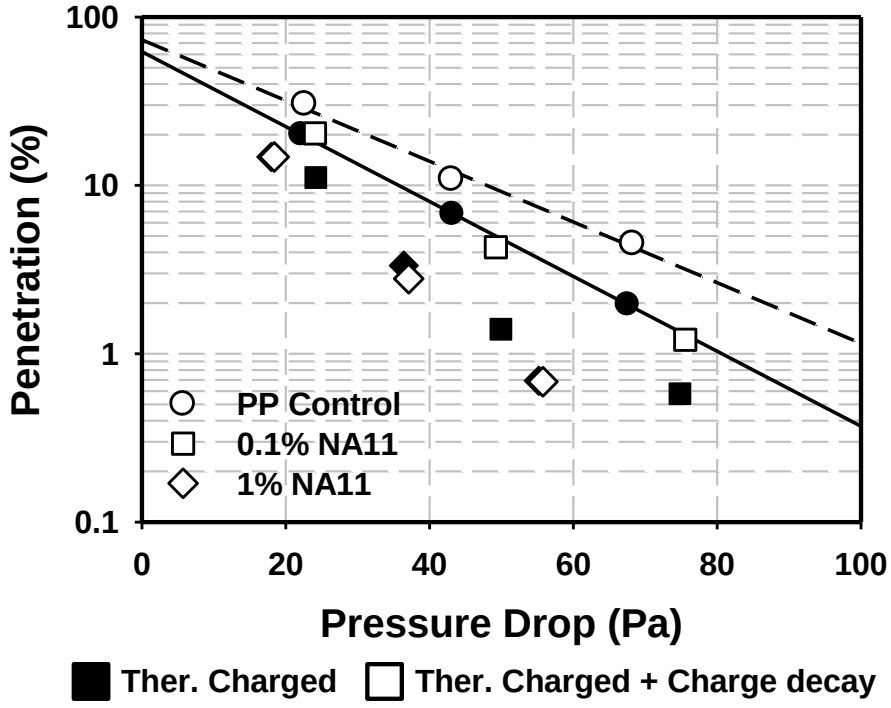

Figure 9.10 Filtration stability of thermally charged NA11 containing webs. Regression lines corresponds to PP Control sample for comparison

The reasons behind high filtration efficiency of thermal charged nucleating agent containing samples would be explained with better charging characteristics. Various web properties such as solidity and surface area will affect the measured surface potential. After finding electric field approximately by dividing absolute difference between face and back of the fabrics with fabric thickness ($\vec{E} = -\frac{|V_a - V_b|}{d}$), calculated values were normalized according to surface area

and solidities. As shown in Figure 9.13 and Figure 9.13, the electric field through thermally charged samples is significantly higher than that of cold charged samples, which resulted with higher quality factor values. The reason behind high efficiency of thermal charged webs would be improved charging conditions, softening of the polymer and enhanced mobility of dipolar molecules. Since nucleating agent content resulted with profound effect on such properties, rather than first two reasons, enhanced mobility for polarization of dipolar molecules would be analyzed.

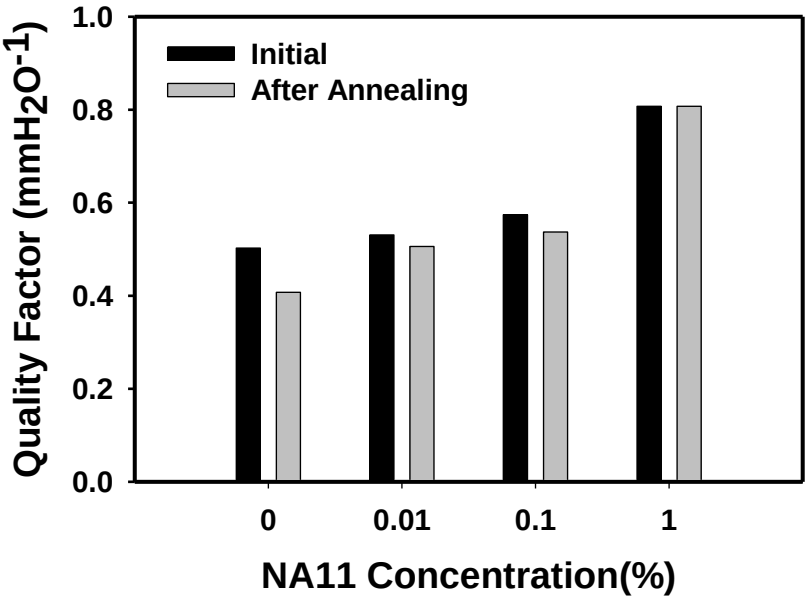

Figure 9.11 Quality factor vs concentration for thermally charged NA11/PP webs after annealing at 80°C for 24h

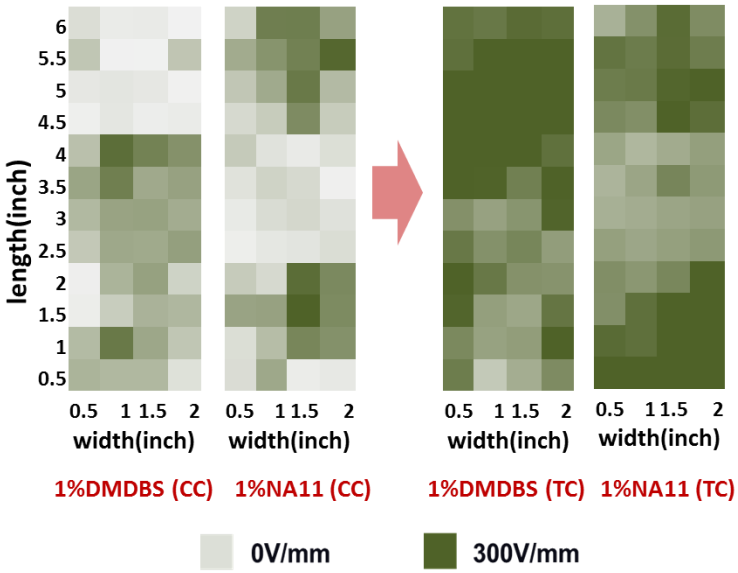

Figure 9.12 Normalized electric field through cold and thermally charged webs

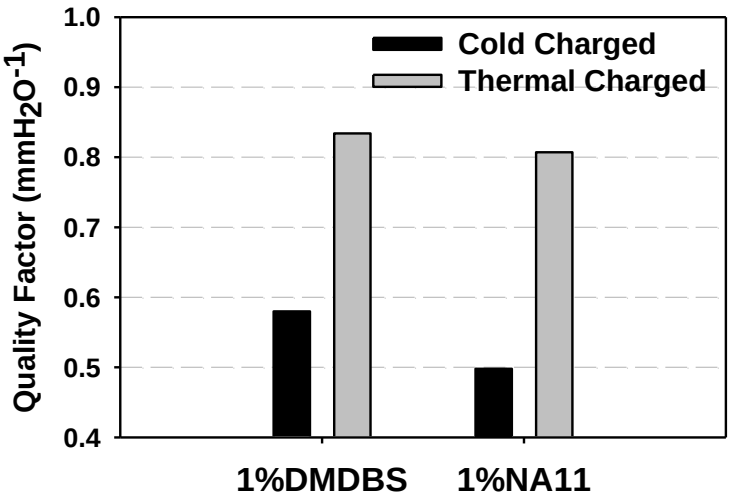

Figure 9.13 Quality factors for cold and thermally charged webs

Polarization mechanism after additives is more likely orientational polarization due to molecular structure. Temperature dependence of orientational polarization was observed in superior electrostatic filtration properties of thermally charged samples[4]. To prove orientational polarization, dielectric properties of the sample webs were analyzed via dielectric spectroscopy. Samples are fixed within Al electrodes of 3.8cm diameter.

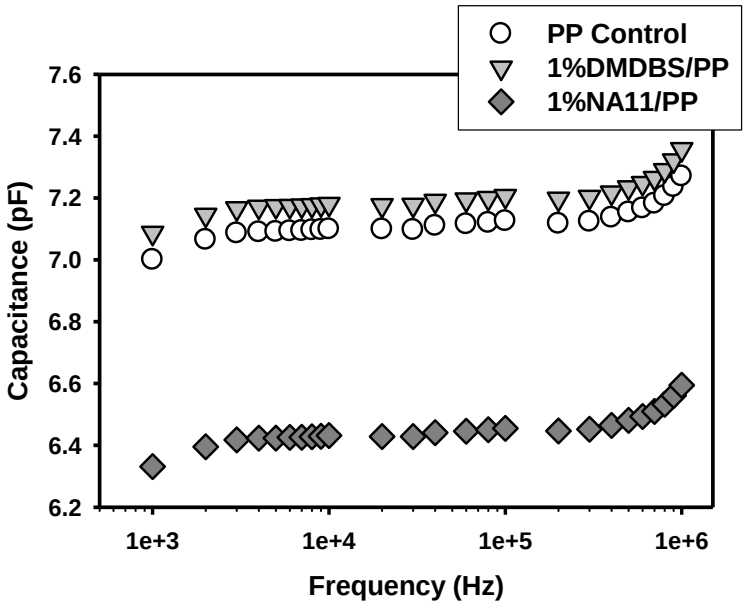

Figure 9.14 Measured capacitance of the webs over a frequency range of 1kHz to 1MHz. Samples were layered to reach a thickness of 1.5±0.2mm

As seen in Figure 9.14 1%DMDBS containing webs exhibited higher capacitance values compared to reference sample, whereas there is a drop after NA11 addition. However since fibrous webs are highly porous, to compare relative permittivity in this range capacitance values were normalized according to solidity. It was impossible to conduct normalization according to parallel and series connection calculations, because fibrous webs are highly anisotropic. After the normalization (Figure 9.15), a significant increase in dielectric values was observed. We can conclude superior electret properties of thermally charged nucleating agent containing webs to the increased concentration of dipolar species.

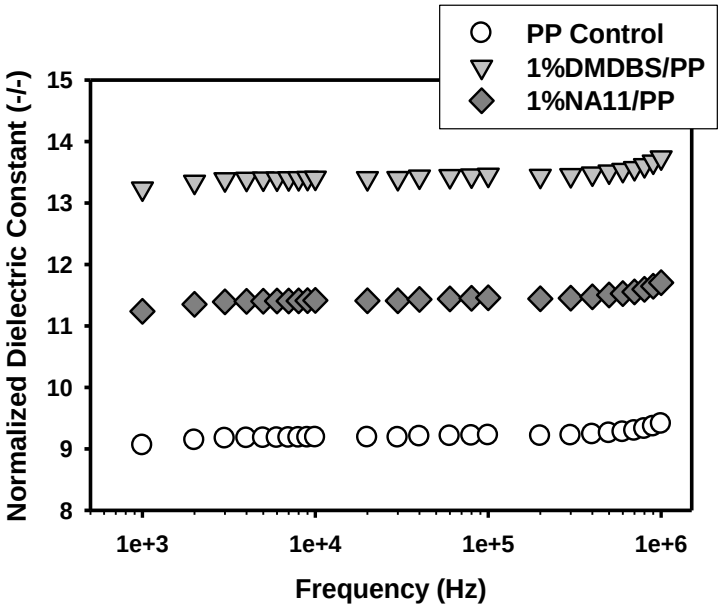

Figure 9.15 Normalized dielectric constants of the webs over a frequency range of 1kHz to 1MHz. Solidity was calculated according to equation1.

9.4 Conclusion

In this study effects of nucleating agent addition on electrostatic filtration properties were investigated. Important web properties on filtration did not change abruptly. However either of the nucleating agents exhibited profound effects on electret properties after thermal charging. Enhancement in filtration properties were conducted with higher potential values, which is related to dielectric properties. Since it was critical to handle all analysis using fibrous webs, inevitable normalization procedures were applied.

9.5 References

1. Mohmeyer, N. *et al.* Additives to improve the electret properties of isotactic polypropylene. *Polymer* 48, 1612–1619 (2007).

2. Hillenbrand, J., Behrendt, N., Altst\ädt, V., Schmidt, H. W. & Sessler, G. M. Electret properties of biaxially stretched polypropylene films containing various additives. *Journal of Physics D: Applied Physics* 39, 535 (2006).

3. Erhard, D. *et al.* Recent Advances in the Improvement of Polymer Electret Films. *[Advances in Polymer Science]* 1–53 (2010).

4. Behrendt, N. *et al.* Charge storage behavior of isotropic and biaxially-oriented polypropylene films containing α-and β-nucleating agents. *Journal of applied polymer science* 99, 650–658 (2006).

5. Mohmeyer, N., Schmidt, H. W., Kristiansen, P. M. & Altst\ädt, V. Influence of chemical structure and solubility of bisamide additives on the nucleation of isotactic polypropylene and the improvement of its charge storage properties. *Macromolecules* 39, 5760–5767 (2006).

6. Hillenbrand, J. *et al.* Charge retention in biaxially-oriented polypropylene films containing various additives. *Electrets, 2005. ISE-12. 2005 12th International Symposium on* 276–279 (2005).

7. Behrendt, N., Altstadt, V., Schmidt, H. W., Zhang, X. & Sessler, G. M. Development of porous polypropylene blends with NA11 particles and glass hollow spheres by biaxial stretching for electret applications. *Dielectrics and Electrical Insulation, IEEE Transactions on* 13, 992–1000 (2006).

8. Pritchard, G. *Plastics additives: an A-Z reference*. (Springer: 1998).

9. Zweifel, H., Maier, R. D. & Schiller, M. *Plastics Additives Handbook*. (Hanser Verlag: 2009).

10. Gächter, R., Müller, H. & Andreas, H. *Plastics additives handbook: stabilizers, processing aids, plasticizers, fillers, reinforcements, colorants for thermoplastics*. (Hanser: 1985).

11. Mohmeyer, N. *et al.* Nucleation of isotactic polypropylene by triphenylamine-based trisamide derivatives and their influence on charge-storage properties. *Polymer* 45, 6655–6663 (2004).

12. Influence of quenching on the charge stability of polymer electrets. 543–547 (1988).doi:10.1109/ISE.1988.38622

13. Kravtsov, A. G., Brünig, H. & Zhandarov, S. F. Analysis of the polarization state of melt-spun polypropylene fibers. *Journal of Materials Processing Technology* 124, 160–165 (2002).

14. Wang, X. & Ke, Q. Experimental investigation of adhesive meltblown web production using accessory air. *Polym. Eng. Sci.* 46, 1–7 (2006).

15. Shambaugh, R. L. A macroscopic view of the melt-blowing process for producing microfibers. *Industrial & Engineering Chemistry Research* 27, 2363–2372 (1988).

16. Milligan, M. W., Lu, F., Buntin, R. R. & Wadsworth, L. C. The use of crossflow to improve nonwoven melt-blown fibers. *J. Appl. Polym. Sci.* 44, 279–288 (1992).

17. Kristiansen, M. *et al.* The Binary System Isotactic Polypropylene/Bis(3,4-dimethylbenzylidene)sorbitol: Phase Behavior, Nucleation, and Optical Properties. *Macromolecules* 36, 5150–5156 (2003).

18. Mercurio, D. J. & Spontak, R. J. Morphological characteristics of 1, 3: 2, 4-dibenzylidene sorbitol/poly (propylene glycol) organogels. *The Journal of Physical Chemistry B* 105, 2091–2098 (2001).

19. Shepard, T. A. *et al.* Self-organization and polyolefin nucleation efficacy of 1, 3: 2, 4-di-p-methylbenzylidene sorbitol. *Journal of Polymer Science Part B Polymer Physics* 35, 2617–2628 (1997).

20. Kao, K.-C. *Dielectric phenomena in solids: with emphasis on physical concepts of electronic processes*. (Academic Press: 2004).

CHAPTER 10

10 Effect of Stabilizers on Corona Discharged PP Electret Filters

Abstract

A study on the effects of stabilizers on electrostatic filtration properties of corona discharged polypropylene (PP) meltblown webs is reported. Two widely known commercial stabilizers were used: Irgafos 168 -Tris(2,4-di-*tert*-butylphenyl)phosphite which acts as hydroperoxide decomposer during melt extrusion and Tinuvin 622LD -Poly(4-hydroxy-2,2,6,6-tetramethyl-1-piperidine ethanol-alt-1,4-butanedioic acid) which is a hindered amine type ligth stabilizer. In experimental additives were blended in two phase extrusion (masterbatch and meltblowing) where resultant concentration was kept in 0.01-1% range. Other than basic webs properties such as fiber diameter, soldity, surface potential and composition were also analyzed since they also affect initial elecrostatic filtration efficiency and stability. Results on charged samples showed that stabilizers barely enhanced filtration efficiency after cold charging, whereas thermal charging dropped the efficiency and stability most probably due to changes in surface composition.

10.1 Introduction

One of the basic issues in high performance aerosol filtration is energy expenses, which is directly related with airflow resistance. To reduce flow resistance without affecting particle capture efficiency, fibrous webs are charged, which are widely known as “electret” or “electrostatic filters”[1,2]. Since particles are captured by means of electrostatic forces, coarser fibers would be used and fiber-fiber distance would be kept larger, meaning solidity would be lowered. This comes with the advantage of high breath comfort for facemasks and respirators [3]. On the other side more open web structure will lead to higher dust holding capacity prior to clogging, which extends filter replacing frequency [4].

However for electret filters one of the basic problems is stability of electrostatic property under storage and filtration conditions[5,6]. In recent years several studies were published on novel charging methods and additives that would enhance filtration efficiency and stability. Corona discharge[5], splitting of charged films[7,8], carding webs composed of fibers of different triboelectric properties[9,10], hydrocharging with high speed liquid jets[11] and electrospinning[12] are methods to impart charges or polarize such filters. Studies are mostly concentrated on polypropylene due to its tailorability and low price. Looking at PP at molecular scale we see a fully sp3 furnished chemistry resulting with a saturated structure which leads insulating properties and very low polarizability. To enhance filtration performance further additives with different dielectric and electronic properties are incorporated to modify electret properties of PP. Among them are nucleating agents[13],

inorganic dielectrics[14], oily mist resisting agent[3,15], charge enhancing additives[84] were investigated so far. Stabilizers, one of the largest additive families might also be a good candidate to enhance electrostatic properties of polymers. Several studies in the literature [90,155,322] indicated their effect on space charge formation, which is an undesirable property for HV cable insulation since they catalyze breakdown of the dielectric. However space charge formation would be beneficial for electret filter applications. Due to difference in their electronic structure those additives would act as deep charge traps[20] which may modify electrostatic features of polymer, so as their filtration properties. In this study we compared the effect of two commercial stabilizers on electrostatic filtration properties of meltblown PP webs. Irgafos 168 and Tinuvin 622LD were selected and blended with PP webs through melt blowing.

10.2 Experimental

Materials and Meltblown Web Production. Achieve 6936G1 propylene polymer resin with a melt flow rate of 1550 was kindly provided from ExxonMobil. Irgafos 168 and Tinuvin 622LD was kindly donated by BASF. To provide better uniformity, initially PP masterbatch pellet at 1%(w/w) Irgafos and 10%(w/w) Tinuvin concentration was prepared by Techmer PM (Clinton, TN). Then, masterbatch was re-extruded with pure resin to produce

additive/PP composite webs with concentration of 0.01%, 0.1%, 1%(w/w). The chemical formulas of the additives were given in Figure 10.1.

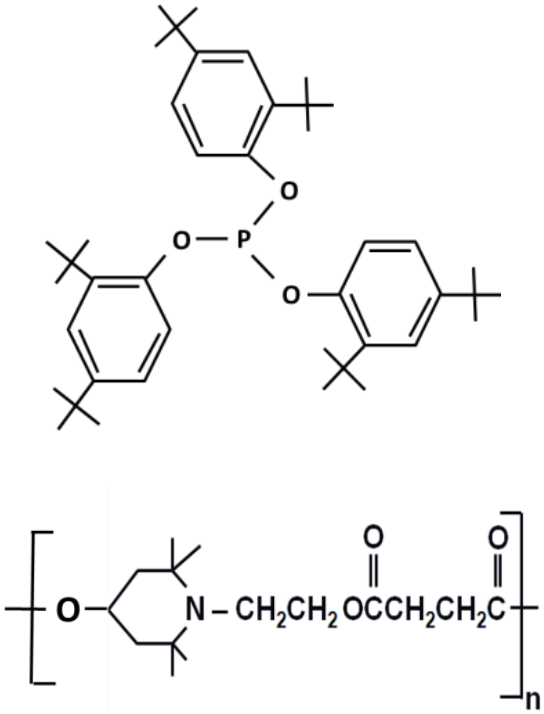

Figure 10.1 Chemistry of Irgafos (above) and Tinuvin (below)

Small melt blowing line used in the web preparation had a 6-inches MB die which has 120 holes, each of which is 0.15mm in diameter (i.e ~ 25 holes/inch). Polymer pellets are melted and pressurized using a 1 1/4" C.W. Brabender extruder, mounted horizontally. The heating in the extruder involves four zone temperature controls. The die is manufactured by

the Reifenhäuser KG. The air plate angle is 60° with the air gap of 0.3 mm and the die tip is outset the die face by 1mm. The temperature profile is tabulated in Table 10.1.

Table 10.1 Temperature profile during meltblowing process

	Z1	**Z2**	**Z3**	**Z4**	**Pump**
Temp. [°C]	190	220	230	250	248
	Transfer	**Turning**	**Die**	**Air Fed**	**Air measured**
Temp. [°C]	250	250	250	339	260-270

Meltblowing is not a specifically controllable process compared to melt spinning process. It means by changing process conditions such as die/air temperature, polymer throughput, air pressure, die-collector distance, belt velocity one can produce samples having different fiber diameter distributions and solidity [21–23]. Dominating melt blowing parameters, throughput value and air pressure were selected as 0.2-0.25ghm and 20-25psi respectively. Belt speed was changed according to desired basis weight. Important parameters for aerosol filtration such as basis weight, thickness, fiber diameter and distribution, solidity and air permeability were measured.

Basis weight measurements were done via weighing 5 specimen of $1dm^2$ area and averages were calculated thereof. Web thickness was measured according to ASTM D 5729 procedure where thickness testing gage (AMES, BG1110-04) with a presser foot diameter of

25.4 mm at pressure of 4.14kPa was used. From measured basis weight and thickness solidity of the webs were calculated from the following equation.

$$solidity = \frac{basisweight}{thickness * density} \qquad \text{Equation 10.1}$$

Fiber Diameter. SEM images of the meltblown samples were taken with a Phenom FEI scanning electron microscope. 100 measurements were taken from 15 pictures and average and standard deviations were calculated thereof.

Air Permeability. For air permeability test the method explained in ASTM D507 and D737 was used. A fixed area (38 cm^2) of sample was subjected to negative pressure of 125 Pa after sealing**.**

Charging. Charging of the samples was carried out with a corona discharger (Mystic Marvels, Model NIP-7E). Applied voltage was fixed at 9 kV, thus an electric field of 3kV/cm was produced within 3cm charging distance. For thermal charging, procedure described by our early work [Chapter 5] was followed. The fibrous material under high electric field is heated to soften and cooled in the presence of the field. Samples were heated to 130°C, which took approximately 1 minute, then polarized for 10 min and cooled to room temperature instantly.

Surface Potential Measurement. The surface potential was measured with electrostatic voltmeter (Monroe 244 Model with 1017AE electrostatic voltage probe)

immediately after charging. The initial measurements (V_0) were taken directly after charging at room temperature. Surface potential of both face and back side of the webs were measured. After that absolute difference between face and back values were calculated since total electric field that particles will be subjected to during filtration will be related to that value. Various web properties such as solidity and surface area will also affect the measured surface potential. After finding electric field approximately by dividing absolute difference between face and back of the fabrics with fabric thickness ($\vec{E} = -\frac{|V_a - V_b|}{d}$), calculated values were normalized according to surface area and solidities.

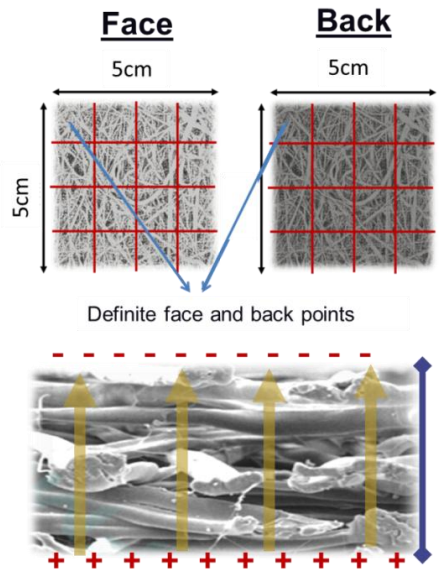

Figure 10.2 Surface potential measurement. 16 specific points were determined.

Surface Chemistry. A Nicolet 510P FTIR spectrometer was used in the range 4000–400 cm^{-1}, with a resolution of 4 cm^{-1}. ATR-FTIR data were analyzed by using Omnic software. 32 scans were collected for each measurement. Three random points were tested, where averages, standard deviations were calculated. Using the equation explained by Kortum[24], the penetration depth of IR in this range was calculated, which is about 0.3μm.

Analysis of Filtration Properties. Filtration properties of webs were evaluated at a face velocity of 5.3 cm/sec. DOP (dioctyl phthalate) aerosols were generated by a collision type atomizer and then evaporated through a membrane dryer, which were selected monodisperse aerosols of 0.3 μm in a long differential mobility analyzer (DMA, TSI, Model 3081, MN, USA) and then neutralized by a Kr-85 radioactive source. The neutralized DOP aerosols were feed into a filter holder with 25.81 cm^2 of effective area and measured their number concentrations at upstream and downstream positions by using two condensation particle counters (CPCs, TSI, Model 3760A, MN, USA). The flow rate and the resistance were measured by a mass flow meter (TSI, Model 4043, MN, USA) and an electronic manometer (TSI, Model 220, MN, USA). Due to unexpected changes in fiber diameter and solidity, normalization of filtration data is inevitable. This would be done simply comparing quality factor values which is negative natural logarithm of penetration of pressure drop ($QF=-\ln P/\Delta p$).

10.3 Results and Discussions

10.3.1 Analysis of Irgafos/PP Meltblown Webs

Addition of Irgafos 168 resulted with more defective (pinholes and shot) PP webs even at 0.01% concentration. Processing problems were also reported during masterbatch production, though Irgafos is a largely used stabilizer for polyolefins. As shown in Figure 10.3 besides shot and pinhole formation, Irgafos addition resulted with larger fiber diameter and lower solidity, which is correlated with increased air permeability.

Cold charged Irgafos containing webs exhibited increase in filtration efficiency compared to control samples. Higher defective structures (shots and pinholes) on the web should have increased penetration. Even after defects, 1% Irgafos containing web was able reach 99% efficiency at an expense of ~70Pa whereas the same was achieved by control sample at an expense of 95Pa.

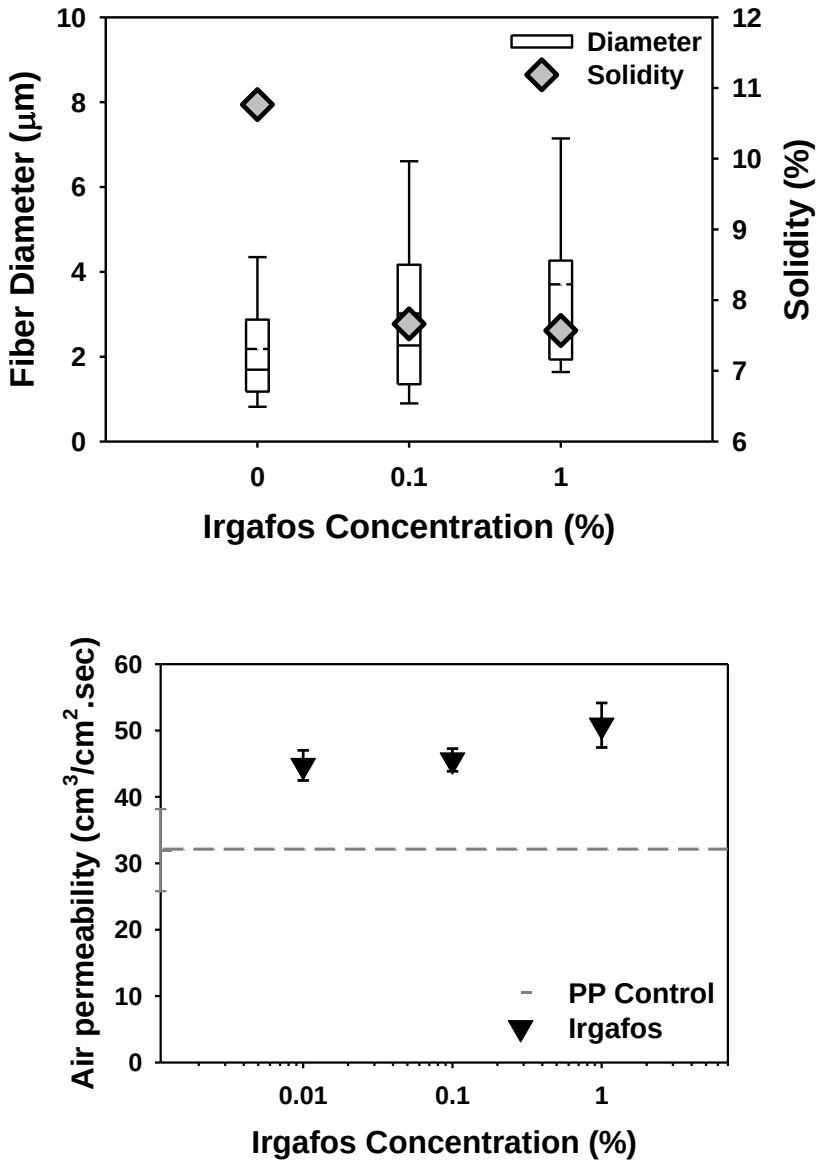

Figure 10.3 Fiber diameter, solidity and air permeability values for Irgafos containing webs (box boundaries indicate upper and lower hinges, whereas dashed line stands for average fiber diameter, solid line for median)

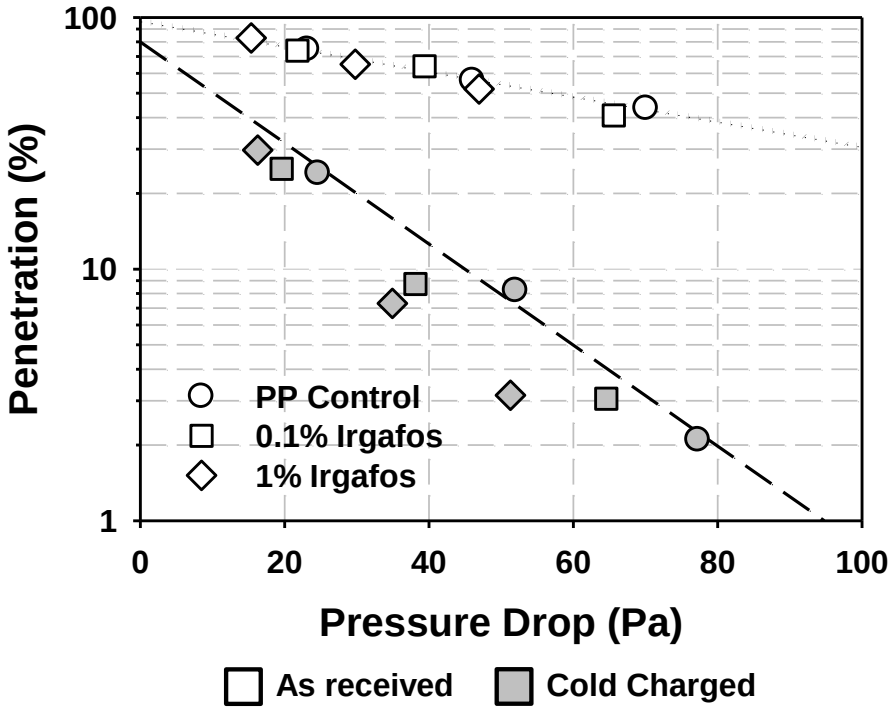

Figure 10.4 Filtration efficiency of as received and cold charged Irgafos containing webs. Measured at a face velocity of 5.3cm/s using 0.3μm DOP particles

Since it is well known that corona charging efficiency increases at high temperatures the samples were also thermally charged. Interestingly we observed that for the case of Irgafos containing webs thermal charging did not work as good as cold charging. As shown in Figure 10.5 1% Irgafos containing cold charged samples were more efficient than thermally charged one.

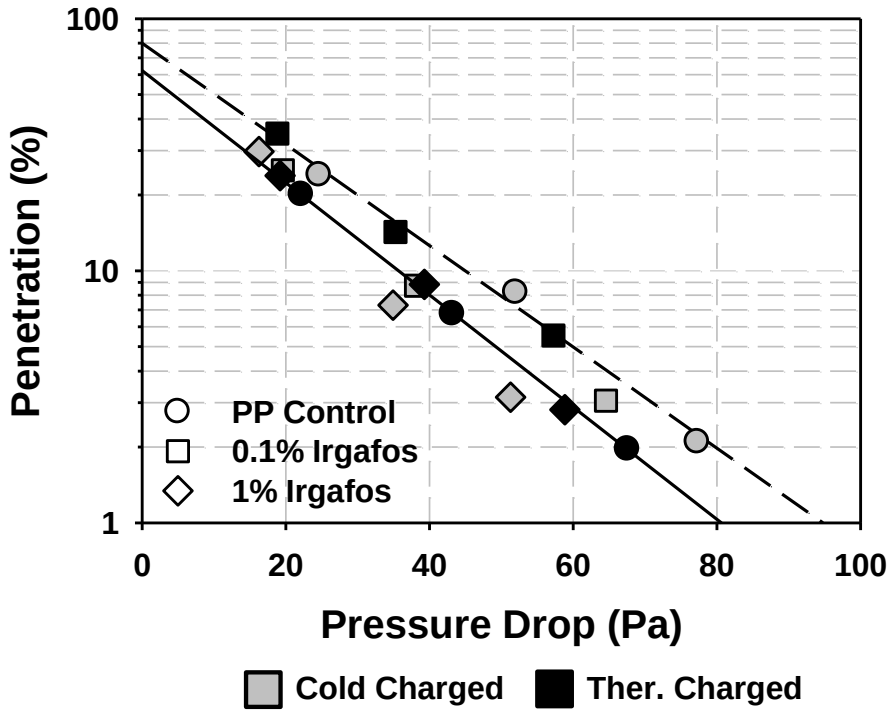

Figure 10.5 Comparison of filtration efficiency after cold and thermal charging. Measured at a face velocity of 5.3cm/s using 0.3µm DOP particles. Samples were charged for 10min and temperature was kept 130°C for thermal charging solid and dashed regression lines correspond to thermal and cold charged PP Control sample respectively.

Results would be compared via calculating quality factors (Figure 10.6). Cold charging 1% Irgafos containing webs resulted with highest initial quality factor, whereas lower than 1% additive incorporation did not lead to a significant change in quality factor, which would be due to consumption of additive against thermal oxidation.

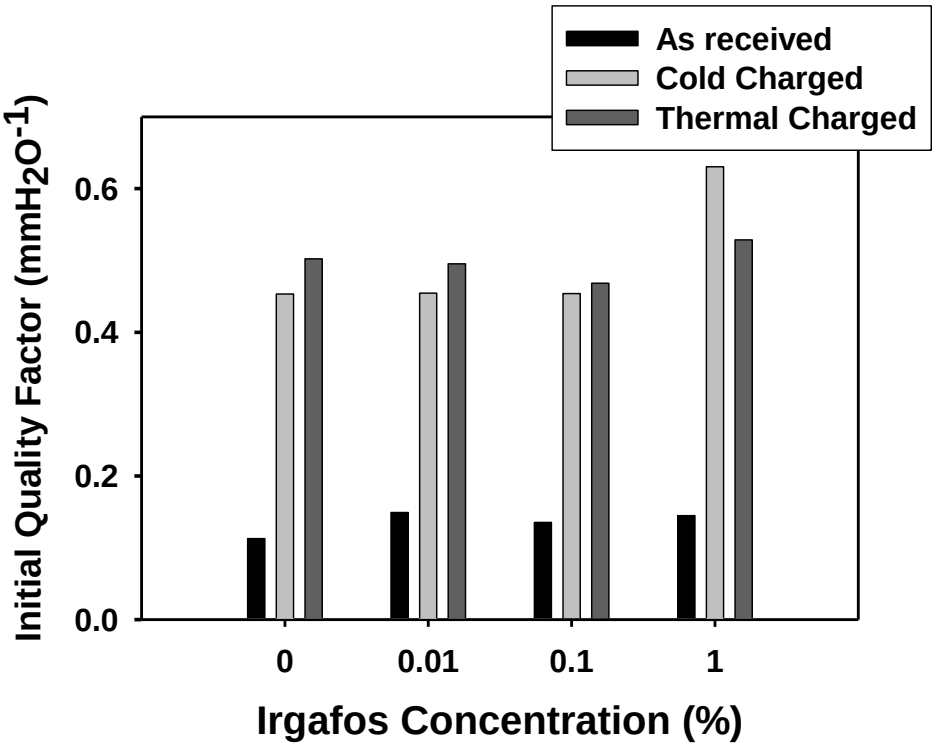

Figure 10.6 Initial quality factor values. Calculated after tests at a face velocity of 5.3cm/s using 0.3μm DOP particles

The stability of electrostatic filtration was analyzed after 24h isothermal charge decay at 80°C. Thermally charged sample exhibited comparatively stable filtration properties (Figure 10.7). The filtration trend for cold charged sample dropped nearly same efficiency with thermally charged after isothermal decay.

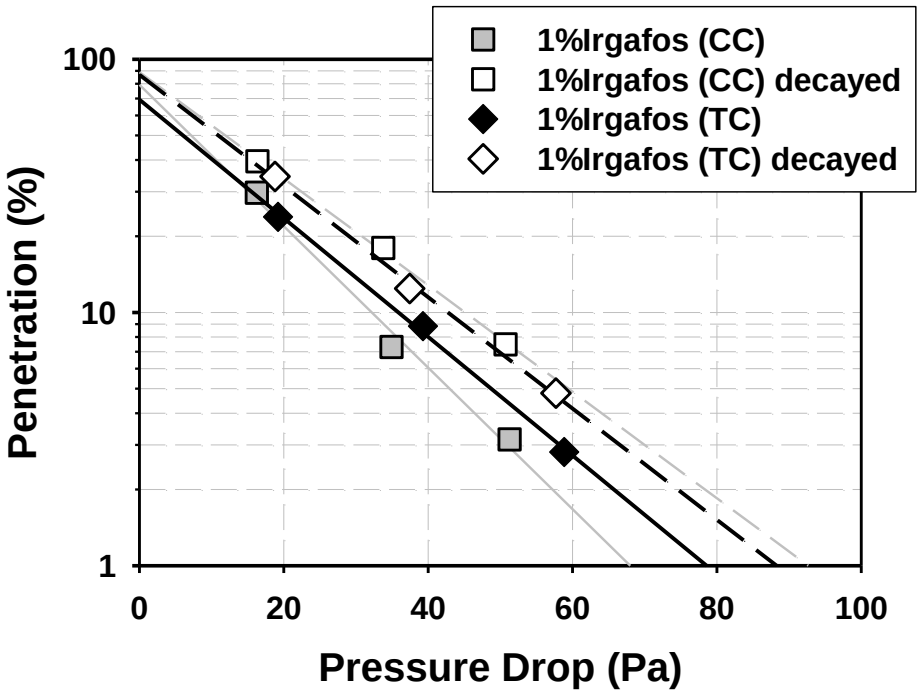

Figure 10.7 Filtration efficiency upon cold and thermal charging. Samples were kept under 80°C for 24h. Solid linear regression lines for initial efficiency, dashed linear regression lines for decayed samples

Results would be seen in quality factor graphs more clearly (Figure 10.8). Interestingly 0.1%Irgafos/PP web exhibited stable filtration efficiency after either cold or thermal charging. Irgafos at 0.1-1% concentration range clearly enhanced filtration efficiency compared to reference sample.

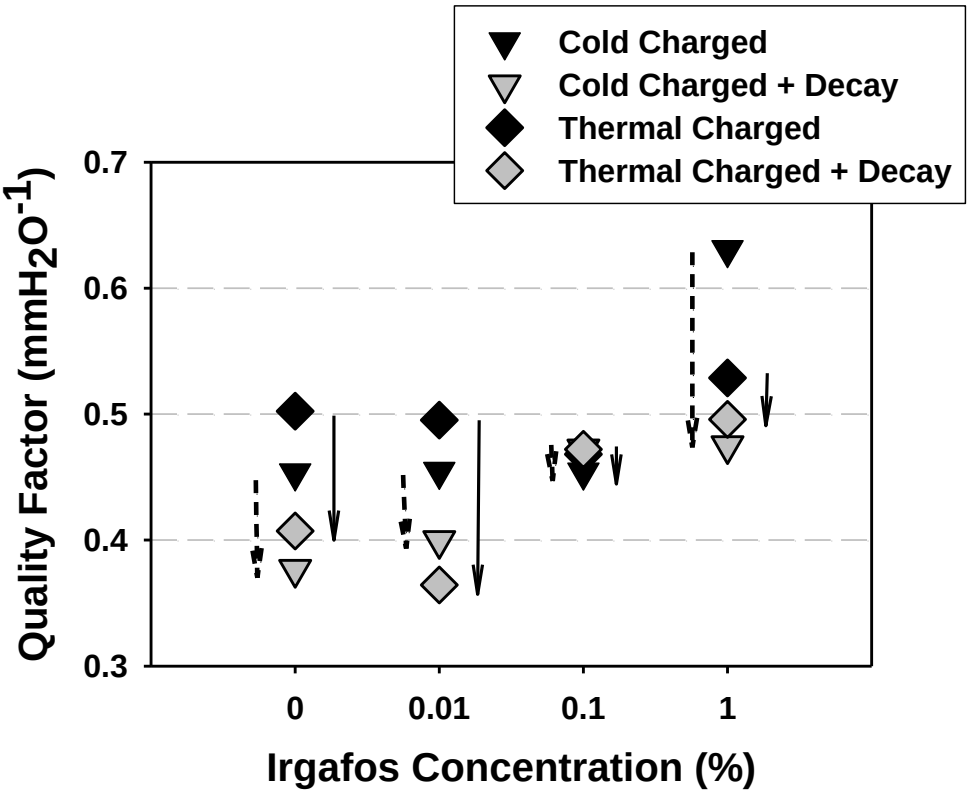

Figure 10.8 Quality factors upon decay under 80°C for 24h. Arrows indicates the drop in quality factor

Similar tendency with filtration properties was also seen in analysis of electrostatic properties. Normalized electric field graphs for cold and thermally charged Irgafos containing webs did not show a significant change (Figure 10.9). At 0.1% Irgafos concentration there is an increase in measured electric field strength, however this did not contribute filtration efficiency which would be due to web defects.

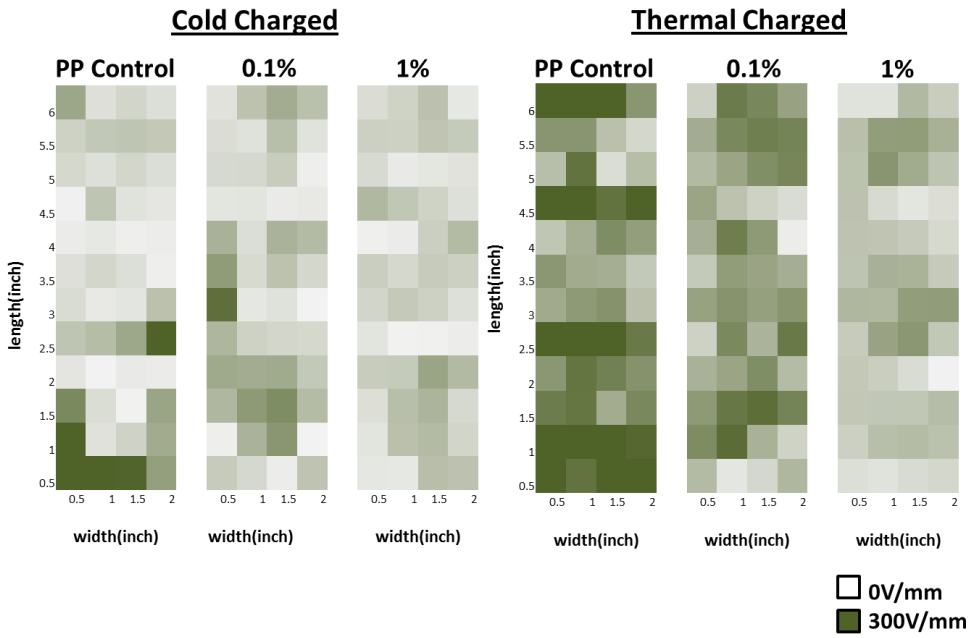

Figure 10.9 Normalized electric field for Irgafos containing webs. Normalization was done according to solidity and surface area calculated from average fiber diameter

10.3.2 Analysis of Tinuvin/PP Meltblown Webs

More uniform and nondefective web structures were obtained upon Tinuvin addition. Similar to Irgafos addition of Tinuvin also resulted with increased fiber diameter and lower solidity. However concentration did not change basic web properties significantly as observed in Irgafos (Figure 10.10). When compared to Irgafos, Tinuvin has even lower melting temperature (softening around 70°C). However it has a linear oligomeric structure which enhances its stability within polymer.

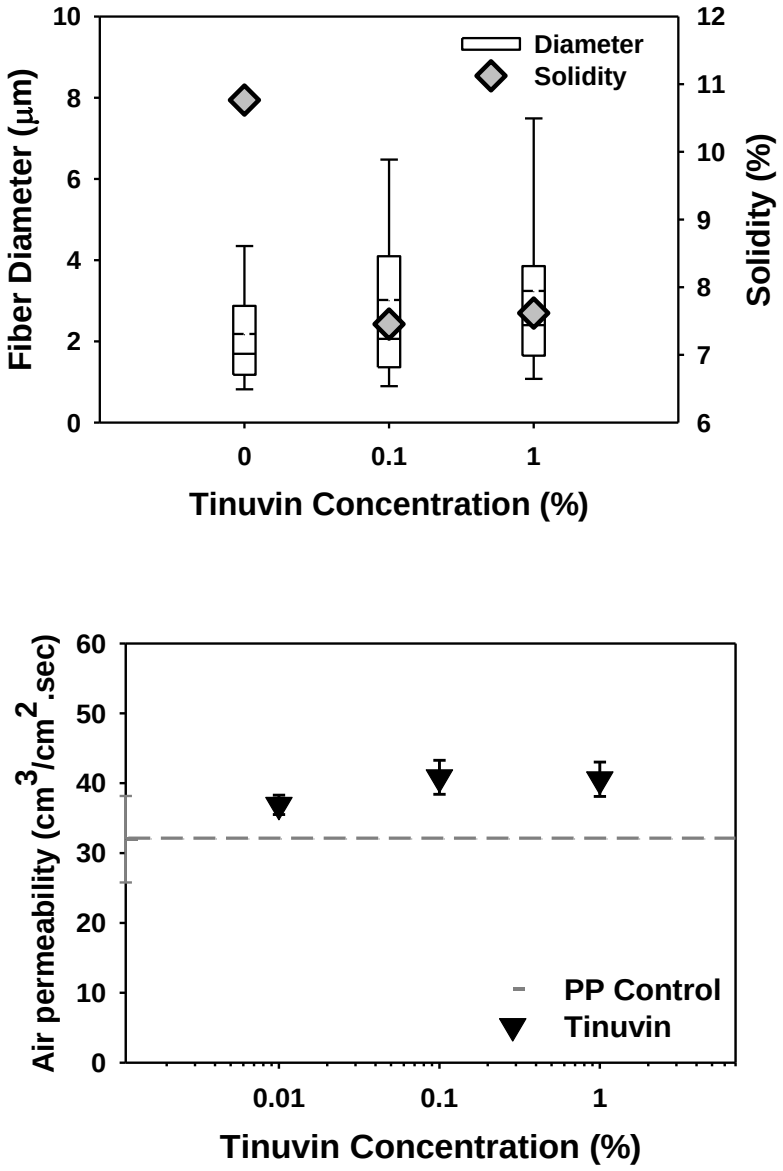

Figure 10.10 Fiber diameter, solidity and air permeability values for Tinuvin containing webs (box boundaries indicate upper and lower hinges, whereas dashed line stands for average fiber diameter, solid line for median)

Even without post charging process there was a noticeable increase in filtration efficiency upon Tinuvin addition. After cold and thermal charging penetration dropped significantly, however same tendency with Irgafos containing webs were observed. As shown in Figure 10.11 thermal charging did not result with a tremendous increase in particle capture efficiency, whereas it was advantageous for PP control web.

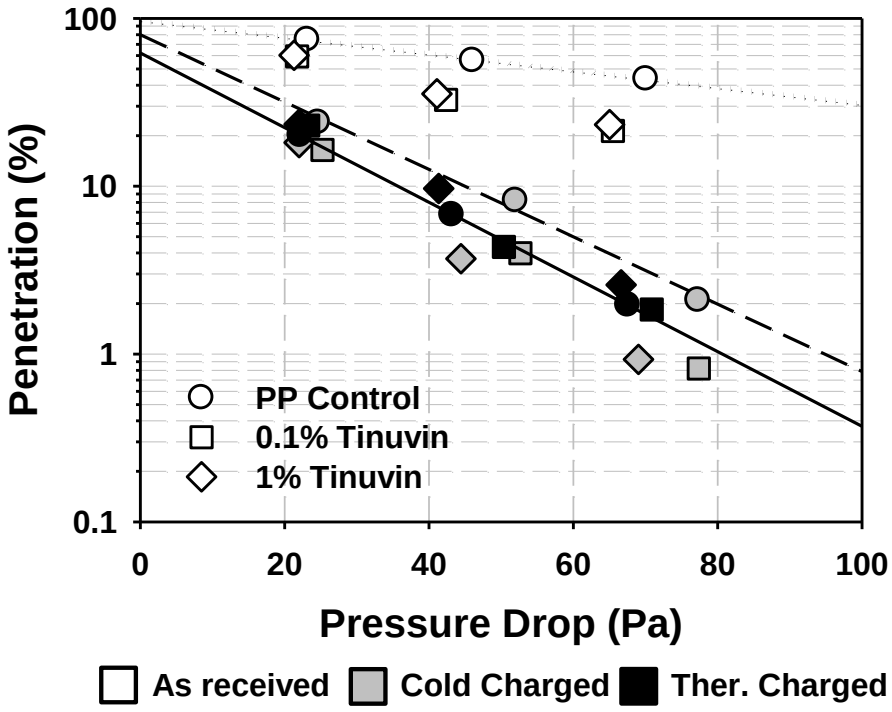

Figure 10.11 Filtration properties of Tinuvin containing webs. Measured at a face velocity of 5.3cm/s using 0.3µm DOP particles. Samples were charged for 10min and temperature was kept 130°C for thermal charging

Looking at quality factors of thermally charged webs, they are significantly low compared to cold charged samples. Even remaining filtration efficiency after 24h of annealing was low for all concentrations. However charge dissipation seems faster for cold charged samples.

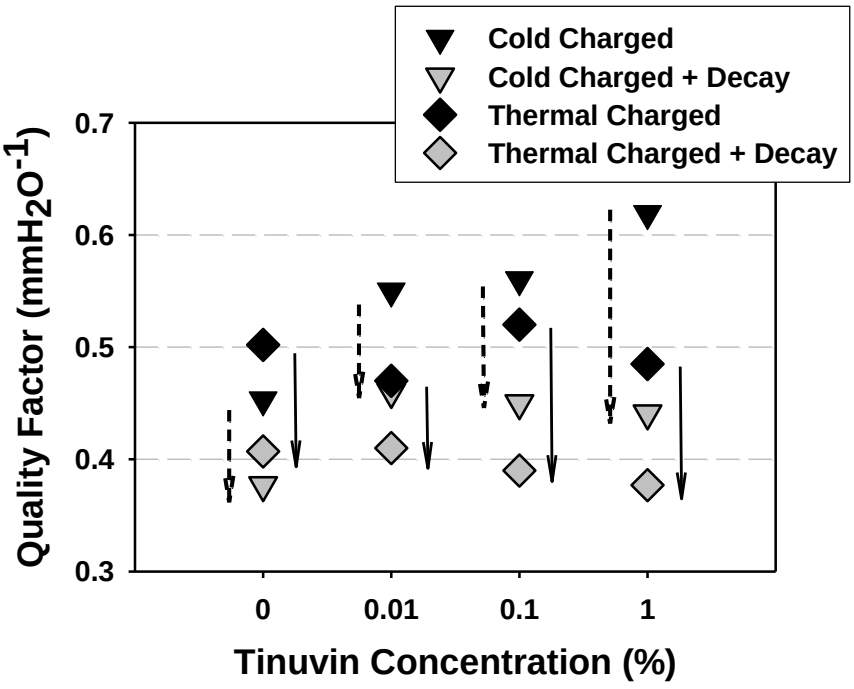

Figure 10.12 Filtration properties of cold and thermally charged Tinuvin containing webs. Calculated from the measurements at a face velocity of 5.3cm/s using 0.3μm DOP particles. Samples were charged for 10min and temperature was kept 130°C for thermal charging

Unlikely Irgafos containing webs, there is a minimal increase in electric field values (darker potential points), however this was not as much as control sample (Figure 10.13). For 1% Tinuvin containing web thermal charging resulted with higher fields through web. This is interesting because the initial quality factor for this sample was not so high which is tested within 1 hour after charging. There seems to be sudden reduction in surface potential which led higher penetration values.

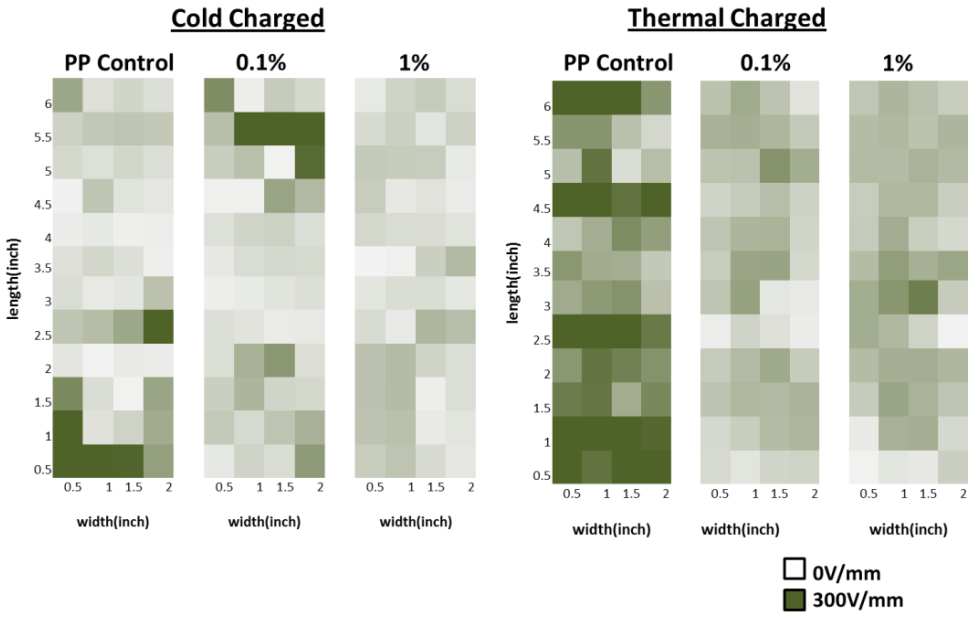

Figure 10.13 Normalized electric field for Tinuvin containing webs

In contrary to several works in the literature[25–28] thermal charging did not produced high efficiency stable electret filters. The substantial drop in filtration properties led us to the question: "changes in surface chemistry". As widely investigated [29–31] one of the basic problems in additive-polymer compositions is blooming of additive over surface and even removal of additive from the host polymer within time. Since thermal charging was done at significantly high temperatures, this would be expected. Unused samples were recharged again under the same conditions and analyzed using ATR spectroscopy. Phosphite and phosphate peaks are characteristic for Irgafos and Irgafos byproducts which is observed at 1191 and 966cm^{-1} respectively [32,33], whereas Tinuvin concentration was analyzed using the peak at 1734cm^{-1}, which corresponds to the absorption of ester groups[34,35]. Absorbance values were normalized according to peaks at 2920cm^{-1} which corresponds antisymmetric CH-CH_2 stretching[36]. As seen in Figure 10.14 there is a significant increase in additive concentration upon thermal charging, which indicates change in surface composition. The change in surface composition may lead to increase in charge escape frequency, which resulted with low charge stability for such webs.

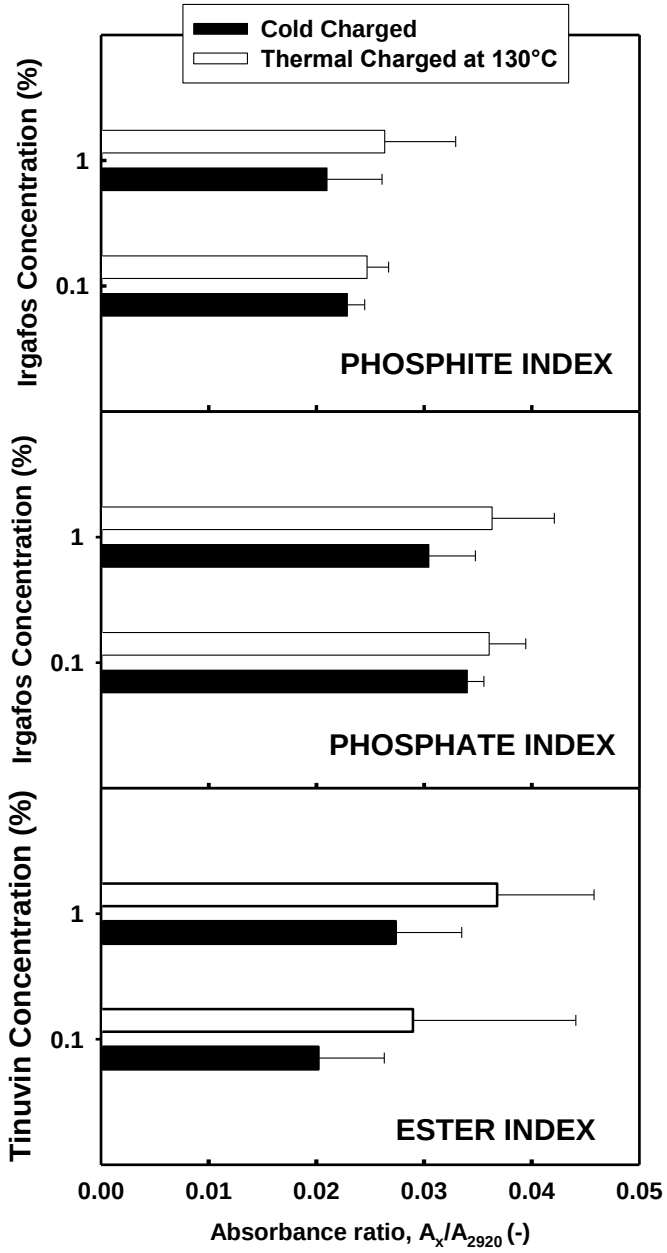

Figure 10.14 Additive blooming through surface upon thermal charging. Absorbance values were normalized according to peak at 2920cm^{-1} which corresponds C-H stretching vibrations.

10.4 Conclusion

Effects of stabilizers electrostatic and electrostatic filtration properties were analyzed. Either of the additives acted positively over electrostatic filtration properties when cold charged, whereas thermal charging did not lead to same results. Blooming of additives during thermal charging is thought to be reason for changes in surface chemistry, which is coupled with low filtration efficiency and stability. A recent patent issued by Sebastian et al[11] describes hydrocharging Irgafos 168 containing meltblown webs using a solution producing high zeta potential over fiber surface. For hydrocharged samples using acetic acid solution quality factor calculated for 0.3µm particles at a face velocity of 6.9cm/sec was significantly high ($1.83 mm H_2O^{-1}$) compared to our samples charged with either cold or thermal corona discharge. This indicates not only additives, but also charging procedure influences electrostatic filtration properties.

10.5 References

1. Nakao, E. Method of manufacturing an electret filter. (1986).at <http://www.google.com/patents?id=pmQ6AAAAEBAJ>
2. Brown, R. G. & Brown, R. G. Electrostatic Filter Unit with High Stable Charge and Its Manufacture. (1970).at <http://www.google.com/patents?id=suweAAAAEBAJ>

3. Huberty, J. S. Oily-mist resistant filter that has nondecreasing efficiency. (2003).at <http://www.google.com/patents?id=-98NAAAAEBAJ>

4. Healey, D. T. Filter media with enhanced stiffness and increased dust holding capacity. at <http://www.google.com/patents?id=-sWJAAAAEBAJ>

5. Gangjin Chen, Huiming Xiao & Xin Wang Study on parameter optimization of corona charging for melt-blown polypropylene electret nonwoven web used as air filter. *Properties and Applications of Dielectric Materials, 2009. ICPADM 2009. IEEE 9th International Conference on the* 389–391 (2009).doi:10.1109/ICPADM.2009.5252406

6. Song, X., Zhou, S., Wang, Y., Kang, W. & Cheng, B. Mechanical and electret properties of polypropylene unwoven fabrics reinforced with POSS for electret filter materials. *Journal of Polymer Research* 19, 1–8 (2012).

7. Romay, F. J., Liu, B. Y. H. & Chae, S. J. Experimental study of electrostatic capture mechanisms in commercial electret filters. *Aerosol science and technology* 28, 224–234 (1998).

8. Van Turnhout, J. & Rieke, J. C. *Method for manufacturing a filter of electrically charged electret fiber material and electret filters obtained according to said method*. (Google Patents: 1983).

9. Smith, P. A., East, G. C., Brown, R. C. & Wake, D. Generation of triboelectric charge in textile fibre mixtures, and their use as air filters. *Journal of Electrostatics* 21, 81–98 (1988).

10. Barrett, L. W. & Rousseau, A. D. Aerosol loading performance of electret filter media. *American Industrial Hygiene Association* 59, 532–539 (1998).

11. Sebastian, J. M. *et al. Method of making electret articles based on zeta potential*. (Google Patents: 2010).

12. Yeom, B. Y., Shim, E. & Pourdeyhimi, B. Boehmite nanoparticles incorporated electrospun nylon-6 nanofiber web for new electret filter media. *Macromolecular Research* 18, 884–890 (2010).

13. Jackson, F. L. & Pittman, P. L. Gas filtration media and method of making the same. (2000).at <http://www.google.com/patents?id=mscDAAAAEBAJ>

14. Myers, D. L., Lassig, J. J., Turkevich, L. A. & Midkiff, D. G. *Stable electret polymeric articles*. (Google Patents: 2003).

15. Jones, M. E. & Rousseau, A. D. *Oily mist resistant electret filter media and method for filtering*. (Google Patents: 1995).

16. Rousseau, A. D., Jones, M. E. & Angadjivand, S. A. *Electret filter media containing filtration enhancing additives*. (Google Patents: 1999).

17. Mizutani, T. Effects of additives and morphology on space charge in LDPE. *Electrical Insulating Materials, 2001. (ISEIM 2001). Proceedings of 2001 International Symposium on* 487 –492 (2001).doi:10.1109/ISEIM.2001.973710

18. Tanaka, Y. *et al.* Effect of additives on morphology and space charge accumulation in low density polyethylene. *Dielectrics and Electrical Insulation, IEEE Transactions on* 10, 148–154 (2003).

19. Cartwright, G. A., Davies, A. E., Swingler, S. G. & Vaughan, A. S. Effect of an antioxidant additive on morphology and space-charge characteristics of low-density polyethylene. *Science, Measurement and Technology, IEE Proceedings*- 143, 26–34 (1996).

20. Teyssedre, G. & Laurent, C. Charge Transport Modeling in Insulating Polymers: From Molecular to Macroscopic Scale. *IEEE Transactions on Dielectrics and Electrical Insulation* 12, (2005).

21. Wang, X. & Ke, Q. Experimental investigation of adhesive meltblown web production using accessory air. *Polym. Eng. Sci.* 46, 1–7 (2006).

22. Shambaugh, R. L. A macroscopic view of the melt-blowing process for producing microfibers. *Industrial & Engineering Chemistry Research* 27, 2363–2372 (1988).

23. Milligan, M. W., Lu, F., Buntin, R. R. & Wadsworth, L. C. The use of crossflow to improve nonwoven melt-blown fibers. *J. Appl. Polym. Sci.* 44, 279–288 (1992).

24. Kortum, G. & Korta1/4m, G. *Reflectance Spectroscopy: Principles, Methods, Applications*. (Springer: 1969).

25. Nishiura, E. & Ando, K. Electret materials and the method for preparing the electret materials. (1991).at <http://www.google.com/patents?id=iY4nAAAAEBAJ>

26. Felton, C. D., Gibson, B. D., Jamison, C. E., McWhorter, W. O. & Serad, G. A. Electret making process using corona discharge. (1986).at <http://www.google.com/patents?id=f1c2AAAAEBAJ>

27. Moosmayer, P., Budliger, J.-P., Zurcher, E. & Wadsworth, L. C. Apparatus for electrically charging meltblown webs (B-001). (1990).at <http://www.google.com/patents?id=O1sCAAAAEBAJ>

28. Gerhard-Multhaupt, R. Electrets: Dielectrics with Quasi-Permanent Charge or Polarization. *Electrical Insulation, IEEE Transactions on* EI-22, 531 –554 (1987).

29. Spatafore, R. & Pearson, L. T. Migration and blooming of stabilizing antioxidants in polypropylene. *Polymer Engineering & Science* 31, 1610–1617 (1991).

30. Duwez, A.-S., Poleunis, C., Bertrand, P. & Nysten, B. Chemical Recognition of Antioxidants and UV-Light Stabilizers at the Surface of Polypropylene: Atomic Force Microscopy with Chemically Modified Tips. *Langmuir* 17, 6351–6357 (2001).

31. Heiserman, W. M., Can, S. Z., Walker, R. A., Begley, T. H. & Limm, W. Interfacial behavior of common food contact polymer additives. *Journal of Colloid and Interface Science* 311, 587–594 (2007).

32. Djouani, F., Patel, B., Richaud, E., Fayolle, B. & Verdu, J. Antioxidants loss kinetics in polyethylene exposed to model ethanol based biofuels. *Fuel* (2011).

33. Djouani, F., Richaud, E., Fayolle, B. & Verdu, J. Modelling of thermal oxidation of phosphite stabilized polyethylene. *Polymer Degradation and Stability* 96, 1349–1360 (2011).

34. Scoponi, M., Cimmino, S. & Kaci, M. Photo-stabilisation mechanism under natural weathering and accelerated photo-oxidative conditions of LDPE films for agricultural applications. *Polymer* 41, 7969–7980 (2000).

35. Hussain, I. & Redhwi, H. H. Development of polypropylene-based ultraviolet-stabilized formulations for harsh environments. *Journal of materials engineering and performance* 11, 317–321 (2002).

36. Nuzzo, R. G., Dubois, L. H. & Allara, D. L. Fundamental studies of microscopic wetting on organic surfaces. 1. Formation and structural characterization of a self-consistent series of polyfunctional organic monolayers. *J. Am. Chem. Soc.* 112, 558–569 (1990).

CHAPTER 11

11 Effect of Surface Morphology on NA11 containing PP Electret Filters

Abstract

A study on the effects of surface morphology on electrostatic filtration properties of corona charged polypropylene (PP) electret filters is reported. To enhance electrostatic properties meltblown electret filters were initially modified with a commercial nucleating agent, NA11 (sodium 2,2'-methylene-bis(4,6-di-tertbutylphenyl)-phosphate). Then both neat and additive containing webs were heat treated to modify their surface crystallinity. Results showed that webs composed of fibers with high surface crystallinity exhibits more stable electrostatic filtration properties compared to that of having lower crystallinity. Attenuated Total Reflection-FTIR was used to measure surface cyrstallinity, whereas electrostatic filtration stability was analyzed after decaying samples at 80°C for 24h.

11.1 Introduction

Electret filters composed of charged/polarized fibers exhibit high filtration efficiency with low flow resistance. However their electrostatic properties may be lost somehow, which

may lead to intolerable drop in particle capture performance. Due to that reason there are still ongoing discussions on their reliability[1,2]. So far several studies were published either in academia or industry to improve their filtration performance and stability[3–10]. Various additives were found to be useful to improve electret properties of PP films[11–18]. For instance by adding nucleating agents smaller spherulites were observed in films whose boundaries are traps for space charges[12]. For the case of nonsoluble nucleating agents microvoids were observed upon stretching which prohibit charge migration [19]. On the other hand NA11 and some conventional nucleating agents do not dissolve in PP. Their electret characteristics were thought to be depending on formation of elongated voids which act as charge barriers against decay. Upon stretching effect of formed cavities becomes more dominant for NA11 containing films which resulted in longer stability[13,15].

On the other hand for the case of nonmetallized electrets as in charged fibers of electrostatic filters *surface* properties will be important due to their larger surface area/volume ratio compared to electret films. The penetration depth of charges through polymer thickness is dependent on polymer properties and charging conditions. Using thermally stimulated discharge current method Cresswell and Perlman[20] measured depth of penetration at most 5% of the 25.4 μm-thick corona charged Mylar films under 12kV/cm. According to Laser Induced Pressure Pulsed (LIPP) studies on irradiated 36 μm thick PP films, charge penetration depth was found to be strongly dependent on energy of electrons.

The depth of charges were found 1.5-2μm when electron energy was kept 10eV, whereas penetration through thickness was observed when electron energy increased to 50eV[21].

Surface properties will directly determine charged fiber interaction with surrounding environment. Air surrounding fibers carry significant amount of ionic species, particularly coming from humidity. Those ionic species will form a double layer, which consist of a fixed Stern layer and diffuse layer. In recent studies enlightening proofs were found that charge transfer during triboelectrification is dominated by ionic layer over near surface[22,23]. Not only acting on triboelectrification, ions on upper surface will be effective on charge transport. Field induced mobility of such counterions will give rise to surface conductivity, which increases total conductivity[24].

Due to exclusion during crystallization, upper surface is composed of lower molecular weight polymer chains. GPC analysis confirmed significant reduction in molecular weight when upper layers of PP films were dissolved in hot toluene[25]. In general after the same thermal and mechanical history lower molecular weight polyolefins would be expected to have higher order, however quite opposite would be found over fiber or film surfaces during high speed extrusion processes. Differences in thermal history, tendency to oxidative reactions and mechanical stresses will cause significant changes between surface and inner layers. Migration of defective structures to lower energy surface is one other factor to change crystal structure [26]. Looking at atomic scale the difference is also apparent from the aspect of coordination numbers. Say an atom in an FCC structure has 12 nearest neighbors, whereas it

will have fewer than 12 on the surface. And it is well known, systems form bonds maximally to lower their energy. So less number of bonds on the surface will give higher energy than bulk. Thus molecular mobility within amorphous region would be expected to be larger which will fasten discharge process. Also amorphous structure is open to decay via ions and volatile organic compounds which was proven experimentally using organic solvent vapour induced charge decay studies[27]. On the other hand amorphous region contains more impurities, oxidized species which leads to charge decay and oxidized species on surface lower hydrophobicity of the PP surface[28,29].

Due to mentioned reasons we investigated the effect of surface crystallinity on electrostatic filtration properties of the webs, rather than bulk properties. Samples were also modified with NA11 which is shown to be charge enhancing additive[11]. Surface crystallinity, which was modified via annealing under two different temperature regimes, were analyzed via Attenuated Total Reflectrion FTIR (ATR-FTIR) spectroscopy. Initial and isothermally decayed filtration properties of the corona charged samples were tested to compare electrostatic filtration stability.

11.2 Experimental

Materials and Melt Blown Web Production. Achieve 6936G1 propylene polymer resin with a melt flow rate of 1550 was kindly provided from ExxonMobil. NA11 was kindly

donated by BASF. To provide better uniformity, initially PP masterbatch pellet at 10%(w/w) additive concentration was prepared by Techmer PM (Clinton, TN). Then, masterbatch was re-extruded with pure resin to produce additive/PP composite webs with concentration of 0.01%, 0.1%, 1%(w/w). The chemical formula of NA11 was given in Figure 11.1.

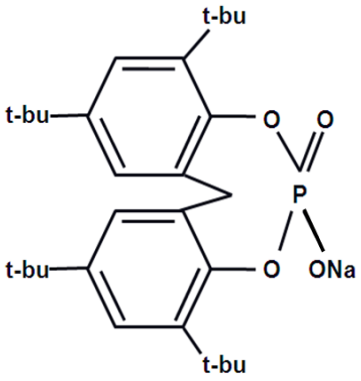

Figure 11.1 Chemistry of NA11

Small melt blowing line used in the web preparation had a 6-inches MB die which has 120 holes, each of which is 0.15mm in diameter (i.e ~ 25 holes/inch). Polymer pellets are melted and pressurized using a 1 1/4" C.W. Brabender extruder, mounted horizontally. The heating in the extruder involves four zone temperature controls. The die is manufactured by the Reifenhäuser Reicofil GmbH & Co. KG. The air plate angle is 60° with the air gap of 0.3

mm and the die tip is outset the die face by 1mm. The temperature profile is tabulated in Table 11.1.

Table 11.1 Temperature profile of MB process

	Z1	**Z2**	**Z3**	**Z4**	**Pump**
Temp. [°C]	190	220	230	250	248
	Transfer	**Turning**	**Die**	**Air Fed**	**Air measured**
Temp. [°C]	250	250	250	339	260-270

Meltblowing is not a specifically controllable process compared to melt spinning process. It means by changing process conditions such as die/air temperature, polymer throughput, air pressure, die-collector distance, belt velocity one can produce samples having different fiber diameter distributions and solidity[30-32]. Dominating melt blowing parameters, throughput value and air pressure were selected as 0.25ghm and 25psi respectively. Belt speed was changed according to desired basis weight, which is 20-25gm^{-2} per layer.

After meltblowing webs were heat treated for 12h under 70 and 110°C to enhance surface crystallinity.

Charging. Charging of the samples was carried out with a corona discharger (Mystic Marvels, Model NIP-7E). Applied voltage was fixed at 9 kV, thus an electric field of 3kV/cm was produced within 3cm charging distance.

Analysis of Filtration Properties. Filtration properties of webs were evaluated at a face velocity of 5.3 cm/sec. DOP (dioctyl phthalate) aerosols were generated by a collision type atomizer and then evaporated through a membrane dryer, which were selected monodisperse aerosols of 0.3 μm in a long differential mobility analyzer (DMA, TSI, Model 3081, MN, USA) and then neutralized by a Kr-85 radioactive source. The neutralized DOP aerosols were feed into a filter holder with 25.81 cm^2 of effective area and measured their number concentrations at upstream and downstream positions by using two condensation particle counters (CPCs, TSI, Model 3760A, MN, USA). The flow rate and the resistance were measured by a mass flow meter (TSI, Model 4043, MN, USA) and an electronic manometer (TSI, Model 220, MN, USA). Since for the uncharged media maximum penetrated particle size is around 300nm, filters are tested in this range[33]. Due to unexpected changes in fiber diameter and solidity, normalization of filtration data is inevitable. This would be done simply comparing quality factor values which is negative natural logarithm of penetration of pressure drop ($QF=-\ln P/\Delta p$).

Surface Crystallinity Analysis. IR spectroscopy is a largely investigated, reliable method for understanding chemical composition of materials. When subjected to IR radiation, all molecules having inherent frequencies of vibrations will absorb radiations at specific wavelengths. Examination of the transmitted light gives how much energy was absorbed at each wavelength. In other words an IR beam at all wavelengths will be directed, but only one with the same frequency with molecular vibration will be absorbed and

detected. So it would be possible to identify structure[34]. Based on total internal reflection, ATR crystal produces an evanescent wave which extends radiation into the sample. Due to that reason for attenuated total reflection spectroscopy, IR will penetrate into sample partially. That is why for surface crystallinity analysis; ATR is preferred instead of transmission infrared (T-IR) spectroscopy. Penetration depth of infrared will be limited, which is described as the depth that the field of radiation decays to a definite value, ie intensity where it decays to 1/e th of incident[35]. Depth of the penetration of IR radiation depends on various factors such as wavelength of IR peak under consideration (λ), refractive indexes of sample (n_s) and ATR element (n_c) and incident angle (θ). According to the equation explained by Kortum[36], we found a penetration depth of approximately 0.33μm for our measurements. Deeper surface can be probed either at lower incidence angle or with a low refractive index crystal such as KRS-5 instead of diamond. Absorbance ratio at wavenumbers of 997 and 972 cm^{-1} is directly related with isotacticity and density of PP[24], which is a used for calculating crystallinity.

11.3 Results and Discussions

According to ATR analysis surface crystallinity values corresponding to uppermost surface (0.33μm) were measured. As seen in Figure 11.2 upon heat treatment surface crystallinity of the fibers increased 10-50%.

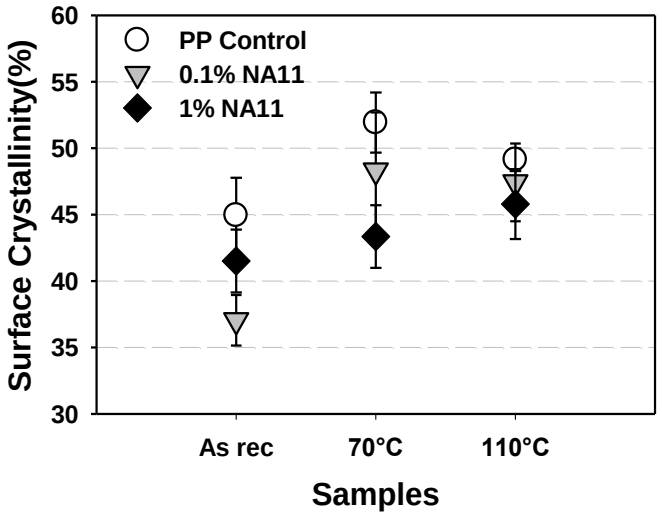

Figure 11.2 Surface crystallinity of as received and heat treated samples. Error bars for standard deviation over 3 measurements.

For the case of control and 0.1%NA11 containing webs heat treatment at 70°C resulted with higher surface order compared to ones treated at 110°C, whereas crystallinity for the 1%NA11/PP web increased continuously.

Upon heat treatment not only order of chains on the surface, but also chemical composition would be expected to be changed. Particularly impurities such as oxidized species and additives would migrate towards surface. Their presence was also analyzed from ATR studies. The value of carbonyl index was obtained from the ratio of the carbonyl peak ($1715cm^{-1}$) and a reference peak ($2722cm^{-1}$) [37–39]. On the other hand migration of NA11

towards surface was also calculated from the ratio of peaks at 1100cm^{-1} and 2720cm^{-1}. As shown in Figure 11.3 heat treatment at 110°C resulted with similar NA11 concentration on upper surface. On the other side carbonyl index increased for all heat treated samples other than 1%NA at 110°C. Interestingly relative change in chemical composition after heat treatment was found similar. Due to that reason filtration properties of untreated and 110°C heat treated samples were compared.

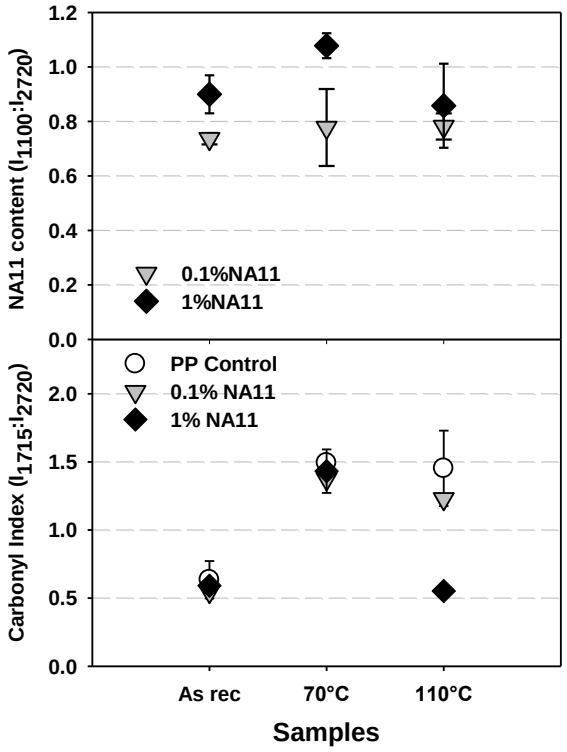

Figure 11.3 Carbonyl index and NA11 content on heat treated samples.

As shown in Figure 11.4 upon heat treatment, NA11 containing webs exhibited an increase in filtration efficiency, while there is a drop in control sample. However change in electrostatic filtration properties were not substantial.

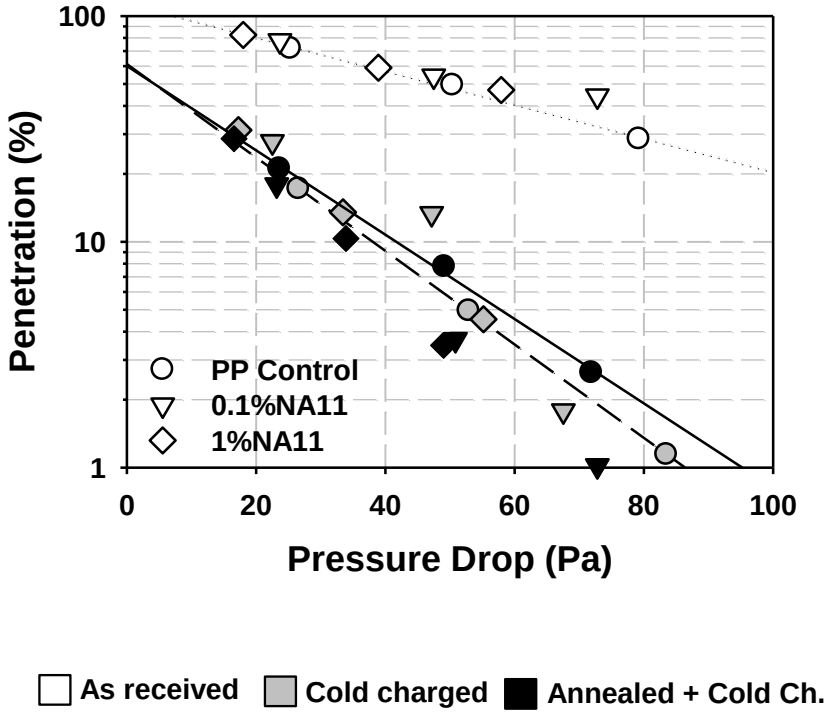

Figure 11.4 Filtration properties of as received, cold charged, heat treated+cold charged samples. Linear regression lines corresponds PP control sample for ease of tracking.

Since there are differences in basic web properties such as fiber diameter, solidity, inevitable differences were observed in filtration properties. Due to that reason samples were compared according to quality factor values. As shown in Figure 11.5 the drop in quality factors (upon heat treatment at 80°C for 24h) of heat treated samples are not as high as untreated samples. For reference sample and 0.1%NA11 containing webs lower surface crystallinity resulted with worse charge stability. For the case of 1% NA11/PP webs the drop is high but also initial quality factor is high and even after decay for 24h at 80°C filtration efficiency is still same with initial efficiency of the only cold charged web.

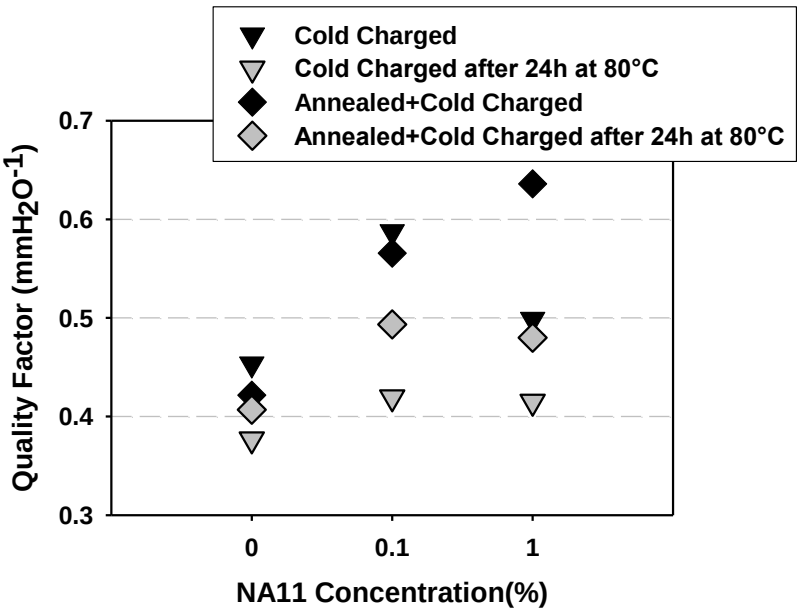

Figure 11.5 Drop in quality factors and change in surface crystallinty of heat treated NA11 containing samples

For the case of reference and 0.1%NA11/PP sample heat treatment reduced drop in quality factor, whereas more than filtration stability. As shown in Figure 11.6 higher surface crystallinity led more stable filtration efficiency for reference and 0.1%NA11 containing web. This is an interesting result since we were expecting higher drop in quality factor due to high carbonyl index for this samples. On the other hand exhibiting a similar carbonyl index drop in quality factor for heat treated 1%NA11 containing web was found higher.

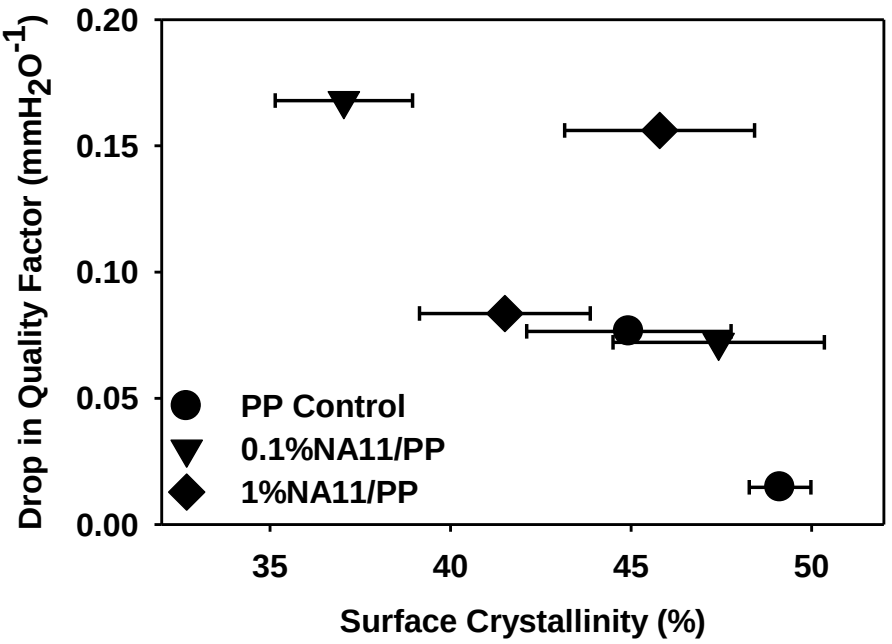

Figure 11.6 Surface crystallinity vs drop in quality factor. Error bars for measurement of 3 points.

11.4 Conclusions

In this study we showed heat treatment enhances electrostatic filtration properties, ie either its initial efficiency or stability. Enhanced surface crystallinity upon heat treatment would affect filtration stability for unmodified samples. Nucleating agent addition gave rise to filtration efficiency, even much more increase was observed upon heat treatment. Interestingly increase in carbonyl index upon heat treatment did not resulted with faster charge decay, which would be more dominant effect of surface morphology. Blooming of nucleating agents was not so significant.

11.5 References

[1] M. Lehtimäki and K. Heinonen, "Reliability of electret filters," *Building and Environment*, vol. 29, no. 3, pp. 353–355, Jul. 1994.

[2] P. C. Raynor and S. J. Chae, "The long-term performance of electrically charged filters in a ventilation system," *Journal of occupational and environmental hygiene*, vol. 1, no. 7, pp. 463–471, 2004.

[3] D. L. Myers and B. D. Arnold, "Electret media for HVAC filtration applications," *INJ Winter*, pp. 43–54, 2003.

[4] J. C. Kim, Y. Otani, D. Noto, N. Namiki, and K. Kimura, “Initial collection performance of resin wool filters and estimation of charge density,” *Aerosol science and technology*, vol. 39, no. 6, pp. 501–508, 2005.

[5] R. C. Brown and R. C. Brown, *Air filtration*. Pergamon Press, 1993.

[6] A. D. Rousseau, M. E. Jones, and B. Z. Mei, “Method of making electret articles and filters with increased oily mist ...,” U.S. Patent 606879930-May-2000.

[7] P. D. Eitzman, A. D. Rousseau, M. E. Jones, and S. A. Angadjivand, *Method of making a fibrous electret web using a nonaqueous polar liquid*. Google Patents, 2002.

[8] J. Dahringer, E. A. Albers, W. Groh, and A. Heyer, *Non-wovens of electret fiber mixtures having an improved charge stability*. Google Patents, 1998.

[9] P. T. . Klaase and J. Van Turnhout, *Method for manufacturing an electret filter medium*. Google Patents, 1986.

[10] J. Van Turnhout, J. W. C. Adamse, and W. J. Hoeneveld, “Electret filters for high-efficiency air cleaning,” *Journal of Electrostatics*, vol. 8, no. 4, pp. 369–379, 1980.

[11] N. Behrendt, V. Altstadt, H. W. Schmidt, X. Zhang, and G. M. Sessler, “Development of porous polypropylene blends with NA11 particles and glass hollow spheres by biaxial stretching for electret applications,” *Dielectrics and Electrical Insulation, IEEE Transactions on*, vol. 13, no. 5, pp. 992–1000, 2006.

[12] N. Mohmeyer, N. Behrendt, X. Zhang, P. Smith, V. Altstadt, G. M. Sessler, and H. W. Schmidt, “Additives to improve the electret properties of isotactic polypropylene,” *Polymer*, vol. 48, no. 6, pp. 1612–1619, 2007.

[13] J. Hillenbrand, N. Behrendt, N. Mohmeyer, V. Altstadt, H. W. Schmidt, and G. M. Sessler, “Charge retention in biaxially-oriented polypropylene films containing various additives,” in *Electrets, 2005. ISE-12. 2005 12th International Symposium on*, 2005, pp. 276–279.

[14] N. Behrendt, N. Mohmeyer, J. Hillenbrand, M. Klaiber, X. Zhang, G. M. Sessler, H. W. Schmidt, and V. Altst\ädt, “Charge storage behavior of isotropic and biaxially-oriented polypropylene films containing α-and β-nucleating agents,” *Journal of applied polymer science*, vol. 99, no. 3, pp. 650–658, 2006.

[15] J. Hillenbrand, N. Behrendt, V. Altst\ädt, H. W. Schmidt, and G. M. Sessler, “Electret properties of biaxially stretched polypropylene films containing various additives,” *Journal of Physics D: Applied Physics*, vol. 39, p. 535, 2006.

[16] N. Mohmeyer, H. W. Schmidt, P. M. Kristiansen, and V. Altst\ädt, “Influence of chemical structure and solubility of bisamide additives on the nucleation of isotactic polypropylene and the improvement of its charge storage properties,” *Macromolecules*, vol. 39, no. 17, pp. 5760–5767, 2006.

[17] N. Mohmeyer, B. Müller, N. Behrendt, J. Hillenbrand, M. Klaiber, X. Zhang, P. Smith, V. Altstädt, G. M. Sessler, and H.-W. Schmidt, "Nucleation of isotactic polypropylene by triphenylamine-based trisamide derivatives and their influence on charge-storage properties," *Polymer*, vol. 45, no. 19, pp. 6655–6663, Sep. 2004.

[18] D. Erhard, D. Lovera, C. von Salis-Soglio, R. Giesa, V. Altst\ädt, and H. W. Schmidt, "Recent Advances in the Improvement of Polymer Electret Films," *[Without Title]*, pp. 1–53, 2010.

[19] N. Behrendt, N. Mohmeyer, J. Hillenbrand, M. Klaiber, X. Zhang, G. M. Sessler, H.-W. Schmidt, and V. Altstädt, "Charge storage behavior of isotropic and biaxially-oriented polypropylene films containing alpha- and beta-nucleating agents," *Journal of Applied Polymer Science*, vol. 99, no. 3, pp. 650–658, 2006.

[20] R. A. Creswell, "Thermal Currents from Corona Charged Mylar," *J. Appl. Phys.*, vol. 41, no. 6, p. 2365, 1970.

[21] L. Tingji and G. M. Sessler, "An experimental study of charge distributions in electron-beam irradiated polypropylene films," *Electrical Insulation, IEEE Transactions on*, vol. 26, no. 2, pp. 228–235, 1991.

[22] A. F. Diaz and R. M. Felix-Navarro, "A semi-quantitative tribo-electric series for polymeric materials: the influence of chemical structure and properties," *Journal of Electrostatics*, vol. 62, no. 4, pp. 277–290, Nov. 2004.

[23] L. S. McCarty and G. M. Whitesides, “Electrostatic charging due to separation of ions at interfaces: Contact electrification of ionic electrets,” *Angewandte Chemie International Edition*, vol. 47, no. 12, pp. 2188–2207, 2008.

[24] R. Pethig, “Review Article—Dielectrophoresis: Status of the theory, technology, and applications,” *Biomicrofluidics*, vol. 4, p. 022811, 2010.

[25] T. Umemura, K. Akiyama, and D. Couderc, “Morphology and electrical properties of biaxially-oriented polypropylene films,” *Electrical Insulation, IEEE Transactions on*, no. 2, pp. 137–144, 1986.

[26] N. Kawamoto, H. Mori, K. Nitta, S. Sasaki, N. Yui, and M. Terano, “Microstructural characterization of polypropene surfaces using grazing incidence X-ray diffraction,” *Macromolecular Chemistry and Physics*, vol. 199, no. 2, pp. 261–266, 1998.

[27] Y. Arita, S. Sha Shiratori, and K. Ikezaki, “A method for detection and visualization of charge trapping sites in amorphous parts in crystalline polymers* 1,” *Journal of Electrostatics*, vol. 57, no. 3–4, pp. 263–271, 2003.

[28] M. Strobel, C. Dunatov, J. M. Strobel, C. S. Lyons, S. J. Perron, and M. C. Morgen, “Low-molecular-weight materials on corona-treated polypropylene,” *Journal of adhesion science and technology*, vol. 3, no. 1, pp. 321–335, 1989.

[29] M. Strobel, V. Jones, C. S. Lyons, M. Ulsh, M. J. Kushner, R. Dorai, and M. C. Branch, "A Comparison of Corona-Treated and Flame-Treated Polypropylene Films," *Plasmas and Polymers*, vol. 8, no. 1, pp. 61–95, Mar. 2003.

[30] X. Wang and Q. Ke, "Experimental investigation of adhesive meltblown web production using accessory air," *Polym. Eng. Sci.*, vol. 46, no. 1, pp. 1–7, Jan. 2006.

[31] R. L. Shambaugh, "A macroscopic view of the melt-blowing process for producing microfibers," *Industrial & Engineering Chemistry Research*, vol. 27, no. 12, pp. 2363–2372, Dec. 1988.

[32] M. W. Milligan, F. Lu, R. R. Buntin, and L. C. Wadsworth, "The use of crossflow to improve nonwoven melt-blown fibers," *J. Appl. Polym. Sci.*, vol. 44, no. 2, pp. 279–288, Jan. 1992.

[33] L. Golanski, A. Guiot, F. Rouillon, J. Pocachard, and F. Tardif, "Experimental evaluation of personal protection devices against graphite nanoaerosols: fibrous filter media, masks, protective clothing, and gloves," *Human & experimental toxicology*, vol. 28, no. 6–7, pp. 353–359, 2009.

[34] B. H. Stuart, *Infrared spectroscopy: fundamentals and applications*. John Wiley and Sons, 2004.

[35] J. P. Hobbs, C. S. P. Sung, K. Krishnan, and S. Hill, "Characterization of surface structure and orientation in polypropylene and poly(ethylene terephthalate) films by

modified attenuated total reflection IR dichroism studies," *Macromolecules*, vol. 16, no. 2, pp. 193–199, Feb. 1983.

[36] G. Kortum and G. Korta1/4m, *Reflectance Spectroscopy: Principles, Methods, Applications*. Springer, 1969.

[37] J. F. Li, R. Yang, and J. Yu, "Natural Photo-Oxidation Degradation of Polypropylene Containing Nucleating Agent," *Advanced Materials Research*, vol. 26–28, pp. 1075–1078, 2007.

[38] J. Guisandez, P. Tiemblo, and J. M. Gomez-Elvira, "Change of thermal and dynamic-mechanical behaviour of a metallocene isotactic polypropylene during low-temperature thermo-oxidation," *Polymer degradation and stability*, vol. 87, no. 3, pp. 543–553, 2005.

[39] A. R. Horrocks, J. Mwila, M. Miraftab, M. Liu, and S. S. Chohan, "The influence of carbon black on properties of orientated polypropylene 2. Thermal and photodegradation," *Polymer Degradation and Stability*, vol. 65, no. 1, pp. 25–36, 1999.

CHAPTER 12

12 Overall Conclusions

- Despite being one of the oldest observations of scientists electrostatic charging is still a fascinating phenomena that still needs to be enlightened[1]. Dealing with atomic, subatomic charge carriers and their interaction with a surface of a few hundred nanometers thickness[2,3]; the difficulties are still referred to sensitive measurement instruments for either charge analysis and surface characterization. Surface potential decay method was explained for analyzing electrostatic properties of fibrous samples. Sample thickness, isotropy, cleanliness, fixed positioning are important factors that change the measured value. Without fixing such parameters, measured value would be misleading with a high deviation.
- A significant increase in charge stability upon charging 1min was obtained for barium titanate and maleic anhydride containing PP filaments. It was shown longer charging times are not proper for charge retention probably due to oxidation of filament surface.
- Charging at 130°C -which is also known as Curie temperature- resulted in the highest initial potential and longest stability for $BaTiO_3$/PP filaments and webs. The effect of $BaTiO_3$ was apparent for concentrations above 1%.

- DMDBS and NA11 did not contribute to cold charging efficiency of fibers. Interestingly thermal charging improved electret properties significantly as observed in $BaTiO_3$/PP samples. Other than factors such as softening of the polymer, improved corona conditions the enhancement was found to be due to additional orientational polarization of additive which was tested via dielectric spectroscopy.
- Antioxidants enhanced electrostatic and electrostatic filtration properties when cold charged, whereas thermal charging did not lead to same results. Blooming of additives during thermal charging is thought to be reason for changes in surface chemistry, which is coupled with low filtration efficiency and stability.
- Heat treatment enhances electrostatic filtration properties, ie either its initial efficiency or stability. Enhanced surface crystallinity upon heat treatment would affect filtration stability for unmodified samples. Nucleating agent addition gave rise to filtration efficiency, even much more increase was observed upon heat treatment.

CHAPTER 13

13 Suggested Future Works

- As indicated in Chapter 4, 9 and 10 properties of additives should be considered before deciding charging method. In general corona discharge is based on gas (plasma)-solid interactions, whereas hydrocharging is on liquid-solid interactions and carding, needlepunching are on solid-solid interactions. The charging method and polymer properties should be investigated simultaneously.
    - For instance, when PP -a nonpolar polymer- is modified with polarizable additives, it requires to be charged with a mechanism that can produce both polarization and charge enhancing. Due to limitations coming from molecular mobility, thermal corona discharge is preferable for the case of $BaTiO_3$ and nucleating agents. There are several highly polarizable additives that would show similar even better tendency. For instance Rochelle salt having a very low Curie temperature[1] would be proper even charging at room temperature.
    - As a second example antioxidant containing webs did not exhibit tremendous increase in filtration properties upon corona discharge. In a recent patent[2], their electrophilic characteristic was utilized for producing high zeta potential in a special solution. Webs containing such additives would rather be charged via liquid contact based method. Hydroentanglement procedure which is

mostly used for bonding nonwoven webs would be proper for producing contact mechanism.

- Models explaining the phenomena are still lack of simulating real matter due to complexity of the systems from the aspect of electrostatic charging. However recent works dealing with electrochemical interactions[75,355] are encouraging to understand the behavior of the matter. Based on such electrochemical properties of the surfaces, filter media would be modified using required additive and even novel charging methods would be proposed[2].
- Even though there is a large patent and academic literature in charge enhancing additives, polymer blends were considered in a few studies[121]. For the case of interfacial polarization and triboelectrification, polymer blends with relatively low miscibility would work effectively.
- Novel polymers with ionic character would also be useful to enhance electrostatic performance. Ionic groups are generally incorporated during polymerization process. Such polymers would be blended with nonpolar polymer, thus web would be charged just after extrusion.
- Due to scope of the project basic web properties were not investigated widely. Electrostatic filtration is a surface dependent process. Other than additives web solidity and fiber diameter affect the electrostatic filtration properties. Since capture

of particles is dependent on the time they spend within filter media, optimized conditions should be determined for any particle velocity.

13.1 References

1. Mueller, H. Properties of Rochelle salt. *Physical Review* **57**, 829 (1940).
2. Sebastian, J. M. *et al. Method of making electret articles based on zeta potential*. (Google Patents: 2010).
3. Liu, C. & Bard, A. J. Nature Materials. *Vol* **7**, 505 (2011).
4. McCarty, L. S. & Whitesides, G. M. Electrostatic Charging Due to Separation of Ions at Interfaces: Contact Electrification of Ionic Electrets. *Angewandte Chemie International Edition* **47**, 2188–2207 (2008).
5. Erhard, D. *et al.* Recent Advances in the Improvement of Polymer Electret Films. *[Without Title]* 1–53 (2010).

APPENDIX1

14 Measuring Electrostatic Properties of Fibrous Materials: A Review and a Modified Surface Potential Decay Technique

Abstract

A reliable, simple surface potential measurement method for fibrous materials was reported. Large variations in potential measurements were found to be mostly due to structural nonuniformity such as packing density, thickness and fiber-fiber proximity. Particularly thermal responses during isothermal decay test were eliminated by fixing fibers bidirectionally. It also includes reviews of different measurement techniques reported in the literature.

14.1 Introduction

Charge retention is one of the oldest observed characteristics of insulators which can be needed or unintentionally occurs during use. Due to low conductivity charged or polarized state is so stable that sometimes it takes several years for them to neutralize. To make this quasipermanent property useful as in electrets, one needs to understand its nature and be able to measure it quantitatively. In this study we focused on measurement methods of long term electrostatic properties of fibrous materials, which are different from films. In the literature

methods for measuring charging properties of electret films were directly applied into fibrous samples [1–8], however direct measurement on fibrous electret samples will be improper due to porous, anisotropic structure. In the first stage previous methods were reviewed whereas in the experimental part corona charged polypropylene (PP) filaments were tested via isothermal surface potential decay test.

14.2 Literature Review

Methods for measuring charge storage characteristics of fibrous materials can be divided as direct and indirect methods. Direct methods can be either measurement of stimulated discharge currents upon heating or potential difference between a capacitive probe and sample surface. On the other hand indirect methods such as derivation from electrostatic filtration analyses are advantageous from some aspects.

14.2.1 Direct methods

Thermally stimulated discharge current (TSDC)[1–3], electrostatic force microscopy (EFM) [9] and non-contact electrostatic voltmeters for surface potential decay measurement [4,7,8,10] are direct methods for measuring electrostatic characteristics. Undoubtedly data obtained from each have some meaning, however as explained later some necessary modifications should be done and results should be analyzed carefully for fibrous materials.

14.2.1.1 Thermally Stimulated Discharge Current (TSDC)

TSDC is a widely investigated method to obtain information about the charge storage mechanism and its depth distribution. Charge accumulation or depolarization is measured with a sensitive ampermeter upon heating the electret at a constant rate. A schematic that illustrates open circuit TSDC mechanism was shown in Figure 14.1.

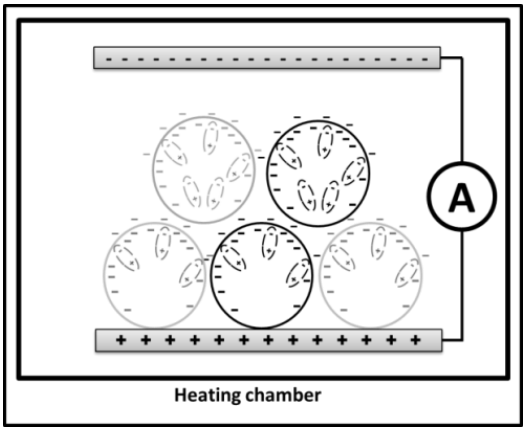

Figure 14.1 Measurement of TSDC for charged fibrous samples (open circuit condition) [adapted from[11]]

The position and size of the current signals is directly related to intrinsic relaxation temperatures, such as glass transition, β, or γ relaxations [16] TSDC is a comprehensive method, not only reveals charge storage properties and relaxation time but also gives idea about other physical properties such as activation energy and trap structure of materials [12].

Activation energy of the trap levels indicates the stability of charges which can be determined using Grossweiner equation [13].

$$E_t = \frac{1.51kT_mT'}{T_m - T'} \qquad \text{Equation 14.1}$$

where T_m is peak temperature, k Boltzmann constant, T' the temperature at which the low temperature side of discharge curve attains one half of its maximum height.

TSC results are informative long term bulk properties for metallized or somehow isolated electrets, however for filtration or any other long term investigation, other than bulk the fibrous sample will also be open to decay via bombardment of air ions and surface conductivity [14]. On the other hand position and height of the TSD peak due to space charge motions will depend on electrode material, because charge injection or charge neutralization at metal-polymer interface will be different depending on the work function of electrode material [15]. For fibrous samples such interfaces will involve not only larger metal-fiber interface but also fiber-fiber interfaces. Baba and Ikezaki[16] criticized the early literature due to significant differences between measured peak temperatures for negatively charged PP films. Controversies with other literature were conducted to the type of metal electrode interface which is formed at high temperatures after vacuum evaporation onto polymer samples. Kravtsov et al[5] filled the gap between the sample surface and the measuring electrode using a 100μm thick PTFE spacer, but did not mention the effect of this

arrangement. On the other hand same group reported enlightening results from the open circuit discharge analysis of charged PP filaments [6] . Three peaks were obtained from TSDC test. The first peak, obtained at a low-temperature (T_{max}=50-60°C), was conducted to the Maxwell-Wagner polarization in which, charge carriers are localized at interfacial trapping sites. The medium-temperature peak between 110 and 120°C is attributed, to the release of both inherent and injected charge carriers and dipole polarization. The highest-temperature TSC peaks (T_{max} = 170-175°C) which is very close to the melting temperature was thought to be due to release of the injected charges upon melting of polypropylene.

In summary TSDC can be a reliable method, however the information is mostly explanatory for bulk properties and one needs to be careful for the noise due to interfaces. Particularly fiber-fiber interface would affect outcome of measurement, since charged fiber can show bipolarity around periphery. Other than thermal stimulation laser induced pressure pulses (LIPP) [17,18] and pulsed electroacoustic waves [19,20] were used to stimulate and analyze charge traps within films. A charge map through depth of the specimen can be drawn using these methods, however according to our knowledge neither of them was applied on fibrous materials so far.

14.2.1.2 Electrostatic Force Microscopy (EFM)

Kim et al[9] used scanning probe microscopy on single charged fibers. Electrostatic force microscopy with a specialized probe was used to measure potential values from theoretically atomic scale fiber area. Thus due to nature of the system the data obtained from scanning microscopy will be particular on a very small region, which requires long testing time for applying in electret filters with a reliable statistical validity. Also method is not informative on charge stability. On the other hand circular geometry of the filaments will disturb the measured potential value, since electric force is inversely proportional to the square of the distance [9].

14.2.1.3 Electrostatic Voltmeters for Surface Potential Decay Measurement

In some other literature non-contact surface potential measurement via electrostatic voltmeter was preferred over direct charge measurement techniques [4,7,8,10,21,22]. The probe at a distance of 1-10mm from sample surface is set to the potential of the charged surface according to the vibrating capacitance principle. A simple drawing of electrostatic voltmeter was given in Figure Figure 14.2[23].

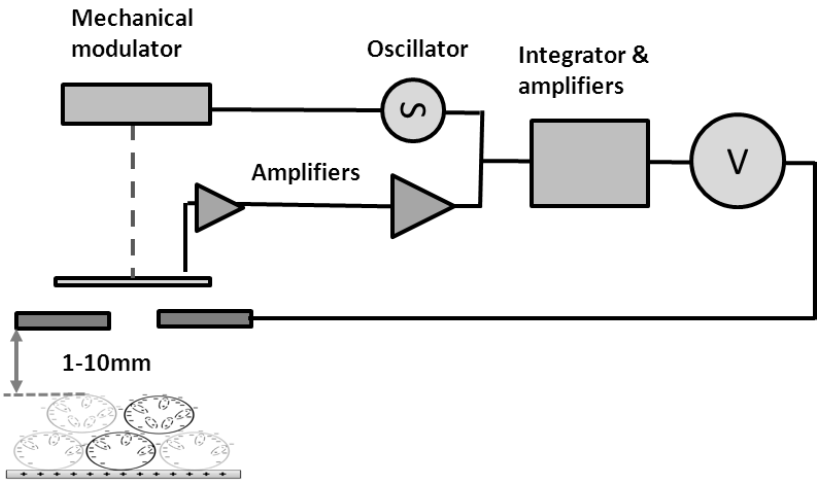

Figure 14.2 Simple schematic drawing of electrostatic voltmeter (adapted from [23])

Complete dissipation of charges or depolarization of the polymer electrets sometimes takes several years. However the decay rate may be boosted at elevated temperatures to perform faster analysis. This accelerated test is called isothermal surface potential decay test (ISPD). Generally initial discharge occurs faster, which is in agreement with Kravtsov's finding[1] of loss of Maxwell-Wagner polarization at low temperatures. This leads to exponential decay curves. For those of the exponential decay curves relaxation times which correspond to a remaining potential of 1/e th of initial potential would be calculated to interpret charge stability (Figure 14.3).

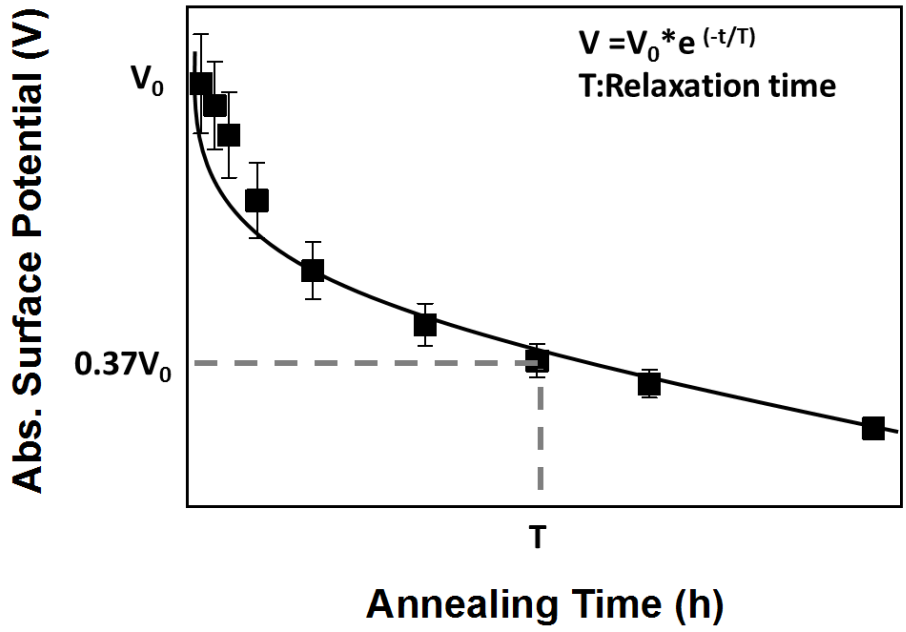

Figure 14.3 Isothermal surface potential decay curve at elevated temperatures [Real data from charged PP filaments]

When compared to nonisothermal TSDC, isothermal potential decay test is time consuming [12], but nondestructive at least for fibrous structure. So far isothermal surface potential decay was applied by many researchers both for film and fibrous electrets. This will be discussed in experimental part deeply since the proposed method in our study is also based on isothermal surface potential decay technique.

14.2.2 Indirect Methods

Indirect methods were derived from the response of charged material to energetic radiation or aerosol particles of known charge density. An early work was reported by Baumgartner[24] who studied on individual fiber through which particles of known charge density and size were sent. The trajectories of particles were recorded with a high speed camera. This method was thought to be improper due to sensitive experimentation and being difficult to apply for 2-D split fibers [25].

Brown utilized X-ray radiation to discharge electret filters. X-rays produced bipolar ions which was attracted to fibers and discharged them. Penetration was measured after exposing webs for particular timings. Total dose of radiation which decayed the filters was found to be correlated with electrostatic capture performance of filter [26]. Romay et al[27] criticized this method since the recombination of bipolar ions in a filter is inevitable, which results in an overestimated charge density prediction. Instead they developed a method based on neutralization of electrical charge with bipolar ions generated by Alpha-ray irradiation from Po-210 (A rare and highly radioactive element with no stable isotopes). In this system recombination might have been problem during ion generation, however it was stated that recombination was negligible at a saturation level. From gradual discharge after exposing filters to alpha radiation for specific time slots, filtration efficiency was calculated [27]. Those of the methods are mostly informative on initial charge density of the samples. However decay conditions should be more realistic and practical to apply into real world. In another

study Kim et al[28] applied a modified version of the Brown's filtration model on the experimental filtration results that were taken from resin wool filter. From the measured initial filtration efficiency charge density in single fiber was estimated. Quite correlated results were obtained [29]. However the measured charge density will depend on the accuracy of the theoretical models which were not proved completely. On the other hand such models to predict charge density will be advantageous since particle capture efficiency will be independent from the sign of polarity of constituent fibers.

In summary both direct and indirect methods have unique advantages. Nondestructive potential measurement would be preferred for comparative studies if exact charge density is not intended to be analyzed as in TSC. Using special tips electrostatic probe microscopy would be used to investigate atomic scale interaction between fibers and particles. Direct methods still seems to be insufficient to analyze webs composed of bipolar charges, which can be analyzed via aerosol filtration test.

14.3 Experimental

14.3.1 Material

PP resin of 34 MFR value (melt flow rate for 10 min at 230°C) was kindly provided from Sunoco Chemicals. PP resin had a number average molecular weight of ~55,000g/mole, whereas weight average molecular weight is ~180,000g/mole. Samples were melt-spun in the

Hills multifilament spinning line in the Nonwovens Institute (single- screw extruder with L: D ratio 1:24, the number of holes in spinhead is 72) in which the spinning speed was 2000 m/min and the throughput was 0.58 g/h/min. Temperature of spin head was fixed at 235°C. Resultant yarns were composed of 72 filaments having diameters of 20μm.

14.3.2 Corona Discharge

Corona discharge occurs when a sufficiently high potential difference exists between electrodes having asymmetric shapes such as a fine wire or point and a surface. Because of the high electric field near the emitting electrode, the air which is normally an insulator becomes ionized. The ions are driven towards the low electric field electrode[30]. Using corona, the surface can be charged in a controlled manner [31]. Charging of the samples was carried out with a negative corona discharger (Mystic Marvels, Model NIP-7E) and the applied voltage was fixed at 9kV where maximum output direct current of the emitter needle was about 160 μA. Charging was done for 1min from a distance of 2cm under laboratory conditions in which relative humidity was kept fixed between 54-58% RH at 22-23°C temperature.

14.3.3 Electrostatic Voltmeter

Monroe 244 Electrostatic voltmeter was utilized to measure surface potential. The instrument is capable of measuring voltage in the range of ±3kV at a temperature range of -50-80°C. Probe has sizes of 9mm x 9mm x 72mm. It enables to take responses lower than 3-4ms.

14.3.4 Sample Preparation for ISPD Test

Multifilament samples were washed with deionized water at 45°C for 6 h to remove impurities and spinfinish applied during melt spinning process. The washing fluid was replaced every 2h. Use of any detergent or surface active was not preferred; since samples might be contaminated with those chemicals even after rinsing. Yarns wounded on washing tubes were dried overnight. After drying they were aligned parallel on aluminum sample holders with a given spacing (10 yarns/cm) as shown in Figure 14.4. It was observed that any fiber protruding from specimen caused significant variations on measured value, so to fix protruding fibers perpendicular yarns were aligned at a distance of 0.7cm from each other. The filaments were fixed carefully by using conductive tape and epoxy to prevent errors that can occur due to position changes during charging and decay tests. *Three trials at three different days* were conducted. Three samples were tested at each trials and average values and standard deviations were calculated thereof. 15 specific points across the sample surface

were used for evaluation. The initial measurements (V_0) were taken directly after charging. All following measurements for surface potential decay test were carried out after fixed annealing times at 80°C. The periods in the oven were 0.5h, 1h, 2h, 4h, 8h, 12h, 16h, and 24h. Due to the nature of decay, periods kept shorter initially. Samples after annealing were cooled for 10 minutes in a desiccator to prohibit the effect of moisture in atmosphere.

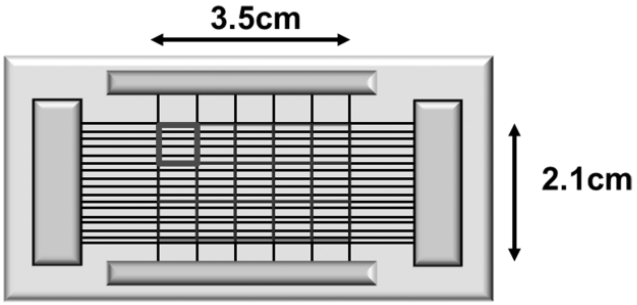

Figure 14.4 Specimen for ISPD test and surface potential detection points

14.4 Results and Discussion

14.4.1 Results

In the initial studies it was noticed that the high variation in observed potential values were due to structural nonuniformity. in x, y, z direction. Since largely used in aerosol filter media initially we aligned yarns randomly as in nonwoven fabrics. A significant variation was observed after random alignment (Figure 5). When yarns were aligned at a spacing of

10fiber/cm, still we observed a high standard deviation. Due to difficulties during preparation of samples using rubber gloves, we saw some of the fibers were protruding in z-direction, which changes measured potential enormously. This was also mentioned in a theoretical study by Horenstein[32]. Due to that reason in the initial studies it was noticed that the high variation in observed potential values were due to structural nonuniformity.

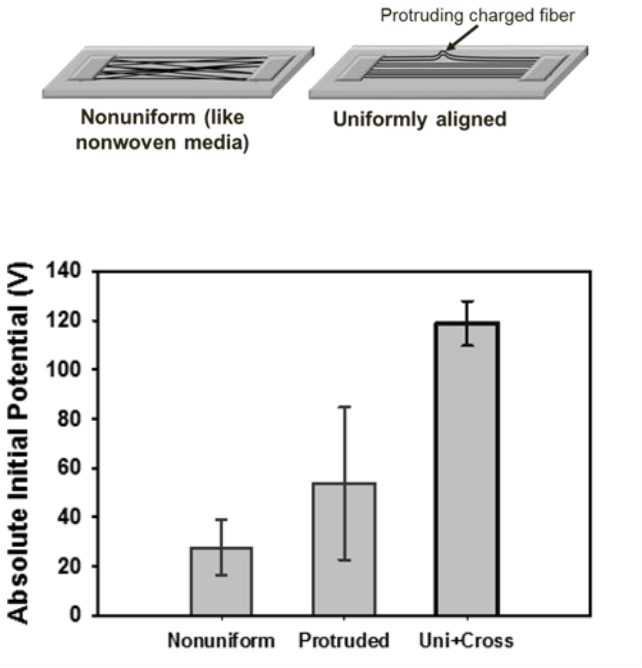

Figure 14.5 Surface potential measurements after various fiber alignments

Those of the large variations were reduced using constant fiber diameter, yarn density and uniform fiber distribution and sample thickness. Because of that reason yarns of definite thickness and density were preferred rather than highly anisotropic nonwovens. As seen in Figure 14.6 even all 9 samples tested in three different days have close decay curves besides initial potential. We think that small variations in fiber density in inspected area, temperature and humidity would be the reason behind negligible differences in initial potentials.

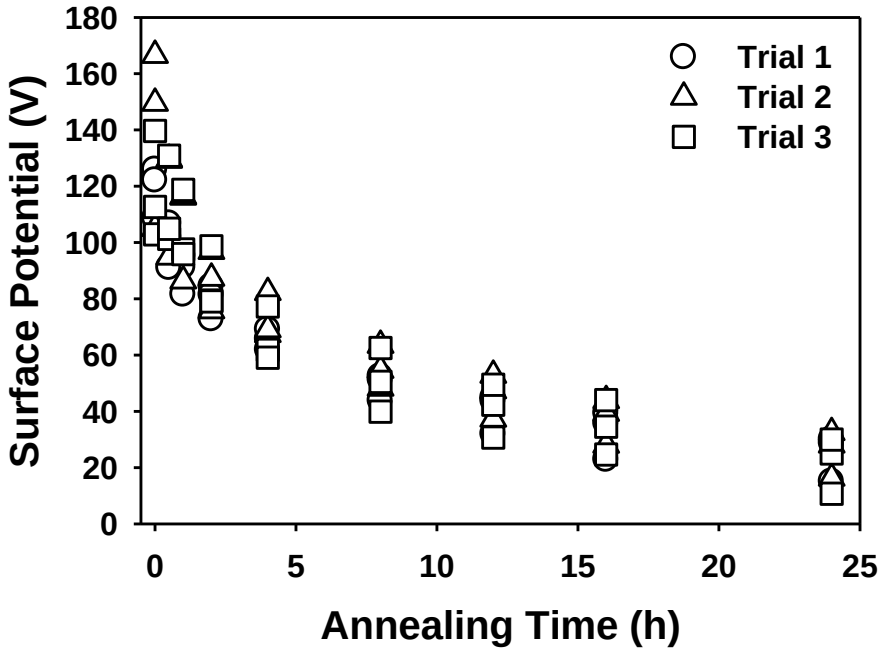

Figure 14.6 Surface potential decay of all 9 samples at 80°C

Figure 14.7 shows the results after taking averages of the three samples that were charged in the same day. After decay of 4 hours variation between samples drops below 10%, which indicates repeatable results were taken from the aspect of charge stability.

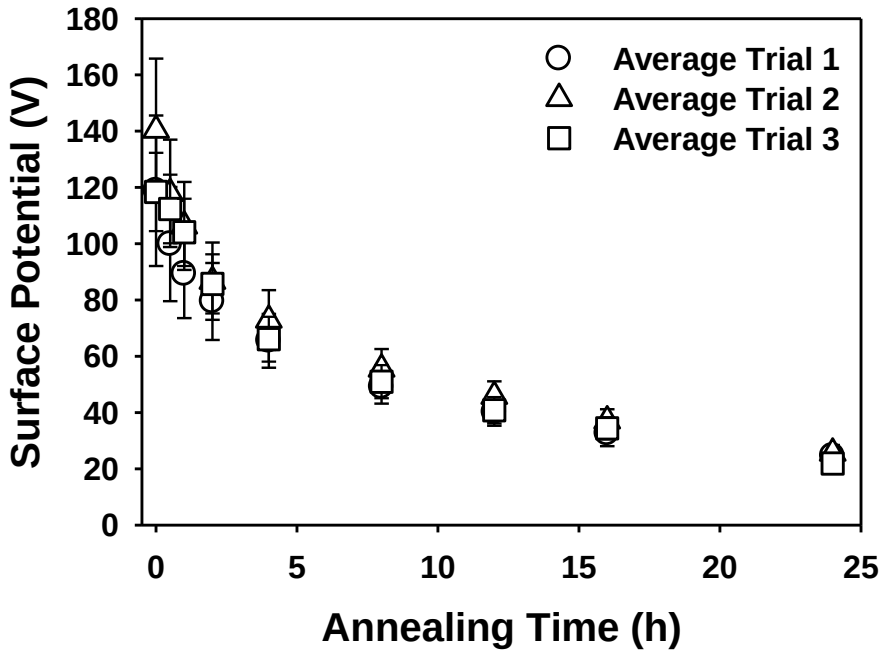

Figure 14.7 Average surface potentials of the samples that were charged on the same day

Figure 14.8 summarizes the relaxation times calculated from the averages of each sample and their initial potential values. It was found that at 80°C approximately 12h was needed to reduce the charge density into 1/e th of the initial. At the end of 24h remaining

potential was about the 20% of the initial value. The error bars indicate the variation within the specimen which comes from the nonuniformity of the corona current density as explained elsewhere [31].

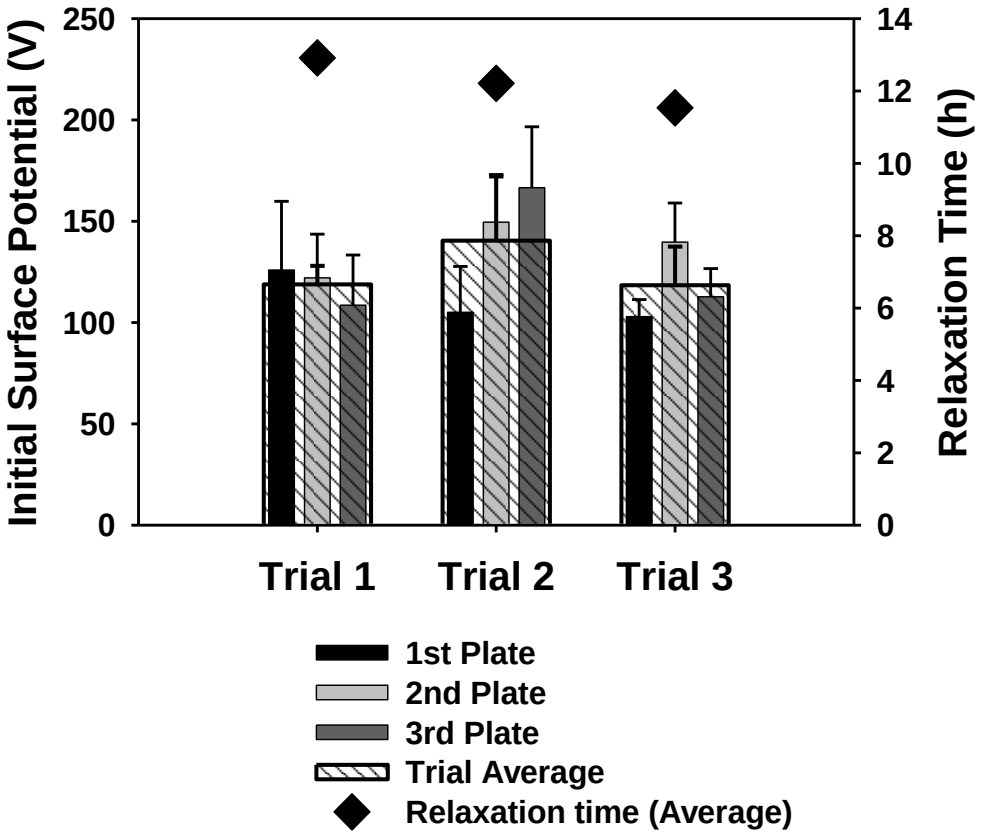

Figure 14.8 Initial potentials and calculated relaxation times of the samples

To understand the meaning of relaxation time, decay test was also applied at different temperatures, including room temperature. The temperature range was kept significantly lower than melting point of PP. Normalized curves upon decay at room temperature, 50°C, 80°C and 110°C shown in Figure 14.9 were obtained.

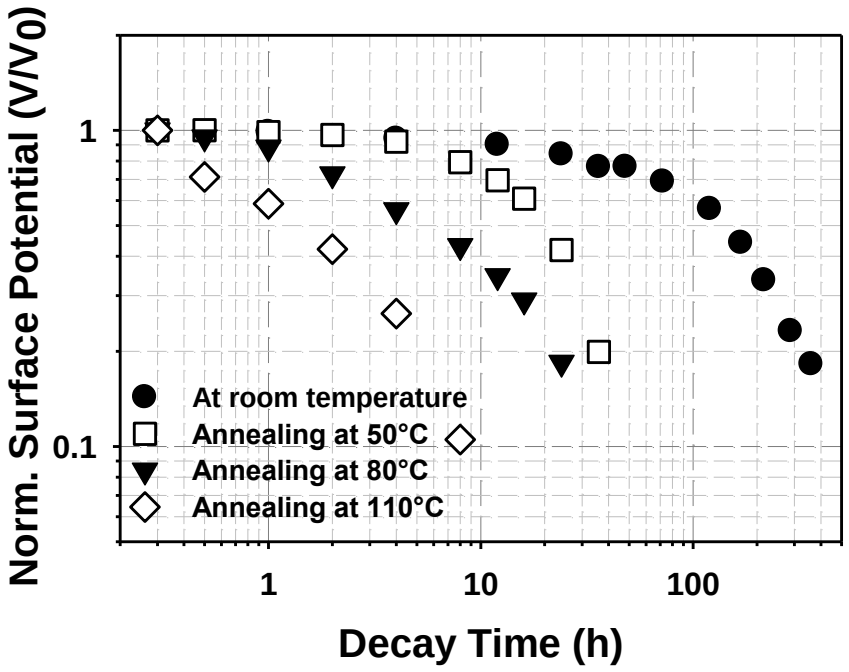

Figure 14.9 Surface potential decay test at various annealing temperatures

If there occurs more than one relaxation mechanism with distinct temperature dependences, in general superposition doesnot hold[33]. However a linear relation between log

relaxation times and 1/T was found from measurement at four temperature values, which shows isothermal accelerated test is meaningful to investigate charge holding properties of filaments.

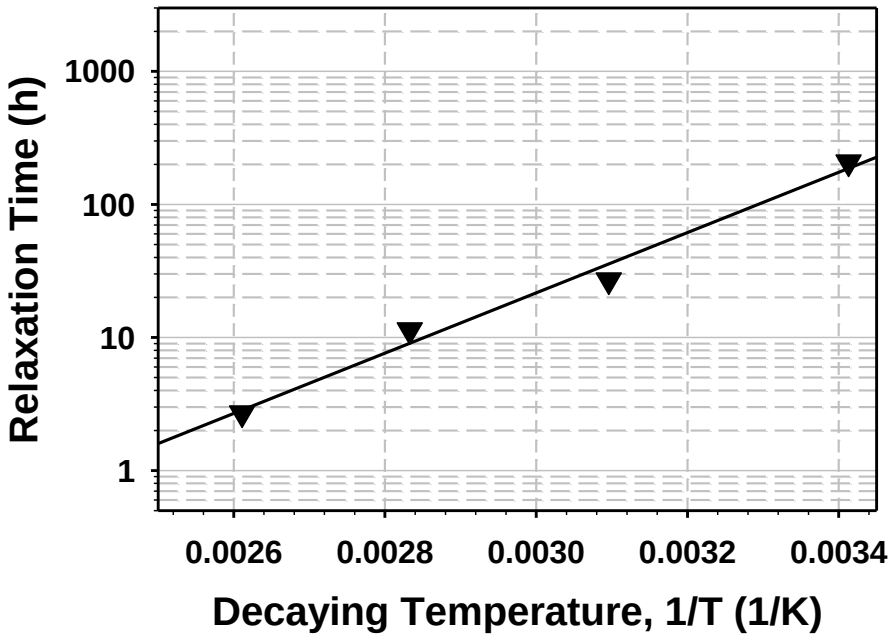

Figure 14.10 Relaxation times at various temperatures

14.4.2 Discussion

When fibrous electrets are considered, it is not easy to design an experimental setup to measure the electrostatic property. Although there are several works explained in the

previous part, when compared to films, nonwoven webs have more anisotropic macro- and microstructures. Firstly, thickness and yarn density (or packing density for webs) should be kept constant. Assuming those filament- electrode samples as capacitors charge and produced voltage will be directly proportional (Equation 14.2).

$$Q = C.V \qquad \text{Equation 14.2}$$

where Q stands for charge, C for capacitance and V for potential. Here the capacitance will be proportional to area/thickness ratio as shown in equation 3.

$$C = \varepsilon_0 \frac{A}{d} \qquad \text{Equation 14.3}$$

This will give us $V = \frac{Q.d}{\varepsilon_0.A}$. So measured potential will be dependent on thickness and area of the capacitance which should be kept constant, if electret characteristics of pure polymer structure is being analyzed.

Secondly every individual filament has a charge at a degree. In the form of a yarn or any 3D structure, the filaments will affect each other, which will also change the measured potential value. This effect probably causes electrostatic stresses within the macrostructure, which may be effective on decay.

Thirdly, fibers are cylindirical objects and will exhibit potential in all directions, which makes the difference with two dimensional films. The potential applied by filaments

through the capacitive probe of voltmeter can change with any motion of charged filaments. On the other hand image charges formed on the metal electrode will be effective on the measured potential since a porous structure is in question. One needs to keep the fiber positions fixed to reduce the effect of image charges on measured value.

Due to explained difficulties sample yarns were aligned uniformly on metal plates like a film structure. To provide a smooth sample surface, yarn density in this 2cm spacing were kept constant and any filaments protruding from the sample were discarded. Main reasons that are thought to be behind obtained 50% CV values in the literature [34] would be overcome using aligned filaments configuration. This CV value is reasonable and even inevitable due to varying fiber chemistry and microstructure. The disadvantage of explained method can be its inappropriateness for triboelectrified fibers. The authors are still looking for developing a reliable method for those of the fibers.

14.5 Conclusion

Surface potential decay analysis is a reasonable method for testing electrostatic properties of fibrous samples. Roughly saying all three charge decay mechanisms; ie bulk conductivity, surface conductivity and ionic attacks from the surrounding environment [14] are taken into account. Here an easy and reliable technique was explained to measure surface potential of fibrous materials which are prone to decay by all three mechanisms. A linear

relationship between relaxation times at different annealing temperatures was found which shows practical applicability of the method. Small variations in measurements are thought to be limited to inevitable contamination and change in chemical composition of surface and morphological properties. Large standard deviation mentioned in the literature seems to be due to variation in packing density, thickness and fiber-fiber proximity within fibrous samples. Under tedious control, deviations were minimized significantly.

14.6 References

1. Kravtsov, A. G., Brünig, H. & Zhandarov, S. F. Analysis of the polarization state of melt-spun polypropylene fibers. *Journal of Materials Processing Technology* 124, 160–165 (2002).
2. Kravtsov, A. G. & Brünig, H. Characteristics of electret charge formation in polypropylene fibres. *Fibre Chem* 32, 180–186 (2000).
3. Kravtsov, A. G. & Gol'dade, V. A. Optimization of the Electret State of Polymer Fibres. *Fibre Chemistry* 33, 189–192 (2001).
4. Tabti, B. *et al.* Corona-Charging and Charge-Decay Characteristics of Nonwoven Filter Media. *Industry Applications, IEEE Transactions on* 46, 634–640 (2010).

5. Kravtsov, A., Br\ünig, H., Zhandarov, S. & Beyreuther, R. The electret effect in polypropylene fibers treated in a corona discharge. *Advances in Polymer Technology* 19, 312–316 (2000).

6. Kravtsov, A. G., Zotov, S. V. & Brunig, H. Peculiarities of the electret state of melt-spun and melt-blown fibrous polypropylene materials. *Mechanics of composite materials* 36, 491–496 (2000).

7. Tabti, B., Dascalescu, L., Plopeanu, M., Antoniu, A. & Mekideche, M. Factors that influence the corona charging of fibrous dielectric materials. *Journal of Electrostatics* 67, 193–197 (2009).

8. Tabti, B. *et al.* Factors That Influence the Decay Rate of the Potential at the Surface of Nonwoven Fabrics After Negative Corona Discharge Deposition. *Industry Applications, IEEE Transactions on* 46, 1586–1592 (2010).

9. Kim, J., Jasper, W. & Hinestroza, J. Charge Characterization Of An Electrically Charged Fiber Via Electrostatic Force Microscopy. *Journal of Engineered Fibers and Fabrics* 1, 30–46 (2006).

10. Lovera, D. *et al.* Charge storage of electrospun fiber mats of poly (phenylene ether)/polystyrene blends. *Polymer Engineering & Science* 49, 2430–2439 (2009).

11. Erhard, D. *et al.* Recent Advances in the Improvement of Polymer Electret Films. *[Without Title]* 1–53 (2010).

12. Bauer, S. *et al.* Thermal stability of the dipole orientation in nonlinear optical guest-host, side-chain and cross-linked polymer electrets. *Electrets, 1994.(ISE 8), 8th International Symposium on* 800–805 (1994).

13. Grossweiner, L. I. A Note on the Analysis of First-Order Glow Curves. *J. Appl. Phys.* 24, 1306 (1953).

14. Jonassen, N. *Electrostatics*. (Springer: 2002).

15. Sessler, G. H., Sessler, G. M., Broadhurst, M. G. & Gerhard-multhaupt, R. (CON) *Electrets*. (Laplacian Press: 2000).

16. Baba, A. & Ikezaki, K. Thermally stimulated currents from corona-charged polypropylene films: A thermal effect of vacuum deposition of metallic electrodes. *Journal of applied physics* 57, 359–365 (1985).

17. Sessler, G. M., West, J. E., Gerhard-Multhaupt, R. & von Seggern, H. Nondestructive Laser Method for Measuring Charge Profiles in Irradiated Polymer Films. *Nuclear Science, IEEE Transactions on* 29, 1644–1649 (1982).

18. Mizutani, T. Space charge measurement techniques and space charge in polyethylene. *Dielectrics and Electrical Insulation, IEEE Transactions on* 1, 923–933 (1994).

19. Liu, R., Takada, T. & Takasu, N. Pulsed electro-acoustic method for measurement of space charge distribution in power cables under both DC and AC electric fields. *J. Phys. D: Appl. Phys.* 26, 986–993 (1993).

20. Vázquez, Chen, G., Davies, A. E. & Bosch, R. Space charge measurement using pulsed electroacoustic technique and signal recovery. *Journal of the European Ceramic Society* 19, 1219–1222 (1999).

21. Yeom, B. Y., Shim, E. & Pourdeyhimi, B. Boehmite nanoparticles incorporated electrospun nylon-6 nanofiber web for new electret filter media. *Macromol. Res.* 18, 884–890 (2010).

22. Antoniu, A., Tabti, B., Plopeanu, M.-C. & Dascalescu, L. Accelerated Discharge of Corona-Charged Nonwoven Fabrics. *Industry Applications, IEEE Transactions on* 46, 1188–1193 (2010).

23. Vosteen, W. E. A high speed electrostatic voltmeter technique. *Industry Applications Society Annual Meeting, 1988., Conference Record of the 1988 IEEE* 1617–1619 vol.2 (1988).doi:10.1109/IAS.1988.25274

24. Baumgartner, H., Loffler, F. & Umhauer, H. Deep-Bed Electret Filters: The Determination of Single Fiber Charge and Collection Efficiency. *Electrical Insulation, IEEE Transactions on* EI-21, 477–486 (1986).

25. Siag, A. M., Tennal, K. B. & Mazumder, M. K. Determination - Of - Fiber - Charge - Density - Of - Electret - Filters - Pb - Taylor & Francis. *Particulate Science and Technology: An International Journal* 12, 351 (1994).

26. Brown, R. C. Electrically charged filter materials. *Engineering Science and Education Journal* 1, 71–79 (1992).

27. Romay, F. J., Liu, B. Y. . & Chae, S. J. Charge density measurement of electret filters using alpha-ray ionizing radiation. *Filtration & separation* 36, 51–56 (1999).

28. Brown, R. C. Capture of dust particles in filters by linedipole charged fibres. *Journal of Aerosol Science* 12, 349–356 (1981).

29. Kim, J., Otani, Y., Noto, D., Namiki, N. & Kimura, K. Initial collection performance of resin wool filters and estimation of charge density. *Aerosol science and technology* 39, 501–508 (2005).

30. Giacometti, J. A. & Oliveira, O. N. Corona charging of polymers. *Electrical Insulation, IEEE Transactions on* 27, 924–943 (1992).

31. Goldman, M., Goldman, A. & Sigmond, R. S. The corona discharge, its properties and specific uses. *Pure & Appl. Chem* 57, 1353–1362 (1985).

32. Horenstein, M. N. Measuring isolated surface charge with a noncontacting voltmeter. *Journal of Electrostatics* 35, 203–213 (1995).

33. van Gurp, M. & Palmen, J. Time-temperature superposition for polymeric blends. *Rheol Bull* 67, 5–8 (1998).

34. Tsai, P. P., Schreuder-Gibson, H. & Gibson, P. Different electrostatic methods for making electret filters. *Journal of Electrostatics* 54, 333–341 (2002).